UNCLASSIFIED

[redacted]

UNCLASSIFIED

Classification Changed

JPL Letter to Authority NASA-Langley
on Nov. 4 1970, signed by W. E. Hansen

Date: Jan. 4, 1971 By: [signature]

Space Programs Summary No. 37-30, Volume I

for the period September 1, 1964 to October 31, 1964

The Lunar Program

(Title Unclassified)

JET PROPULSION LABORATORY
LIBRARY
DEC 30 1964

CALIFORNIA INSTITUTE OF TECHNOLOGY

Copy No. 193

THIS COPY ISSUED FOR J.P.L. USE ONLY

JET PROPULSION LABORATORY
CALIFORNIA INSTITUTE OF TECHNOLOGY
PASADENA, CALIFORNIA

November 30, 1964

[redacted]

CONFIDENTIAL

[redacted] declassified after 12 years

UNCLASSIFIED

166750
Lab 9601

Preface

The *Space Programs Summary* is a six volume, bimonthly publication designed to report on JPL space exploration programs, and related supporting research and advanced development projects. The subtitles of all volumes of the *Space Programs Summary* are:

Vol. I. The Lunar Program (Confidential)

Vol. II. The Planetary–Interplanetary Program (Confidential)

Vol. III. The Deep Space Network (Unclassified)

Vol. IV. Supporting Research and Advanced Development (Unclassified)

Vol. V. Supporting Research and Advanced Development (Confidential)

Vol. VI. Space Exploration Programs and Space Sciences (Unclassified)

The *Space Programs Summary,* Volume VI consists of an unclassified digest of appropriate material from Volumes I, II, and III and a reprint of the space science instrumentation studies of Volumes I and II.

W. H. Pickering, *Director*
Jet Propulsion Laboratory

Space Programs Summary No. 37-30, Volume I

Copyright © 1964, Jet Propulsion Laboratory, California Institute of Technology

Prepared under Contract No. NAS 7-100, National Aeronautics & Space Administration

This document contains information affecting the national def[redacted] United States, within the meaning [redacted] Espionage Laws, Title 18, U.S.C., [redacted] 793 and 794, the [redacted] mission or revelation of which in any manner to an unauthorized person is prohibited by law.

UNCLASSIFIED

Contents

I. *Ranger* Project 1
A. Introduction 1
B. Project Engineering 2
C. Systems 7
D. Supporting Activities 19
II. *Ranger* TV Subsystem, Block III 20
A. System Engineering 20
B. Cameras 21
C. Telecommunications 21
D. Systems Control and Electrical Power 21
III. *Surveyor* Project 22
A. Introduction 22
B. Space Flight Operations Documentation 22
IV. *Surveyor* Spacecraft System 24
A. System Engineering 27
B. Scientific Payload 32
C. System Analysis 48
D. Flight Control 65
E. Electronics 74
F. Electrical Power Supply 78
G. Thermal Control 85
H. Engineering Mechanics 101
I. Propulsion 114
J. Spacecraft Vehicle and Mechanisms for Basic Bus 123
K. Reliability, Quality Assurance, and System Test 129
L. Launch Operations 148
M. Support of Study on Critical Data Recorder 157

UNCLASSIFIED

UNCLASSIFIED

I. *Ranger* Project

A. Introduction

The *Ranger* Project was established to develop a space flight technology for transporting engineering and scientific instruments to the Moon and planets. Nine *Ranger* launchings, using *Atlas D–Agena B* vehicles, are now planned; seven of these flights have been made.

Rangers 1 and *2* (Block I) were not lunar-oriented, but were engineering evaluation flights to test the basic systems to be employed in later lunar and planetary missions. Several scientific experiments were carried on a non-interference basis. Both spacecraft performed satisfactorily within the constraints of the obtained satellite orbit. *Rangers 3, 4,* and *5* (Block II) carried a gamma-ray instrument, a TV camera, and a rough-landing seismometer capsule; all three of these flights experienced failures.

The objective of the *Ranger* Block III (*Rangers 6* through *9*) flights is to obtain pictures of the lunar surface, at least an order of magnitude better than those obtainable from Earth-based photography, which will be of benefit to both the scientific program and the U.S. manned lunar flight program. The *Ranger 6* spacecraft, which was launched from Cape Kennedy, Florida, on January 30, 1964, and impacted the Moon essentially on target on February 2, 1964, did not accomplish the primary flight objective due to a failure of the TV subsystem to transmit pictures. An extensive analysis of the TV subsystem failure was conducted, new and reworked parts were assembled as the *Ranger 7* TV subsystem, and extensive testing of the reassembled TV subsystem was performed. The *Ranger 7* spacecraft was launched from Cape Kennedy, Florida, on July 28, 1964, and impacted the Moon on target on July 31, 1964. The mission flight objective was accomplished. The outstanding events of the mission were the precision of the midcourse maneuver and the transmission of 4304 video pictures of the lunar surface.

Testing of the proof test model was completed. *Rangers 8* and *9* are in varying stages of assembly; preliminary subsystem and system testing is being performed.

UNCLASSIFIED

UNCLASSIFIED

B. Project Engineering

1. Investigation of Launch-to-Injection Environment for Ranger Missions

Subsequent to the *Ranger 6* flight, questions were raised regarding the possible effects of the launch vehicle and the launch-to-injection environment upon the operation of the spacecraft. Investigations were started in the areas of electrical transients, accumulated high electrostatic charges, mechanical and electrical operations of the umbilical plug and door, ionized gases, and blast waves at booster ejection. It was intended to determine through these investigations: (1) whether this environment could have affected the operation of the *Ranger 6* TV circuits, and (2) whether the changes introduced on the *Ranger 7* spacecraft would preclude any deleterious effects because of the above mentioned phenomena. The specific purposes of the investigations were to identify areas in the launch-to-injection phase of flight which were believed to be problem areas and to establish a general test plan to prove or disprove the existence of problems within these areas.

a. Problem areas. A list was prepared of hypothetical problems based on suspected environmental conditions. The problems fell generally into two categories: unknown environmental conditions and unknown spacecraft susceptibilities.

Launch vehicle electrostatic problems had occurred in other space programs, and the circumstances of the occurrences were carefully evaluated. The extent of charge or degree of voltage buildup on the *Ranger* launch vehicle in relation to time and the discharge characteristics of the static charge when arcing or dissipating posed major questions. A knowledge of the degree of ionization of gases in flight and the effects of ionized gases in combination with an electrostatic charge on the surface of the launch vehicle was also desired.

The susceptibility of the spacecraft and launch vehicle had not been fully determined from the viewpoint of knowing the points at which electrical transients, static charges, and electrical discharges became critical. Also, the integrity of the launch vehicle and spacecraft grounding systems in the presence of high static charges and discharges had not been verified.

b. Test plans and activities. Two approaches were followed in an attempt to determine the conditions under which the TV command switch on *Ranger 6* could have been triggered. One approach was analytical and was directed toward determining the theoretical characteristics of the launch-to-injection environment. The other approach was realistic and was directed toward determining susceptibilities of spacecraft circuits.

Analytical efforts. A mathematical model of the spacecraft and launch vehicle in the flight configuration was developed to provide an analysis of high-voltage effects. A preliminary investigation was made concerning the nature of the plume which occurs during flight at the time of *Atlas* staging. It was believed that a blast wave, possibly accompanied by ionization, takes place at this time. Available information concerning the extent of static charges on the launch vehicle was reviewed.

Tests. The following experimental tests were performed:

(1) Electrical measurements were made at the umbilical connector immediately upon the start of the investigations. These measurements, made prior to the transient and high-voltage tests, were taken under both quiescent and actual operating conditions of spacecraft equipment.

(2) Specific mechanical tests were conducted to determine the mechanical operating characteristics of the *Ranger–Agena* adapter umbilical door.

(3) Laboratory test programs were performed independently in two separate areas. RCA performed tests which included attempts to activate the TV turn-on circuit by electrostatic and electromagnetic means. JPL initiated a series of tests to determine the effects on the spacecraft due to characteristics of launch vehicle circuits, especially at the time of staging of the *Atlas* booster.

(4) High-voltage tests were conducted by charging the structural test model of the spacecraft, adapter, shroud, and *Agena* forward equipment rack (in the flight configuration) and by arcing the accumulated charge to ground. Tests were made simultaneously by RCA and JPL on typical circuits and isolated elements on the spacecraft. This constituted a brute-force method of actually determining whether or not a static charge would trigger the TV turn-on circuit. Fig. 1 shows the general test arrangement used for the high-voltage static tests. Discharge arcs after voltage buildup are shown in Fig. 2. The JPL tests are described below in Part 2.

UNCLASSIFIED

UNCLASSIFIED

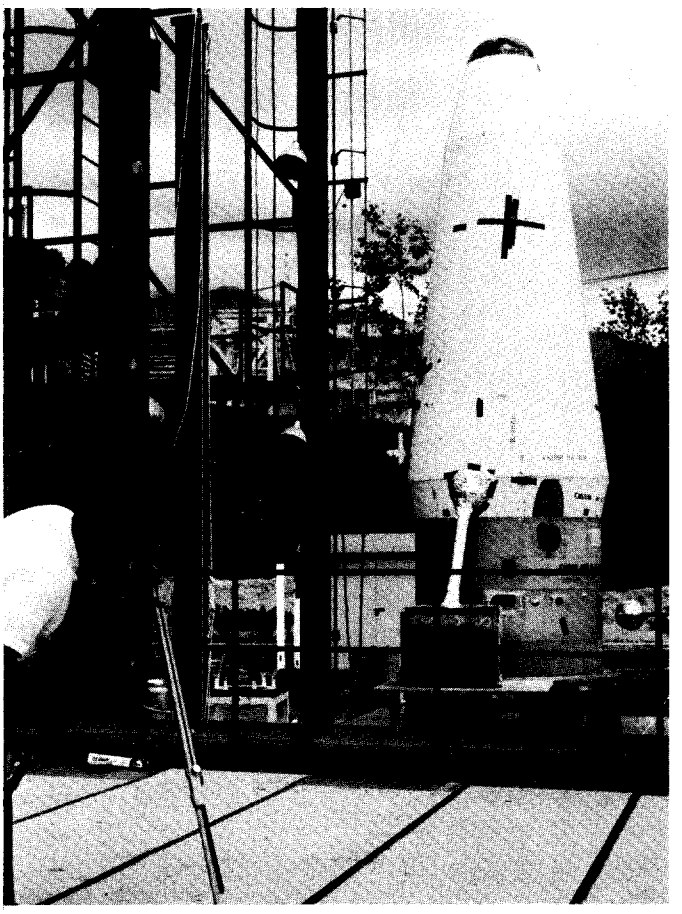

Fig. 1. General configuration for high-voltage static tests

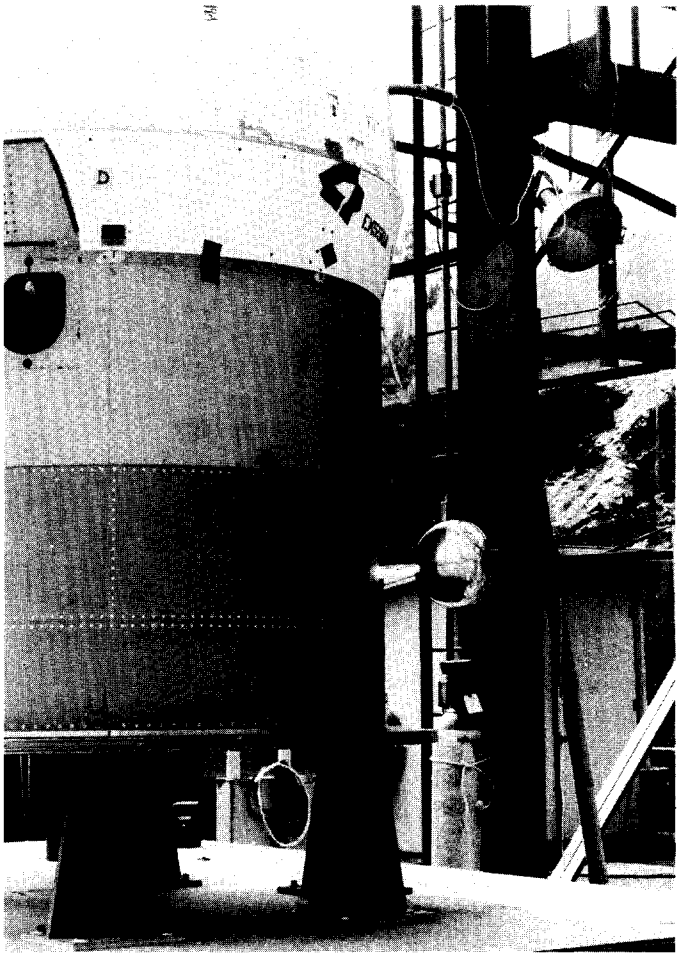

Fig. 2. Discharge arcs after voltage buildup

c. Recommendations. As a result of these investigations, the following were recommended:

(1) Additional tests to determine the answers to specific questions and to resolve certain discrepancies between the theoretical and actual results which appeared during the first tests.

(2) Further experiments and calculations to determine the hazards of transients and high voltages in combination with an ionized blast wave for similar missions.

(3) A complete design review of all flight doors as a result of the umbilical door tests.

(4) A verification that proper system grounding techniques are used throughout the launch vehicle and spacecraft systems.

(5) Continuation of the investigation of the ionized gas problem at staging.

(6) Investigation of the possibility of disconnecting the *Agena* spin fitting a few seconds prior to ignition.

(7) Instrumentation of launch vehicles to provide actual and accurate flight data in order to better understand the flight environment and more specifically determine the electrostatic charging and discharging rates.

2. Ranger Static-Charge Analysis and Susceptibility Tests

a. Introduction. Extensive analyses and tests of *Ranger* spacecraft susceptibility to high-voltage charge and discharge transients were performed during this reporting period (refer to Part 1, above). The purpose of the high-voltage test program was to determine whether charging of the spacecraft and launch vehicle due to the rocket engines, or subsequent discharge of a charged vehicle to clouds or exhaust trail, could create a mechanism for spacecraft degradation or failure.

CONFIDENTIAL UNCLASSIFIED

UNCLASSIFIED CONFIDENTIAL

b. Charging and discharging model and analysis. A preliminary investigation showed that the charge would be removed from (or placed on) the vehicle surface, i.e., the shroud around the spacecraft. If this shroud were a perfect conducting surface without any aperture, there would be no field inside the shroud to induce voltage into internal circuitry. However, since the shroud is not perfect, some field will exist inside and be available to induce voltage into spacecraft circuitry. The original model proposed for analysis is shown in Fig. 3. This is a simplified model. A more complex model has been developed by Dr. G. I. Cohn, a consultant.

Fig. 3 shows an element A which may be a circuit isolated from structure and shroud or any isolated device having some resistance R_i and capacitance C_i to structure. C_l is a leakage capacitance through the shroud to infinity and is related to the imperfections of the shroud assembly. C_e is the capacitance of the total vehicle to ground or other reference. The current generator represents the vehicle charging mechanism. An analysis of the above model yields the following relationships for charge and discharge, respectively:

$$V_{charge} = \frac{R_i C_l I}{C_e}\left(1 - e^{-t/R_i C_i}\right)$$

$$V_{discharge} = \frac{C_l V_0}{C_i} e^{-t/R_i C_i}$$

where V_0 is the vehicle voltage at time of discharge. These voltages represent the voltage difference between the element A and the shroud structure. The values of R_i, C_i, C_e, and C_l were measured on the thermal control model (TCM).

c. Spacecraft TCM tests. The spacecraft with shroud installed was mounted on top of an *Agena* adapter ring and *Agena* forward equipment rack. The complete assembly was then mounted on an insulated table. A high-voltage generator was used to raise the potential of the assembly to various levels up to 300 kv. The assembly was then discharged through a discharge sphere and ground strap. The purpose of these tests was to determine the magnitude of induced transients into typical spacecraft circuitry and to evaluate the possibility of these transients as failure-producing effects. Tests on the TCM with simulated circuitry aboard (no power applied to circuits) yielded transients of 100 to 200 mv during spacecraft discharge from 200 kv. Although this value is not a probable cause of catastrophic failure, the possibility did exist of a temporary malfunction of a live spacecraft. As a result of these tests it was proposed that the proof test model (PTM) be subjected to this high-voltage environment.

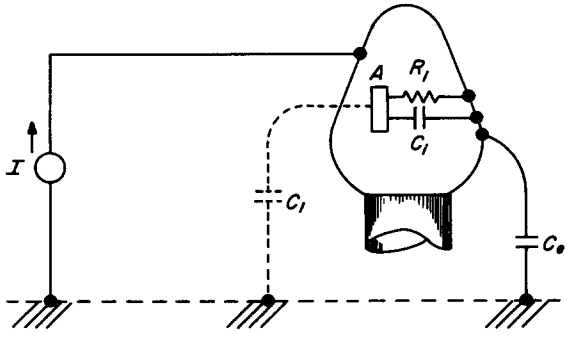

Fig. 3. High-voltage charging and discharging model

d. Spacecraft PTM tests. On July 17, 1964, the *Ranger 7* configuration PTM was installed on the insulated table with antennas connected to establish two-way lock with the spacecraft command transponder and the ground receiver, and to check out the TV subsystem subsequent to each series of discharges. The PTM was placed in the launch mode with the CC&S inhibited. A launch verification test was performed. All external cabling to the spacecraft was removed. Two-way RF lock was established, and the spacecraft was raised to 10, 30, 60, 100, and 200 kv. At each level, the spacecraft was allowed to arc over to the discharge sphere. Telemetry was monitored during the breakdown period. After several arcs, the high voltage was removed and complete engineering measurements were made. Also at this time, the TV subsystem was turned on and the 90-point telemetry was transmitted to the RCA checkout equipment.

No temporary or permanent malfunction or failure occurred on the PTM as a result of these high-voltage tests.

3. Ranger Electromagnetic Interference Transient Tests

a. Summary. The non-normal events which occurred during the *Ranger 6* launch prompted an investigation concerning the susceptibility of the *Ranger* spacecraft to electrical transients on its umbilical lines. During testing of the PTM spacecraft in the *Ranger 7* electrical configuration (changed from *Ranger 6*), some lines were shown to be sensitive to transients, but no anomalies similar to the *Ranger 6* events were noted.

b. Background. Because a non-normal *Ranger 6* flight event (Channel-8 telemetry turn-on) occurred near the

UNCLASSIFIED CONFIDENTIAL

UNCLASSIFIED
CONFIDENTIAL

Atlas booster jettison event, effects of electrical transients were investigated, particularly those associated with the booster jettison event. A launch vehicle transient could be coupled from the *Agena* to the *Ranger* spacecraft via the two baseband telemetry wires (the only *Agena-Ranger* hard-line connection). Investigation showed that these wires are isolated in both the *Ranger* and the *Agena* by isolation transformers. However, discussions (but no documentation) with Lockheed Missiles and Space Corporation and General Dynamics/Astronautics indicated that currents of 20 amp and voltages as large as 100 v are interrupted during flight sequencing, so it is thought that large electrical transients could be present. Since the net transient environment at the spacecraft was unknown, it was decided to test selected umbilical lines regardless of the environment and regardless of the coupling path. The goals were to determine if critical subsystems are susceptible to electrical transients on the umbilical lines.

c. Description of the transient. It was decided to adapt the transient generator used in the Air Force specification GM-07-59-2617A, *Electro-Interference Control Requirements for Minute Man.* This transient simulates a capacitive discharge. A schematic of the generator is shown in Fig. 4. It is triggered by a variable repetition rate pulse generator at a rate of 10 pulses/sec, this rate being in the range used in the Air Force specification. The peak transient voltage can be adjusted continuously from 1 to 75 v, positive or negative polarity. Since the test was not meant to be destructive, the maximum amplitude of 75 v with respect to chassis ground was in some cases reduced by the subsystem cognizant engineers on the basis of component voltage ratings. The transient waveform is shown in Fig. 5; it varies depending on the circuit under test.

d. Transient tests performed. The first test was performed on July 13, 1964. The test operating configuration and procedure were intended to simulate the condition of launch plus 1 min. The *Ranger* PTM spacecraft was ungrounded in a no-cable configuration; one exception to this was the operational support equipment (OSE)

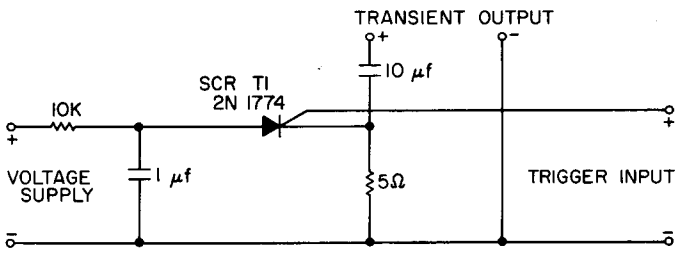

Fig. 4. Transient generator schematic

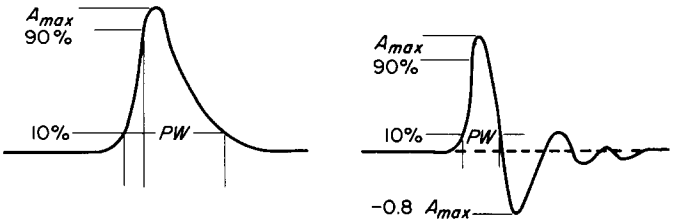

PULSE WIDTH (*PW*): 10-15 μsec
RISETIME: 0.5-1 μsec

PULSE WIDTH (*PW*): 6-7 μsec
RISETIME: 0.5-1 μsec

A_{max}: MAXIMUM AMPLITUDE

(a) HIGH-IMPEDANCE CIRCUIT (b) LOW-IMPEDANCE CIRCUIT

Fig. 5. Typical injected transient pulses

battery simulator cable which was used because the duration of the test would have discharged the spacecraft batteries considerably. Another exception was the use of two wires from the central computer and sequencer (CC&S) OSE to inhibit CC&S at the 1-min-after-launch operating mode. The spacecraft was commanded and monitored by the system test complex by a two-way RF link during the test. Channel-8 telemetry was turned on (a non-standard launch mode) because it is the only method of monitoring the TV subsystem. In this mode, the electrical transients were injected into the umbilical wires one at a time (Fig. 6). The voltage was increased until 75 v (or the reduced level set by the cognizant engineer) was reached or an indication of susceptibility was noticed on the central recorder. If an indication of susceptibility was noticed, the threshold was determined by coordination of the transient generator operator (next to the spacecraft) and the central recorder operators (on the system test complex) through the missile operations paging system communications set. Once the threshold of susceptibility was determined, the transient voltage was increased until the test director halted the proceedings or the maximum voltage for that line was reached. This procedure was followed for negative and positive polarity transients for each line. Soon after the first test, the criterion for selection of those particular umbilical lines was questioned; it was decided to repeat the test on all umbilical lines. On July 22 and 23 the second test was performed. It made use of information from the first test. The transient generator setup in particular was improved for ease of operation.

e. Test results. The results of the second test confirmed the results of the first test on those wires tested both times. The results did not indicate a non-normal event similar to that on *Ranger 6*. This does not rule out the possibility that the *Ranger 6* failure was due to a transient.

CONFIDENTIAL
UNCLASSIFIED

UNCLASSIFIED
CONFIDENTIAL

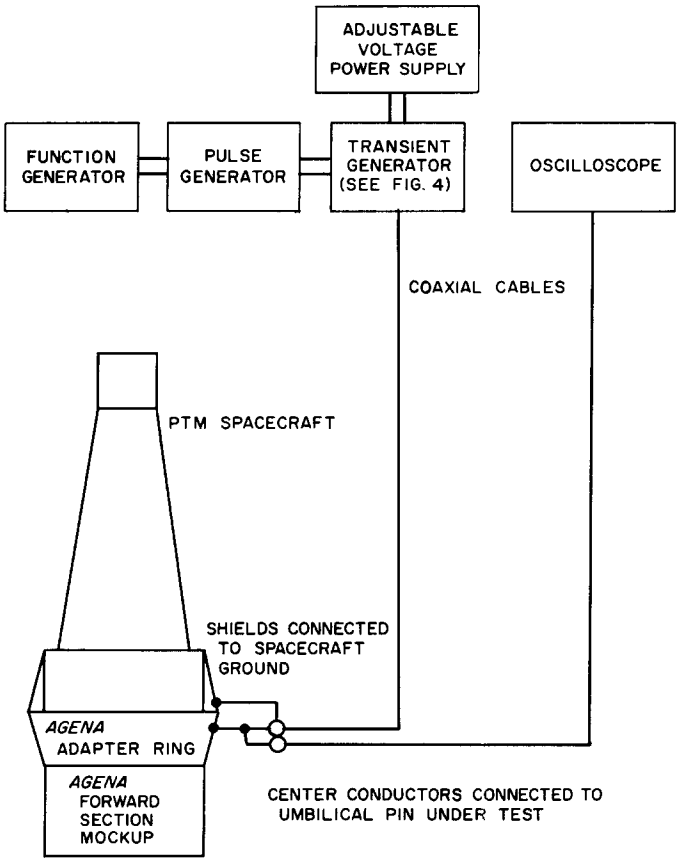

Fig. 6. Block diagram of *Ranger* PTM transient test configuration

The actual transient environment is unknown so it is possible that the test did not simulate the actual environment. Also, some circuitry had been changed to the *Ranger 7* configuration, making test results not directly applicable to *Ranger 6*.

The most sensitive umbilical circuit was the external mode change line. The spacecraft started changing data modes when the transient amplitude reached +17.5 v. At +25 v, the mode change relay was chattering and could be heard outside the spacecraft. The next most sensitive lines were all DC return lines. Transients injected in these lines caused the central recorder readout to be noisy, particularly Channels 2 and 3, when the transient voltage level reached +25 to 50 v.

4. Spacecraft Assembly and Test Operations

During the reporting period, the *Ranger* proof test model (PTM) was up-dated and the TV, data encoder, and attitude-control subsystems were extensively tested and modified where necessary. *Rangers 8* and *9* were in varying stages of assembly and had entered preliminary subsystem and system testing phases.

a. Proof test model. During the week of August 3, the PTM electronic assemblies were removed from the spacecraft and returned to the technical divisions for incorporation of engineering change requirements (ECR) and up-dating to the *Ranger 8* and *9* configuration. Some TV subassemblies were returned to RCA for the same reason. The intent was to perform all changes to PTM hardware and harnessing prior to changing the flight equipment. The PTM spacecraft bus equipment was reassembled by August 17.

The PTM TV subsystem was completely disassembled during the week beginning August 17. Minor mechanical rework and paint touch-up were accomplished on the structure. After return of all items from RCA, the PTM TV subsystem was reassembled. New transmitter and transmitter power supplies were also incorporated. After reassembly, the TV subsystem was checked out and the F-camera video was found to be non-operational. Investigation revealed a sequencer problem and the assemblies were returned to RCA. Rework in New Jersey failed to resolve the problem, which was corrected after return of the sequencer to JPL.

No spacecraft problems were reported in the attitude-control and data encoder subsystem checks ending September 2.

During the RF full-power checks on the TV subsystem, no power was obtained from the P-channel. A partial short-circuit in the transmitter power supply was corrected and subsequent checks indicated normal operation except for a polarity reversal at a telemetry monitor point. Following modification by RCA, the subsystem checks were resumed without abnormal operations.

Following the TV subsystem checks, a series of tests was performed on the attitude-control power supply and the spacecraft power subsystem; no problems were noted. The TV subsystem was mated to the spacecraft and electromagnetic interference checks were performed. No anomalies were detected with spacecraft RF lock or degradation of telemetry data.

A system test on September 10–11 was conducted without serious problems. This test completed the schedule for the PTM, which was then to be maintained in the

UNCLASSIFIED
CONFIDENTIAL

UNCLASSIFIED

Ranger 8 and 9 configuration and used to evaluate problems that might develop during the mission.

b. Ranger 8. The *Ranger* 8 spacecraft was released from storage and mechanical build-up was started. The electrical assemblies were returned to the technical divisions for checks and ECR incorporation. During test, the pyrotechnic subsystem failed to fire one-half of the midcourse motor turn-on squibs and the suspected assembly was replaced.

Mechanical assembly operations were completed. Ground wiring and integrity checks were then run without incident. After initial power application on October 5, subsystem checkout and calibration indicated no problem more serious than a defective attitude-control module.

During October 13–16, power calibrations were made with telemetry, and a back-up command timer and system test was performed. No major problems were experienced.

On October 19, a power survey was conducted on the spacecraft bus and the midcourse motor with the new squib ignition harness was installed. Following the power survey, a TV subsystem test showed favorable results. The initial system test produced only a telemetry channel failure. The pyrotechnic subsystem test was repeated because of spacecraft modifications; results were satisfactory.

A back-up functions system test on October 23 showed abnormal behavior in the radio and central-computer-and-sequencer operational support equipment. Neither problem was considered significant. The spacecraft was subjected to attitude-control gas system checks.

Following completion of ring harness modifications on September 8 and minor mechanical up-dating and ECR incorporation, the spacecraft bus was given an attitude-control gas subsystem quantitative leak check, which was well within specification.

c. Ranger 9. During the first week of October, the *Ranger* 9 spacecraft was removed from storage and the ring harness was modified. The bus structure was checked for proper screw and bolt torque values and, after the incorporation of miscellaneous ECR's, the *A* and *S* planes of the bus were checked, as were the TV mating surface and the Sun sensor mounting pads.

C. Systems

1. Ranger 7 Trajectory Analysis

a. Launch phase. The *Ranger 7* spacecraft was launched at 16:50:07:873 GMT on July 28, 1964, from the Air Force Eastern Test Range at Cape Kennedy, Florida, using an *Atlas D–Agena B* boost vehicle. The inertial launch azimuth was 96.6 deg east of north. After liftoff, the booster rolled to an azimuth of 97.1 deg and performed a programmed pitch maneuver until booster cutoff. During the sustainer and vernier stages, adjustments in vehicle attitude and engine cutoff times were commanded as required by the ground guidance computer to adjust the altitude and velocity at *Atlas* vernier engine cutoff. After *Atlas–Agena* separation, there was a short coast period prior to the first ignition of the *Agena* engine. At a preset value of sensed velocity increase, the *Agena* engine was cut off. At this time the *Agena*–spacecraft combination was coasting in a nearly circular parking orbit in a southeasterly direction at an altitude of 188 km and an inertial speed of 7.80 km/sec. After an orbit coast time of 19.97 min, as determined by the ground guidance computer and transmitted to the *Agena* during the *Atlas* vernier stage, a second ignition of the *Agena* engine occurred. 89 sec later, the *Agena* was cut off with the *Agena*–spacecraft combination in a nominal Earth–Moon transfer orbit. The launch-phase ascent trajectory profile is illustrated in Fig. 7; a sequence of events from launch to acquisition of the Earth by the spacecraft is shown in Fig. 8.

b. Cruise phase. Injection (second *Agena* cutoff) occurred at 17:20:01 GMT over the western coast of South Africa at a geocentric latitude and longitude of −12.89 and 15.07 deg, respectively. The *Agena*–spacecraft combination was at an altitude of 192 km and traveling at an inertial speed of 10.949 km/sec. At 1 min, 32 sec after injection, the *Agena*–spacecraft combination entered the Earth's shadow. The *Agena* separated from the spacecraft 2 min, 35 sec after injection, performed a programmed 180-deg yaw maneuver, and ignited its retrorocket. The retrorocket impulse was designed to eliminate interference with the spacecraft operation and reduce the chance of the *Agena* impacting the Moon. Tracking data indicated that the *Agena* passed the upper trailing edge of the Moon at an altitude of 4170 km about 3 hr after *Ranger 7* impact.

Ranger 7 left the Earth's shadow 40 min, 5 sec after injection after a total shadow duration of 38 min, 33 sec. Sun acquisition had been initiated 9 min, 58 sec prior to leaving the Earth's shadow and was accomplished 5 min after leaving the Earth's shadow. Within 1 hr after

CONFIDENTIAL
UNCLASSIFIED

UNCLASSIFIED
CONFIDENTIAL

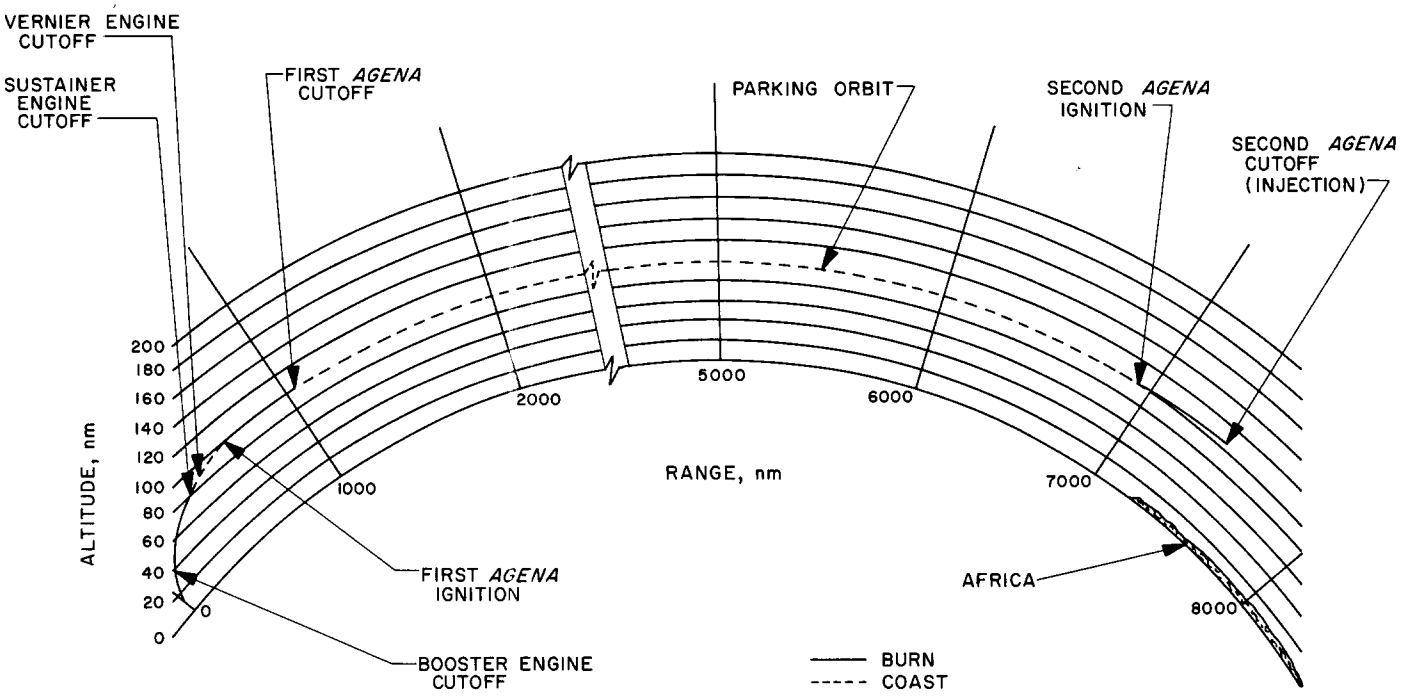

Fig. 7. Ascent trajectory profile

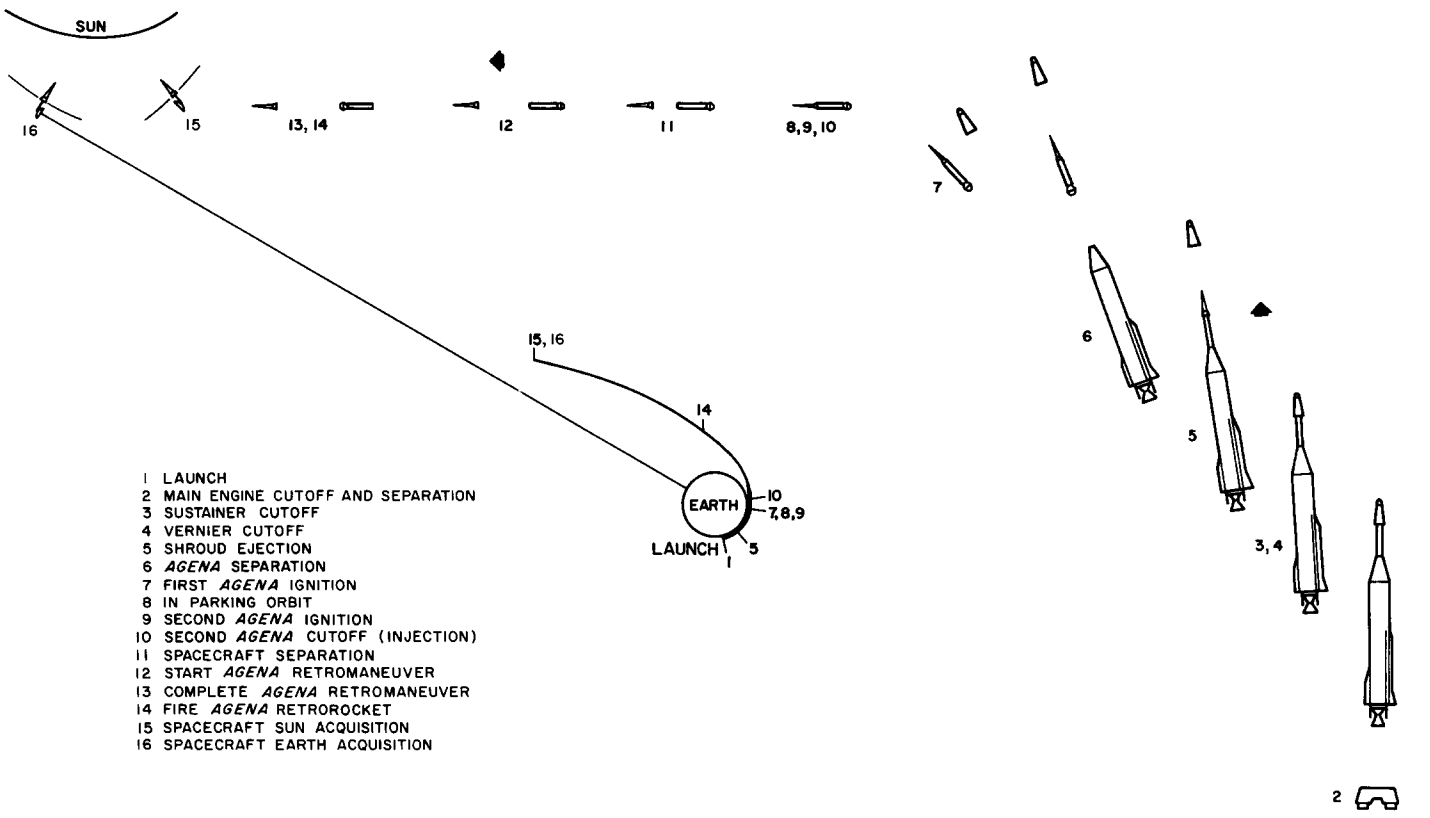

Fig. 8. Sequence of events to Earth acquisition

UNCLASSIFIED
CONFIDENTIAL

UNCLASSIFIED

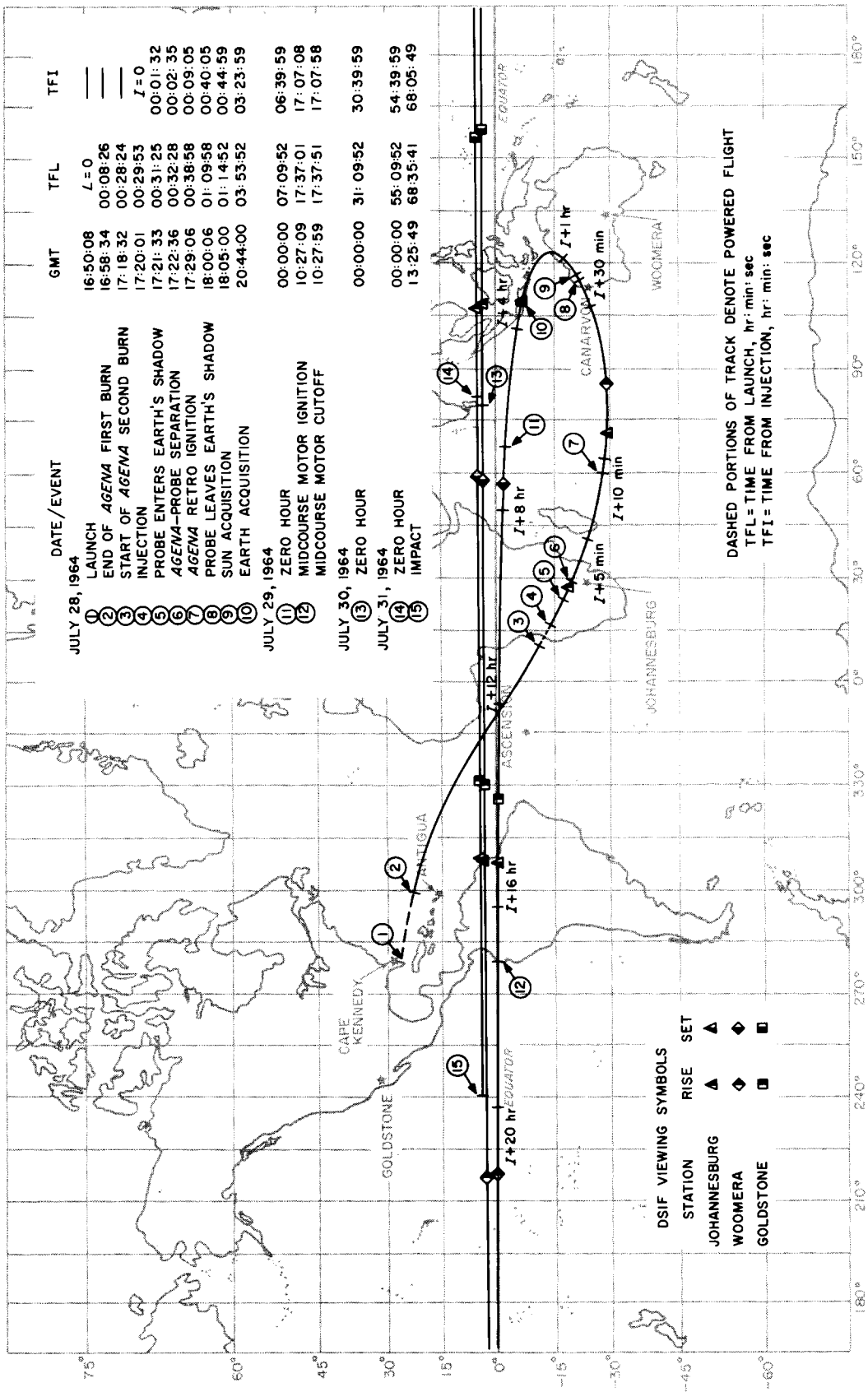

Fig. 9. Earth track of *Ranger 7* trajectory

UNCLASSIFIED

UNCLASSIFIED

injection, the spacecraft was receding from the Earth in almost a radial direction with decreasing speed. This reduced the geocentric angular rate of the spacecraft (in inertial coordinates) until, at 1.4 hr after injection, the angular rate of the Earth's rotation exceeded that of the spacecraft. This caused the Earth's track of the spacecraft (Fig. 9) to reverse its direction from increasing to decreasing Earth longitude. Plots of the geocentric distance and inertial speed of the probe as well as the Earth-probe-Sun (EPS), Sun-probe-Moon (SPM), and Earth-probe-Moon (EPM) angles as functions of time from launch are presented in Figs. 10 through 12.

Tracking data gathered and analyzed prior to the midcourse maneuver indicated that, without a correction, the spacecraft would impact the back side of the Moon at a selenocentric latitude and longitude of −12.3 and 204.0 deg, respectively. The transit time from injection to impact would have been 67.391 hr. The *Ranger* 7 transfer trajectory is illustrated in Fig. 13.

c. Midcourse maneuver phase. In order to alter the trajectory so as to impact a selected aiming point at a selenocentric latitude of −11 deg and longitude of −21 deg, midcourse maneuver calculations indicated a requirement

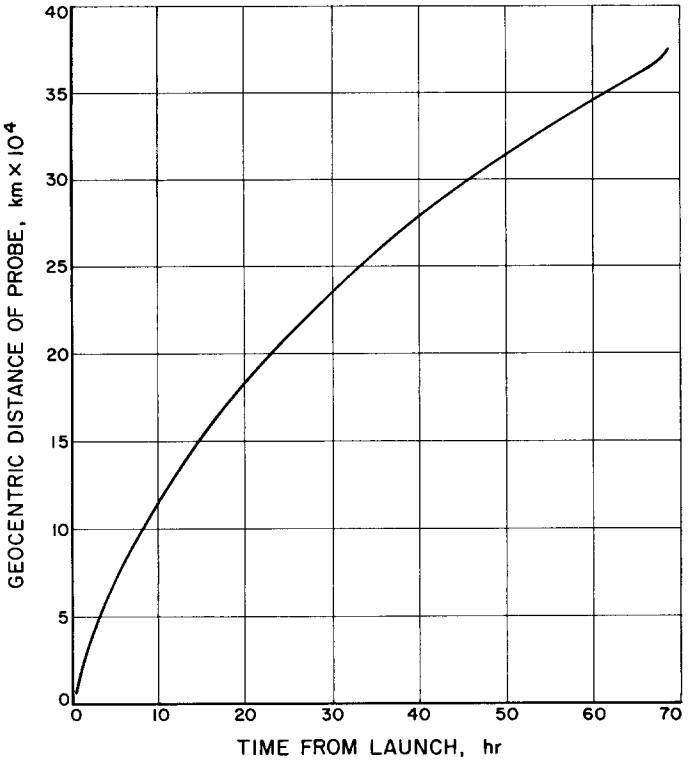

Fig. 10. Geocentric distance of probe vs time from launch

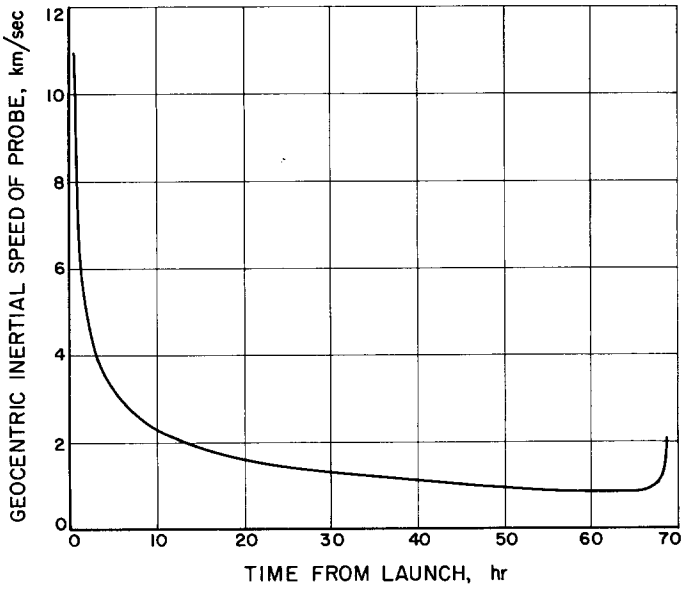

Fig. 11. Geocentric inertial speed of probe vs time from launch

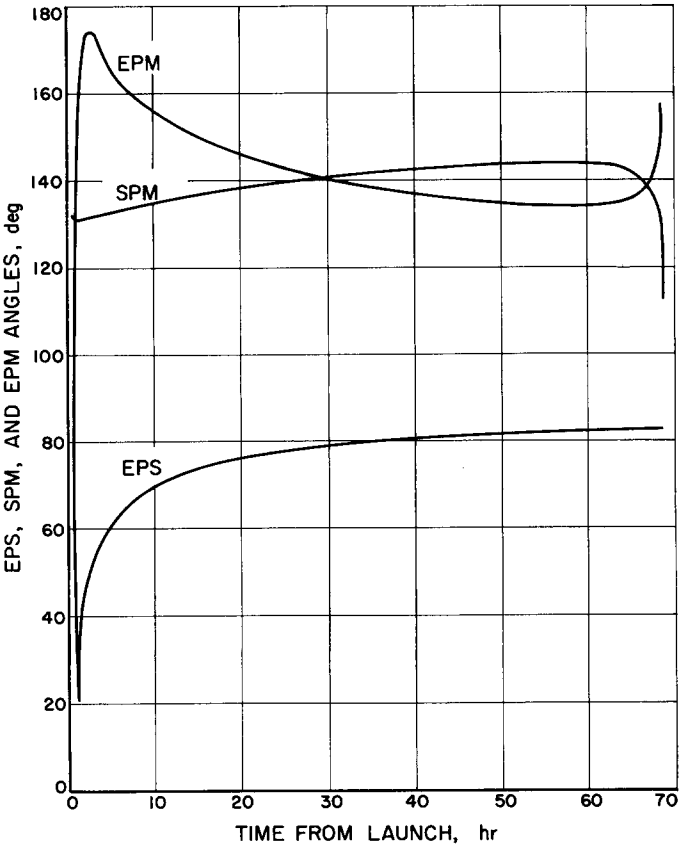

Fig. 12. Earth-probe-Sun, Sun-probe-Moon, and Earth-probe-Moon angles vs time from launch

UNCLASSIFIED

UNCLASSIFIED
CONFIDENTIAL

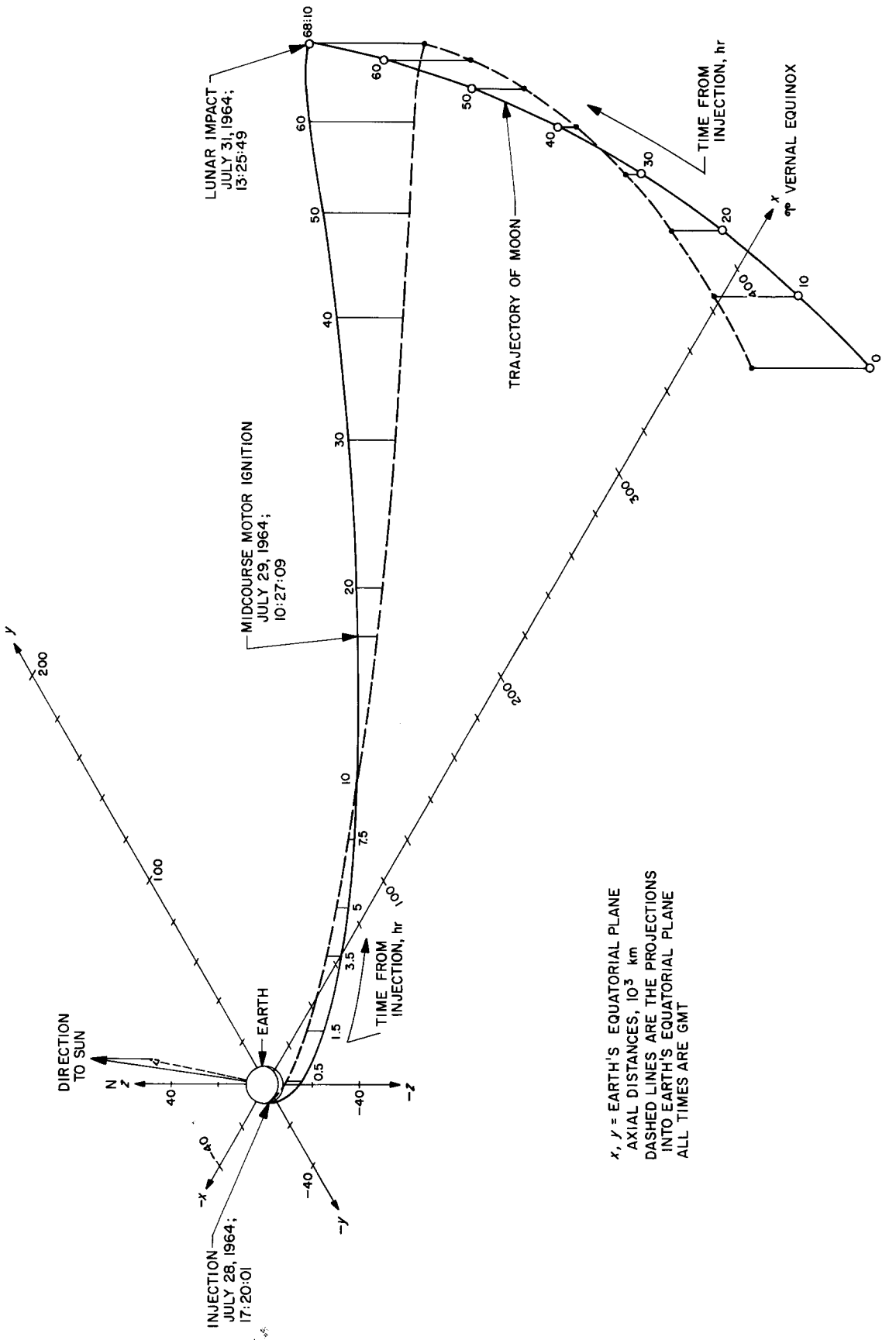

Fig. 13. *Ranger 7* transfer trajectory

CONFIDENTIAL
UNCLASSIFIED

UNCLASSIFIED

for a 29.89-m/sec increment of velocity (60-m/sec maximum capability). In addition, this correction was selected to adjust the flight time from injection to impact to be 68.09 hr, thus allowing the TV camera backup turn-on clock to be utilized as designed. To properly align the thrust direction of the midcourse motor for the burn, a 5.56-deg roll turn and −86.80-deg pitch turn were required. The midcourse motor was ignited at 10:27:09 GMT on July 29, 1964, at which time the spacecraft was at a geocentric distance of 169,000 km and traveling with an inertial speed of 1.786 km/sec relative to the Earth. At the end of the 50-sec burn of the midcourse motor, the geocentric distance had increased to 169,075 km, and the inertial speed relative to the Earth had decreased to 1.756 km/sec. Analog data received at the Goldstone Tracking Station and relayed to the JPL Space Flight Facility gave positive indication that the midcourse maneuver and motor burn had been executed precisely. This was further verified by the observed doppler data, which were essentially the same as those predicted for the maneuver. Injection and encounter conditions for the pre-midcourse orbit used to determine the midcourse maneuver are given in Table 1.

d. Postmidcourse maneuver cruise phase. Following the midcourse maneuver, the spacecraft reacquired the Sun and Earth, thus returning to the cruise mode. At about 63 hr from injection and at a geocentric distance of 355,300 km, the spacecraft's inertial speed relative to the Earth reached a minimum value of 0.850 km/sec. At this point, the spacecraft was about 28,300 km from the lunar surface with an inertial speed of 1.36 km/sec relative to the Moon. Due to the lunar gravitational field, the spacecraft's velocity then began to increase.

Table 1. Orbit used for determination of the *Ranger 7* midcourse maneuver

Initial conditions[a]	
Epoch	July 28, 1964; 17:19:56 GMT
Earth-fixed sphericals	
R	6567.6350 km
ϕ	−12.676075 deg
θ	14.647727 deg
V	10.533237 km/sec
γ	1.3798852 deg
σ	117.37931 deg
Inertial Cartesians	
x	−4833.6829 km
y	−4206.2223 km
z	−1441.1942 km
$\dot{x}$	7.0598554 km/sec
$\dot{y}$	−6.8711888 km/sec
$\dot{z}$	−4.7802415 km/sec
Orbital elements	
a	269557.90 km
e	0.97564876
i	28.957643 deg
Ω	17.045773 deg
ω	204.26350 deg
ν	2.6878172 deg
Impact parameters	
Impact epoch	July 31, 1964; 12:43:29.17 GMT
Selenocentric latitude	−12.344962 deg
Selenocentric longitude	203.95135 deg
Time of flight from injection	67.391 hr[b]
$\lvert \mathbf{B} \rvert$	3869.9779[c] km
$\mathbf{B} \cdot \mathbf{T}$[d]	−3794.9573 km
$\mathbf{B} \cdot \mathbf{R}$[d]	758.30590 km

[a] See Table 2 for definition of symbols.
[b] 1σ uncertainty of 5.2 sec.
[c] 1σ uncertainty of 15.9 km.
[d] $\mathbf{B} \cdot \mathbf{T}$ and $\mathbf{B} \cdot \mathbf{R}$ are referenced to the true lunar equator (Fig. 14). (For *Ranger 7* work, the true lunar equator is used as the reference plane. If $\mathbf{N}$ is a unit vector in the lunar north direction, then $\mathbf{T} = \mathbf{S}_I \times \mathbf{N}$ and $\mathbf{R} = \mathbf{S}_I \times \mathbf{T}$.)

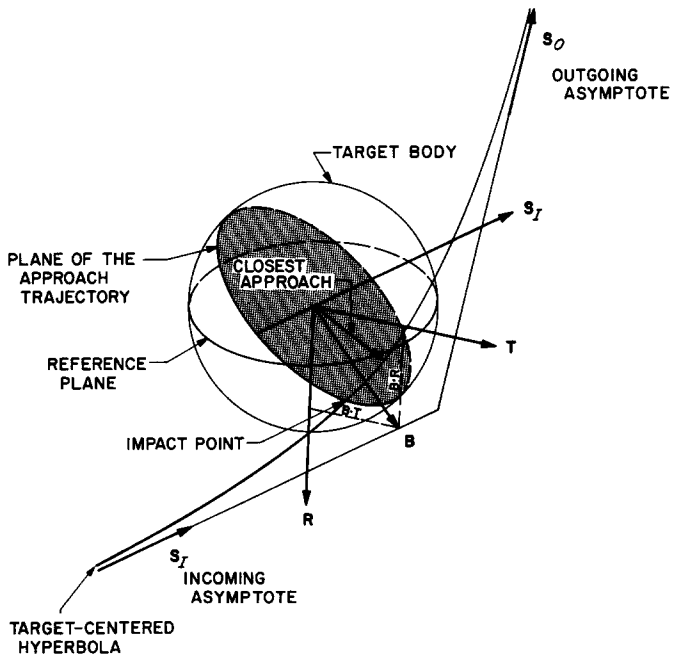

Fig. 14. Definition of the miss parameter B

Postmidcourse tracking data up to within 0.5 hr before impact were analyzed and resolved the lunar encounter conditions to a high degree of accuracy. Lunar impact was indicated to occur at a selenocentric latitude and longitude of −10.68 and −20.68 deg, respectively, with a flight time from injection of 68.097 hr. The encounter

UNCLASSIFIED

UNCLASSIFIED

Table 2. Definition of symbols (with Earth as central body)

R	probe radius distance, km
ϕ	probe geocentric latitude, deg
θ	probe east longitude, deg
V	probe Earth-fixed velocity, km/sec
γ	path angle of probe Earth-fixed velocity vector with respect to local horizontal, deg
σ	azimuth angle of probe Earth-fixed velocity vector measured east of true north, deg
x, y, z	vernal equinox Cartesian coordinates, in km, in a geocentric equatorial system. The origin is the center of the central body. The principal direction (x) is the vernal equinox direction of date, and the principal plane (x, y) is the Earth equatorial plane of date. z is along the direction of the Earth's spin axis of date.
$\dot{x}, \dot{y}, \dot{z}$	first-time derivatives of x, y, and z, respectively: i.e., Cartesian components of the probe space-fixed velocity vector, km/sec.
a	semimajor axis, km
e	eccentricity
i	inclination, deg
Ω	longitude of the ascending node, deg
ω	argument of pericenter, deg
ν	true anomaly, deg

conditions and the corresponding postmidcourse initial conditions are presented in Table 3.

Table 3. Last postmidcourse orbit of *Ranger 7*

Postmidcourse conditions[a]	
Epoch	July 29, 1964; 10:27:58 GMT
Earth-fixed sphericals	
R	169075.11 km
ϕ	2.7386728 deg
θ	277.82452 deg
V	12.070902 km/sec
γ	8.1207532 deg
σ	270.95860 deg
Inertial Cartesians	
x	156674.78 km
y	63040.835 km
z	8078.5225 km
$\dot{x}$	1.4342630 km/sec
$\dot{y}$	0.97256602 km/sec
$\dot{z}$	0.28116494 km/sec
Orbital elements	
a	244087.41 km
e	0.97401678
i	28.706807 deg
Ω	16.907167 deg
ω	203.78348 deg
ν	161.92545 deg
Impact parameters	
Impact epoch	July 31, 1964; 13:25:48.50 GMT
Selenocentric latitude	−10.671182 deg
Selenocentric longitude	−20.68303 deg
Time of flight from injection	68.0965 hr[b]
$\lvert \mathbf{B} \rvert$	1811.2719 km[c]
$\mathbf{B} \cdot \mathbf{T}^d$	1623.8932 km
$\mathbf{B} \cdot \mathbf{R}^d$	802.29478 km

[a]See Table 2 for definition of symbols.
[b]1σ uncertainty of 1.0 sec.
[c]1σ uncertainty of 14.7 km.
[d]$\mathbf{B} \cdot \mathbf{T}$ and $\mathbf{B} \cdot \mathbf{R}$ are referenced to the true lunar equator (Fig. 14). (For *Ranger 7* work, the true lunar equator is used as the reference plane. If $\mathbf{N}$ is a unit vector in the lunar north direction, then $\mathbf{T} = \mathbf{S}_t \times \mathbf{N}$ and $\mathbf{R} = \mathbf{S}_t \times \mathbf{T}$.)

e. Encounter phase. During the encounter phase of the *Ranger 7* flight, the spacecraft raced toward destruction by lunar impact with increasing acceleration due to the pull of the lunar gravitational field. This effect is shown in Fig. 15, where the *Ranger 7* trajectory to lunar encounter is compared with a hypothetical *Ranger 7* trajectory resulting from a massless Moon. At 1 hr before impact, at a lunar altitude of 6390 km, the speed of the probe relative to the Moon had increased to 1.551 km/sec. No terminal maneuver to realign the TV cameras' pointing direction was necessary.

About 45.5 min before impact, the spacecraft crossed the lunar equator at an altitude of 4933 km. At 13:08:36 GMT, while at an altitude of 2126 km above the lunar surface, Channel-F full power was verified. At 13:12:09 GMT, at an altitude of 1723 km, Channel-P full power was also verified. At 13:25:49 GMT on July 31, 1964, *Ranger 7* crashed onto what was to be named the lunar "Mare Cognitum" at an impact speed of 2.616 km/sec and at a path angle of −64.1 deg. The spacecraft had encountered the Moon in a direct motion along a hyperbolic trajectory, the incoming asymptote direction being at an angle of −5.57 deg to the lunar equator and with the orbit plane inclined 26.84 deg to the lunar equator.

The trace of the trajectory on the lunar surface from injection to impact is given in Fig. 16; the traces of the lunar approach portions of the premidcourse and postmidcourse orbits are illustrated in Fig. 17. Figures 18 through 22 present trajectory parameters plotted versus GMT prior to impact of the *Ranger 6* spacecraft on the Moon.

UNCLASSIFIED

UNCLASSIFIED
CONFIDENTIAL

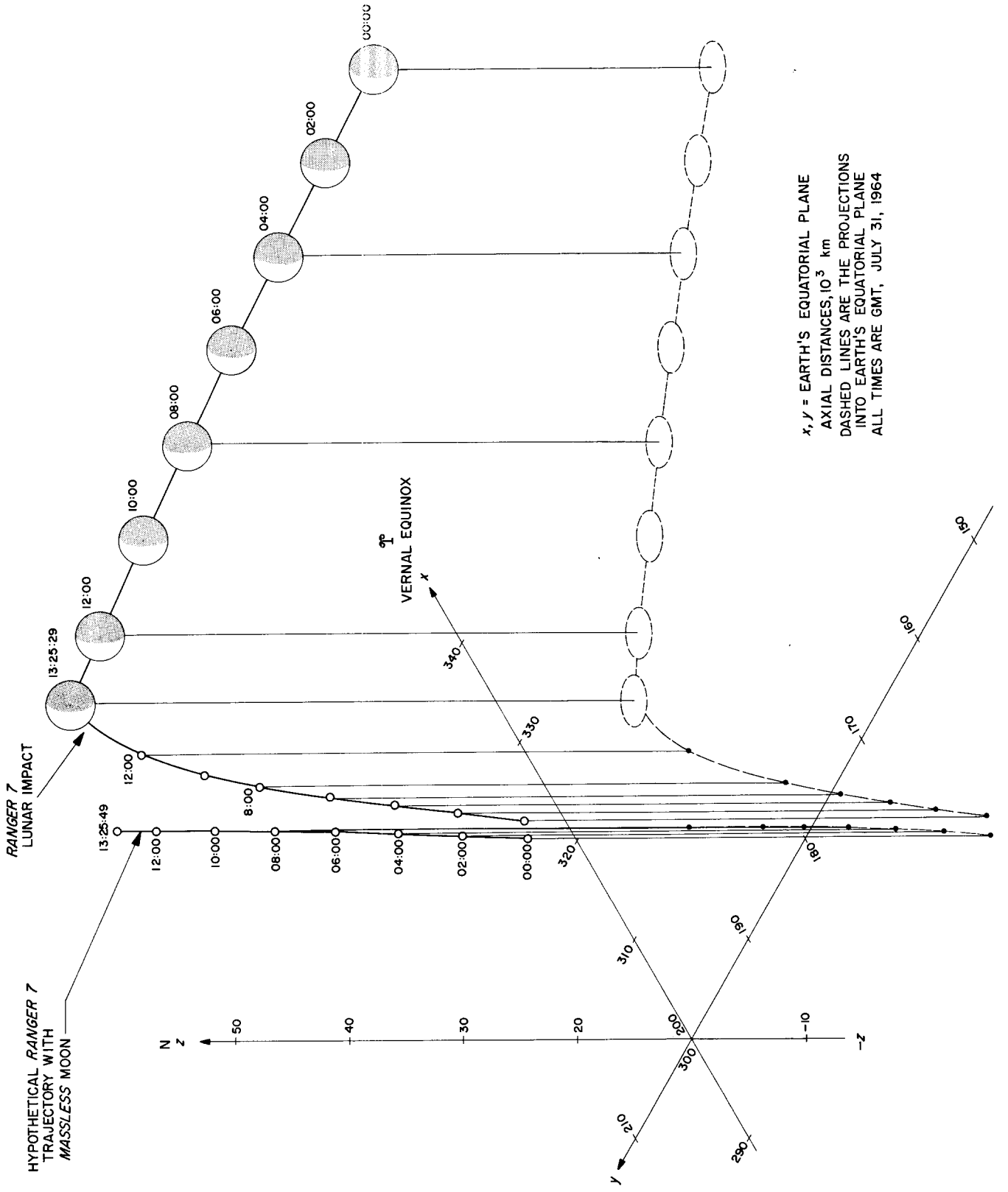

Fig. 15. Effect on *Ranger 7* trajectory due to lunar gravitational attraction

UNCLASSIFIED
CONFIDENTIAL

UNCLASSIFIED

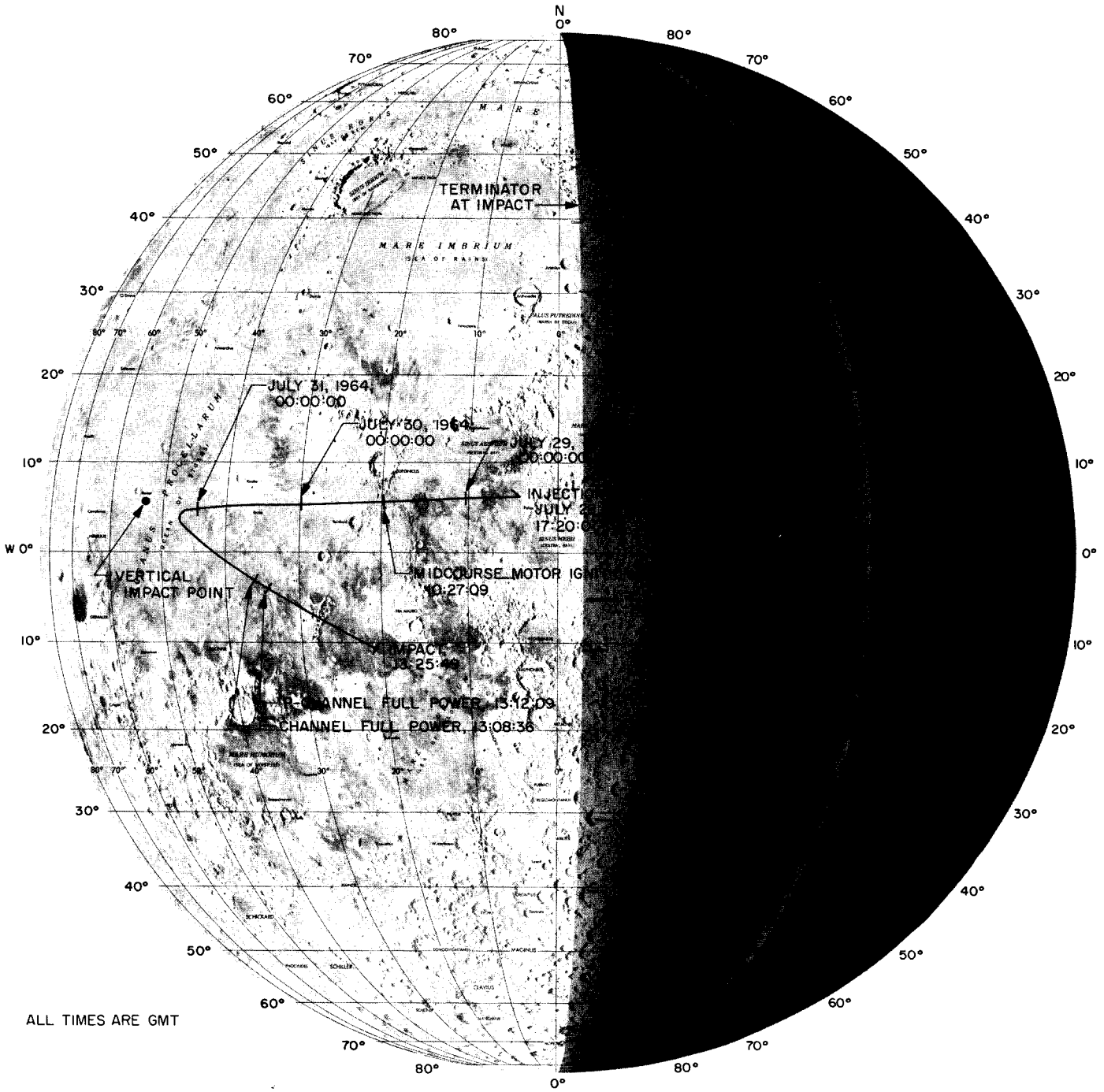

Fig. 16. Lunar track of *Ranger 7* trajectory

UNCLASSIFIED

UNCLASSIFIED

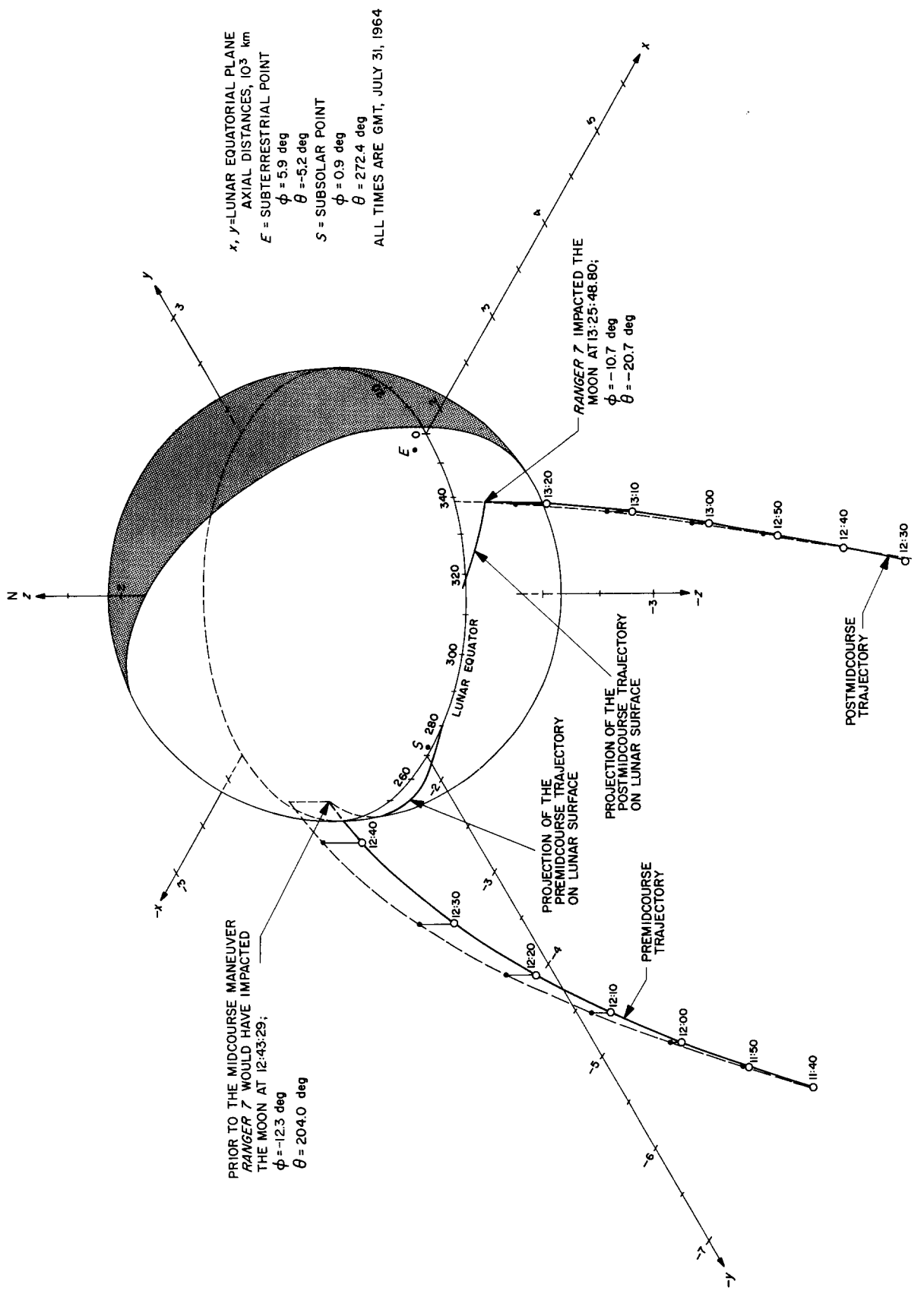

Fig. 17. *Ranger 7* premidcourse and postmidcourse encounter trajectories

UNCLASSIFIED

UNCLASSIFIED
CONFIDENTIAL

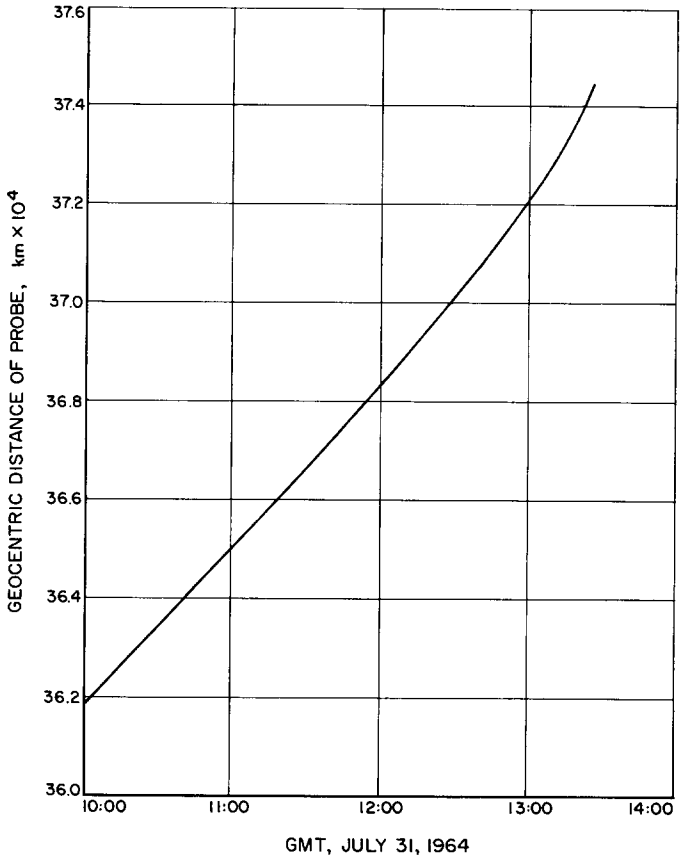

Fig. 18. Geocentric distance of probe vs GMT at lunar encounter

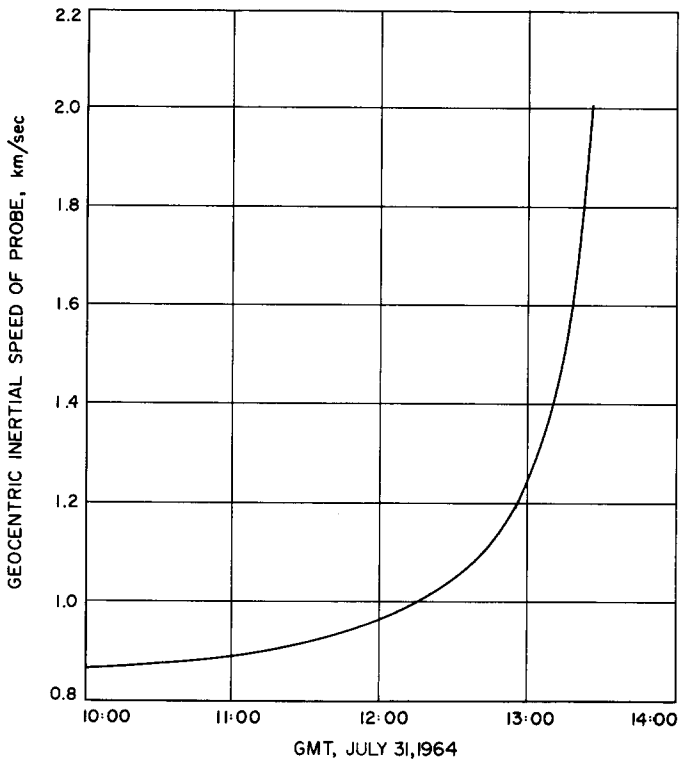

Fig. 19. Geocentric inertial speed of probe vs GMT at lunar encounter

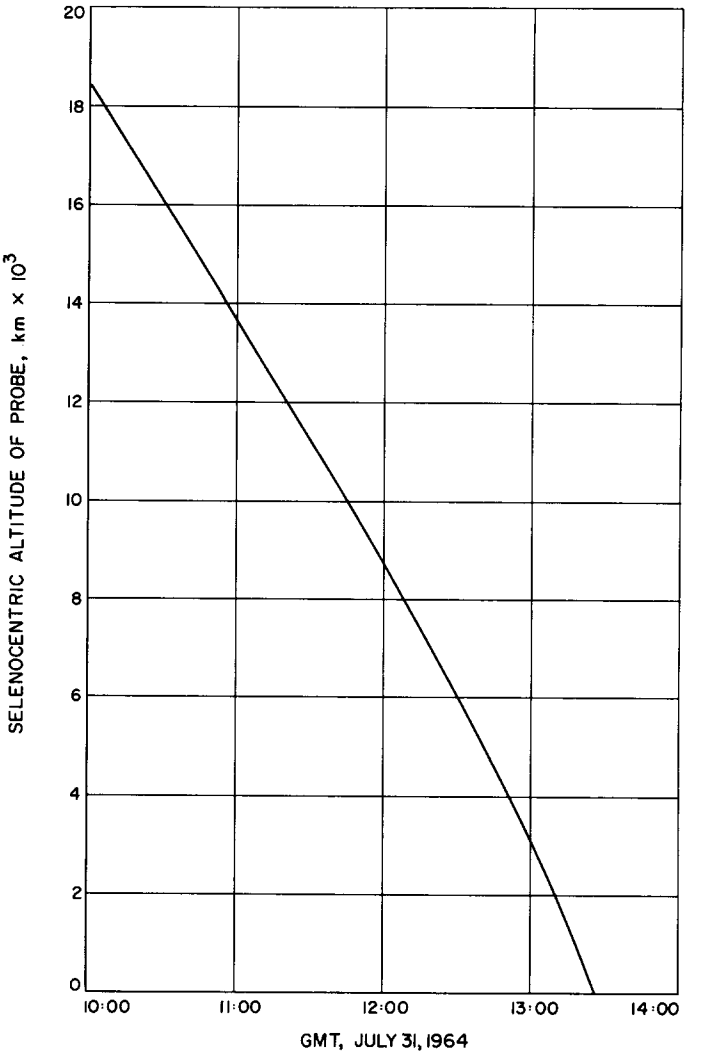

Fig. 20. Selenocentric altitude of probe vs GMT at lunar encounter

CONFIDENTIAL
UNCLASSIFIED

UNCLASSIFIED

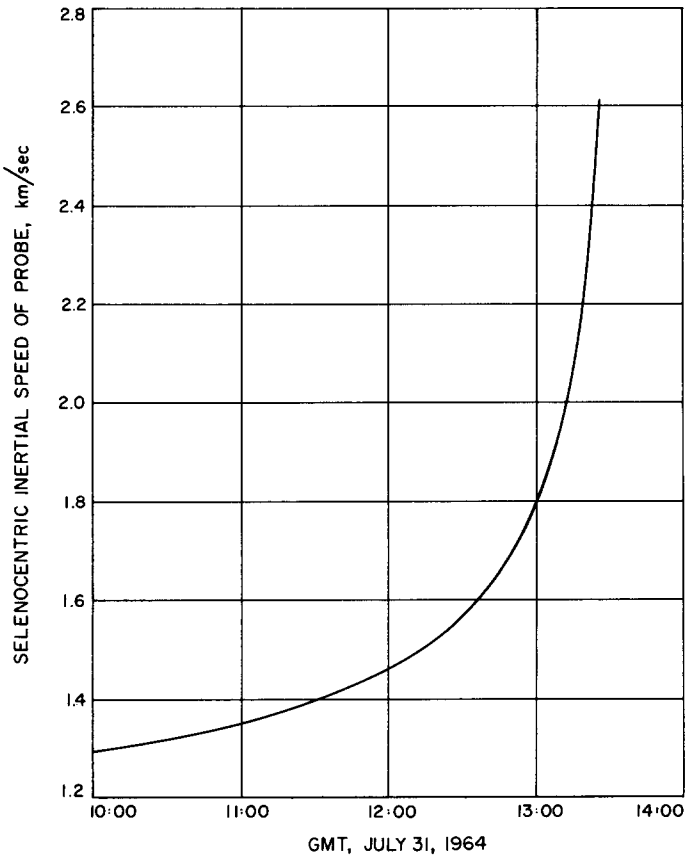

Fig. 21. Selenocentric inertial speed of probe vs GMT at lunar encounter

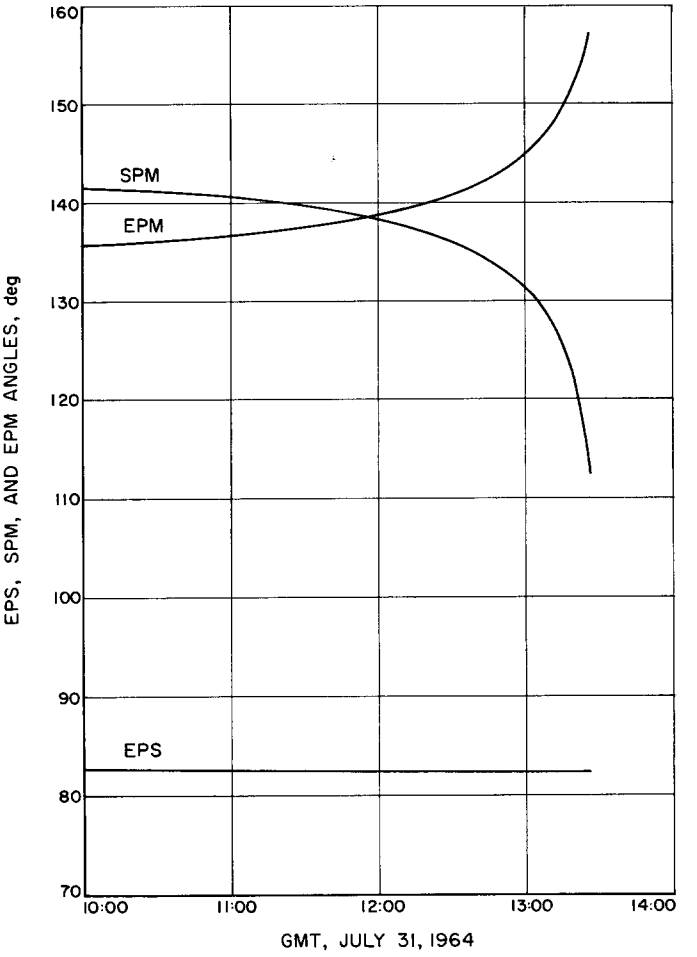

Fig. 22. Earth-probe-Sun, Sun-probe-Moon, and Earth-probe-Moon angles vs GMT at lunar encounter

2. *Master Data Table, Ranger 7*

A Master Data Table (MDT) for the *Ranger 7* mission is being prepared by the Data Operations and Program Development Group. The MDT is a file of magnetic tapes which contain a time sequential record of the best telemetry data recorded by the Deep Space Instrumentation Facility (DSIF), and a time sequential record of DSIF station automatic-gain-control (AGC) data for each station's pass.

The format of the data in the MDT is compatible with the existing operational flight telemetry Reduction, Analysis, and Engineering Plot Programs. The MDT, when complete, will be the prime source of the *Ranger 7* spacecraft telemetry and station AGC data and will be available to the various JPL Technical Divisions for detailed post flight analysis.

The MDT is comprised of either raw spacecraft telemetry data recorded on magnetic tapes by Air Force Eastern Test Range and DSIF stations, or real-time digitized and/or teletype data. The processing required in preparation of the MDT is essentially as follows (Fig. 23):

(1) DSIF-recorded magnetic tapes are shipped to the JPL Space Flight Operations (SFO) Document Control.

(2) The SFO Document Control forwards the tapes to the Telemetry Processing Station (TPS), where a digital tape is generated.

(3) Data is extracted from the digital tapes by an IBM 7094 computer Input Processor Program, which provides a tabular output of formatted engineering raw data.

(4) The engineering raw data records are reviewed by the Data Operations and Program Development Group for deficiencies and/or discrepancies. Where

UNCLASSIFIED

UNCLASSIFIED
CONFIDENTIAL

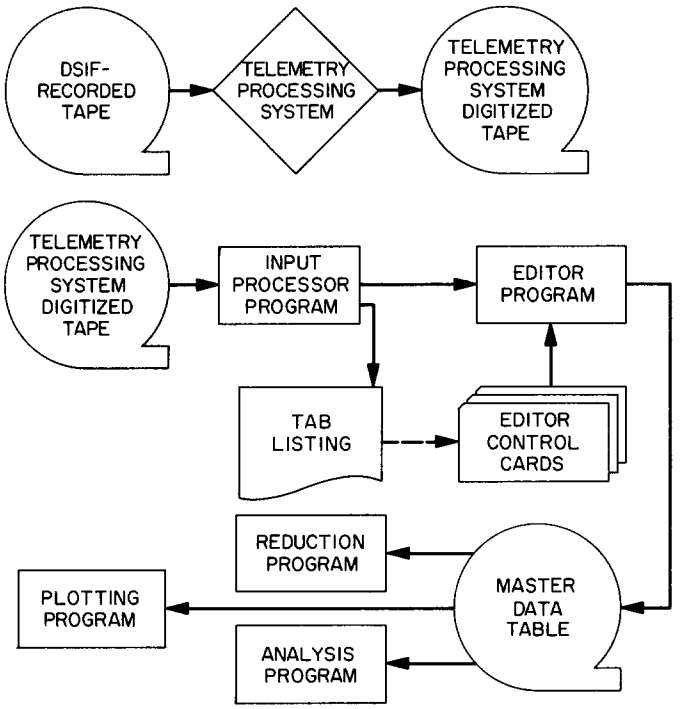

Fig. 23. Processing diagram for preparation of master data table

deficiencies and/or discrepancies exist, the real-time data is reviewed and the better data is used in compiling the MDT.

(5) After all the data is reviewed, inputs which suppress all discrepancies in the data stream are prepared for the Editor Program; where deficiencies exist, the inputs instruct the Editor Program to merge a secondary source into the data stream.

(6) The Editor Program outputs the data on the magnetic tapes which constitute the Master Data Table for the *Ranger 7* mission.

D. Supporting Activities

From mid-August to mid-October, 1964, 32 experimental, 15 type-approval, and 31 flight acceptance tests associated with the *Ranger* Block III Project were completed by the JPL Environmental and Dynamic Testing Laboratory (Table 4).

Table 4. *Ranger* usage of JPL Environmental and Dynamic Test Laboratory from August 15 to October 15, 1964

Facility	Number of tests
Vibration	47
Acoustic	0
Centrifuge	4
Shock	0
Handling shock	0
Temperature	11
Explosive atmosphere	0
Vacuum	12
Total	74

UNCLASSIFIED
CONFIDENTIAL

UNCLASSIFIED

II. *Ranger* TV Subsystem, Block III

The primary objective of *Rangers 6–9* (Block III) is to produce high-resolution TV pictures of the lunar surface. To implement this objective, a TV subsystem has been developed by RCA under contract to JPL. The subsystem mates with the JPL bus, as did the lunar capsule of the *Ranger 3–5* (Block II) series.

The subsystem structure consists of three major assemblies: (1) the central box which houses the main electronic components, (2) the camera subassembly with associated bracketry and equipment, and (3) the thermal shield. A view aperture for the cameras is provided in the thermal shield.

The following material relating to the subsystem development is abstracted from the RCA report: *Ranger TV Subsystem, Block III, Nineteenth Bimonthly Progress Report*, October 2, 1964, covering the period from July 9, 1964, to September 15, 1964.

A. System Engineering

1. Flight Model III-3

During this reporting period, modifications to assemblies for Flight Model (FM) III-3 were completed, and a series of acceptance vibration and thermal-vacuum tests was performed. Following these tests, the assemblies were delivered for integration with the FM III-3 TV subsystem.

The initial turn-on and command system performance check was completed, and the communications and camera alignment procedure was performed. All telemetry points except those related to temperatures were calibrated. The TV subsystem is expected to complete the test cycle and be shipped to JPL during the next reporting period.

2. Flight Model III-4 and Spares

The rework and testing of assemblies for FM III-4 continued. All available units and harnesses were mounted on the FM III-4 structure.

Rework and refinishing of the spare structure to the latest configuration was completed. Assembly of all available spare components on the spare structure was accomplished in preparation for electrical testing to be performed in parallel with FM III-3 testing.

3. Proof Test Model

The proof test model (PTM) testing program at JPL continued during this reporting period, with the following tests being performed: pyrotechnic shock test, System Test 16, umbilical shock test, special electromagnetic interference high-voltage test, System Test 17, inadvertent

UNCLASSIFIED

UNCLASSIFIED

turn-on test, a second umbilical cable transient test, and TV subsystem and bus interface compatibility test. The TV subsystem operated normally during these tests, except for noisy Channel 8 telemetry during the second umbilical cable transient test.

The PTM was then completely disassembled, and all components were either placed in controlled stock or returned to RCA for rework. All mechanical modifications were completed on the structure.

During a subsystem checkout, the P-channel operated normally, but the F-channel cameras were inoperative. After connecting an open ground and making all connections consistent with the flight configuration, another check was made. The F-channel then operated normally, but the P-channel did not go into full power. Also, trouble was noted in the transmitter power supply. The transmitter and power supply were sent to RCA for troubleshooting; the failure analysis is still in process. After the reinstallation of these units at JPL, two checkouts were made with satisfactory results. The TV subsystem was then checked out with the bus, and System Test 18 was performed.

B. Cameras

The partial-scan vidicon procurement effort was completed during this reporting period, with seven vidicons having been accepted. A full-scan vidicon procurement effort was initiated to replace the depleted spare vidicon stock and to fill an existing camera assignment. The new tube is similar to the former vidicon, differing only in target construction, mask orientations, and mesh density. Qualification tests for the denser mesh construction are scheduled during the next reporting period.

A six-camera bench evaluation was performed to determine the relative performance of the equipment with regard to shutter bumpering and to align the cameras. Electrical noise levels were significantly higher in this test than in the equipment tests, making an exact observation of microphonics difficult. Performance of the assembled FM III-3 during a later test indicated the same problems that occurred during this bench test. As a result of an evaluation of shutter-induced camera microphonics, a Camera P4 was replaced. Efforts are now under way to establish sufficient tests to verify the extent of system microphonics prior to the delivery of a camera assembly to mechanical integration for system assignment. These tests will be conducted in a partial system configuration. Also, investigations of methods for minimizing system microphonics are being conducted.

C. Telecommunications

Modification of all transmitter and transmitter power supplies to incorporate the Resdel-design intermediate power amplifiers (IPAs) was completed. Requalification of a transmitter with the Resdel IPA, incorporating new Varactor diodes in the $\times 4$ multiplier circuit, was performed. The test results indicate an appreciable improvement in power profile with this transmitter over that with the FM III-2 configuration.

All assemblies for the PTM, FM III-3, and FM III-3 spare TV subsystems were delivered for integration. All assemblies for the FM III-4 TV subsystem and the remaining assemblies for Spare 2 will be delivered for integration during the next reporting period.

Three new harnesses were completed, and the harness for the PTM was modified to the FM III-3 and -4 configuration.

D. Systems Control and Electrical Power

During this reporting period, the distribution control units (DCUs) for the PTM and the qualification test model, two spare DCUs, and the command control unit for the PTM were reworked to the configuration of FMs III-3 and -4.

All high-current voltage regulator flight and spare units have been released for integration. The use of Fifth Dimension, Inc., commutators in the telemetry assembly reduced the power drain on the low-current voltage regulator. As a result, all flight and spare units have been readjusted and returned for integration.

The flight and flight-spare batteries for FMs III-3 and -4 have been completed and are in storage at the vendor's facility.

CONFIDENTIAL
UNCLASSIFIED

UNCLASSIFIED
CONFIDENTIAL

III. *Surveyor* Project

A. Introduction

The *Surveyor* Project will take the next step in developing lunar technology by attempting soft landings on the Moon with a group of test missions whose objective is to demonstrate successful soft landing by post-landing spacecraft operation. An engineering payload including elements of redundancy, increased diagnostic telemetry, touchdown instrumentation, and survey TV will be used.

Following the test missions, the general objective is to conduct lunar exploration to extend our knowledge of the nature of the Moon and to discover and verify the suitability of sites for *Apollo* spacecraft landings. These flights will carry a scientific payload selected from the following experiments: two-camera TV, micrometeorite ejecta, single-axis seismometer, alpha-particle scattering, soil properties (surface sampler), and touchdown dynamics.

Through 1966 spacecraft will be injected into the lunar trajectory by direct ascent, using single-burn *Atlas–Centaur* vehicles. For launches prior to 1966 a 50-m/sec midcourse correction capability will exist. Launches performed in 1966 will require a 30-m/sec midcourse correction capability.

Hughes Aircraft Company is under contract to develop and manufacture the first seven spacecraft.

B. Space Flight Operations Documentation

Surveyor Operations System Schedule. The preliminary issue of this schedule was published on October 20, 1964. This document provides a comprehensive description of all *Surveyor* SFO schedules, and is to be updated, revised, and reissued once each month. This scheduling document will also constitute one section of an overall Project document titled "*Surveyor* Project Operating Schedules."

UNCLASSIFIED
CONFIDENTIAL

UNCLASSIFIED

Surveyor Spacecraft–Space Flight Operations Interface Document. The first revision of this document was published on October 19, 1964. Text revisions include the sections on document philosophy and organization, document and interface control, and spacecraft–space flight operations requirements.

Additional mission events were also specified in this issue. While the preliminary document only outlined and gave specific examples of the way system compatibility would be examined, this revision completes the task of translating all portions of the system into document format.

Surveyor Deep Space Instrumentation Facility (DSIF) Detailed Operating Procedures. The preliminary issue of this document was published on September 30, 1964. It contains the detailed procedures to which DSIF *Surveyor* mission-dependent personnel are to operate in order to conduct the *Surveyor* mission. Additionally, the Detailed Operating Procedures contain for reference the procedures used by DSIF mission-independent personnel, interfacing the DSIF mission-dependent operation. This preliminary document contains only a portion of the procedures used under standard conditions, and outlines the requirements for those standard and nonstandard procedures to be provided in subsequent revisions.

UNCLASSIFIED

UNCLASSIFIED CONFIDENTIAL

IV. *Surveyor* Spacecraft System

The following material relating to the *Surveyor* spacecraft system was prepared by the Hughes Aircraft Company. The principal model designations and vehicles discussed are defined in Table 1.

Table 1. Model and vehicle designations

Designation	Description
SC-1–4	Flight spacecraft with engineering payload
SC-5–7	Flight spacecraft with scientific payload
A-21	Model designation for spacecraft with engineering payload (SC-1–4)
A-21A	Model designation for spacecraft with scientific payload (SC-5–7)
T-21	Model A-21 prototype system test spacecraft
T-21A	Model A-21A prototype system test spacecraft
T-2	Simplified spacecraft for evaluation of terminal descent propulsion and flight control
S-2	Test spaceframe for vibration, shock, and static structural tests
S-6, -7	Test spaceframe for vernier propulsion system tests
S-8	Test spacecraft for flight control buzz tests

System engineering. The transponder for the SD-2 dynamic test spacecraft was tested at Goldstone and accepted by JPL in mid-September. A main power switch is being added to the spacecraft as a safety provision to enable cutoff of all spacecraft power up to launch. A preliminary telemetry calibration and error analysis handbook is being coordinated with the users. In tests at Lewis Research Center, spacecraft hardware showed no ill effects from gas impingement during operation of the *Centaur* shroud ejection system.

Scientific payload. Design was completed on a change to the alpha scattering experiment to provide for five additional data signals; an engineering change proposal for an improved instrument is being prepared. A change proposal has been completed on incorporating current limiting in the power circuits for the alpha scattering, micrometeorite ejecta detection, and seismological experiments. Vibration tests were performed on the soil mechanics/surface sampler. Type approval testing of the television camera is approaching completion. Photometric

UNCLASSIFIED CONFIDENTIAL

UNCLASSIFIED
CONFIDENTIAL

charts for TV camera calibration on the Moon have been designed. A preliminary thermal analysis of the television cameras has been performed.

System analysis. Studies were made to show the effects of midcourse velocity distribution on vernier propellant requirement and the effects of increasing retro-engine separation time on terminal descent parameters. Landing accuracy was evaluated in a Monte Carlo simulation program. The use of a coherent-type threshold leading edge detector in the television system for horizontal synchronization was analyzed. A sequence analysis for the soil mechanics/surface sampler was made, and methods of reducing operating time were studied. A command verification and transmission computer program is being developed for integration into the SFOF.

Flight control. The flight control electronics unit completed type approval testing successfully. Further evaluation of a delayed square wave power source for the gyro and Canopus sensor motors indicated an efficiency increase with three-phase power. Work was initiated to incorporate the slit-type acquisition Sun sensor on the first flight spacecraft. The first set of flight-type gas jet valves passed acceptance tests.

Electronics. Excessive phase jitter in the receiver and transmitter is being eliminated through ribbon mounting of the crystals. The circuitry for the RF transfer switch drive was modified to remove potential failure modes. Improvements were incorporated in the boost regulator and the battery charge regulator.

Electrical power supply. The solar panel wiring harness was redesigned for compatibility with the new mast harness and the first three flight panels were reworked to incorporate the changes. Solar cells were space-calibrated in JPL balloon flights for use as primary standard cells. Infrared radiometry is being evaluated for use in solar panel testing. Five prototype main batteries passed type approval vibration and shock tests; four have successfully passed the 300-hr type approval thermal-vacuum test.

Thermal control. An upgraded analysis indicates that the A-21 compartment system has a positive heat dissipation capability at lunar noon and a night heat loss of 20 w, compared to 60 w previously estimated. The paint pattern on the helium tank has been changed to prevent overheating in the transit phase. Special test hardware for solar-thermal-vacuum testing of the T-21 spacecraft has been defined, and a data monitoring system has been checked out. A comprehensive thermal test program employing a new spacecraft thermal control model has been started.

Engineering mechanics. Shock absorber tube failures were traced to excessive chuck pressure during machining, and corrective steps were taken. Revision of the mathematical model used in the forced-response computer program to accommodate upgrading of the S-2 vehicle to the S-2A configuration is continuing. Type approval vibration testing of S-2A was carried out, except for certain low-frequency tests that will be conducted with a redesigned motor housing in the antenna/solar panel positioner housing; the housing failed in a lateral shake test at 9.6 cps. Structural analysis and redesign were performed on the equipment compartments and the retro-engine supports.

Propulsion. The first four quality assurance firings of the main retro-rocket engine were made at AEDC; ballistic performance was satisfactory and preliminary data indicate that thrust vector excursion met specifications. An inert engine with a modified hinge joint was vibration tested. In the vernier propulsion system program, two expulsion unbalance tests with the S-6 vehicle using simulated propellant were completed. The 30-day storage test with the S-7 vehicle, involving firings at 5-day intervals was started. Type approval testing of the 6 Al-4 Va titanium propellant tanks is complete, except for the vibration phase.

Spacecraft vehicle and mechanisms for basic bus. Vehicle assembly operations included assembly of SC-1 for the beginning of system tests and upgrade of T-21; T-21A, SC-2, T-1, and T-2SS are in process of assembly at the close of the period. Strengthened mechanisms for deployment of the omnidirectional antennas have performed satisfactorily in vibration testing of the S-2A vehicle. A redesigned motor housing is being fabricated to replace the one that failed in S-2A vibration. Type approval testing of pyrotechnic squibs is nearly complete.

Reliability, quality assurance, and system test. In the reliability assurance test program, Canopus sensors incorporating a structural improvement have performed satisfactorily in vibration and thermal-vacuum tests; two sensors have survived 1500 hr of mission simulation and the tests are continuing. The upgraded T-21 system test spacecraft is receiving functional tests prior to the start of thermal-vacuum tests about November 1; the test equipment has been checked out with generally satisfactory results. Preparations are being made for the T-21

CONFIDENTIAL
UNCLASSIFIED

UNCLASSIFIED
CONFIDENTIAL

vibration and shock tests. The T-2S descent test vehicle completed closed-loop tests simulating the first drop test scheduled for October 20. A vibration test of the S-8 vehicle with RADVS installed, using simulated vernier engine vibration inputs, is being planned. The S-8 buzz test suspension system was checked out. The STEA 3 system is being prepared for testing the SC-2 spacecraft.

Mission operations. Planning details for the *Surveyor/Centaur* combined system test are being coordinated. The three operations consoles for use at AFETR have undergone tests and one has been modified for use with the *Surveyor* dynamic models. Compatibility testing of the dynamic model transponder for SD-2 in conjunction with DSIF equipment was completed at the Goldstone Pioneer site. Microwave installation and testing was conducted at AFETR.

Support of study on critical data recorder. Hughes provided technical support to the Aeronutronics Division of Philco in their study of a critical data recorder (CDR) for installation on the *Surveyor* spacecraft. The purpose of the CDR is to sense and transmit data on spacecraft structural condition and orientation even after a landing hard enough to make the spacecraft inoperative. The Hughes effort included coordination and preliminary design on CDR mounting, data channel assignments, mechanical loads, thermal and radiation environments, a breakwire sensing system, and test and operations requirements.

UNCLASSIFIED
CONFIDENTIAL

CONFIDENTIAL UNCLASSIFIED

A. System Engineering

1. A-21 Spacecraft Configuration

The first four flight spacecraft are designed to carry an engineering instrument payload to evaluate spacecraft performance and lunar soft-landing characteristics. These spacecraft are designated SC-1 through SC-4 (Model A-21), and their general arrangement is shown in Fig. 1.

By direction of JPL, the material of the nitrogen tank is being changed to 6Al-4Va titanium alloy from 7Al-4Mo titanium alloy. The incorporation of this change requires redesign of the tank support structure and attachment details.

The current A-21 weight summary is shown in Table 1 and includes changes up to, but not including, the effects of the nitrogen tank change. A more detailed weight breakdown is given in Table 2. The A-21 balance summary showing the center-of-gravity location is given in Table 3.

2. A-21A Spacecraft Configuration

The fifth, sixth, and seventh flight spacecraft (SC-5, SC-6, and SC-7) will have a scientific instrument payload for the measurement and evaluation of lunar surface characteristics. The scientific payload configuration is designated A-21A. There have been no significant changes in the configuration or the mass properties of A-21A since the last report. The latest detailed A-21A weight breakdown and weight summary is shown in Tables 4 and 5.

3. Dynamic Model SD-2

Flight acceptance testing the transponder for the *Surveyor* dynamic model SD-2 was completed on September 16, 1964. The transponder was accepted by JPL on September 18, 1964. Delivery to GD/A at San Diego for combined system test is scheduled for October 26, 1964. Compatibility testing of this transponder with the Goldstone Deep Space Instrumentation Facility was conducted during the week of October 5, 1964. A detailed discussion will be found in Section L, *Mission Operations*.

4. Publications

The *Surveyor* equipment design specification is in the final stages of editing and is scheduled for publication early in the next reporting period.

The model descriptions of both the A-21 and A-21A spacecraft were published during this reporting period.

Table 1. A-21 spacecraft weight summary

Item	Current design weight, lb
Total separated weight	2158.69
Basic bus	697.74
Usable propellant	1398.41
Engineering payload	62.54

5. Main Power Switch

Inclusion of a main power switch into the *Surveyor* spacecraft has become a mandatory safety requirement. The switch will be located electrically between the auxiliary battery control unit and the main power distribution bus. The switch removes all spacecraft battery power from the vehicle: (1) to eliminate the "hot pin" problem that would occur during *Surveyor/Centaur* mating; and (2) to provide a safety precaution in the event of propellant leakage. Switch actuation is limited to use prior to completion of 2-in. motion at launch. A motor-driven design was selected to preclude inadvertent switch actuation after launch with subsequent loss of spacecraft power. Fail-safe features are incorporated into the launch circuitry to preclude loss of the safety provisions. Critical restraints that governed selection of the switch include:

(1) Efficient (low voltage drop) handling of all spacecraft power.

(2) Fit available space envelope within Compartment A.

(3) Be an off-the-shelf space-qualified switch, preferably used on other space programs.

The main power switch incorporation change is in progress. T-21, SC-1, and SC-2 will receive switches during their respective upgrade periods. However, type approval testing and qualification of the switch will not be completed until the first quarter 1965.

The major modifications to the *Surveyor* system to accommodate the main power switch include:

(1) Incorporation of mounting inserts in the Compartment A thermal tray for the physical attachment of the switch (involving rework of T-21 and SC-1).

(2) Revision of Compartment A wiring harness to route power leads through switch and add switch motor control leads (involves building a new harness for SC-1 and reworking the old SC-1 harness for T-21).

(3) Revision of Basic Bus 1 wiring harness: – route motor control leads from Compartment A to *Surveyor/Centaur* connector.

CONFIDENTIAL UNCLASSIFIED

UNCLASSIFIED
CONFIDENTIAL

Table 2. A-21 spacecraft weight breakdown

Item	Current design weight, lb	Item	Current design weight, lb
Basic bus (total)	697.74	Spacecraft vehicle	217.33
Flight control	53.51	Spacecraft basic structure	
Sensor group		Equipment attaching hardware	
Secondary solar sensor		Landing gear installation	
Attitude control system		Paint	
Electronics	112.77	Equipment Compartments A and B	
Data link (antenna, RF switches, transmitter — diplexer, command receiver, and transponder)		Electrical wiring	
Central command decoder		Pneumatic lines attitude control	
Central signal processor		Release mechanism, retro-rocket	
Altitude marking radar		Engineering measurement sensors	
Doppler velocity sensor and altimeter		Latch — spacecraft to *Centaur*	
Boost regulator		Spacecraft propulsion (not including usable propellant)	227.62
TV Camera 4		Rocket engine, main retro	
Engineering data processing		Vernier propulsion system	
Mechanisms auxiliaries		Unusable vernier propellant	
Heater control		Helium	
Signal processing auxiliary		Insulation — main retro engine	
Battery charge regulator		Safety and arming device — main retro	
Low data rate auxiliary		Usable propellant (total)	1398.41
Electrical power	54.90	Retro-rocket propellant	
Solar panel		Vernier propellant	
Battery		Buoyancy — retro propellant	
Mechanisms	28.60	Weight tolerance	2.50
Positioner, antenna/solar panel		Buoyancy — basic bus	0.51
Antenna mechanism, omnidirectional		Engineering payload (total)	62.54
Separation sensing and arming provisions		Survey Camera 3 and auxiliary	21.51
		Auxiliary battery installation	28.46
		Engineering instrumentation (added)	12.54
		Buoyancy — payload	0.03

Table 3. A-21 spacecraft weight and balance summary

Condition	Weight, lb	Vertical center of gravity Z[a]-axis, in.	Lateral X-axis, in.	Center of gravity Y-axis, in.
Current design weight				
Total separated weight (after *Centaur* separation)	2158.69	12.10	0.13	—0.11
Maximum touchdown weight	643.67	16.88	0.15	—0.11
Minimum touchdown weight	603.77	17.55	0.16	—0.04

[a] Inches above landing gear hinge line (spacecraft station 47.48).

(4) Revision of *Surveyor/Centaur* launch complex wiring for control of switch.

(5) Revision of system test equipment assembly wiring for control of switch.

A description of the power circuitry changes to incorporate the power switch will be found in Section F.

6. *Telemetry Calibration and Error Analysis Handbook*

On October 1, 1964 a preliminary version of the Telemetry Calibration and Error Analysis Handbook was printed and distributed. The handbook will provide information to: (1) personnel monitoring the operation of central command and data handling consoles (CDC) at the DSIF stations, (2) personnel responsible for programming the computer at the Space Flight Operational Facility for real-time data reduction, (3) those conducting detailed postflight data reduction, (4) system test personnel, and (5) others associated with the *Surveyor* telemetry system.

The handbook is not complete; of the telemetry measurements that exist on the spacecraft, approximately 40% of the 334 commutated analog measurements were analyzed (the 130 bi-state measurements need no analysis). A preliminary handbook has been issued at this time to those who will be using the information to obtain

UNCLASSIFIED
CONFIDENTIAL

UNCLASSIFIED
CONFIDENTIAL

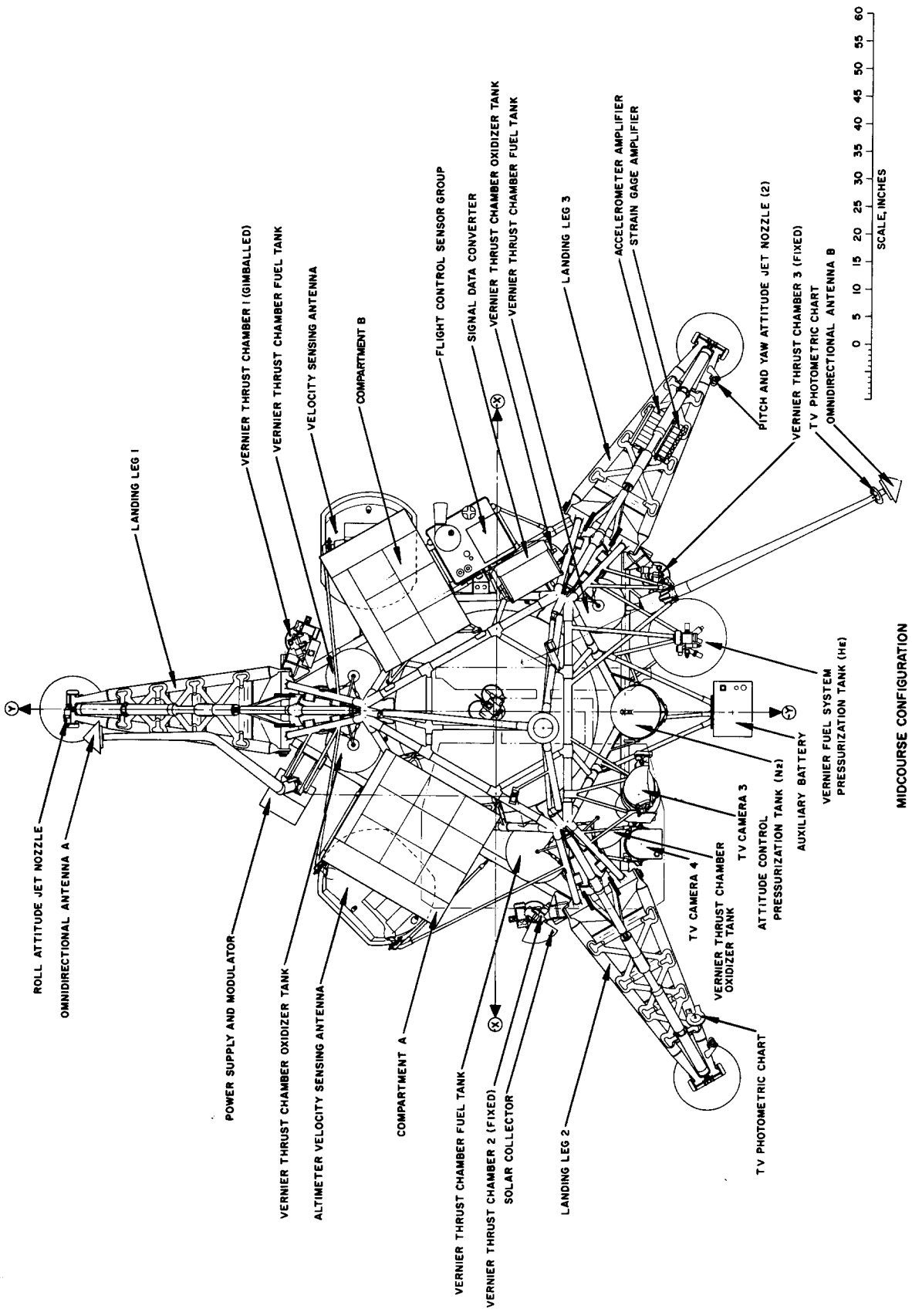
ROLL ATTITUDE JET NOZZLE
OMNIDIRECTIONAL ANTENNA A
LANDING LEG 1
POWER SUPPLY AND MODULATOR
VERNIER THRUST CHAMBER OXIDIZER TANK
ALTIMETER VELOCITY SENSING ANTENNA
VERNIER THRUST CHAMBER 1 (GIMBALLED)
VERNIER THRUST CHAMBER FUEL TANK
VELOCITY SENSING ANTENNA
COMPARTMENT A
COMPARTMENT B
VERNIER THRUST CHAMBER FUEL TANK
VERNIER THRUST CHAMBER 2 (FIXED)
SOLAR COLLECTOR
LANDING LEG 2
FLIGHT CONTROL SENSOR GROUP
SIGNAL DATA CONVERTER
VERNIER THRUST CHAMBER OXIDIZER TANK
VERNIER THRUST CHAMBER FUEL TANK
LANDING LEG 3
ACCELEROMETER AMPLIFIER
STRAIN GAGE AMPLIFIER
PITCH AND YAW ATTITUDE JET NOZZLE (2)
VERNIER THRUST CHAMBER 3 (FIXED)
TV PHOTOMETRIC CHART
OMNIDIRECTIONAL ANTENNA B
SCALE, INCHES
0 5 10 15 20 25 30 35 40 45 50 55 60
VERNIER FUEL SYSTEM PRESSURIZATION TANK (He)
AUXILIARY BATTERY
ATTITUDE CONTROL PRESSURIZATION TANK (N2)
TV CAMERA 3
TV CAMERA 4
VERNIER THRUST CHAMBER OXIDIZER TANK
TV PHOTOMETRIC CHART
MIDCOURSE CONFIGURATION
ANTENNA AND SOLAR PANNEL POSITIONER
OMITTED FROM VIEW FOR CLARITY

Fig. 1. A-21 general arrangement

UNCLASSIFIED
CONFIDENTIAL

UNCLASSIFIED
CONFIDENTIAL

Table 4. A-21A spacecraft weight breakdown

Item	Current design weight, lb	Item	Current design weight, lb
Basic bus (total)	698.67	Spacecraft vehicle	218.26
Flight control	53.51	Spacecraft basic structure	
Sensor group		Equipment attaching hardware	
Secondary solar sensor		Landing gear installation	
Attitude control system		Paint	
Electronics	112.77	Equipment Compartments A and B	
Data link (antenna, RF switch, transmitter — diplexer, command receiver, and transponder)		Electrical wiring	
Central command decoder		Pneumatic lines attitude control	
Central signal processor		Release mechanism, retro-rocket	
Altitude marking radar		Engineering measurement sensors	
Doppler velocity sensor and altimeter		Latch — spacecraft to *Centaur*	
Boost regulator		Spacecraft propulsion (not including usable propellant)	227.62
TV Camera 4		Rocket engine, main retro	
Engineering data processing		Vernier propulsion system	
Mechanisms auxiliaries		Unusable vernier propellant	
Heater control		Helium	
Signal processing auxiliary		Insulation — main retro engine	
Battery charge regulator		Safety and arming device — main retro	
Low data rate auxiliary		Usable propellant (total)	1387.71
Electrical power	54.90	Retro-rocket propellant	
Solar panel		Vernier propellant	
Battery		Buoyancy — retro propellant	
Mechanisms	28.60	Weight tolerance	2.50
Positioner, antenna/solar panel		Buoyancy — basic bus	0.51
Antenna mechanism, omnidirectional separation sensing and arming provisions		Scientific payload (allowable payload weight based on spacecraft injected weight of 2150 lb)	63.62

Table 5. A-21A spacecraft weight summary

Item	Current design weight, lb
Total separated weight	2150.00
Basic bus	698.67
Usable propellant	1387.71
Scientific payload	63.62

comments and criticism regarding format and content before final publication.

Most analog measurements will have two graphs and one page of data corrections. The first graph plots telemetered voltage (0 to 5 v) expressed as a percentage of full scale (the CDC consoles are so calibrated) versus the parameter being measured (volts, temperature, frequency, dbm, degrees, amperes, pressure, etc.). A second graph plots the rss error as a function of the parameter being measured and is obtained by calculating the 3-σ distribution error of each error contributor: transducer, conditioning circuit, supply voltage, analog/digital converter, harness drops, commutator switches, amplifier gain variation and nonlinearity, offsets, etc.; they are then combined in a rss manner. Those error contributors whose value can be measured or calculated are then subtracted from the gross errors and another curve is plotted on the second graph to indicate the improvement that can be obtained by making the error corrections. The method of making these corrections is then described.

The final version of the handbook will contain an analysis of every commutated and continuous analog measurement and will also describe the methods used to compute the errors and the means whereby they can be minimized.

Each spacecraft will have its own handbook, because a large portion will contain calibration data corresponding only to those specific units mounted on that par-

UNCLASSIFIED
CONFIDENTIAL

UNCLASSIFIED
CONFIDENTIAL

ticular spacecraft. The handbook under preparation at this time will be for T-21 and will be followed by a handbook for the SC-1 spacecraft.

7. Shroud Ejection Test Support at Lewis Research Center

Hughes is supplying spacecraft hardware and technical assistance to Lewis Research Center for the *Centaur* shroud ejection tests. The first test using the Hughes-supplied hardware was conducted on August 31, 1964. Preliminary analysis of the test data showed that no significant stresses occurred in the antenna/solar panel positioner and mast assembly structure. The maximum pressure transient measured was approximately 0.5 lb/in^2 at 0.05 sec at the area adjacent to the top of the mast. The maximum pressure measured at the bottom of the planar array was 0.19 lb/in^2. The gas blast from the nose shroud separation bottles continued for approximately 1.4 sec causing a low level vibration of the mast of approximately 12 cps. The amplitude was minimal; the maximum stresses measured were insignificant. The installation of the pressure transducers on the planar array was incorrect and the data is thought to show higher pressures than actually existed.

Inspection of the solar panel immediately after the test showed no damage that could be attributed to the gas impingement. Even though nitrogen ice particles were present (because the ambient pressure was below the triple point of nitrogen) and were evident in the high-speed motion pictures of the test, the solar cells showed no resulting damage.

Another test using the same hardware, except for the substitution of an actual planar array for the simulated panel and incorporating further changes in the GD/A nose shroud and separation system to reduce further the gas impingement effects, is scheduled for about November 1, 1964.

CONFIDENTIAL
UNCLASSIFIED

UNCLASSIFIED
CONFIDENTIAL

B. Scientific Payload

1. Payload System Engineering

a. General system integration. Activities during this period have been devoted primarily to an analysis of proposed instrument changes, the conduct of special studies, and the comparison of command and date channel allocations. Typical of these activities was a study related to a *Surveyor* critical data recorder (see Section M).

Engineering change requests to current limit 29-v dc regulated power used by the seismometer alpha scattering instrument, micrometeorite ejecta detector, and soil mechanics/surface sampler have been received from JPL. These changes would protect the spacecraft 29-v dc regulated (non-essential) bus in case of a malfunction in instrument power circuits. Current limiting circuits would also provide protection for an instrument in case of a temporary short circuit. Engineering change proposals have been prepared to describe the technical, cost, and schedule effects of the proposed changes.

b. Alpha scattering experiment subsystem. The alpha scattering experiment will be used for compositional analysis of lunar surface materials. The experiment provides a capability to allow measurement of materials at several locations on the lunar surface when used in conjunction with the soil mechanics surface sampler experiment.

Subsystem integration. Recent approval of an engineering change proposal provides for the transmission of five additional engineering data signals to Earth during operation of the alpha scattering instrument. The engineering for this change, which includes three voltage monitors and two command verification signals, has been released and implementation is in progress.

Hughes is also preparing an engineering change proposal describing the technical, cost, and schedule effect of incorporating the redesigned alpha scattering instrument (Type 2). Although the improved instrument will result in approximately 2.2 lb increase in spacecraft weight, the stability and accuracy of data measured will be greatly enhanced. However, it is expected that the increase in instrument (sensor head) weight may result in major redesign of the alpha scattering instrument deployment mechanism. Other effects of the change include a minor increase in instrument power, revision of experiment interconnections, modification of instrument output data format, and revision in instrument outline and mounting provisions. Payload and system test activities will require revisions to test requirements and associated ground support equipment.

JPL has requested Hughes to perform a thermal analysis of the alpha scattering sensor head (Type 1). The study, which includes the conditions listed below, will be utilized by JPL to supplement a thermal analysis of the sensor head in the deployed positions recently completed by the Illinois Institute of Technology Research Institute. The study will determine:

(1) Equilibrium temperature of the sensor for the transit coast phase. (Normal transit attitude, non-operating.)

(2) Sensor temperature for an equatorial lunar noon landing (non-operating).

(3) Sensor temperature for a lunar night landing (non-operating).

(4) Equilibrium temperature of the sensor for an equatorial lunar noon landing with the sensor head in the stowed position (non-operating).

(5) Transient sensor temperature during a standard sample count (operating for a 3-hr period with an equatorial lunar noon thermal environment). The initial temperatures for the standard sample count operation will be determined by the steady-state thermal analysis of item (4).

This study is expected to be completed by mid-November 1964.

The alpha scattering instrument auxiliary (S/N X-1) has passed all unit functional tests and will be integrated with the JPL supplied P-1 instrument in late October.

Alpha scattering instrument auxiliary. Fabrication of the type approval and T-21A units has started. Type approval test (TAT) and flight acceptance test (FAT) specifications for this unit are 75% complete and the related unit test equipment is 50% complete.

Alpha scattering deployment device. The alpha scattering sensor head stowage and deployment mechanism provides the means for stowing the sensor head on the spaceframe during launch, transit, and lunar landing. After landing, the mechanism positions the sensor head for taking a standard sample count, a background count, and a lunar surface count. A recent design change allows the soil mechanics/surface sampler to redeploy the sensor head to another location.

Deployment of the instrument cable was a problem in the mechanism redesign. Tests to determine the force required to bend the proposed instrument cable at low temperatures were run. The test jig is shown in Fig. 2.

CONFIDENTIAL
UNCLASSIFIED

UNCLASSIFIED

The prototype cable used in the test consisted of four 22 gauge single conductors, seven 24 gauge single conductors, four 24 gauge shielded conductors and one triple conductor 24 gauge shielded cable in a woven glass sleeving. In the test setup, the cable was clamped in a 4 in. long block in a manner that allowed 6 in. of free cable to protrude from one end. A dry ball bearing at the free end prevented sag and reduced sliding friction to a minimum. A small wire hook was fastened to the cable at the 6 in. point. A 0 to 150 gram scale was used to measure the bending force. The installation of the test sample in the cold chamber is shown in Fig. 3. The results in Table 6 were obtained. A subsequent analysis indicated that under worst slope conditions (15 deg), the expected cable forces would tip the sensor head.

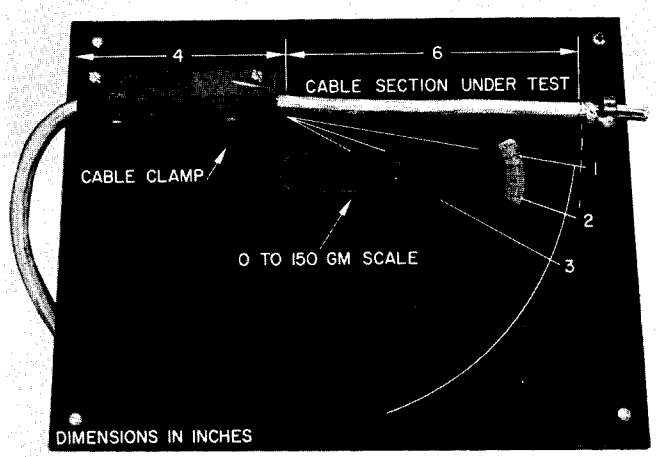

Fig. 2. Alpha scattering cable bend test fixture

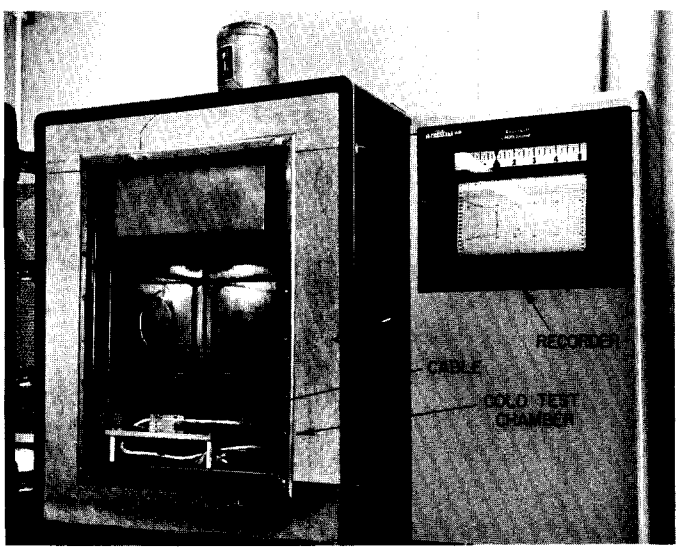

Fig. 3. Alpha scattering cable bend test setup

Table 6. Results of prototype alpha scattering instrument cable in cold chamber

Deflection, in.	Bending force, grams, at temperature indicated			
	+65°F	0°F	−50°F	−100°F
1	25	28	33	57
2	40	27	61	93
3	55	69	82	123

A survey of other cable designs was made. As a result, a flat ribbon type ("contour") cable was selected. In turn, a redesign of the sensor head stowage bracket was made to incorporate a cable stowage container. The proposed contour cable will have 14 convolutions when stowed in the container. It will be released from the container when the sensor head is moved to the background count position. The design provides for a "soft" service loop to the sensor head and allows a maximum extension of approximately 56 in. Two cables have been fabricated for the developmental test model (X-1) and the payload evaluation unit (X-2).

c. Micrometeorite ejecta detection experiment subsystem. The *Surveyor* micrometeorite ejecta detector will provide data regarding the number, momentum, and kinetic energy of individual lunar ejecta resulting from meteoroids impacting on the lunar surface.

Subsystem integration. During this reporting period Hughes completed a thermal analysis of the micrometeorite ejecta detector sensor assembly. This analysis included a determination of the optimum thermal paint pattern for the sensor assembly, a unit temperature profile for lunar day operation with this paint pattern, evaluation of heater effect on near day/night terminator operation, and recommendations for special thermal problems. For details of the analysis see Section G of this report.

Hughes is evaluating a JPL engineering change request to update instrument outline and mounting drawings to indicate latest instrument design.

The micrometeorite ejecta detector auxiliary (S/N X-1) has passed all unit functional tests, and will be integrated with the JPL supplied P-1 instrument in late October.

Micrometeorite ejecta detector auxiliary. Fabrication of the type approval and T-21A units has started. TAT and FAT specifications for this unit are 75% complete and the related unit test equipment is 50% complete.

d. Seismological experiment subsystem. The seismological experiment subsystem is composed of a short-

UNCLASSIFIED

UNCLASSIFIED

period vertical seismometer sensor (hard-mounted to the *Surveyor* spaceframe), an electronics assembly, and an electronics auxiliary (located within Compartment B).

Seismometer sensor. The seismometer sensor is used to measure the number, magnitude, spatial distribution of natural Moon quakes, and the seismic background noise. This data, when correlated with the effects of temperature of the lunar surface materials, will aid in determining the elastic properties and structure near the lunar surface.

Electronics assembly. The electronics assembly consists of a high gain, low noise amplifier required to amplify the very small sensor signal output to levels which are compatible with the telecommunications subsystem.

Auxiliary. The auxiliary consists of the electronics required to provide command decoding, buffering of data from the sensor, power management for the auxiliary, and control of electromechanical devices.

Subsystem integration. At JPL request, changes to the experiment were recently proposed. Specifically, the following subsystem changes were provided:

(1) Provide current limiting, such that under short circuit conditions the spacecraft shall not supply greater than 200ma for a period greater than 100 msec.

(2) Provide a 0.20-amp fuse in the sensor heater circuits.

(3) Increase the sensor power dissipation from 0.5 to 1.0 w.

In addition, JPL has requested Hughes to perform a thermal analysis of the single axis seismometer, in its natural environment on the spacecraft, during a prelaunch, transit, and touchdown sequence. Results of the study will be discussed in subsequent progress reports.

Seismometer auxiliary. Fabrication on the type approval and T-21A units has started. TAT and FAT specifications for this auxiliary are 75% complete. The unit test position is 50% complete.

e. Soil mechanics-surface sampling experiment subsystem

Subsystem integration. During this reporting period, a mission analysis study of the soil mechanics-surface sampling experiment was completed. The study, made at JPL request, resulted in a determination of elapsed time, power consumption, and number of commands necessary to complete a given proposed sequence of lunar operations. For purposes of the study, it was assumed that the spacecraft was on a level lunar surface. The sequence to be performed consisted of surface mapping and surface bearing strength tests at 14 points and drop and drag tests at 6 points. All points were evenly distributed in the instrument field of operation. This sequence was then translated into elapsed times, number of commands, and consumption of electrical energy. Results of the study revealed that completion of the prescribed sequence will be time consuming unless the command generation and transmission process is highly mechanized. As an example, 75 hr would be required to complete the sequence if individual commands or groups of commands were generated in the Space Flight Operations Center, sent to the Deep Space Net at Goldstone to be punched on tape, sent back to the Space Flight Operations Center for verification, and the verification and authorization to transmit sent back to Goldstone. The study also revealed that the total operating time for the instrument would be small, possibly less than 15 min. The electrical energy consumed by the experiment would be approximately 3 w-hr if the experiment were turned off after each series of commands. Further study of operating criteria, command programming, and lunar sequencing will be required to reduce operating time and assure optimum utilization of electrical energy.

JPL has recently initiated an engineering change request to update, correct, and clarify the soil mechanics-surface sampler interface specification. Preliminary work has been initiated and Hughes will prepare an engineering change proposal.

It was recently noted that a short circuit in the spacecraft 4.85-v dc potentiometer power supply could disable the commutators in the engineering signal processor. Hughes Aircraft Co. has undertaken a study to determine the total system effects of such a failure. It is expected that the study will be completed in late October, and the results will be reported in *SPS 37-31*, Vol. I.

Soil mechanics/surface sampler. The soil mechanics/surface sampler (SM/SS) is designed for digging, scooping, and picking over a lunar surface area of approximately 25 ft^2. It consists of a pantograph arm and scoop mechanism operated by independent electric motor drives for azimuth, elevation, radial motions, and scoop opening and closing.

Approximately 45% of the unit detail drawings have been released. These drawings reflect the conversion of the original surface sampler to a soil mechanics/surface sampler. Procurement specifications for the shock and strain measuring systems have been completed and requests for bids initiated.

UNCLASSIFIED

CONFIDENTIAL UNCLASSIFIED

Upgrade of previously fabricated surface samplers to the soil mechanics/surface sampler configuration has progressed as follows:

(1) Payload Systems Laboratory unit (X-4) has been completed.

(2) engineering model (X-2) has been completed.

(3) engineering model (X-3) is 50% complete.

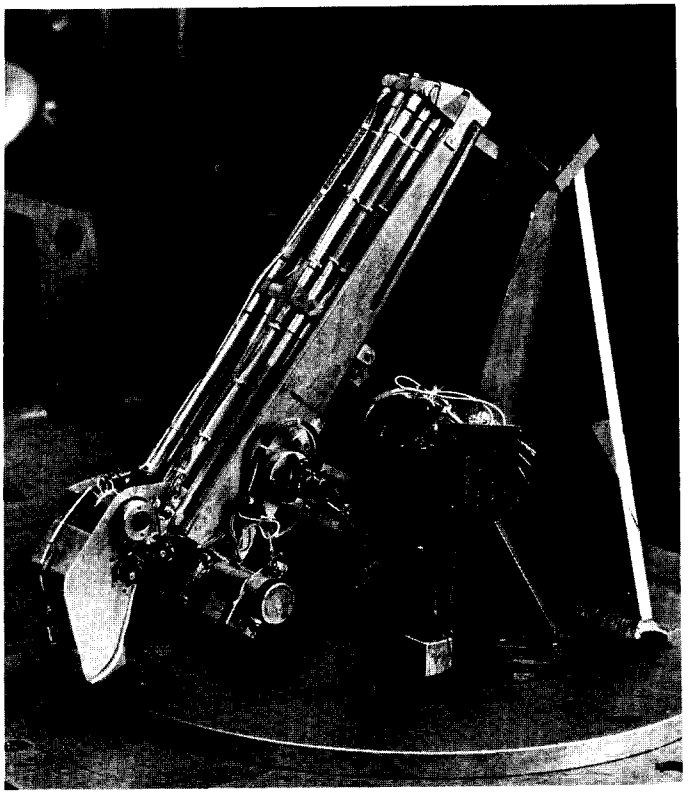

Fig. 4. Soil mechanics/surface sampler development vibration test

Lateral axis vibration tests on an engineering model have been completed. Fig. 4 shows the SM/SS mounted on a vibration test fixture in the Hughes Space Environment Simulation Laboratory. Fig. 5 shows the frequency versus acceleration input to the test unit. The maximum level of the input was 18 g. Fig. 5 shows the resulting accelerations measured at the centerline of the elevation axis. Maximum acceleration occurred at approximately 70 cps. Vertical axis vibration testing is in progress and will be described in subsequent reports.

Preliminary testing of developmental accelerometers has been completed. Fig. 6 depicts deceleration versus time response of the scoop blade when dropped on brick and featherstone samples, respectively.

Soil mechanics/surface sampler auxiliary. Product design of the SM/SS auxiliary has been completed and the unit has been delivered to the Payload System Laboratory. A thermal analysis has been completed on the unit

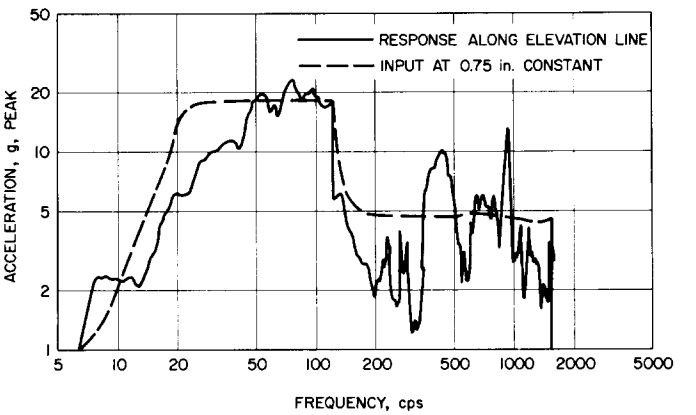

Fig. 5. Lateral vibration test of soil mechanics/surface sampler

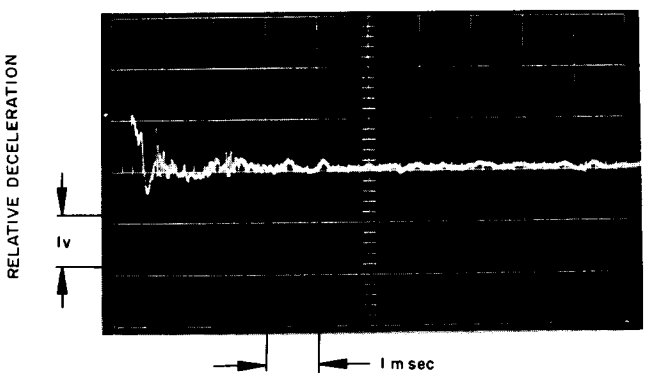

(a) Brick

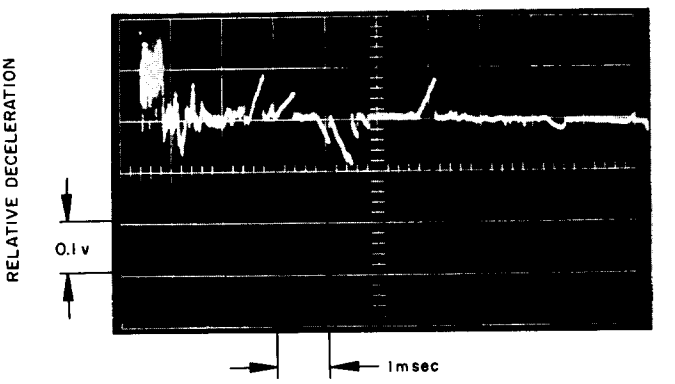

(b) Featherstone

Fig. 6. Deceleration of scoop blade in drop tests from 3-in. height

UNCLASSIFIED CONFIDENTIAL

UNCLASSIFIED CONFIDENTIAL

and design change recommendations are under study. Production planning has been completed for type approval and T-21A units, and unit test equipment design is approximately 50% complete.

2. Payload Systems Laboratory

a. General. Design of Payload Systems Laboratory (PSL) test equipment has been completed and all engineering released for fabrication. Fabrication and checkout of the test equipment is near completion, and the equipment is expected to be operational in late October. Fig. 7 shows three test racks which comprise a part of the total test configuration.

Preparation of preliminary test procedures was initiated in September. These procedures will be broad enough to provide a basis for developmental testing of PSL instruments, auxiliaries, and mechanisms. The procedures will, however, be detailed enough to assure proper sequence of testing and permit the orderly analysis of test results. These documents will in turn provide the framework for the development of detailed procedures to be used on T-21A and subsequent flight units.

Testing and checkout of instrument auxiliaries commenced on October 6, 1964.

b. Soil mechanics/surface sampling experiment subsystem. During this report period, the design and fabrication of the SM/SS junction box, associated cables, and tees were completed. The SM/SS experiment control panel passed unit test and its integration into the total test configuration is in process.

c. Micrometeorite ejecta detection (MED) experiment subsystems. The design and fabrication of the MED junction box, associated cables and tee connectors have been completed. A bench test set has been completed and is currently being utilized for MED auxiliary tests. The experiment panel has passed unit test and its integration into the total test configuration is in progress.

d. Alpha scattering and seismological experiments subsystems. Parallel effort has continued on the functional checkout of the alpha scattering and seismological experiment control panels. Fabrication of these panels was completed during the report period. Bench checks were completed and the panels have been installed in the PSL racks. Integration with the data logging systems and other special test equipment is in progress.

Experiment junction box, tee, and cable designs were released. The junction boxes provide power and signal switching circuits and trouble shooting access test points. Front panels of these units are shown in Fig. 8 and 9

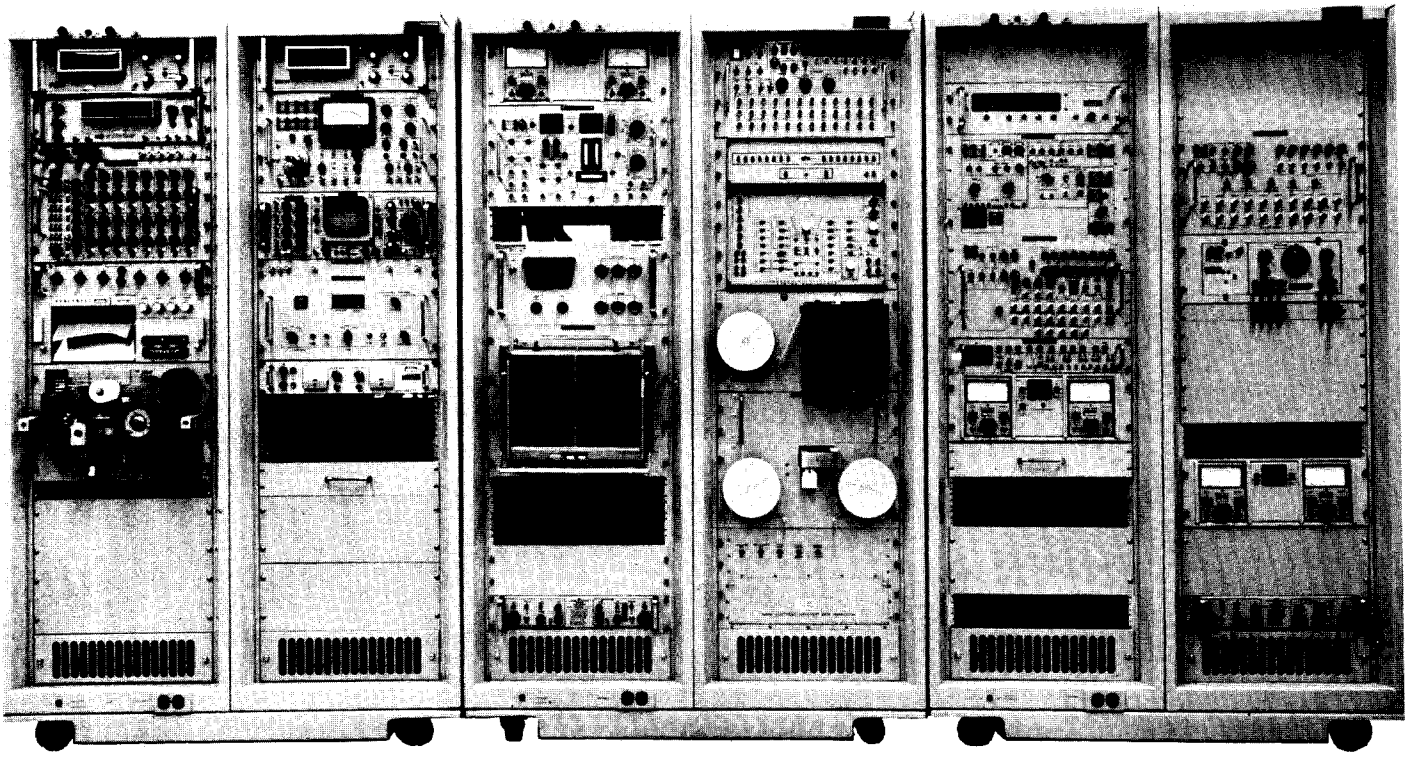

Fig. 7. PSL scientific instruments test racks

UNCLASSIFIED CONFIDENTIAL

UNCLASSIFIED
CONFIDENTIAL

respectively. Final assembly and integration of these units is expected in late October.

Instrument simulators, currently under design, will aid in the final checkout and integration of the PSL test rack complex and the M13 simulated spaceframe. A high confidence of compatibility between instruments and test devices will be thereby assured prior to installation of instruments on M13. In addition, all instruments and auxiliaries will be checked on their respective bench setups. These checks will be accomplished prior to any instrument or auxiliary being mounted on M13.

e. Spaceframe mockup (M13). The basic PSL spaceframe (designated M13) was completed in September and all mechanical payload interfaces have been installed (Fig. 10).

Design of those portions of Compartments A and B electrical harness related to the payload and all individual experiment harnesses have been completed and fabrication is under way. Installation of the harnesses on the spaceframe is expected to occur during the latter part of October.

3. Television Subsystem

a. T-21 television subsystem. The television cameras and auxiliary were removed from the T-21 spacecraft for routine upgrade and functional testing during the scheduled upgrade period. The mirror azimuth end-stop modification was incorporated in the survey camera. The end-stop is a pin that restricts the mirror azimuth rotation to 360 deg. If the mirror assembly were inadvertently commanded beyond 360 deg, the azimuth position potentiometer would be damaged. This modification prevents damage to the potentiometer. Each unit was functionally tested to verify operational integrity.

b. SC-1 television subsystem. All television units for the SC-1 vehicle were installed on the spacecraft on September 1, 1964, and subsystem group testing is underway.

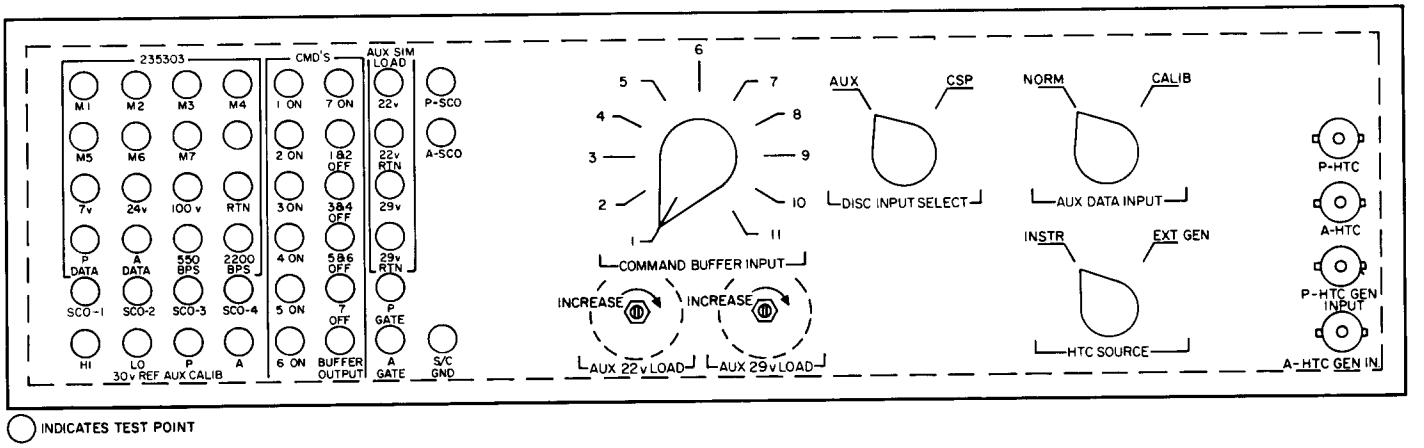

◯ INDICATES TEST POINT

Fig. 8. Front panel of PSL alpha scattering experiment junction box

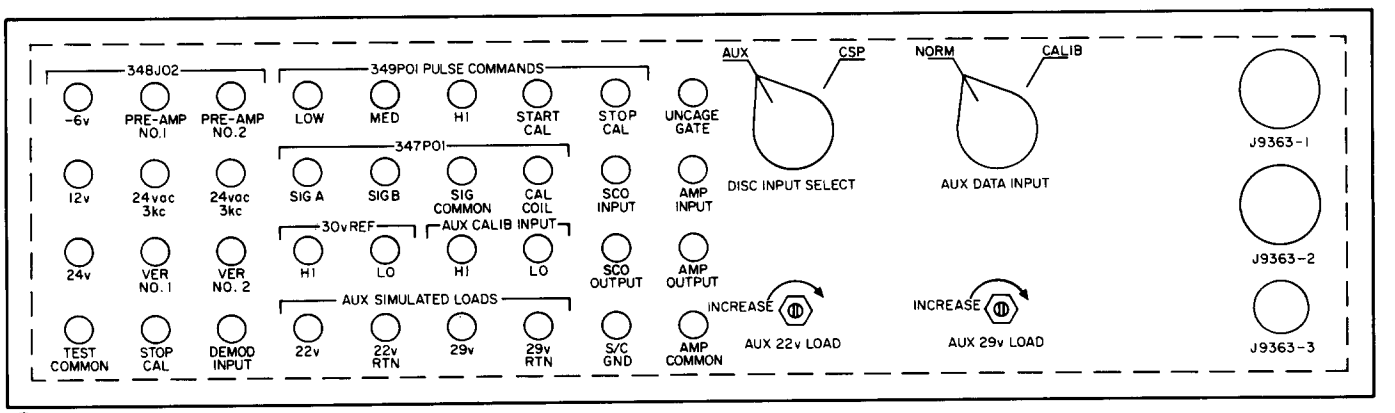

◯ INDICATES TEST POINT

Fig. 9. Front panel of PSL seismometer experiment junction box

CONFIDENTIAL
UNCLASSIFIED

UNCLASSIFIED
CONFIDENTIAL

c. Type approval testing. The type approval test camera has essentially completed environmental testing since the last bimonthly report period. Environmental testing includes thermal-vacuum, vibration, and shock testing.

All portions of the thermal-vacuum sequence were performed with the exception of testing at —50 and —250°F. These temperatures were not attained due to a poor thermal conduction path between the TV camera and the test fixture. The test fixture is presently being redesigned to provide an adequate conduction path. It is planned that the TAT camera will be subjected to low temperature testing when the redesigned fixture is available.

An abbreviated functional test was performed following thermal-vacuum testing. All electrical parameters compared favorably with those obtained from the pre-environmental functional test.

Four significant failures occurred during the vibration portion of the type approval test. The format of the vibration test is to subject the camera to six 2-min sweeps for each principal axis. The camera principal axes are shown in Fig. 11. The mirror assembly was damaged on the first vibration sweep in the X-axis. The damage consisted of the separation of two aluminum doublers and the loss of some thermal paint in the damaged area. The open mirror assembly showing the damaged area is shown in Fig. 12. This same type of failure was observed during type approval testing of the mirror assembly. A redesign of this area had been initiated, however, the redesign was not in the TAT camera and will be incorporated in SC-1 and subsequent mirror assemblies.

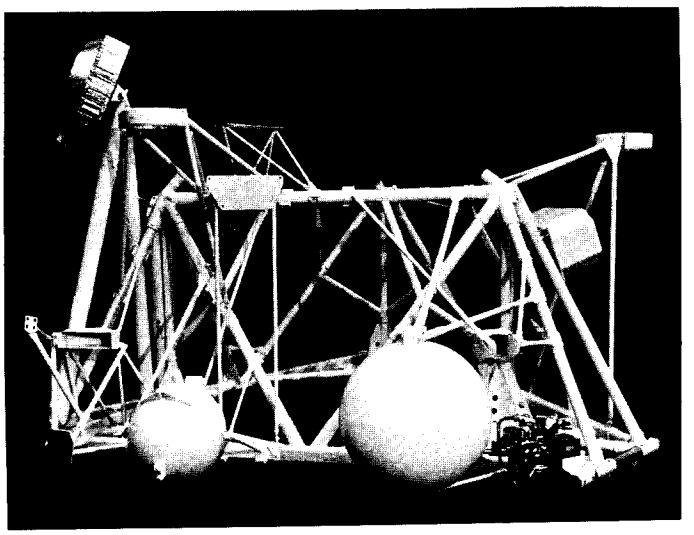

Fig. 10. PSL spaceframe (M-13)

Functional testing, subsequent to the mirror damage, showed that all functions operated properly with the exception of the "start frame." The failure was due to inadequate mounting of the large capacitor (C-1) on

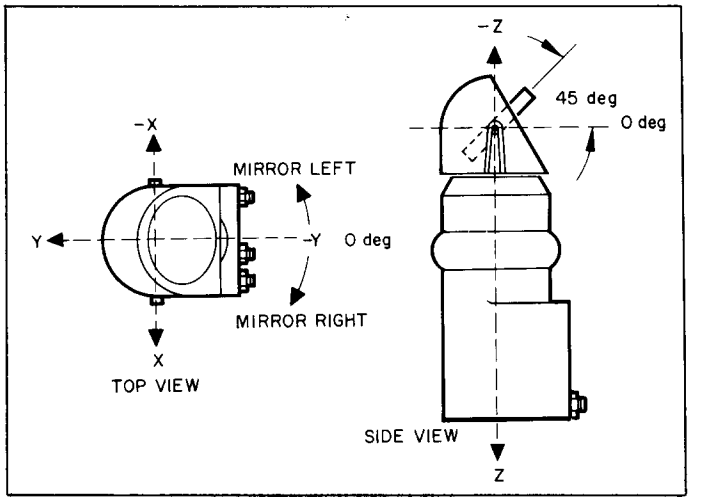

Fig. 11. Survey camera principal axes

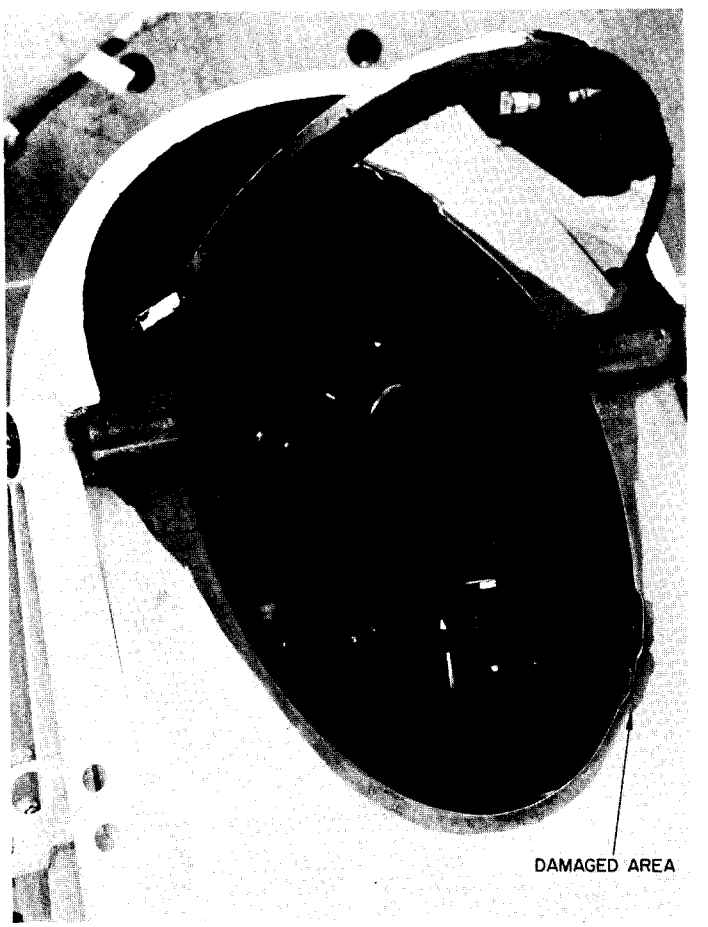

Fig. 12. Mirror assembly damaged in vibration test

CONFIDENTIAL
UNCLASSIFIED

UNCLASSIFIED
CONFIDENTIAL

the electrical conversion unit (ECU) cover plate. The original mounting is shown in Fig. 13. The single clip that mounts this large capacitor had vibrated, resulting in breaking both leads to the capacitor. The new mounting redesign provides more support to the capacitor and, in addition, the leads to the capacitor will be positioned to minimize flexing of the leads with respect to the ECU cover plate. This change was incorporated in the TAT camera prior to finishing the vibration sequence and the failure did not reoccur.

At the completion of the vibration sequence, a functional test disclosed that the shutter and filter wheel had failed. The shutter failed due to a retainer which jammed a shutter blade latch. When the washer was moved back in place, the shutter operated properly. Investigation of this area will determine if this is a random failure or if the failure requires a redesign. The filter wheel failed in two areas during the vibration sequence. Four hollow rivets, used to hold the filter wheel to its shaft failed. The shaft which holds the filter wheel webbing is approximately 0.25 in. in diameter. A V-notch is cut out such that the remaining material is approximately 0.1 in. in diameter. Failure occurred in this V-notch area. Investigation of these two areas is in progress.

The future test sequence of the TAT camera is to complete the low temperature thermal-vacuum portion of type approval testing, perform a detailed functional test, and perform vibration testing a second time after the filter wheel is redesigned.

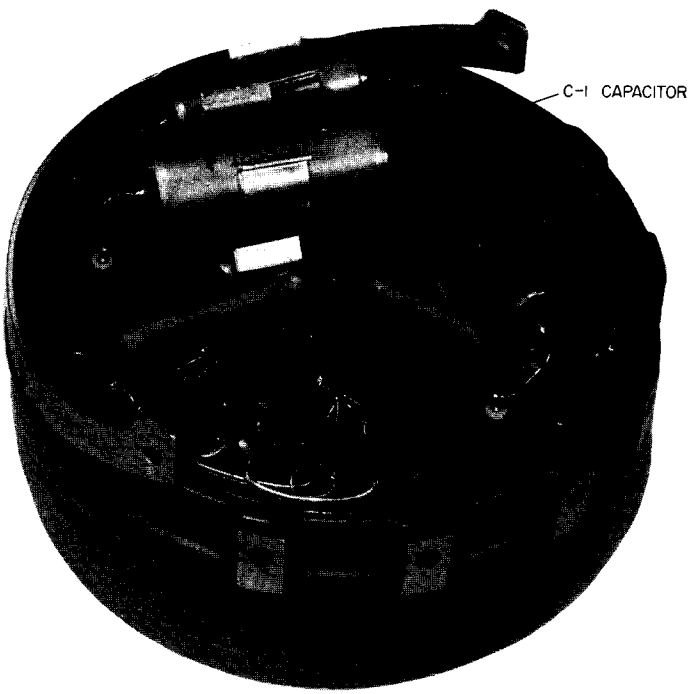

Fig. 13. Original C-1 capacitor mounting on ECU cover plate

d. TV mirror assembly. A study is being made on optical calibration of the mirror assembly in thermal-vacuum environment to augment the ambient room condition calibration procedure now in use. The data obtained under thermal-vacuum calibration will more nearly simulate the mission environment resulting in more meaningful calibration data.

The testing procedure has been designed to meet the following constraints. The complete calibration of both azimuth and elevation axes must be performed at high, low, and room temperature under vacuum conditions. Auxiliary mechanisms used in the vacuum chamber must be designed for extensive vacuum operation and reliability. The increased amount of data must be amenable to reduction by computer. No measuring equipment will be inside the chamber where it could be affected by the environment. In addition, an optical window must be provided in the vacuum chamber to form a coordinate reference in mirror unit coordinates. The position reference must be provided in order to recover coordinate position if the measuring equipment is disturbed or if there is a displacement from thermal gradient between the inside and outside of the chamber.

As now conceived, an autocollimating theodolite will view the mirror unit through an optical quality quartz window in the vacuum chamber. A two-axis positioner will rotate the mirror unit within the vacuum chamber. The positioner does not require precise control since its actual rotation is measured by the theodolite. A mirrored glass block rigidly attached to the specimen baseplate serves as the position reference for elevation and azimuth rotation in mirror coordinates.

e. Photometric charts. It is required to provide a means of calibrating the television camera after the lunar landing. To perform this calibration, three photometric charts, calibrated to Earth standards, will be provided on the spacecraft. One will be placed on landing gear Leg 2 to be viewed by the survey camera in Sector 3. Another will be located on landing Leg 3 to be viewed by the survey camera in Sector 2, and a third chart will be located on the omnidirectional antenna B, which can be viewed by both survey cameras. Fig. 14 shows the location of both survey cameras and the three photometric charts on the A-21A spacecraft configuration. Fig. 15 shows the A-21 spacecraft configuration which has only one survey camera and two photometric charts.

Selection of the colors and paints for the photometric charts has been completed. The spectral response of the

CONFIDENTIAL
UNCLASSIFIED

UNCLASSIFIED
CONFIDENTIAL

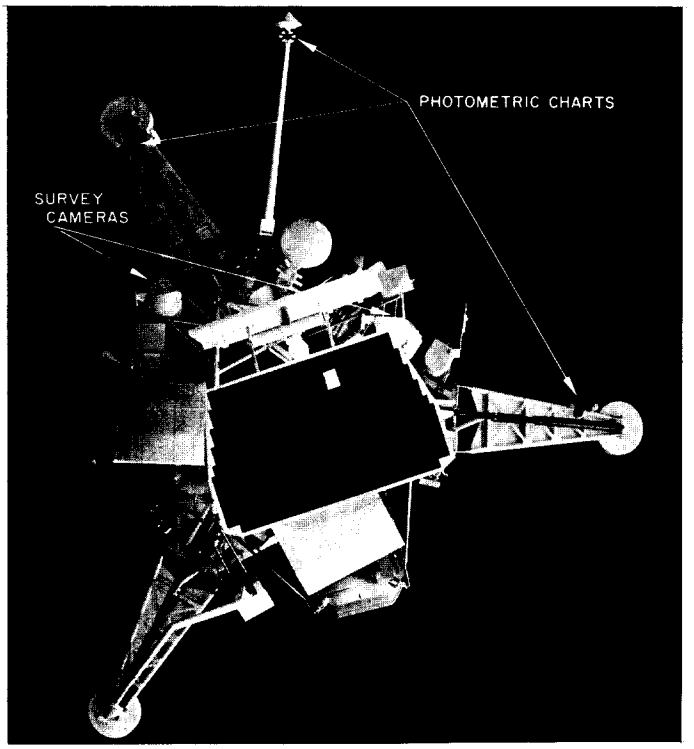

Fig. 14. Photometric charts on A-21A

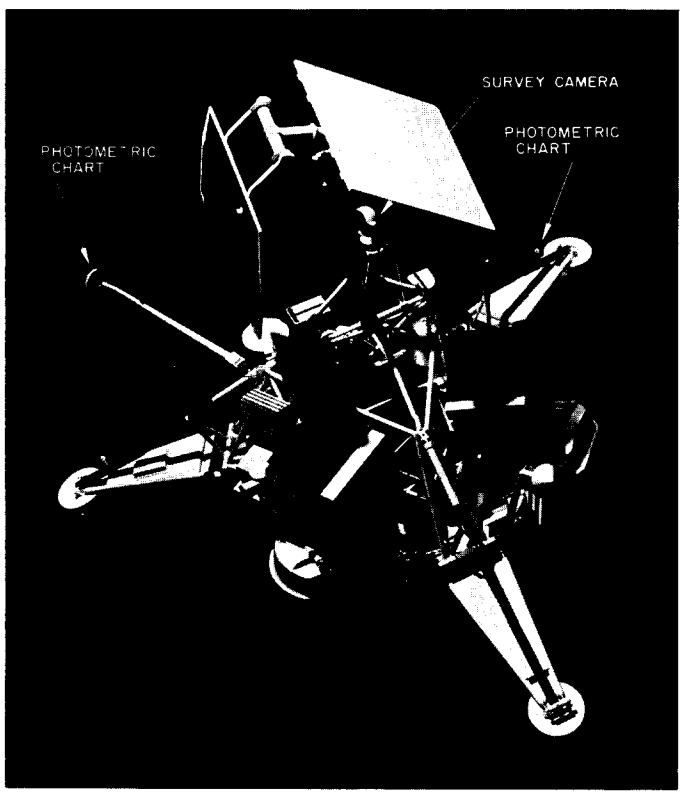

Fig. 15. Photometric charts on A-21

vidicon and the transmission of the filter elements had to be considered in order to select appropriate colors that would provide useful video voltages for all combinations of lens, iris, and filter wheel positions.

Fig. 16 shows typical spectral response for the General Electrodynamics Corporation (GEC) vidicon used in the television cameras. Fig. 17 shows a typical transmission coefficient plotted as a function of wavelength for the survey camera variable focal length lens. Fig. 18 shows typical transmission coefficients for each filter element. These data are combined to get an overall spectral response curve for each condition of filter color, iris setting, and expected luminance level. The colors selected for the charts are orange-black, blue-black, and green. Their reflectances plotted as a function of wavelength are shown in Fig. 19.

The substrate material used for the two charts on the spacecraft legs is 0.030-in. sheet aluminum, whereas the

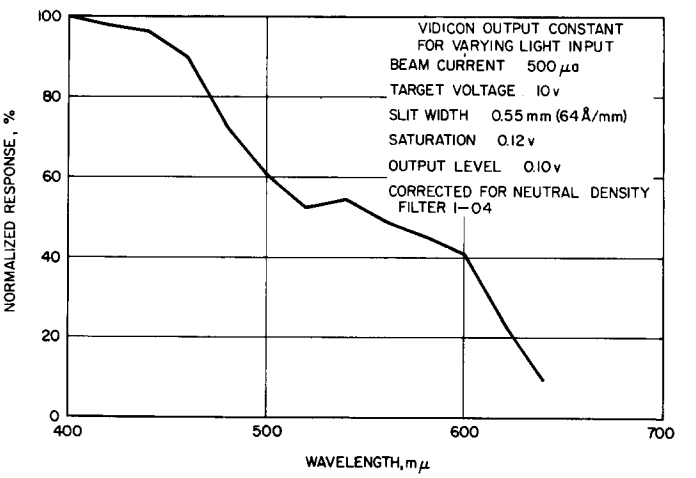

Fig. 16. Typical spectral response for survey vidicon

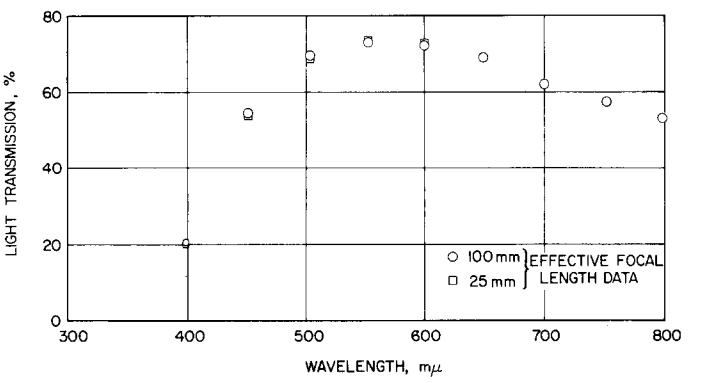

Fig. 17. Transmission coefficient for survey camera variable focal length lens

UNCLASSIFIED
CONFIDENTIAL

UNCLASSIFIED
CONFIDENTIAL

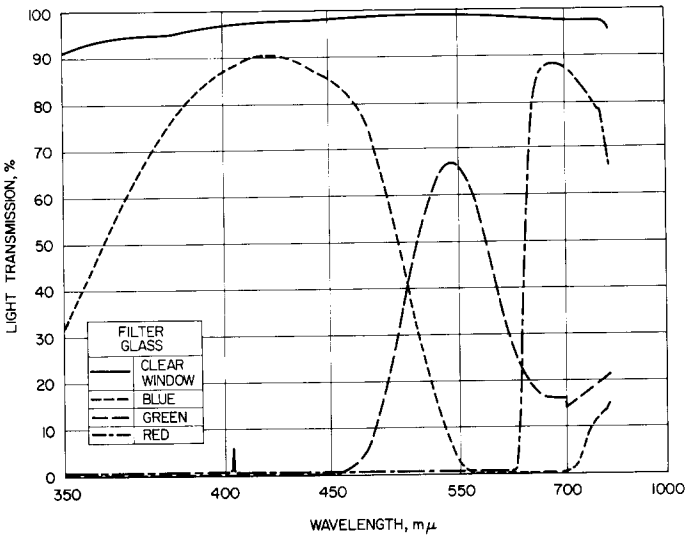

Fig. 18. Transmission coefficients for typical filter elements

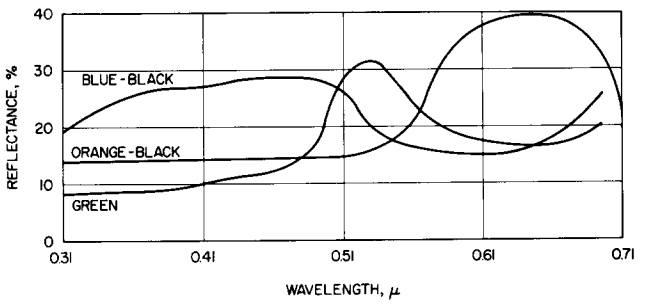

Fig. 19. Typical reflectance coefficients for points on photometric charts

material used for the chart on the omnidirectional antenna boom is 0.060-in. thick epoxy-glass material. This is required so that the chart does not affect the antenna radiation pattern. In addition to the colored paints, there are several shades of gray so that photometric properties of the Moon's surface can be determined. Fig. 20 shows the photometric chart.

f. Stray magnetic field problem. Observation of the TV raster with various orientations of the camera with respect to the Earth's magnetic field has shown that the TV raster shifts. There is a conetic magnetic shield around the deflection yoke area of the vidicon. A study has been initiated to determine if the magnetic shielding could be improved. Several shields and shielding procedures have been investigated. During the investigation, a 60-cps, 0.1 Gauss magnetic field was impressed in a direction perpendicular to the axis of the vidicon. The induced signal voltage was measured at the vidicon faceplate. Table 7 summarizes the results of this testing.

The configurations are defined as follows:

(1) Configuration 1 has the yoke, vidicon, and shield as used in the TV cameras.

(2) Configuration 2 is the same as Configuration 1 with hydrogen annealing of the yoke shield.

(3) Configuration 3 adds a conetic foil to the outside of the vidicon cell assembly. All necessary holes are punched through the conetic foil.

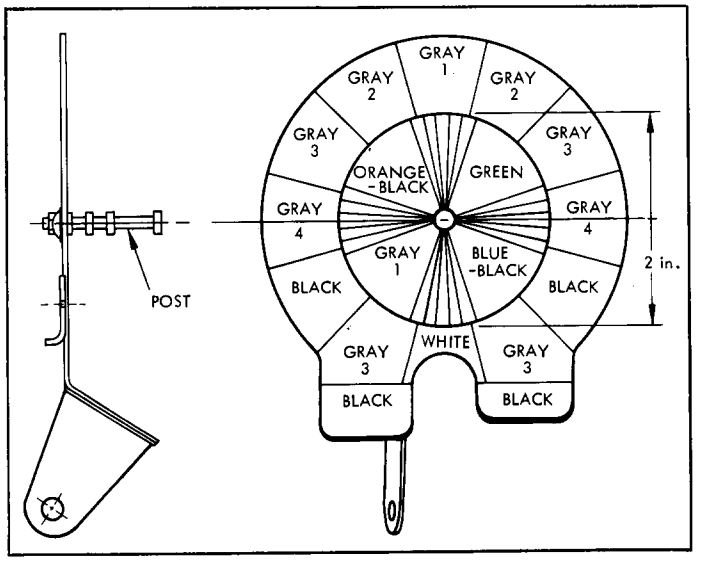

Fig. 20. Photometric chart

Table 7. Improvement of various configurations of magnetic shielding

	Configuration	Field strength (Gauss) 60 cps	60-cps pickup, v	Factor by which pickup is reduced relative to Configuration 1
1	Non-annealed yoke shield only	0.1	3	1
2	Annealed yoke shield only	0.1	1.1	2.7
3	Annealed yoke shield and outer liner	0.1	0.75	4.0
4	Annealed yoke shield and inner liner	0.1	0.60	5.0
5	Annealed yoke shield and both liners	0.1	0.46	6.5
6	Annealed yoke shield and ¾-in. conetic wrapped around front of vidicon	0.1	0.46	6.5

UNCLASSIFIED
CONFIDENTIAL

UNCLASSIFIED
CONFIDENTIAL

(4) Configuration 4 is the same as Configuration 2 with the addition of an inner foil liner.

(5) Configuration 5 utilizes both inner and outer linings of conetic foil.

(6) Configuration 6 utilizes an annealed yoke shield and ¾-in. conetic foil shielding around the glass of the vidicon near the vidicon faceplate. Although this configuration resulted in one of the greatest reduction of magnetic field effects, it is not practical to implement this change into hardware because the conetic foil introduces approximately 4 pf of capacitance at the input of the video amplifier, and would degrade resolution.

Employing the outer liner method is the most simple from the viewpoint of manufacturing since the conetic foil can be wrapped around the vidicon cell assembly and bonded in place without disturbing the cell assembly. One such liner was bonded to the exterior of a vidicon cell and suffered no damage when purged with liquid nitrogen. Additional investigation is planned to determine the best method of improving magnetic shielding before a method is selected for implementation in the hardware.

g. TV camera thermal analysis. A detailed thermal analysis is being performed on the TV cameras to determine if the present thermal design is adequate for the *Surveyor* mission. The survey cameras will be analyzed for transit, terminal descent, and lunar environment phases; the approach camera will be analyzed only for transit and terminal descent phases.

A thermal model valid for both survey cameras has been defined. The process of defining the model was to choose a number of areas within the camera assumed to be uniform in temperature. Fifty-six such areas, called nodes, were chosen for the survey camera thermal model. The next step in defining a thermal model was to evaluate terms for radiation and conduction. These terms are essentially the paths whereby energy can pass between the nodes causing their temperatures to change. The survey camera thermal model has 148 conduction terms and 187 radiation terms which connect the 56 nodes. Fig. 21 shows the nodes chosen for the survey camera. Table 8 is a listing of the 56 nodes. It might be noted here that a rather detailed analysis is necessary to define the terms. If the radiation and conduction terms are grossly in error, the thermal model will not predict accurate temperatures. The final step in defining the thermal model is to choose proper view factors for the exterior nodes. The view factors take into consideration the surroundings of the TV camera, i.e. spacecraft, solar radiation, free space, and when applicable, the lunar surface. The view factors or thermal parameters have been defined for TV 3 and are described in Fig. 22 and Table 9. The view factors were measured by use of a form factometer button in conjunction with a full-scale engineering mockup of the *Surveyor* spacecraft and a one-fifth scale engineering model. Modification of the view factors provides

Table 8. Survey camera nodes

Node	Location	Node	Location
1	Top of mirror hood	15	Curved portion of lens support structure
2	Flat portion of mirror hood	16	Chassis 1
3	Mirror	17	Lens structure housing under chassis 1
4	Elevation motor side of mirror hood	18	Chassis 2
5	Plug side of mirror hood	19	Lens structure housing under chassis 2
6	Elevation drive assembly	20	Upper shroud Chassis 1 side
7	Filter wheel assembly	21	Upper shroud Chassis 2 side
8	Azimuth drive assembly	22	Upper shroud Chassis 1 side below Node 20
9	Mirror assembly base	23	Upper shroud Chassis 2 side below Node 21
10	Mirror to lens assembly junction	24	Vidicon faceplate
11	Lens assembly	25	Top glass portion of vidicon
12	Teflon support ring	26	Middle portion of vidicon
13	Boron nitride collar	27	Lower portion of vidicon
14	Shutter base plate	28	Gun structure in vidicon

UNCLASSIFIED
CONFIDENTIAL

CONFIDENTIAL UNCLASSIFIED

Table 8 (continued). Survey camera nodes

Node	Location	Node	Location
29	Vidicon cell assembly cap	43	Support leg between Chassis 4 and 5
30	Socket, cathode, heater of vidicon tube mounting structure	44	Chassis 6
31	Vidicon cell assembly housing	45	Lower shroud facing Chassis 6
32	Vidicon yoke and shield	46	Lower shroud below Node 34
33	Lower shroud facing Chassis 4	47	Lower shroud below Node 33
34	Lower shroud facing Chassis 5	48	Lower shroud below Node 45
35	Lower shroud facing Chassis 3	49	Lower shroud below Node 46
36	Chassis 3	50	Lower shroud below Node 47
37	Chassis 4	51	Base of lower shroud
38	Main deck structure	52	Top cover of ECU
39	Chassis 5	53	ECU chassis
40	Support leg between Chassis 3 and 4	54	ECU transformer
41	Support leg between Chassis 3 and 5	55	Side of ECU cover
42	Vidicon radiator	56	Base of ECU cover

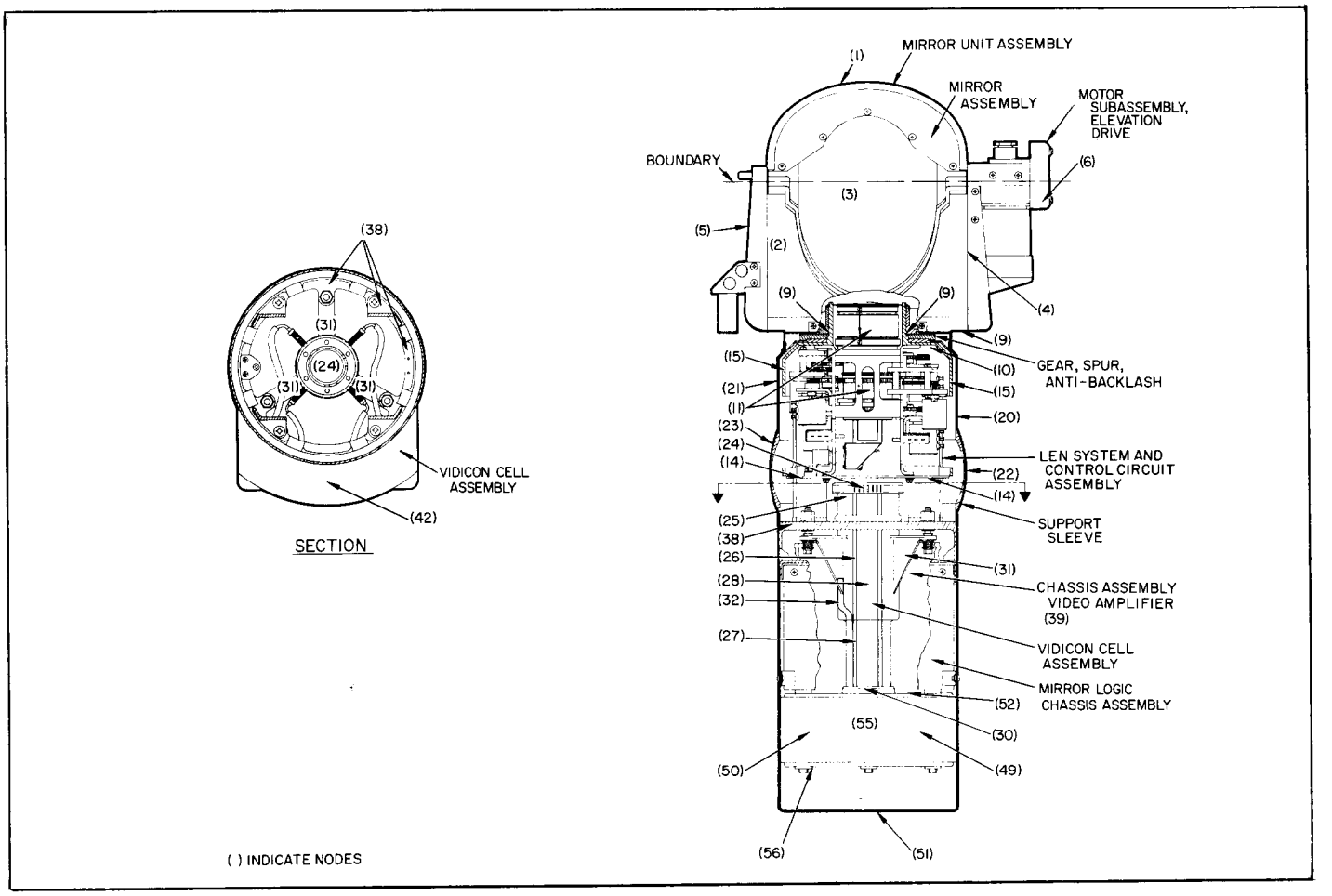

Fig. 21. Location of nodes in survey camera for thermal analysis

CONFIDENTIAL UNCLASSIFIED

UNCLASSIFIED
CONFIDENTIAL

the means whereby the initial conditions can be changed providing the input to study the several phases of the missions.

The final step in providing a thermal model was to translate the model into a computer program. An IBM 7090 computer has been used in conjunction with the thermal model to predict the nodal temperatures during transit for survey Camera 3. For this transit analysis, all nodes were assumed to be initially at 85°F and the spacecraft was assumed to be in its normal transit attitude (survey Camera 3 shielded from solar radiation by the solar panel). Results from some of the more significant nodes are summarized in Table 10. The most rapid rate of temperature decrease occurred on the mirror hood (—33°F/min); the slowest rate of temperature decreases occurred on lower portions of the vidicon tube in the vicinity of the deflection yoke. The thermal model will be verified by correlating data which is to be obtained from the T-21 vehicle solar-thermal-vacuum testing.

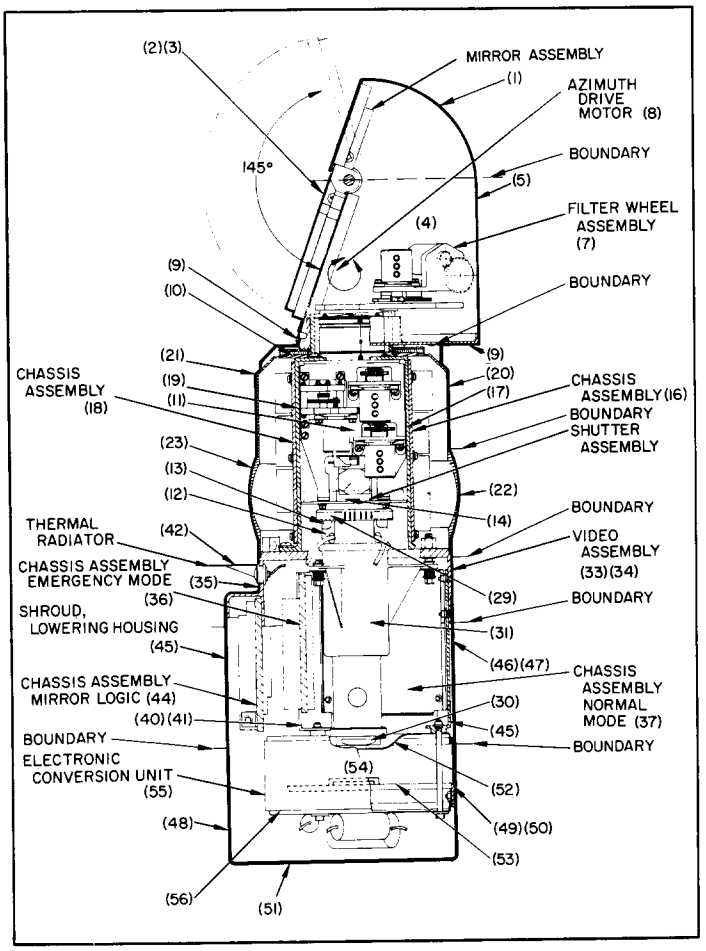

Fig. 21 continued. Location of nodes in survey camera thermal analysis

A more refined thermal model is being defined that will utilize approximately 110 nodes. Each radiation and conduction term will be reevaluated and the choice of the exterior shroud nodes will be optimized by considering the view factors examined for the survey Camera 3. In addition to the more refined model for the survey camera, a thermal model will be defined for the approach camera. Further analysis will be made to study the heating capability of the camera heaters during steady-state transit conditions.

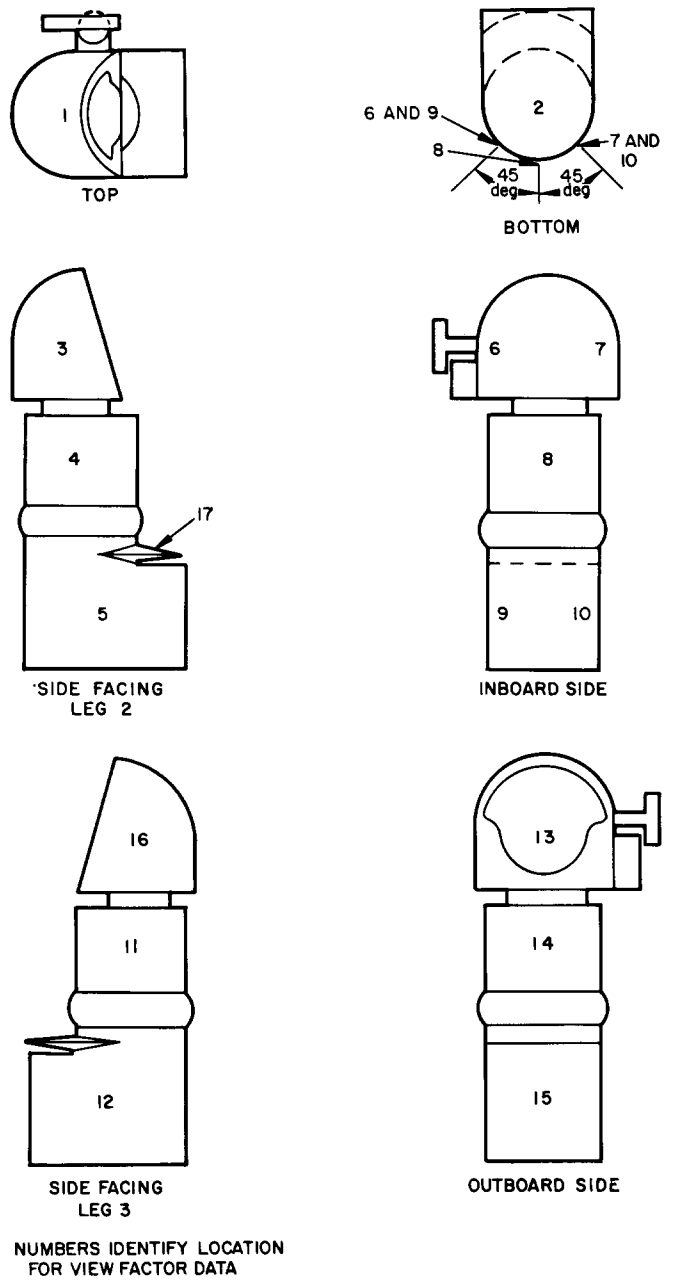

Fig. 22. Form factometer button locations on Camera 3

UNCLASSIFIED
CONFIDENTIAL

CONFIDENTIAL UNCLASSIFIED

Table 9. Camera 3 thermal parameters for A-21 in transit configuration

i	From factometer button location (i)	View factor F_i		Effective thermal properties as seen by element (i) Absorptance (α)	Emittance (ϵ)
1	Top	Solar panel	0.07	0.30 ± 0.02[a]	0.84 ± 0.02
		Spaceframe	0.11	0.18 ± 0.02[b]	0.87 ± 0.02
		Space	0.82	—	1.0
2	Bottom	Spacecraft	0.30	0.18 ± 0.02[b]	0.87 ± 0.02
		TV 4	0.06	0.14 ± 0.02	0.46 ± 0.02
		Blanketed tank	0.04	0.16 ± 0.02	0.66 ± 0.03
		Retro-engine	0.08	0.16 ± 0.02	0.66 ± 0.03
		Space	0.52	—	1.0
3	Leg 2 side	Spaceframe	0.03	0.18 ± 0.02[b]	0.87 ± 0.02
		Space	0.97	—	1.0
4	Leg 2 side	Spacecraft	0.05	0.18 ± 0.02[b]	0.87 ± 0.02
		Space	0.95	—	1.0
5	Leg 2 side	Spacecraft	0.07	0.18 ± 0.02[b]	0.87 ± 0.02
		Space	0.93	—	1.0
6	Hood assembly	Spacecraft	0.28	0.18 ± 0.02[b]	0.87 ± 0.02
		Retro-engine	0.06	0.16 ± 0.02	0.66 ± 0.03
		Space	0.66	—	1.0
7	Hood assembly	Spacecraft	0.25	0.18 ± 0.02[b]	0.87 ± 0.02
		Retro-engine	0.05	0.16 ± 0.02	0.66 ± 0.03
		Space	0.70	—	1.0
8	Inboard side	Spacecraft	0.15	0.18 ± 0.02[b]	0.87 ± 0.02
		Retro-engine	0.08	0.16 ± 0.02	0.66 ± 0.03
		Space	0.77	—	1.0
9	Inboard side	Spacecraft	0.30	0.18 ± 0.02[b]	0.87 ± 0.02
		Retro-engine	0.15	0.16 ± 0.02	0.66 ± 0.03
		Space	0.55	—	1.0
10	Inboard side	Spacecraft	0.15	0.18 ± 0.02[b]	0.87 ± 0.02
		Space	0.85	—	1.0
11	Leg 3 side	Spacecraft	0.40	0.18 ± 0.02[b]	0.87 ± 0.02
		Retro-engine	0.15	0.16 ± 0.02	0.66 ± 0.03
		Space	0.45	—	1.0
12	Leg 3 side	Spacecraft	0.40	0.18 ± 0.02[b]	0.87 ± 0.02
		Retro-engine	0.25	0.16 ± 0.02	0.66 ± 0.03
		Space	0.35	—	1.0
13	Mirror surface	Spacecraft	0.10	0.18 ± 0.02[b]	0.87 ± 0.02
		Retro-engine	0.02	0.16 ± 0.02	0.66 ± 0.03
		Space	0.88	—	1.0
14	Out-board side	Spacecraft	0.05	0.18 ± 0.02[b]	0.87 ± 0.02
		Space	0.95	—	1.0
15	Out-board side	Spacecraft	0.05	0.18 ± 0.02[b]	0.87 ± 0.02
		Space	0.95	—	1.0
16	Hood assembly	Spacecraft	0.32	0.18 ± 0.02[b]	0.87 ± 0.02
		Retro-engine	0.08	0.16 ± 0.02	0.66 ± 0.02
		Space	0.60	—	1.0
17	Vidicon radiator	TV 3	0.30	0.18 ± 0.02[b]	0.87 ± 0.02
		Space	0.70	—	1.0

[a] After 350 solar equivalent hours of ultraviolet exposure, α will increase 0.15.
[b] After 500 solar equivalent hours of ultraviolet exposure, α will increase 0.05 and after 1000 solar equivalent hours α will increase 0.14.

h. Shutter design evaluation test. A design evaluation test (DET) model of the redesigned linear solenoid TV shutter was fabricated and subjected to a thermal-vacuum test equivalent to type approval test (TAT) levels. The schedule of the DET is summarized in Table 11.

Table 10. Camera 3 nodal temperatures during transit

Node description	Maximum rate of temperature fall, °F/min	Temperature, °F After 1 hr	After 10 hr	After 30 hr	After 66 hr
Chassis 1	1.6	16	−131	−155	−156
Chassis 2	1.6	16	−131	−155	−156
Chassis 3	0.8	39	−126	−154	−155
Chassis 4	0.8	40	−126	−154	−156
Chassis 5	0.6	42	−126	−154	−155
Chassis 6	2.8	8	−129	−153	−154
Chassis ECU	0.9	37	−126	−153	−154
Vidicon faceplate	0.9	36	−129	−156	−157
Shutter baseplate	0.9	35	−129	−156	−157
Lens assembly	1.6	21	−131	−156	−157
Mirror baseplate	2.6	4	−134	−158	−159
Elevation drive motor	3.2	−11	−137	−159	−160
Azimuth drive motor	3.1	3	−135	−158	−159

Table 11. Linear solenoid TV shutter thermal-vacuum test operation schedule

No. of cycles	Exposure, msec	Volts applied to control circuit	Desired shutter plate temperature, °F
5000	20	16	+165
5000	150	16	+165
7500	20	22	+165
7500	150	22	+165
2500	20	26	+165
2500	150	26	+165
Check	20 and 150	16	+165
5000	20	16	− 65
5000	150	16	− 65
7500	20	22	− 65
7500	150	22	− 65
2500	20	26	− 65
2500	150	26	− 65
Check	20 and 150	16	− 65

CONFIDENTIAL UNCLASSIFIED

UNCLASSIFIED
CONFIDENTIAL

Prior to thermal-vacuum testing, the shutter was simultaneously operated and vibrated at flight acceptance test (FAT) levels. After vibration, the shutter was operated an additional 1000 cycles and then prepared for thermal-vacuum testing.

Special precautions were taken to ensure a "dry" environment for the shutter during thermal-vacuum testing. In addition to degreasing the shutter prior to installation in the vacuum chamber, an absorption type (molecular sieve) roughing pump, followed by an ion diffusion pump, was selected to produce the required vacuum. This pumping arrangement was used rather than oil diffusion and roughing pumps to avoid extraneous lubrication effects caused by thin oil films forming on moving parts due to minute backstreaming of oil in the pumping system. Thus, in the absence of extraneous lubrication, the shutter moving parts were subjected to maximum wear. The shutter was instrumented with four thermocouples as shown in Fig. 23. Various parts of the shutter are also defined in this photo.

Shutter uniformity of exposure was measured by allowing light to pass through three narrow slits in the shutter plane. The light falls on photo sensors that generate the timing signals. Digital timers were provided to accurately measure the exposure time at each slit. At selected times during the DET, simultaneous readings were taken of exposure times at the leading and trailing slits for each of ten exposures. The results, as shown for typical measurements in Table 12, indicate that the exposure difference between slits never exceeds 0.61 msec. The design requirment is that exposure uniformity shall be less than 1 msec. In addition, the data shows that the time of exposure does not vary significantly as the voltage is changed from the limits of 16 to 26 v applied to the input driving circuits. This can be seen by comparing the average exposure times as a function of voltage; i.e., 18.24 versus 18.31 msec and 18.40 versus 18.87 msec at 26 and 16 v, respectively.

Several anomalies occurred during the testing. At high temperature the B1 solenoid coil which drives the shutter Blade B during the retrace stroke shorted and was inop-

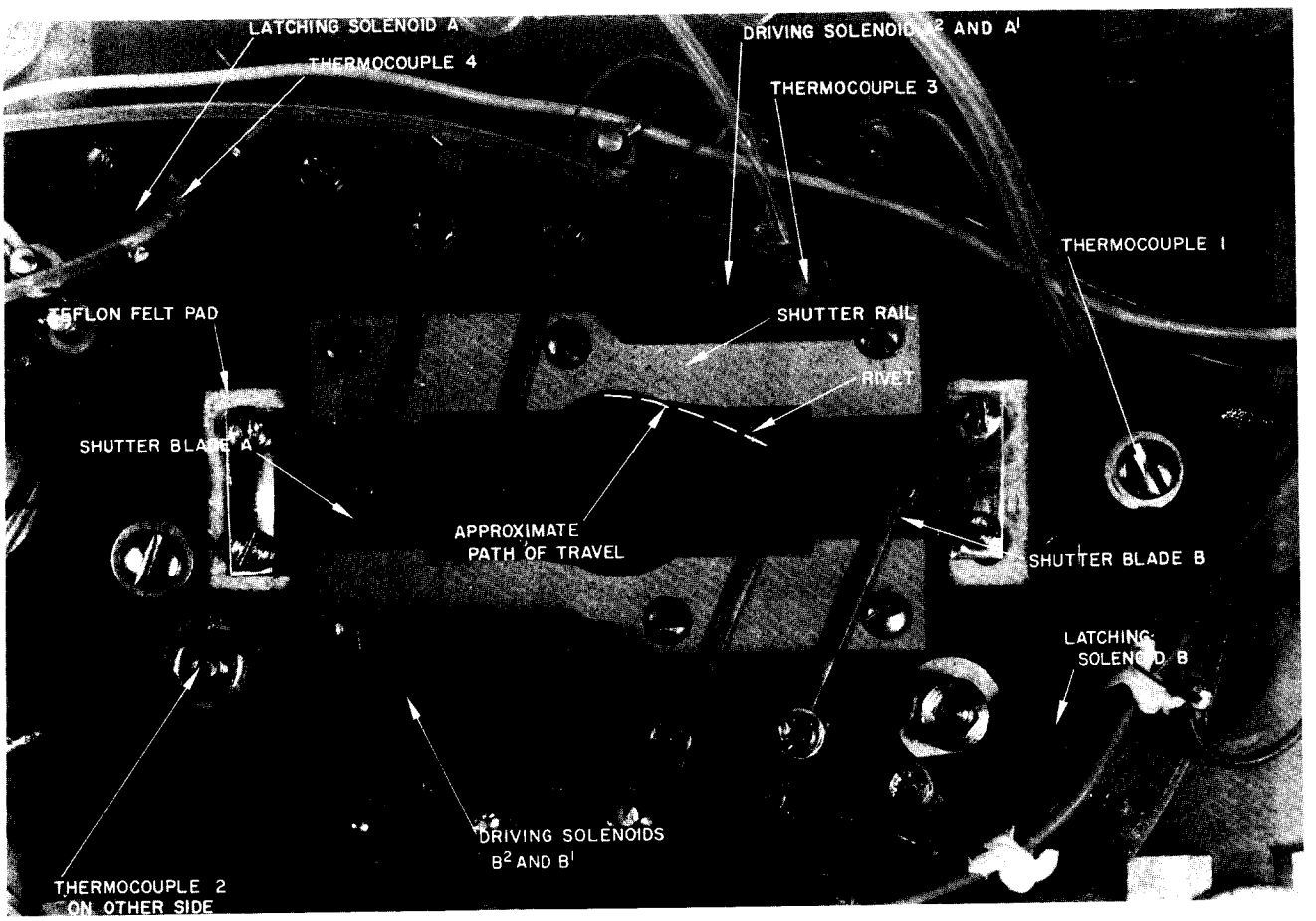

Fig. 23. Design evaluation test shutter

CONFIDENTIAL
UNCLASSIFIED

UNCLASSIFIED
CONFIDENTIAL

Table 12. Shutter exposure time
Temperature ≈ 165°F

Lead slit, msec	Lag slit, msec	Δt, msec
	Voltage = 16v	
18.44	18.96	0.52
18.26	18.71	0.45
18.10	18.40	0.30
18.23	18.64	0.41
18.25	18.73	0.48
18.27	18.76	0.49
18.19	18.60	0.41
18.60	19.09	0.49
18.28	19.79	0.61
18.50	19.02	0.52
18.31 average	18.87 average	
	Voltage = 26 v	
18.17	18.29	0.12
18.27	18.27	0.0
18.33	18.57	0.24
18.23	18.46	0.23
18.16	18.29	0.13
18.25	18.43	0.18
18.41	18.55	0.14
17.99	18.18	0.19
18.07	18.33	0.26
18.49	18.59	0.10
18.24 average	18.40 average	

erative. Thus the trailing Blade A was required to push the leading Blade B during retrace. Each drive solenoid consists of two coils. One coil is energized during exposure while the other is energized during retrace. The shutter operated properly during exposure.

An input of 14 v was adequate to push the Blade B at the beginning of the test. However, a voltage in excess of 16 v was required to accomplish the retrace action at the conclusion of the test. Satisfactory operation of the shutter was demonstrated at the conclusion of testing, however, by demonstrating exposure at 16 v and proper operation of Blade A at 14 v. The shorted coil permitted demonstration of adequate design margin, since two blades were pushed by a single solenoid, and operation would have been satisfactory even though the solenoid was defective.

During the low temperature portion of the test, exposure time became shorter and backflash was observed. Backflash occurs during the retrace stroke when the overlapping shutter blades no longer overlap resulting in a secondary exposure. The backflash observed during the test was considered small and was later determined to be caused by inadequate clearance between a rivet head on the A shutter blade and the edge of the rail in which the shutter blade rides. Fig. 23 shows a similar area on shutter Blade B and its rail which operated properly during the test. The rivet is used to control the overlap of the two shutter blades during retrace. It travels in an arc governed by the driving and latching arms. The initial clearance between the rivet and the rail was inadequate during assembly. The slight wear that occurred during the first 30,000 cycles of operation apparently eliminated the initial clearance. Adequate clearance has subsequently been provided.

After 78,000 cycles of operation, one of the pins holding a latch solenoid armature to the latch arm dropped out when the shutter was inverted. This was considered as a failure due to improper installation. Similar difficulties were experienced during initial assembly of the shutter. The pin on the other latch coil is identical and did not fail. After 189,000 cycles of operation, one of the brass rivets holding the leading shutter blade (during the exposure stroke) to its activating arm failed from fatigue in shear. This was considered a wear-out failure. The rivet was replaced and the test continued. At present the shutter has completed over 131,000 additional cycles without additional failures. This brings the total cycles to over 320,000. The design goal is to provide a life time of 60,000 cycles for the shutter. In summary, the performance of the design evaluation test shutter indicates that the design is now adequate.

CONFIDENTIAL
UNCLASSIFIED

UNCLASSIFIED
CONFIDENTIAL

C. System Analysis

1. Introduction

The analytical work reported in this section covers four main categories: (1) spacecraft guidance and trajectory, (2) trajectory computer programming, (3) mission analysis, and (4) system performance. The first category includes a study of tracking system and *Centaur* interfaces with the spacecraft. Mission analysis includes a study of operational requirements and sequences, mission management requirements, and engineering data needs. System performance analysis includes maintenance of system specifications, determination of certain system test requirements, and formulation of emergency mode operations.

2. Effect of Velocity Distribution on Vernier Propellant Requirements

A study was conducted on the effects of various midcourse velocity distributions on the total required vernier propellant. The *Surveyor* Monte Carlo Vernier Propellant Calculation Program was employed for the analysis. This program is a simplified transit mission simulation that functions essentially as follows. In each cycle, a critical planes midcourse velocity correction is selected from an arbitrary bivariate Gaussian distribution; vernier propellant requirements are computed on the basis of a randomly selected specific impulse error. In the terminal phase, all major error sources are considered and sampled from appropriate distributions: vernier thrust levels during the main retro phase, propellant specific impulse, main retro burning time, burnout velocity and altitude, mixture ratio, and touchdown dispersions. The resultant output is the probability of sufficient fuel and oxidizer with loading ratio and total loaded propellant as parameters.

Best estimate values of constants and errors of the spacecraft employing the Rocketdyne vernier engine system (formerly considered for use on *Surveyor*) were used for the terminal descent phase; the parameters of the midcourse distributions were varied in the study as discussed, with effects on the total vernier propellant requirements as reported here.

Two criteria for choosing a vernier propellant loading were considered. The first was to follow the present design specification, by selecting the fuel loading that provides for 99% of all errors (primarily in the terminal descent phase) when a maximum (3σ) midcourse correction (30 m/sec for A-21A, 50 m/sec for A-21) is made. The second criterion was to select the fuel loading which will provide for 99% of all flights, i.e., the midcourse correction is combined statistically with the terminal phase errors. Clearly, the second criterion will result in a lower fuel requirement than the first and, hence, is a less conservative design. This latter approach was employed in Reference 1.

In the Monte Carlo Vernier Propellant Calculation Program (Reference 2), the critical plane midcourse velocity correction is generated from the relation

$$V_{MC} = 3.28083\sqrt{(\sigma_1 y_1 + \mu_1)^2 + (\sigma_2 y_2 + \mu_2)^2}$$

where

V_{MC} = magnitude of the correction (ft/sec).

3.28083 = conversion from meters to feet.

μ_1, σ_1 = average value and 1σ value of one component of the correction (m/sec).

μ_2, σ_2 = average value and 1σ value of the correction orthogonal to μ_1 (m/sec).

y_1, y_2 = Gaussian random variables with unit variance and zero mean.

A fixed midcourse correction (non-random) can be obtained by setting the σs equal to zero; a Rayleigh distribution is obtained when $\sigma_1 = \sigma_2$ and $\mu_1 = \mu_2$; a "half Gaussian" distribution is obtained when $\mu_1 = \mu_2 = \sigma_2 = 0$; and other combinations can be obtained by adjusting the σs and μs. The figure of merit of the correction is

$$\sqrt{\sigma_1^2 + \sigma_2^2}$$

Since the midcourse velocity correction (V_{MC}) can only be positive, the simulation in effect folds back the negative half of a distribution and adds it to the positive half.

Fig. 24 shows a Gaussian distribution with mean $\mu = 0$. Here x may represent an injection coordinate error and f(x) the probability density function of the error. In Fig. 25, the corresponding "half Gaussian" distribution is shown where the negative portion of the Gaussian distribution has been added to the positive portion. Here x could be the midcourse correction in m/sec and g(x) the probability density function of the correction.

Fig. 26 illustrates a similar case for a Gaussian distribution with mean $\mu \neq 0$. Its non-negative counterpart, shown in Fig. 27 was referred to in this study as a quarter-Gaussian distribution.

Fig. 28 shows a plot of the four midcourse probability density functions discussed above for an actual propellant analysis with a midcourse maneuver of 30 m/sec correcting for 99% of the injection errors. The fixed mid-

CONFIDENTIAL
UNCLASSIFIED

UNCLASSIFIED

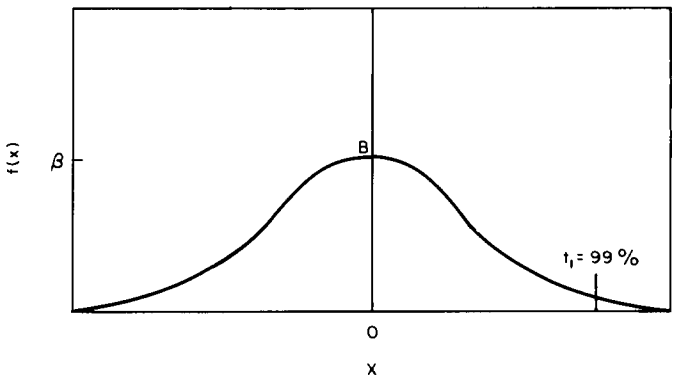

Fig. 24. Gaussian distribution with mean = 0

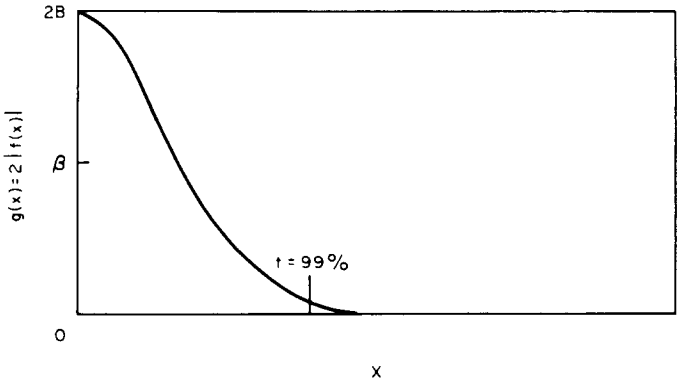

Fig. 25. Half-Gaussian distribution

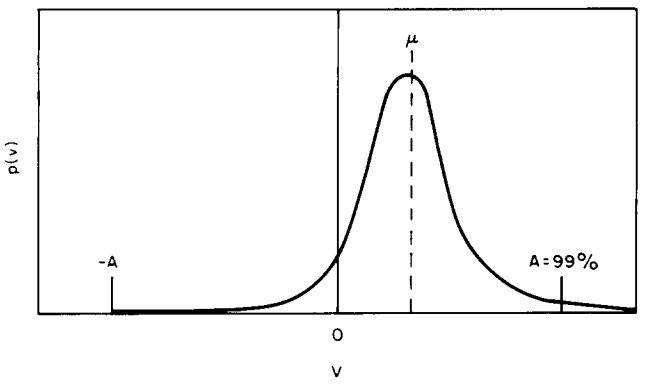

Fig. 26. Gaussian distribution with $\mu \neq 0$

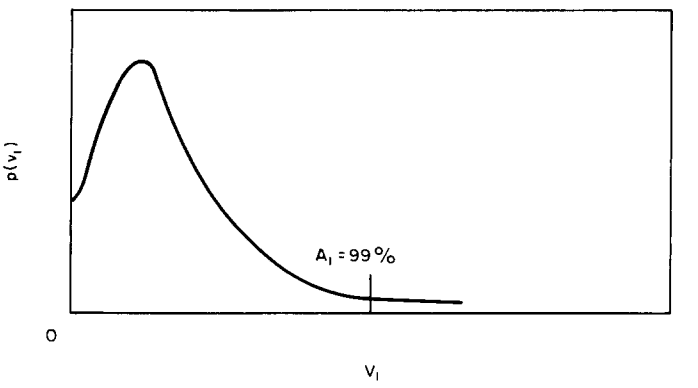

Fig. 27. Quarter-Gaussian distribution

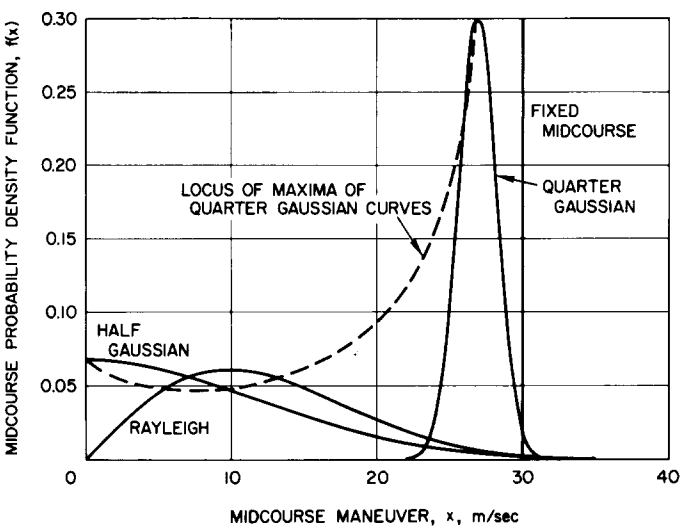

Fig. 28. Midcourse probability density functions for 99% midcourse maneuver = 30 m/sec

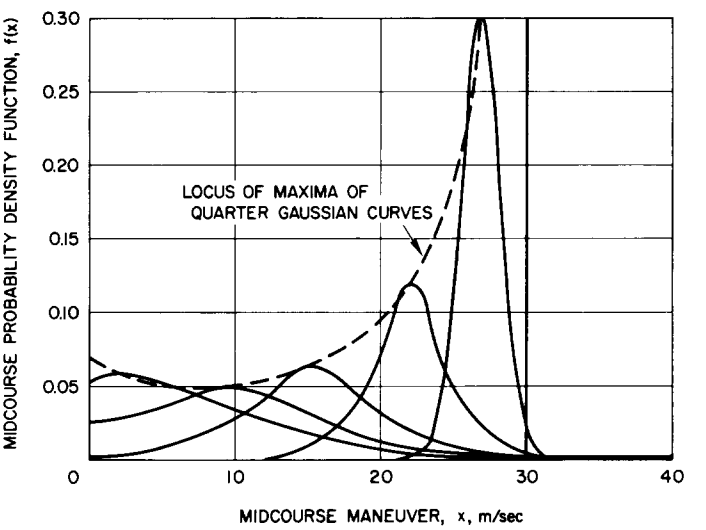

Fig. 29. Several quarter-Gaussian distributions for 99% midcourse maneuver of 30 m/sec

UNCLASSIFIED

UNCLASSIFIED CONFIDENTIAL

course maneuver is an impulse function at 30 m/sec whose area is equal to that under the other curves. The quarter-Gaussian case shown is only one of an infinite number which can be chosen. This one was chosen for the figure because of its similarity to a realistic model of a midcourse maneuver. It can be seen that if the mean and 1σ value of the quarter-Gaussian distribution were varied, keeping the 99% point fixed, every situation between the fixed midcourse and the Rayleigh and Gaussian distributions can be simulated.

For a clearer understanding of quarter-Gaussian distribution, several distributions are shown in Fig. 29. It should be noted that the quarter-Gaussian distribution no longer represents a midcourse correction in the critical plane only. Its derivation has no direct physical significance with respect to injection errors. The reason for including it in this study is because it forms an approximation of an actual midcourse correction dispersion and so midcourse maneuvers of any mean and variance can be studied.

Fig. 30 shows midcourse probability density functions for the three main 99% corrections used in this study. These 99% corrections are 15, 30, and 50 m/sec.

The results of this study show the weight of vernier propellant[a] in pounds required to correct for 99% of all error dispersions assuming various midcourse velocity correction distributions. These results are shown in Table 13.

Two graphs illustrate these results. The first, Fig. 31, shows the weight of vernier propellant required as a function of 99% midcourse corrections for three cases: fixed midcourse, Rayleigh, and half-Gaussian distributions. Similar lines could have been drawn between fixed midcourse and half-Gaussian cases to depict the quarter-Gaussian cases if more data had been obtained.

The second graph, Fig. 32, shows the weight of vernier propellant as a function of the normalized means of the various distributions for 99% midcourse maneuvers of 15, 30, and 50 m/sec. The mean in this report refers to the mean of the Gaussian distribution before the negative portion was folded over and added to the positive portion of the curve. Thus in Fig. 32 the Rayleigh results cannot be plotted. A normalized mean of 1.0 represents a fixed midcourse correction, one of 0.0 a half-Gaussian distribution, and the points in between are quarter-Gaussian distributions.

Both graphs show that the fixed midcourse maneuver requires the maximum amount of propellant and the half-Gaussian requires the least. A Rayleigh distribution re-

[a] The weight of vernier propellant used in this report is the total weight required minus contingency and unusables.

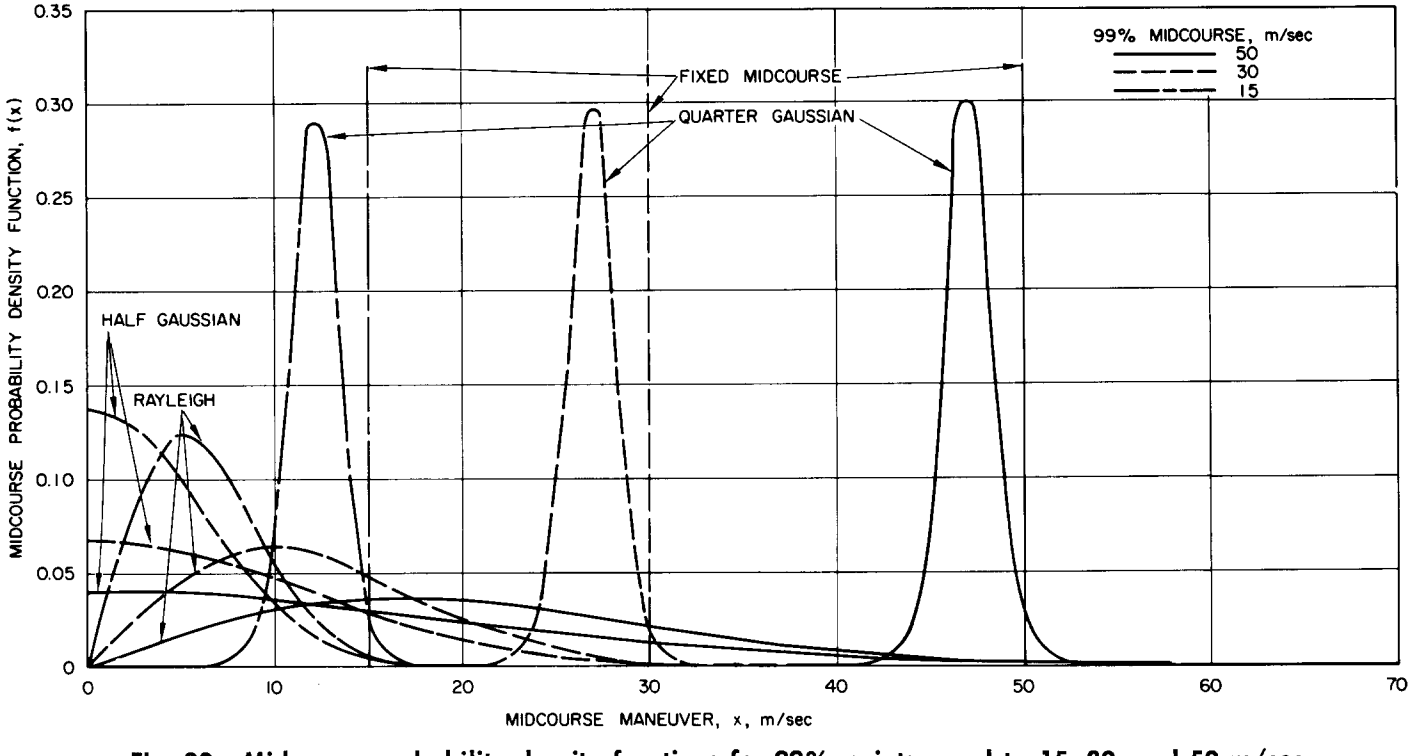

Fig. 30. Midcourse probability density functions for 99% points equal to 15, 30, and 50 m/sec

CONFIDENTIAL UNCLASSIFIED

UNCLASSIFIED CONFIDENTIAL

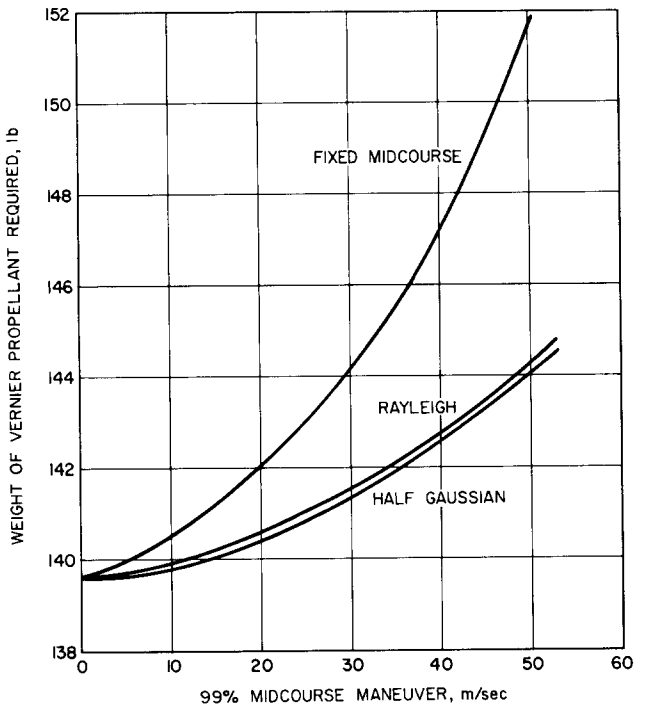

Fig. 31. Weight of vernier propellant versus midcourse maneuver for three midcourse maneuver dispersions

quires slightly more propellant than the half-Gaussian case with the quarter-Gaussian falling in between the half-Gaussian and fixed midcourse maneuvers. Also, the amount of propellant required increases nonlinearly with the 99% midcourse maneuver.

It is interesting to note the relatively small amount of additional propellant required to greatly increase the midcourse maneuver capability when a half-Gaussian or Rayleigh distribution is assumed. For example in Fig. 31, approximately 4 additional lb of propellant are required for a 99% midcourse maneuver of 50 m/sec as opposed to one of 15 m/sec. Approximately 10 additional lb are required for the same increase in capability when designing for a fixed midcourse maneuver.

The rms magnitude of the midcourse correction can be defined using the three components of the midcourse correction velocity. However, this study was concerned only with a critical plane midcourse correction and thus with two dimensions. Given V as a column matrix of the midcourse correction velocity components

$$V = \begin{bmatrix} V_1 \\ V_2 \end{bmatrix}$$

Table 13. Vernier propellant requirement to correct for 99% of launch vehicle guidance errors assuming various error dispersions

Distribution	Propellant weight, lb													
	99% dispersion, m/sec													
	5	10	10.72	12.875	15	16.667	21.45	25.75	30	32.2	35.8	38.6	42.8	50
Fixed midcourse	140.0	140.60			141.22	141.50			144.20					151.63
Quarter Gaussian														
$\mu_1 = 11.9, \sigma, = 1.333$					140.79									
$\mu_1 = 10, \sigma, = 2.147$					140.92									
$\mu_1 = 5.692, \sigma, = 4$					140.64									
$\mu_1 = 5, \sigma, = 4.29$					140.64									
$\mu_1 = 26.9, \sigma, = 1.333$									143.41					
$\mu_1 = 20.692, \sigma, = 4$									142.80					
$\mu_1 = 20, \sigma, = 4.29$									142.79					
$\mu_1 = 10, \sigma, = 8.67$									142.00					
$\mu_1 = 46.9, \sigma, = 1.333$														150.09
$\mu_1 = 40.692, \sigma, = 4$														148.67
$\mu_1 = 30, \sigma, = 8.67$														146.50
$\mu_1 = 15, \sigma, = 15.02$														145.43
Rayleigh			140.36		140.45		140.87		141.49	141.69	142.2			144.29
Half Gaussian				139.93	139.86			141.08	141.34			142.57	143.00	144.08

Note: For propellant weights, tenths and hundreds of a pound are not significant, as variations of ½ lb can be expected depending on the particular random sequence selected in the Monte Carlo simulation.

UNCLASSIFIED CONFIDENTIAL

UNCLASSIFIED CONFIDENTIAL

then Λ_v is the 2×2 covariance matrix of the midcourse correction velocity components where

$$\Lambda_v = \begin{bmatrix} \sigma_1^2 & \rho_{12}\,\sigma_1\sigma_2 \\ \rho_{12}\,\sigma_1\sigma_2 & \sigma_2^2 \end{bmatrix}$$

In using the rms criterion, only the Gaussian and Rayleigh distributions were studied. For each of these distributions, a graph was drawn showing the effect of launch vehicle guidance accuracy on the amount of vernier propellant required. These graphs, Fig. 33 and 34, show the cumulative vernier propellant distribution function and seem to be compatible with the work done by Thornton (Reference 2).

3. *Effect of Increasing Main Retro Separation Time on Terminal Descent Parameters*

The main retro separation phase is initiated by a 3.5 Earth g sensing switch during the main retro tailoff. After an 8.125 sec timed delay (main retro separation time) starting at the 3.5-g point, the main retro separation bolts are exploded. Under most conditions the 8.125 sec delay is sufficient time for the main retro thrust to decrease to a value that allows clean separation of the ejected retro case from the spacecraft. If it is necessary to increase the probability of clean retro separation above the present value, one method of achieving this is by increasing the main retro separation time. This increase in delay time decreases the expected retro thrust at the time the separation bolts are exploded.

Fig. 35 is a plot of variations in dry landed weight, main retro and vernier propellant loading, and main retro ignition range as a function of main retro separation time.

Main retro propellant weight variations are well within the qualification limits and main retro ignition range for the worst case impact angle (45 deg) is well within the

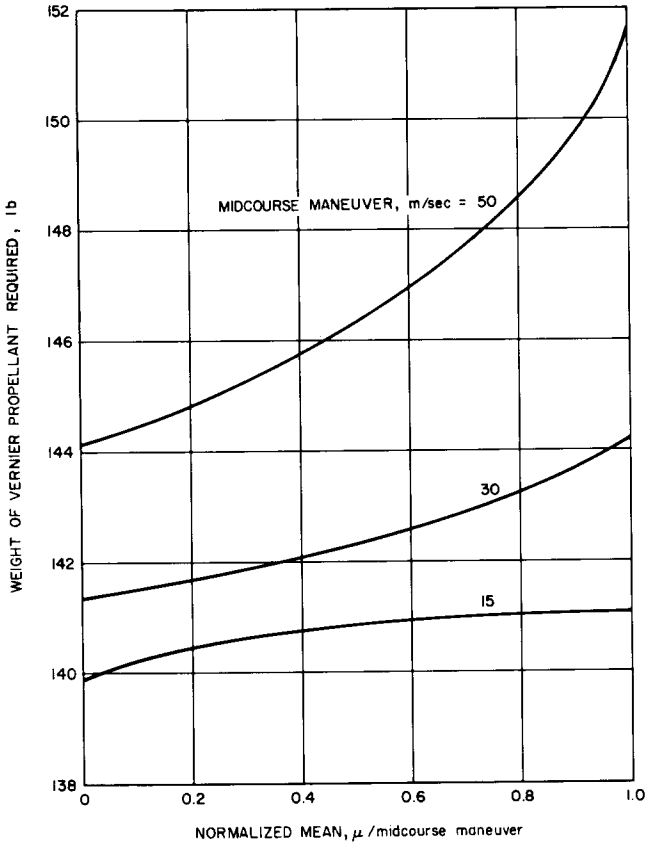

Fig. 32. Weight of vernier propellant versus normalized means of various distributions for three midcourse maneuvers

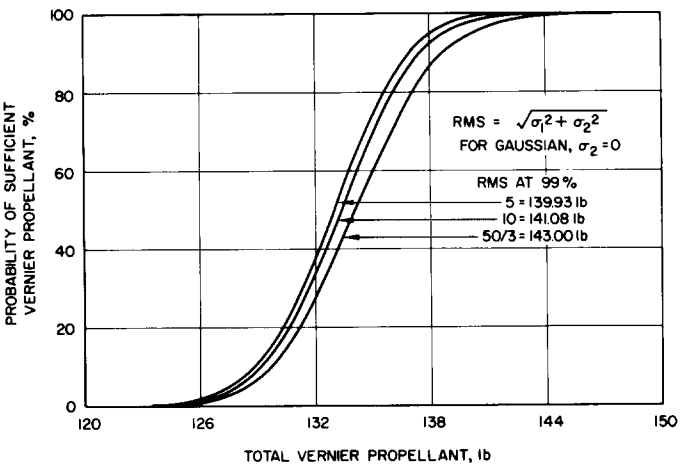

Fig. 33. Effect of launch vehicle guidance accuracy assuming Gaussian distribution

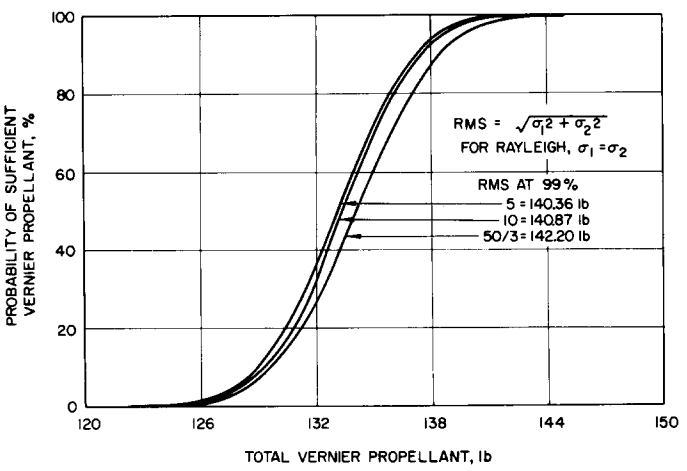

Fig. 34. Effect of launch vehicle guidance accuracy assuming Rayleigh distribution

CONFIDENTIAL UNCLASSIFIED

UNCLASSIFIED

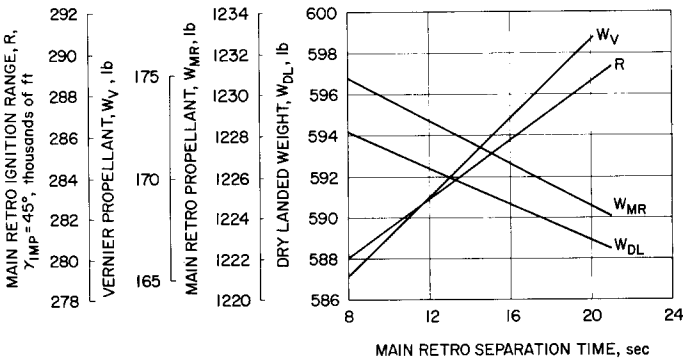

Fig. 35. Effects of main retro separation time

marking radar limit of 60 mi. The cost in dry landed weight (payload) is approximately 0.4 lb/sec increase in separation delay time.

4. Estimate of Landing Location Accuracy

The *Surveyor* landing location accuracy is primarily a function of tracking error, spacecraft mechanization errors, execution time error, and magnitude of the velocity correction. The transit phase Monte Carlo simulation computer program simulates these error sources, except for the execution time error. (Execution time errors are discussed in Reference 3.)

A computer run of 500 Monte Carlo cycles was run for a vertical impact trajectory with injection errors, tracking errors, and midcourse execution errors given by the covariance matrices shown in Table 14. The injection and tracking errors are errors in the state vector: the first three elements are position coordinates x, y, z (km) and the last three are velocity coordinates, $\dot{x}$, $\dot{y}$, $\dot{z}$ (km/sec).

The execution error model assumes bias and proportional errors in the absolute velocity of the midcourse correction and in the two angular maneuvers. Thus, the diagonal elements of the injection error covariance matrix are, respectively, the variances of:

(1) Bias in velocity.

(2) Error proportional to velocity.

(3) Bias in roll.

(4) Error proportional to roll.

(5) Bias in pitch (or yaw).

(6) Error proportional to pitch (or yaw).

The midcourse logic used in the program corrects miss and chooses a $\dot{U}_3$ component which is a function of time of flight, burnout velocity and fuel margin (see Reference 4). This midcourse logic together with the errors assumed in Table 14 results in the following midcourse maneuver statistics:

Average critical plane maneuver = 15.1 m/sec

99% critical plane maneuver = 44.6 m/sec

Average total midcourse maneuver = 35.3 m/sec

99% total midcourse maneuver = 49.7 m/sec

Average $\dot{U}_3$ = −26.7 m/sec

Minimum $\dot{U}_3$ = −41.6 m/sec

Maximum $\dot{U}_3$ = 17.9 m/sec

The covariance matrix of the B·T and B·R components of B-plane miss, calculated from 500 Monte Carlo cycles is

	B·T	B·R
B·T	683.1	−164.2
B·R	−164.2	440.8

From this covariance matrix, standard deviations of these components, and of the semi-major and semi-minor axis are found to be:

$$\sigma_{B\cdot T} = 26.1 \text{ km}$$

$$\sigma_{B\cdot R} = 21.0 \text{ km}$$

$$\sigma_{SMA} = 26.3 \text{ km}$$

$$\sigma_{SMI} = 20.3 \text{ km}$$

Letting $B = \sqrt{(B\cdot T)^2 + (B\cdot R)^2}$ be the total miss, the average total miss is

$$\bar{B} = 29.2 \text{ km}$$

UNCLASSIFIED CONFIDENTIAL

UNCLASSIFIED
CONFIDENTIAL

Table 14. Error covariance matrices

Injection error covariance matrix						
	X	Y	Z	$\dot{X}$	$\dot{Y}$	$\dot{Z}$
X	2.8365906E 00	2.7127827E-01	−1.5353842E 00	1.0350438E-02	−1.8261604E-04	−5.8400184E-03
Y	2.7127827E-01	9.2455901E 00	1.9684962E 00	−8.3310649E-03	4.2776321E-02	8.7400472E-03
Z	−1.5353842E 00	1.9684962E 00	6.9555037E 00	−1.1085860E-02	1.3111059E-02	2.5450447E-02
$\dot{X}$	1.0350438E-02	−8.3310649E-03	−1.1085860E-02	5.3703215E-05	−4.9132419E-05	−4.8878260E-05
$\dot{Y}$	−1.8261604E-04	4.2776321E-02	1.3111059E-02	−4.9132419E-05	2.2004904E-04	5.5308621E-05
$\dot{Z}$	−5.8400184E-03	8.7400472E-03	2.5450447E-02	−4.8878260E-05	5.5308621E-05	1.0598767E-04
Tracking error covariance matrix						
	X	Y	Z	$\dot{X}$	$\dot{Y}$	$\dot{Z}$
X	3.0304630E 01	6.0200336E 00	−1.8058121E 00	4.6083813E-04	2.7531973E-04	−2.5892022E-04
Y	6.0200336E 00	4.6286833E 00	−6.8653917E 00	8.2026986E-05	7.4131152E-05	−1.1089506E-04
Z	−1.8058121E 00	−6.8653917E 00	1.2721119E 01	−2.5490578E-06	−4.2688253E-05	1.1695659E-04
$\dot{X}$	4.6083813E-04	8.2026986E-05	−2.5490578E-06	7.4195237E-09	4.6333960E-09	−4.4606150E-09
$\dot{Y}$	2.7531973E-04	7.4131152E-05	−4.2688253E-05	4.6333960E-09	3.2823698E-09	−3.5737860E-09
$\dot{Z}$	−2.5892022E-04	−1.1089506E-04	1.1695659E-04	−4.4606150E-09	−3.5737860E-09	4.5299886E-09
Midcourse execution error covariance matrix						
	V	KV	θ	Kθ	ϕ	Kϕ
V	2.1800000E-09	0.	0.	0.	0.	0.
KV	0.	1.0900000E-05	0.	0.	0.	0.
θ	0.	0.	1.0900000E-05	0.	0.	0.
Kθ	0.	0.	0.	7.2250000E-07	0.	0.
ϕ	0.	0.	0.	0.	1.0900000E-05	0.
Kϕ	0.	0.	0.	0.	0.	7.2250000E-07

The 99% miss circle has radius

$$B_{0.99} = 75.6 \text{ km}$$

To convert to landing-site errors, it is only necessary to apply the proper focusing factor. Since this factor is approximately 0.64 for a vertical impact trajectory, the radius of the circle containing 99% of the landings is 48.4 km. The landing location error for a trajectory having a 45 deg incidence angle can be found by assuming a 0.92 focusing factor. This results in a 99% landing location circle of radius 69.5 km.

5. Television Synchronization Analysis

The *Surveyor* television subsystem presently utilizes a threshold leading edge detector for horizontal synchronization, with vertical sync derived from these horizontal sync pulses.

This method of sync detection is adequate with respect to sync jitter for values of predetection (signal-to-noise

CONFIDENTIAL
UNCLASSIFIED

UNCLASSIFIED
CONFIDENTIAL

ratio) presently specified for television operation (+11.5 db rms/rms minimum).

However, retrieval of useful information may be possible at lower signal-to-noise ratios than this, extending down to −10 db rms/rms in the predetection bandwidth, for the wide-band FM television link. The corresponding postdetection sync signal-to-noise ratio results in excessive horizontal jitter, with this non-coherent type of detection process. For this reason, a sampled-data phase lock loop detector was constructed for incorporation into the existing television ground data handling system. In order to obtain the very small values of horizontal jitter proposed, additional preconditioning of the sync signal is anticipated. This may take the form of sync tip filtering in the predetection bandwidth or similar signal-to-noise ratio improvement techniques.

The following analysis treats this basic coherent type of detector, relating horizontal sync jitter to its loop parameters such as bandwidth and gain.

a. Equivalent mathematical model. In this study, some properties of the sample data phase lock loop shown in Fig. 36 were investigated.

The input is a periodic series of horizontal sync pulses, as shown in Fig. 37.

The modified pulse generator produces the wave form of Fig. 38.

If q(t) is the single-pulse train shown in Fig. 39,

then

$$g(t) = q(t) - q(t - T_1/2) \tag{1}$$

The behavior of the loop when the input pulse train and VCO output are time shifted in respect to each other was first considered. Let the input pulse train be delayed by ρ and the VCO output by Δ. The objective of the loop then is to attempt to reduce the error $\epsilon = \rho - \Delta$. The output of the multiplier and integrator is thus

$$\phi(T) = \int_{\Delta}^{T_1+\Delta} P(t-\rho)\, g(t-\Delta)\,dt + \int_{\Delta}^{T_1+\Delta} n(t)\, g(t-\Delta)\,dt \tag{2}$$

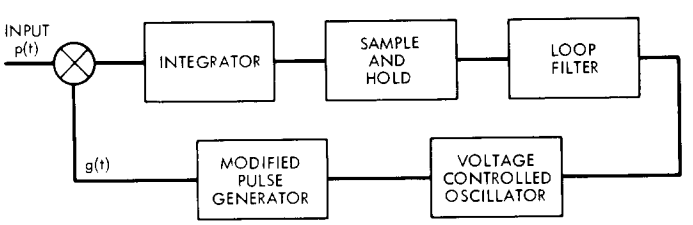

Fig. 36. Sample data phase lock loop

The first integral involves the input pulse signal in Fig. 37 and is therefore

$$k\int_{\Delta}^{T_1+\Delta} P(t-\rho)\, q(t-\Delta)\,dt - k\int_{\Delta}^{T_1+\Delta} P(t-\rho)$$

$$q(t-\Delta-T_1/2)dt = T_1 k\left\{\frac{1}{T_1}\int_{0}^{T_1} P(x+\Delta-\rho)\right.$$

$$\left. q(x)dx - \frac{1}{T_1}\int_{0}^{T_1} P(x+\Delta-\rho)\, q(x-T_1/2)dx\right\} \tag{3}$$

If the cross correlation between P(t) and q(t) is defined as

$$R_{pq}(\tau) = \frac{1}{T_1}\int_{0}^{T_1} P(x+\tau)\, q(x)dx \tag{4}$$

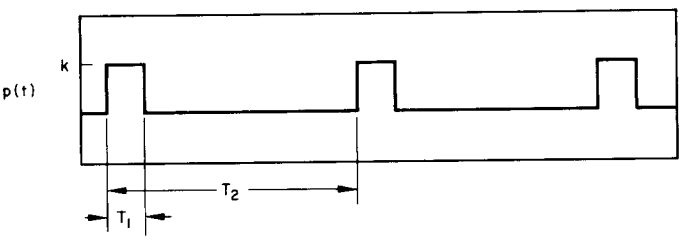

Fig. 37. Input sync pulse

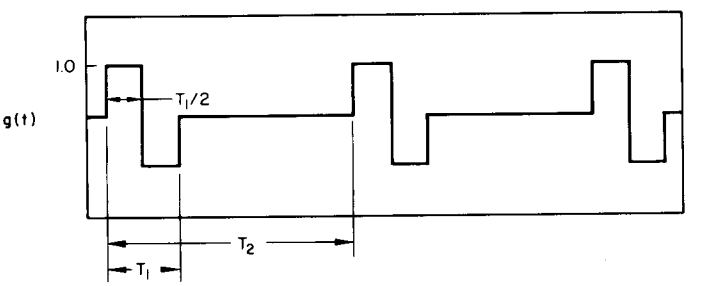

Fig. 38. Modified pulse generator wave form

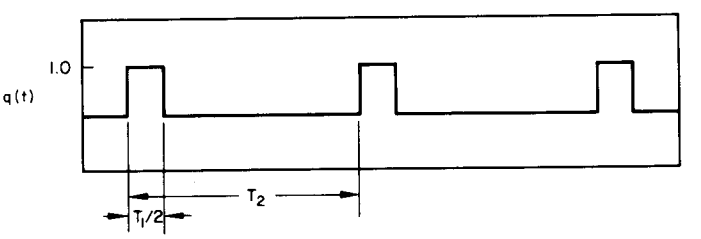

Fig. 39. Single pulse train, q (t)

UNCLASSIFIED
CONFIDENTIAL

UNCLASSIFIED
CONFIDENTIAL

then Equation 3 can be rewritten

$$T_1 k \left\{ R_{pq}(\Delta - \rho) - R_{pq}\left(\Delta - \rho + \frac{T_1}{2} \right) \right\} \qquad (5)$$

For the pulse signals assumed, the above expression has the form shown in Fig. 40, which is periodic in $\Delta - \rho$, repeating at the frequency of the VCO modified pulse train. If ϵ denotes $\Delta - \rho$, then the above function plots the output of the integrator at time T_1 in terms of the time error existing between the input and VCO pulse functions. If the above function is called $D(\epsilon)$, then

$$\begin{aligned} D(\epsilon) &= k \quad |\epsilon| < T_1/2 \\ &= -k \quad T_1 > |\epsilon| > T_1/2 \\ &= 0 \quad T_1 < |\epsilon| \end{aligned} \qquad (6)$$

Hence, the multiplier and integrator can be replaced by a mathematical block wnich yields an output, at completion of integration, given by $D(\epsilon)$. Note that $D(\epsilon)$ is linear for small time differences and acts as an open circuit if $|\epsilon| > T_1$. It must be remembered that it has been assumed that Δ and ρ have not changed during the integration period; however, they may change from period to period.

The second integral in Equation 2 represents the effect of noise at completion of integration, and has the form

$$y_n(T_1, \Delta) = \int_{\Delta}^{T_1 + \Delta} n(t)\, g(t - \Delta)\, dt \qquad (7)$$

$$= \int_0^{T_1} n(x + \Delta)\, g(x)\, dx \qquad (8)$$

If the noise is stationary, the effect of shifting Δ can be eliminated. Therefore

$$y(T_1) = \int_0^{T_1} n(x)\, g(x)\, dx$$

$$= \int_0^{T_1} n(x)\, q(x)\, dx - \int_0^{T_1} n(x)\, q(x - T_1/2)\, dx \qquad (9)$$

The $y(T_1)$ is assumed Gaussian with zero mean and has variance

$$\overline{y^2(T_1)} = \int_0^{T_1} \int_0^{T_1} q(x)\, q(s)\, \overline{n(x)\, n(s)}\, dx\, ds + \int_0^{T_1} \int_0^{T_1} q(x - T_{1/2})\, q(s - T_1/2)\, \overline{n(x)\, n(s)}\, dx\, ds \qquad (10)$$

where the bar denotes averaging. The fact that $q(x)\, q(x - T_1/2) = 0$ eliminates the third term above. Under the assumption of white noise, $\overline{n(x)\, n(s)} = N_o\, \delta(x - s)$ where N_o is the two sided noise level in watts per cps, and substitution yields

$$\begin{aligned} \overline{y^2(T_1)} &= N_o \int_0^{T_1} q^2(x)\, dx + N_o \int_0^{T_1} q^2(x - T_1/2)\, dx \\ &= N_o T_1 \qquad \text{(v-sec)}^2 \end{aligned} \qquad (11)$$

It is concluded that the output of the integrator after complete integration is

$$\phi(T_1) = D(\epsilon) + y(T_1) \qquad \text{v-sec} \qquad (12)$$

where $y(T_1)$ is a Gaussian random variable of variance $N_o T_1$. The instantaneous sample value of $\phi(T_1)$ is then held, filtered by the loop filter, and used to control the time shift of the VCO. The overall system can therefore be represented by the equivalent mathematical model shown in Fig. 41.

The system is basically a negative feedback sampled data loop for an equivalent input composed of the time shift of the input pulse train. The error ϵ is the timing difference between the received and locally generated pulse trains. Noise enters equivalently as a perturbation of the sample value held by the sample and hold network. This perturbation leads to a jitter effect in the

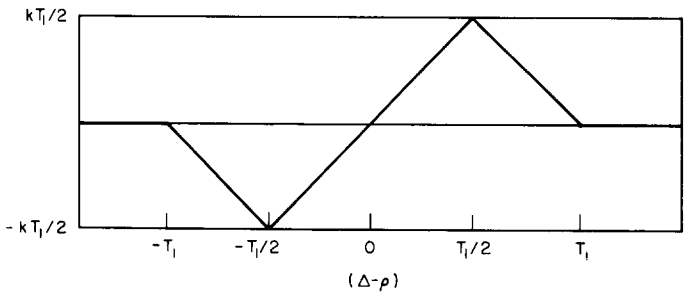

Fig. 40. Form of Equation 5

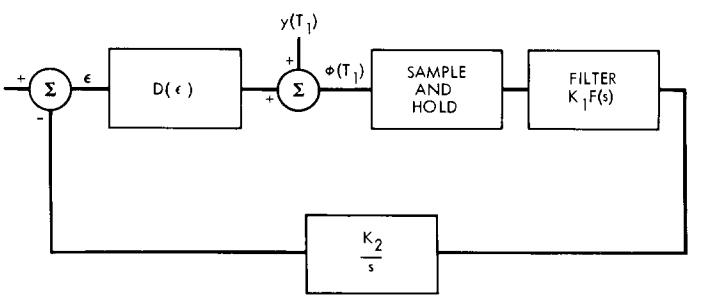

Fig. 41. Equivalent mathematical model

CONFIDENTIAL
UNCLASSIFIED

UNCLASSIFIED

VCO output timing, the magnitude of the rms jitter being related to system parameters and input noise.

b. Time jitter due to noise during lockon. The effect of input noise when the system operates with zero steady-state signal error was investigated. During this lockon phase, the function D (ϵ) becomes a constant gain device and the system can be represented by an equivalent linear sampled data control system. The noise causes variations in the timing signal at the VCO output, that is, in the parameter Δ. The effect of loop gain and filter bandwidth on the mean square jitter in Δ due to the equivalent input noise was investigated. The presence of the sampler forces use of the sampling theory, and this jitter information can be obtained only at the sampling instants.

Consider first the case where no loop filtering is used. If Z [·] represents the z transform of [·], then the loop gain function has the z transform

$$G(z) = Z\left[\frac{D(\epsilon)\, K\, (1 - e^{-T_2 s})}{S^2}\right] \tag{13}$$

where

$K = K_1 K_2 =$ total loop gain (sec/v-sec)

$D(\epsilon) = k$ volts

Define

$$K_0 = kT_2\, K \text{ sec} \tag{14}$$

then

$$G(z) = \frac{K_0 z}{(z-1)^2} - \frac{K_0}{(z-1)^2} = \frac{K_0}{(z-1)} \tag{15}$$

Note that K_0 is essentially a normalized loop gain for the system. The noise transfer function from point of application to tracking error (or VCO output) is then

$$H(z) = \frac{G(z)/k}{1 + G(z)} = \frac{K_0/k}{z + (K_0 - 1)} \tag{16}$$

The mean square jitter at each sample is then given by the relation

$$\sigma^2 = \frac{N_0 T_1}{2\pi j} \oint H(z)\, H(1/z)\, dz/z \tag{17}$$

where no sample-to-sample correlation has been assumed. The above has been tabulated for various H(z) and substitution from Equation 16 yields

$$\sigma^2 = \frac{N_0 T_1 (K_0 T_2)^2}{K_0 (2 - K_0)} \tag{18}$$

Hence, it is required that $K_0 \leq 2$, and a bound is established on the loop gain. The above can be written as

$$\sigma^2 = \left[\frac{N_0}{k^2 T_2}\right] T_1 T_2 \left[\frac{K_0}{2 - K_0}\right] \quad \text{sec}^2 \tag{19}$$

Here the term $N_0/k^2 T_2$ resembles a noise-to-signal power ratio in an ideal bandwidth $B_2 = 1/T_2$, which is denoted as $(N/S)_{B2}$. Note that σ^2 is monotonically decreasing with the normalized loop gain K_0. A case where a simple RC low pass filter is used in the loop is now considered.

Thus, in Fig. 41

$$F(s) = \frac{a}{s + a} \tag{20}$$

and

$$G(z) = Z\left[\frac{k\, K\, a(1 - e^{-T_2 s})}{s^2 (s + a)}\right] = \frac{(k\, Ka)\, \frac{T_2}{a}}{z - 1} - \frac{(k\, Ka)(1 - e^{-aT_2})}{a^2 (z - e^{-aT_2})} = \frac{Ko}{z - 1} - \frac{\frac{Ko}{aT_2}(1 - e^{-aT_2})}{z - e^{aT_2}} \tag{21}$$

where again

$$K_0 = k\, T_2 K$$

Simplifying,

$$G(z) = (K_0)\, \frac{\beta_1 z + \beta_2}{z^2 - \beta_3 z + \beta_4} \tag{22}$$

where

$$\beta_1 = 1 - \frac{1 - e^{-aT_2}}{aT_2}$$

$$\beta_2 = \frac{1 - e^{-aT_2}}{aT_2} - e^{-aT_2}$$

$$\beta_3 = 1 + e^{-aT_2}$$

$$\beta_4 = e^{-aT_2}$$

The resulting loop noise function is then

$$H(z) = \frac{\left[\frac{K_0}{k}\right](\beta_1 z + \beta_2)}{z^2 + C_1 z + C_0} \tag{23}$$

with

$$C_1 = (K_0)\, \beta_1 - \beta_3$$

$$C_0 = \beta_4 + (K_0)\, \beta_2$$

UNCLASSIFIED

UNCLASSIFIED CONFIDENTIAL

Using Equation 23 in Equation 17, the resulting mean square jitter is

$$\beta^2 = T_1 T_2 \left[\frac{N_o}{k^2 T_2}\right] F(aT_2, K_o) \qquad \text{sec}^2 \qquad (24)$$

where

$$F = K_o^2 \frac{(\beta_1^2 + \beta_2^2)(1 + C_o) - 2\beta_1 \beta_2 C_1}{(1 - C_o)(1 - C_1^2 + 2C_o + C_o^2)} \qquad (25)$$

The above function is shown in Fig. 42 as a function of K_o for various values of aT_2. Although this relation is convenient for analysis, it must be further constrained to be useful for system design. If no restriction is placed upon K_o, for example, minimization of σ^2 clearly occurs as K_o approaches zero; i.e., an open circuit.

c. Steady-state tracking errors. One important restriction that must be placed on the system design is its behavior to various inputs in Fig. 41. That is, independent of the jitter, the loop must react favorably to changes in the timing of the input pulse train. If such changes occur, the loop undergoes a transient effect and hopefully settles to some finite steady-state error. As long as the system is considered linear, this steady-state tracking error can be added to the timing jitter to obtain the total timing error in the loop.

Using the final-value theorem in sampled data theory, the steady-state erorr to an input I(z) is

$$e_{ss} = \lim_{z \to 1} \frac{z - 1}{z}\left[\frac{1}{1 + G(z)}\right] I(z) \qquad (26)$$

Substituting from the previous results one can construct the following taubulation for e_{ss}.

Input		*No loop filter*	*Loop filter*
Step in phase	$\Delta = 1\,u(t)$	0	0
Step in frequency	$\Delta = \Delta_o t\,u(t)$	Δ_o/K_o	Δ_o/K_o
Drift in frequency	$\Delta = t^2\,u(t)$	∞	∞

Hence, the system behaves exactly the same, in terms of steady-state error, whether the low pass loop filter is inserted or not. Note that the system cannot track drifts in frequency between the incoming and locally generated pulse trains. This is due to the fact that the loop contains only one integration (VCO). Simple addition of a second integrator to the loop without proper compensation, however, will yield an infinite mean square jitter.

If it is assumed that the most serious input timing change is an instantaneous change in frequency, then a desired steady-state error of e_o sec requires a normalized loop gain of

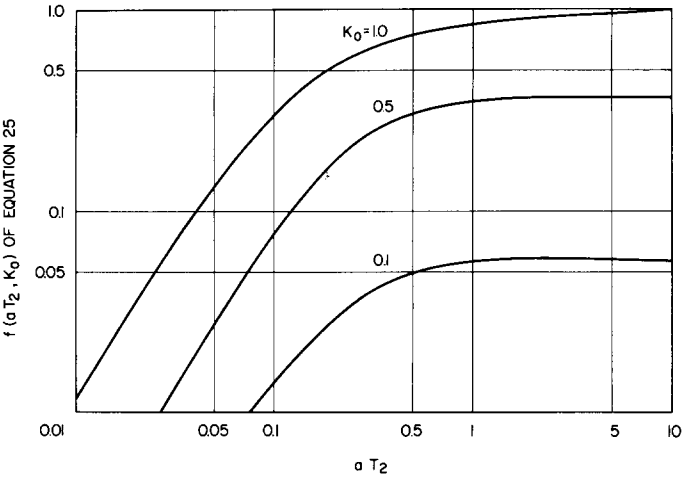

Fig. 42. Plot of (a T_2 K_0) of Equation 24

$$K_o \geq \frac{\Delta_o}{e_o} \qquad \text{sec} \qquad (27)$$

This places a constraint on the minimum loop gain, and the corresponding time jitter for a particular loop filter can be obtained by solving Equation 25. It would be convenient, therefore, to have a plot of Equation 25 for various values of loop gain. This appears in Fig. 42 and the corresponding time jitter can be obtained from Equation 19. Note that the jitter decreases as the filter bandwidth is made smaller, and little increase in jitter occurs for bandwidths greater than $1/T_2$, the pulse repetition frequency. The asymptotic value at large bandwidths corresponds to complete removal of the filter, which is evident by letting $aT_2 \to \infty$ and noting that Equation 25 becomes identical to Equation 16. It is therefore concluded that the sample data loop should operate with as small a bandwidth as possible to minimize the pulse jitter. The lower limit of the bandwidth is determined by the desired system transient response.

Consider the following example:

let

$$T_2 = 1.67 \text{ msec}$$

$$T_1 = 0.133 \text{ msec}$$

$$k = 1 \text{ v}$$

$$K_o = 0.1 \text{ sec}$$

$$a = 1/T_2 \text{ cps}$$

then, from Equation 14, the loop gain required is

$$K \geq \frac{0.1}{1.67 \times 10^{-3}} = 60$$

CONFIDENTIAL UNCLASSIFIED

UNCLASSIFIED

The resulting jitter is obtained from Equation 19 and Figure C-19:

$$\sigma^2 = \left(\frac{N}{S}\right)_2 \left(10^{-8}\right) \text{sec}^2$$

With a $(N/S)_2$ of 30 db in a bandwidth 600 cps, the resulting rms jitter is

$$\sigma = 3.1\ \mu\text{sec}$$

6. Soil Mechanics Surface Sampler Sequence Analysis

A study was performed at JPL request to delineate the time, power, number of commands (see Tables 15 and 16), and operational mode required to perform the soil mechanics surface sampler (SMSS) experiment in a preliminary sequence specified by JPL. Two operational modes were considered in determining the time required to perform this experiment. Mode 1 employed the command generation (SCP), verification and transmission (CVT) programs of the SFOF to send command messages to the DSN. In this mode about 75 hr were required to complete the experiment. Mode 2 employed a direct telephone line connection between the experiments and the command and data handling console (CDC) operator at the DSN. Further, the commands to perform the entire experiment were placed on punched tape at the site in suitable subsequences such that as the experimenter selected each individual task to be performed, the CDC operator placed in the command reader the appropriate subsequence by slewing the tape to an experimenter-directed sequence number. In this mode, the experimenter had full authority to proceed with the test at his own discretion. Under mode 2, the elapsed time to complete the experiment was found to be about 21 hr.

It is evident that even under this high speed mode of operation the time to complete the desired experiment is formidable. This would suggest that the test as designed is either too ambitious when consideration is given to the

Table 15. Soil mechanics surface sampler energy consumption and command total[a]

SMSS movement commands	Number of Commands	Total time ON, sec	Regulated power					Unregulated power				
			Auxiliary		Instrument		Total regulated energy for experiment, w-sec	Auxiliary		Instrument		Total unregulated energy for experiment, w-sec
			Power (for SMSS function), w	Energy, w-sec	Power (for SMSS function), w	Energy, w-sec		Power (for SMSS function), w	Energy, w-sec	Power, (for SMSS function), w	Energy, w-sec	
Coarse (2 sec) commands												
Extend	107	214	3.31	709	—	—		0.36	77.1	7.9	1690	
Retract	96	192	3.31	635	—	—		0.36	69.0	7.9	1517	
Elevate	38	76	3.31	252	—	—		0.4	30.2	8.8	669	
Lower	7	14	3.31	45.4	—	—		0.24	3.4	5.3	74.3	
Right	8	16	3.31	53.0	—	—		0.36	5.8	7.9	126.3	
Left	5	10	3.31	33.1	—	—		0.36	3.6	7.9	79	
Open scoop	1	2	3.31	6.6	—	—		0.1	0.2	2.2	4.4	
Disengage	5	10	1.71	17.1	—	—		0.8	8.0	17.6	176	
Fine (0.1 sec) commands												
Lower	340	34	3.31	112	—	—		0.5	17.0	11.0	374	
Right	7	0.7	3.31	2.3	—	—		0.9	0.6	19.8	13.9	
Left	19	1.9	3.31	6.3	—	—		0.9	1.7	19.8	37.6	
Strain measurement ON		507	1.2	609	4.28	2170		—	—	—	—	
Accelerometer measurement ON		420	0.69	290	1.42	596		—	—	—	—	
Equipment Auxiliary		1553	0.32	498	—	—						
Totals				3268.8		2766	6034.8		216.6		4761.5	4978.1

[a] E_T = 11,013 w-sec
E_T = 3.06 w-hr

UNCLASSIFIED

UNCLASSIFIED
CONFIDENTIAL

command generation problem and the data analysis time, or the test is designed in a non-optimum manner. Recommendations were made that would optimize the mode of lowering the SMSS to the lunar surface. It was also recommended that the SMSS be driven in azimuth arcs when stepping from point to point, in lieu of the test requirement of stepping the SMSS in extension and retraction from point to point. Under these conditions, the elapsed time to complete the experiment would be reduced to approximately 6 hr.

It became evident during the analysis of the SMSS experiment that the required operational sequence could best be developed by deriving the commands necessary to perform each individual task within the experiment. Forty-two individual tasks were catalogued in this manner. The time to execute each task subsequence from the CDC was computed, along with the attendant spacecraft energy dissipation. In deriving each sequential command list for the subsequences, consideration was given to the allowable SMSS motor duty cycles and to the required time to allow the 2-sec timer to complete its period. In the case of television coverage, sufficient time was allocated between television frames, in the same operation, to permit at least three erase scans of the vidicon. The narrow angle (100 mm) television operations were developed with three television pictures per operation. These television pictures are taken at the same azimuth and elevation position of the camera mirror, but with one picture having a focus position two steps less than the nominal focus position for that point – one picture at the nominal focus step position, and one picture at two steps greater than the nominal focus step. The reason for taking three photos at different focus positions was to compensate for the uncertainty in elevation position of the test point and to allow pictures of the scoop in the depression as far as the television is able to perceive, and in addition, to get details of any mounds that may have been created by the scoop. Due to the greater depth of field in the wide angle mode (25 mm) this was not deemed necessary for such television photos.

The detailed analysis can be found in Reference 5.

7. Surveyor Command Verification and Transmission Program (CVT)

An operational computer program is being developed to facilitate the processing of command messages between the Space Flight Operations Facility and the Deep Space Stations. The program is now being coded and is scheduled for integration into the SFOF in the near future. Fig. 43, 44, and 45 show the CVT program logic. The CVT program will perform the following functions:

Table 16. Energy consumption and command count for TV[a]

Energy loss due to camera function operations				Energy loss for equipment on-time		
Commands	Number of commands	Energy factor	w-sec	Item	Energy factor	w-sec
Power ON Camera 3	28	—	—	Camera on-time 296 sec	10.3	3130
Power OFF Camera 3	28	—	—			
Start frame	28	7.9	221			
Step focus in	41	2.48	103	High-power transmitter on-time 78.5 sec	50	3930
Step focus out	63	2.48	156			
Multiple step focus in	8	2.46	19.7			
Step mirror right	6	4.4	26.4	Camera auxiliary on-time 296 sec	5.2	1540
Step mirror left	1	4.4	4.4			
2 step mirror right	12	8.8	105.5			
2 step mirror left	18	8.8	158.5			
Step mirror up	8	4.4	35	Number of commands for subsystem decoder 549	0.2/command	110
Step mirror down	10	4.4	44			
Set 100 mm	14	35	490			
Set 25 mm	14	35	490			
Fill-in	270	—	—			
Totals	549		1853.5			8710

[a] E_T = 10,563 w-sec
E_T = 2.94 w-hr

CONFIDENTIAL
UNCLASSIFIED

UNCLASSIFIED
CONFIDENTIAL

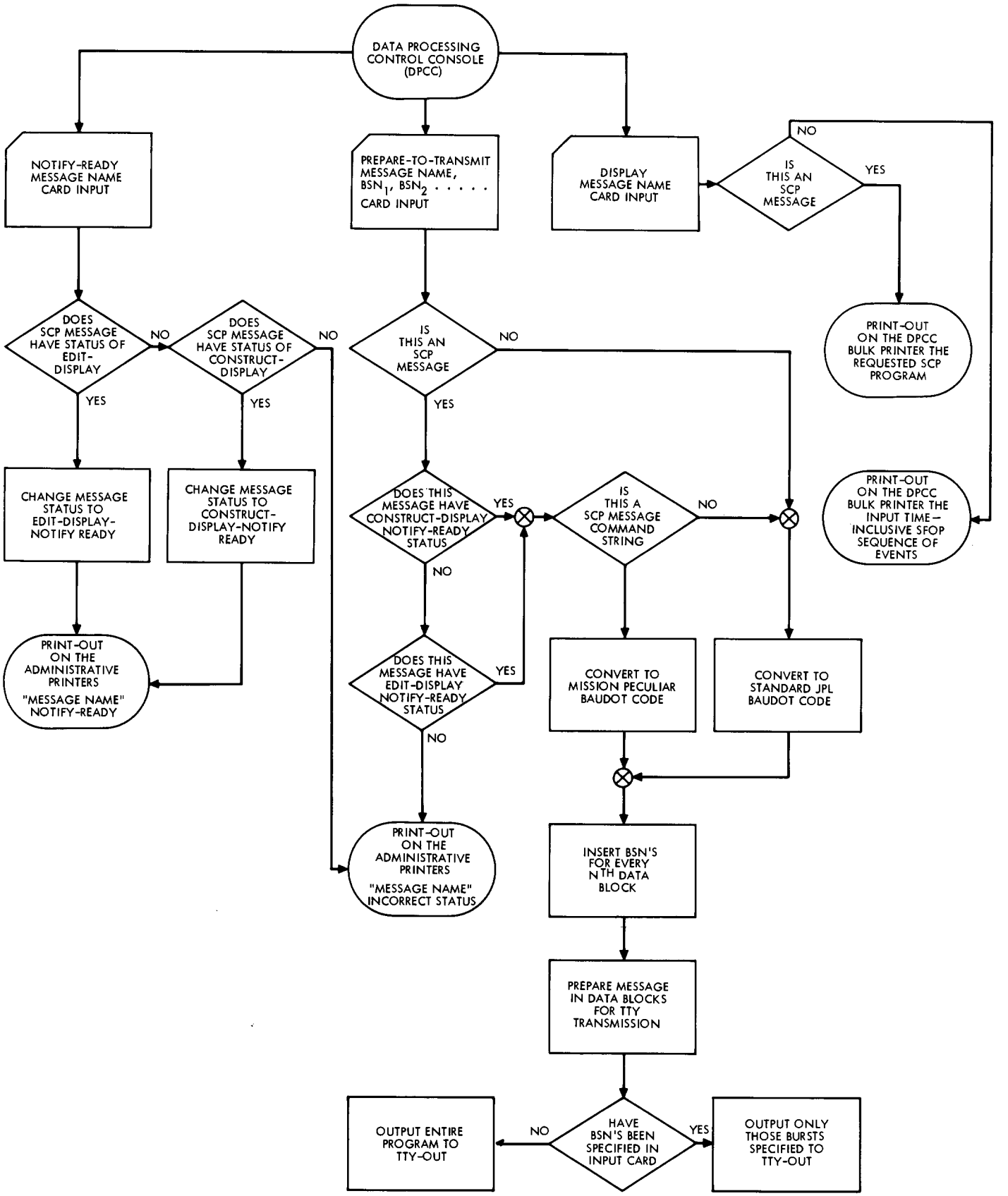
DATA PROCESSING CONTROL CONSOLE (DPCC)
NOTIFY-READY MESSAGE NAME CARD INPUT
PREPARE-TO-TRANSMIT MESSAGE NAME, BSN1, BSN2 . . . . . CARD INPUT
DISPLAY MESSAGE NAME CARD INPUT
IS THIS AN SCP MESSAGE
NO
YES
PRINT-OUT ON THE DPCC BULK PRINTER THE REQUESTED SCP PROGRAM
DOES SCP MESSAGE HAVE STATUS OF EDIT-DISPLAY
NO
YES
DOES SCP MESSAGE HAVE STATUS OF CONSTRUCT-DISPLAY
NO
YES
IS THIS AN SCP MESSAGE
NO
YES
CHANGE MESSAGE STATUS TO EDIT-DISPLAY-NOTIFY READY
CHANGE MESSAGE STATUS TO CONSTRUCT-DISPLAY-NOTIFY READY
DOES THIS MESSAGE HAVE CONSTRUCT-DISPLAY NOTIFY-READY STATUS
YES
IS THIS A SCP MESSAGE COMMAND STRING
NO
PRINT-OUT ON THE DPCC BULK PRINTER THE INPUT TIME—INCLUSIVE SFOP SEQUENCE OF EVENTS
NO
PRINT-OUT ON THE ADMINISTRATIVE PRINTERS "MESSAGE NAME" NOTIFY-READY
DOES THIS MESSAGE HAVE EDIT-DISPLAY NOTIFY-READY STATUS
YES
NO
CONVERT TO MISSION PECULIAR BAUDOT CODE
CONVERT TO STANDARD JPL BAUDOT CODE
PRINT-OUT ON THE ADMINISTRATIVE PRINTERS "MESSAGE NAME" INCORRECT STATUS
INSERT BSN'S FOR EVERY NTH DATA BLOCK
PREPARE MESSAGE IN DATA BLOCKS FOR TTY TRANSMISSION
OUTPUT ENTIRE PROGRAM TO TTY-OUT
NO
HAVE BSN'S BEEN SPECIFIED IN INPUT CARD
YES
OUTPUT ONLY THOSE BURSTS SPECIFIED TO TTY-OUT

Fig. 43. CVT program flow chart

UNCLASSIFIED
CONFIDENTIAL

UNCLASSIFIED
CONFIDENTIAL

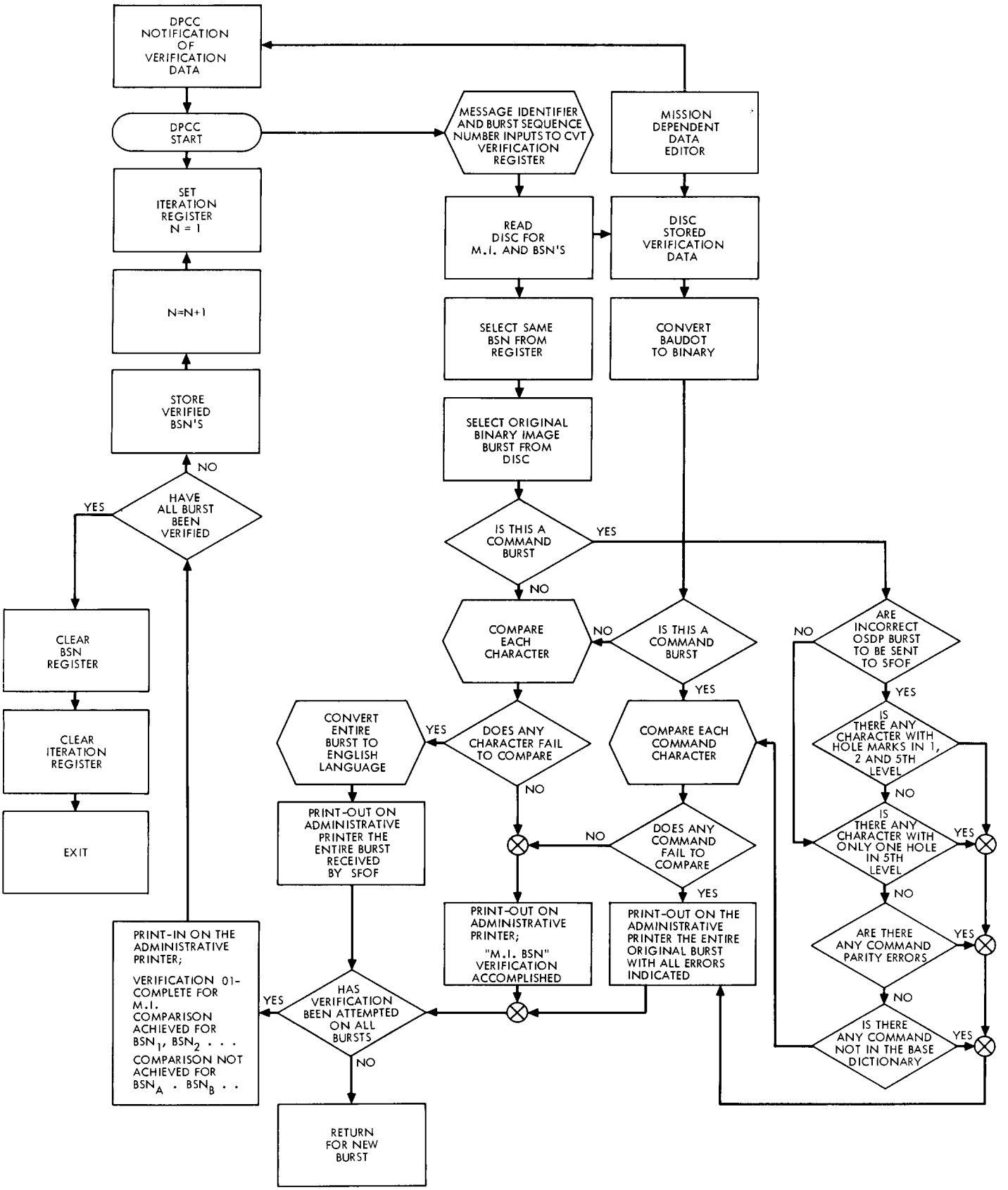
DPCC NOTIFICATION OF VERIFICATION DATA
DPCC START
SET ITERATION REGISTER N = 1
N=N+1
STORE VERIFIED BSN'S
HAVE ALL BURST BEEN VERIFIED
NO
YES
CLEAR BSN REGISTER
CLEAR ITERATION REGISTER
EXIT
PRINT-IN ON THE ADMINISTRATIVE PRINTER;
VERIFICATION 01-COMPLETE FOR M.I. COMPARISON ACHIEVED FOR BSN_1, BSN_2 . . .
COMPARISON NOT ACHIEVED FOR BSN_A . BSN_B . .
MESSAGE IDENTIFIER AND BURST SEQUENCE NUMBER INPUTS TO CVT VERIFICATION REGISTER
MISSION DEPENDENT DATA EDITOR
READ DISC FOR M.I. AND BSN'S
DISC STORED VERIFICATION DATA
SELECT SAME BSN FROM REGISTER
CONVERT BAUDOT TO BINARY
SELECT ORIGINAL BINARY IMAGE BURST FROM DISC
IS THIS A COMMAND BURST
YES
NO
COMPARE EACH CHARACTER
NO
IS THIS A COMMAND BURST
YES
ARE INCORRECT OSDP BURST TO BE SENT TO SFOF
NO
YES
CONVERT ENTIRE BURST TO ENGLISH LANGUAGE
YES
DOES ANY CHARACTER FAIL TO COMPARE
NO
COMPARE EACH COMMAND CHARACTER
IS THERE ANY CHARACTER WITH HOLE MARKS IN 1, 2 AND 5TH LEVEL
NO
YES
PRINT-OUT ON ADMINISTRATIVE PRINTER THE ENTIRE BURST RECEIVED BY SFOF
NO
DOES ANY COMMAND FAIL TO COMPARE
IS THERE ANY CHARACTER WITH ONLY ONE HOLE IN 5TH LEVEL
YES
NO
YES
PRINT-OUT ON ADMINISTRATIVE PRINTER;
"M.I. BSN" VERIFICATION ACCOMPLISHED
PRINT-OUT ON THE ADMINISTRATIVE PRINTER THE ENTIRE ORIGINAL BURST WITH ALL ERRORS INDICATED
ARE THERE ANY COMMAND PARITY ERRORS
YES
NO
IS THERE ANY COMMAND NOT IN THE BASE DICTIONARY
YES
HAS VERIFICATION BEEN ATTEMPTED ON ALL BURSTS
YES
NO
RETURN FOR NEW BURST

Fig. 44. Verification flow chart

UNCLASSIFIED
CONFIDENTIAL

UNCLASSIFIED
CONFIDENTIAL

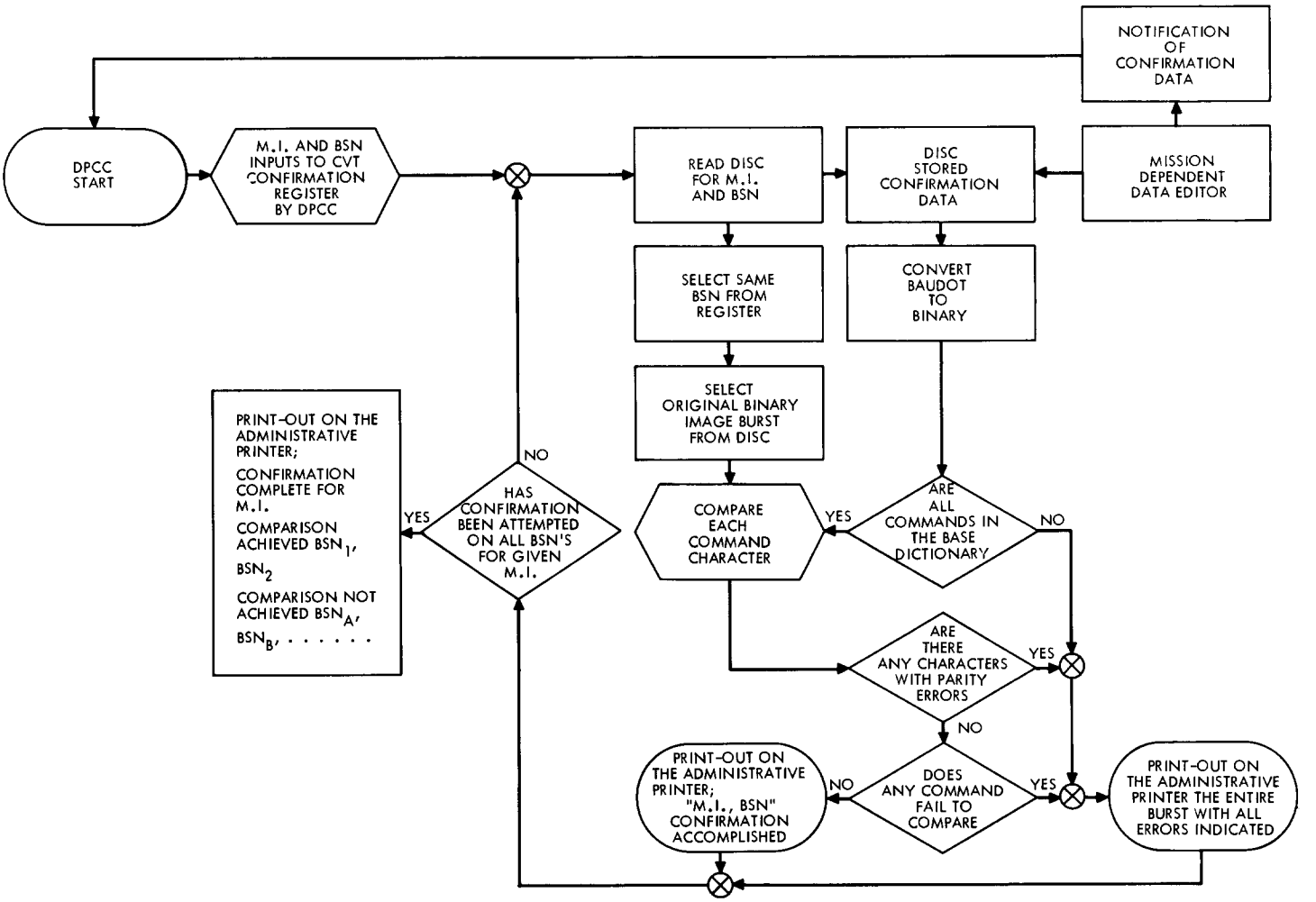
NOTIFICATION OF CONFIRMATION DATA
DPCC START
M.I. AND BSN INPUTS TO CVT CONFIRMATION REGISTER BY DPCC
READ DISC FOR M.I. AND BSN
DISC STORED CONFIRMATION DATA
MISSION DEPENDENT DATA EDITOR
SELECT SAME BSN FROM REGISTER
CONVERT BAUDOT TO BINARY
SELECT ORIGINAL BINARY IMAGE BURST FROM DISC
PRINT-OUT ON THE ADMINISTRATIVE PRINTER;
CONFIRMATION COMPLETE FOR M.I.
COMPARISON ACHIEVED BSN1, BSN2
COMPARISON NOT ACHIEVED BSNA, BSNB, ...
HAS CONFIRMATION BEEN ATTEMPTED ON ALL BSN'S FOR GIVEN M.I.
NO
YES
COMPARE EACH COMMAND CHARACTER
ARE ALL COMMANDS IN THE BASE DICTIONARY
YES
NO
ARE THERE ANY CHARACTERS WITH PARITY ERRORS
YES
NO
PRINT-OUT ON THE ADMINISTRATIVE PRINTER; "M.I., BSN" CONFIRMATION ACCOMPLISHED
NO
DOES ANY COMMAND FAIL TO COMPARE
YES
PRINT-OUT ON THE ADMINISTRATIVE PRINTER THE ENTIRE BURST WITH ALL ERRORS INDICATED

Fig. 45. Confirmation flow chart

- Verify that base dictionary of all possible binary commands is valid when read in from the disc and after being used. Both vertical and horizontal check sums will be used so that command in error can be output on the administrative printer.
- Subdivide each message into transmission bursts by assigning burst sequence numbers to each Nth message block.
- Transform binary command messages and space flight operations plan (SFOP) sequence of events to Baudot code.
- Transform the following teletype (TTY) codes to binary:
  - (1) Standard JPL Baudot code
  - (2) Mission-peculiar command-sequence number Baudot code
  - (3) Command confirmation code
- Write magnetic tape with both Baudot and binary images of command messages or sequence of events.
- Display SFOP sequence of events or command messages.
- Set status of command message to notify when ready and print a message on all user-area administrative printers that message or SFOP has this status.
- Insert carriage returns, line feeds, etc., into outgoing command messages or SFOP sequence of events.

The program will verify commands at the following levels:

Program (internal)

(1) Verify that command messages given to it by *Surveyor* command preparation program (SCP) contain only commands from base dictionary.

CONFIDENTIAL
UNCLASSIFIED

UNCLASSIFIED CONFIDENTIAL

(2) Verify that command messages given to it by SCP have proper status.

User Area

(1) Command Verification. After a command message is transmitted to the DSN it is returned to the SFOF and placed on a disc. The CVT obtains this image from the disc in proper code, transforms it to binary and compares it with the command message prepared by the SCP. The CVT notifies all user areas whether or not the command message compares. If it does not compare with the proper message and the error is in the instruction portion, the line containing the error and the lines preceding and following the error are printed in the data processor control console (DPCC) and command preparation areas. Prepunched tapes will be compared sequence-by-sequence with the prestored sequences. Errors will be indicated in the same manner as if they were in the command portion of a command message.

The following will be identified in command verification:

(a) Command sequence number.

(b) Position of error in sequence.

(c) Octal representation of command as transmitted and as received.

(d) Whether or not offending command is from base dictionary.

(2) Command Confirmation. When command sequences are executed by CDC, they are transmitted to SFOF and placed on disc. The CVT obtains sequences from disc. It transforms them to binary and compares them with original prestored sequences. All errors found are indicated for output in the same manner as in command portion of command messages under command verification, above, with the exception that commands are time tagged with last time received (all administrative printers). All commands returning for confirmation will be written on offline output tape.

UNCLASSIFIED CONFIDENTIAL

UNCLASSIFIED

D. Flight Control

1. Introduction

The flight control subsystem consists of spacecraft units that provide velocity and attitude control during the transit and landing phase of the *Surveyor* mission. These units, which include optical sensors, inertial instruments, attitude controls, and flight control electronics are discussed in this section. Although the lunar radar and propulsion are also functionally included, they are covered in other sections of this report.

2. Progress Summary

Type approval tests were successfully completed on the flight control electronics unit. Following integration testing, the unit was delivered to the T-21 spacecraft as part of the sensor group. The third flight model of the electronics unit was delivered to the subsystem test area.

Additional tests to determine the feasibility of operating the gyro and Canopus sensor motors using a delayed square wave power source were completed. Results indicate a significant increase in the efficiency when three-phase power is supplied to the motors. Square wave tests are also being made at the flight control sensor group level.

Work was initiated to incorporate the slit type acquisition Sun sensor in the first flight spacecraft and performance tests are being made on an engineering development model.

Acceptance tests were completed on the first set of flight model gas jet valves and the valves are available for installation on the spacecraft.

3. System Design

a. Thrust phase control system. A study was made to determine the effect on thrust-phase attitude control system performance of accelerometer offset and vernier engine gain mismatch. Since the accelerometer used to provide acceleration signals is mounted off the spacecraft center of gravity, it senses not only the desired thrust-to-mass ratio, (T/M), but also acceleration terms which depend on the x, y, and z offsets and angular derivatives. With the offset included, the accelerometer senses the following in the —z, or upward direction.

$$\ddot{R}_{(-z)} = -T/M\,[x(\omega_x\omega_z - \dot{\omega}_y) + y\,(\omega_y\omega_z + \dot{\omega}_x) - z\,(\omega_x^2 + \omega_y^2)] \quad (1)$$

where $x = -31.88$ in., $y = 0.74$ in., $z = +0.62$ in., and ω = angular velocity.

A computer study demonstrated that the y and z offsets contribute second-order effects and that the $(x\omega_x\omega_z)$ term is insignificant. Therefore Equation 1 can be rewritten as follows:

$$\ddot{R}_{(-z)} = T/M + x\dot{\omega}_y \quad (2)$$

It was also found that system performance (as a function of x) was only slightly dependent on the presence of the pitch attitude control loop. The simplified system which was analyzed is shown in Fig. 46.

The constants A, B, C, and F are all functions of vernier engine gains. In particular, A and C are both zero when all engine gains are equal. This condition decouples the yaw attitude loop from the acceleration loop. Investigation with the analog computer, including all coupling terms and three angular degrees of freedom, showed that the engine configuration which yields least x gain margin was:

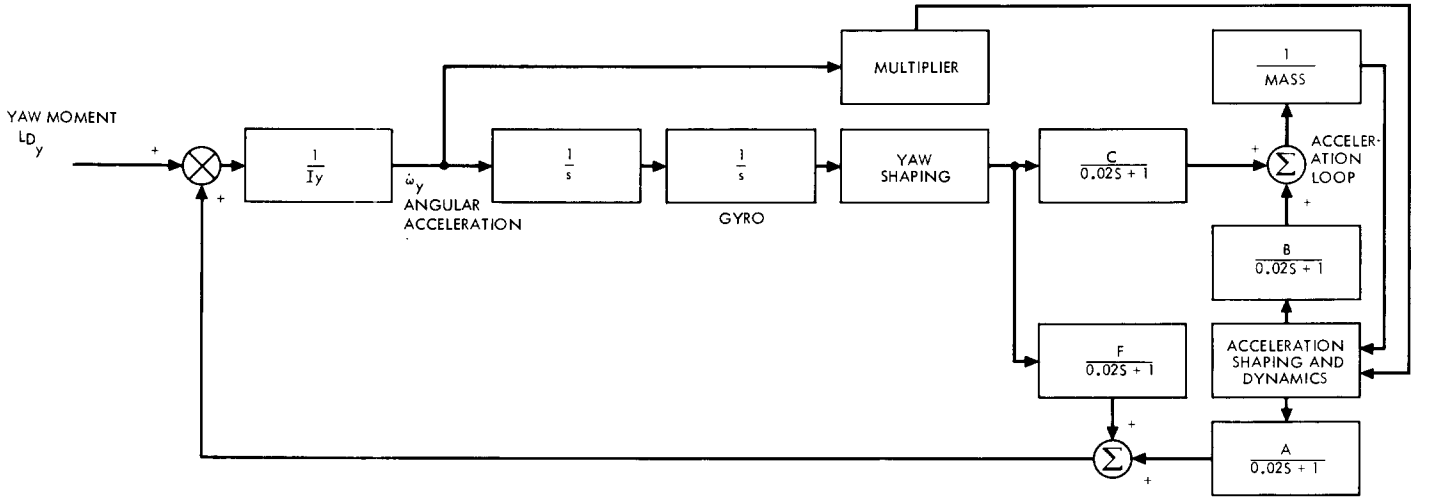

Fig. 46. Yaw attitude loop

CONFIDENTIAL
UNCLASSIFIED

UNCLASSIFIED

Engine 1 Low gain = 0.876

Engine 2 High gain = 1.32

The system root locus plot with these engine gains is shown in Fig. 47. This plot was confirmed by computer results.

With the acceleration loop exercised by step commands and by radar noise, time histories of engine thrust and angular motion were compared to the case where x = 0. No significant degradation in system performance was observed.

Future studies will examine the effect of accelerometer offset on system performance with vernier engine hysteresis and radar noise present.

b. Vernier engine simulation study program. An attempt is being made to revise the computer simulation of the vernier engine thrust chamber assembly to provide a better definition of the effect of system nonlinearities and other system dynamics not included in the present simulations. Although results obtained with the present linear computer simulation have exhibited good correlation with water flow test data (Fig. 48), improvements are expected when the nonlinear effects such as localized compressibility due to gas entrapment or gas generation in the thrust chamber coolant passage are included in the simulation. Revisions will be based primarily upon the block diagram shown in Fig. 49 which shows an improved functional representation of elements in the thrust chamber assembly. The final computer simulation will be used to evaluate the effects of vernier engine design and development changes on throttling dynamics and overall thrust control system performance.

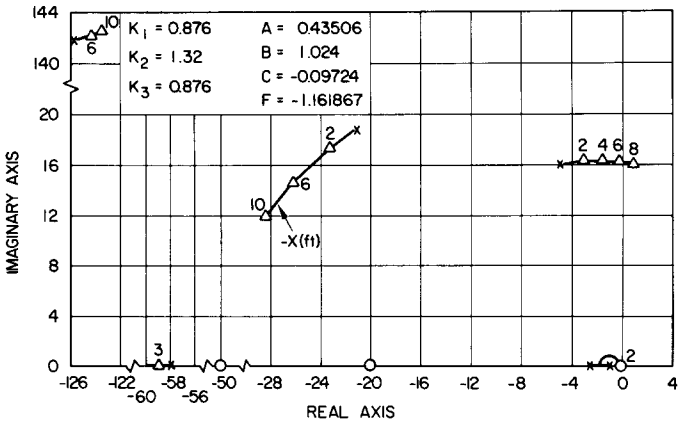

Fig. 47. Yaw attitude loop root locus

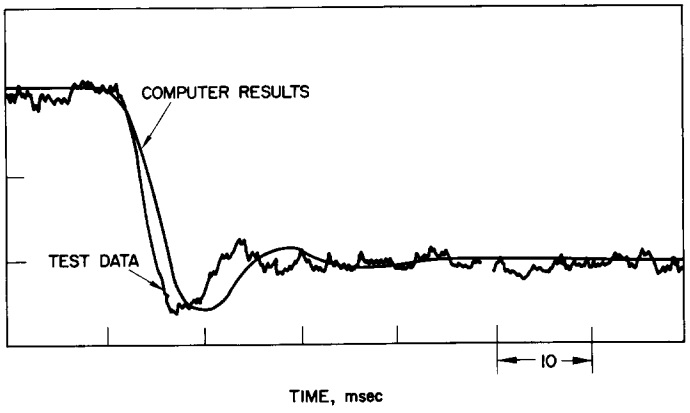

Fig. 48. Vernier engine step response data

4. T-2 Closed Loop Testing

The T-2 closed loop test has been in progress at AFMDC. The purpose of the test is to investigate flight control hardware transient response, phase margin, and gain margin under simulated dynamic conditions. The test results are correlated with the analytically predicted performance to verify proper operation.

The initial closed loop testing of the T-2 flight control electronics unit and the inertial reference unit revealed that the test results could not be correlated with analytical results. Subsequent investigations were conducted at El Segundo to determine the validity of the computer mechanization including the equations used to determine the system response. To facilitate comparison and to ensure a valid set of computer equations, the aerodynamic and lunar gravity parameters were deleted and the two cross-over frequencies and the steady-state gain of the inner rate loop were verified. A gain-phase plot depicting the cross-over frequency points is shown in Fig. 50. Computer runs were made where possible to operate with either actual hardware or simulated hardware as shown in Fig. 51. Good correlation with analytical results was obtained for both the hardware and the simulated hardware runs.

Further investigation disclosed that some of the multipliers in the computer simulation did not function properly at low signal levels during the AFMDC tests. Replacement of the multipliers and re-scaling of the computer has resulted in satisfactory closed loop operation at AFMDC.

Future testing will include the checkout of the T-2 flight control hardware by testing it in conjunction with a computer simulation of engine and spacecraft dynamics. The tests will differ from previous closed loop thrust phase tests in that the lateral velocity, acceleration, and trajectory control loops will be included in the simulation.

UNCLASSIFIED

UNCLASSIFIED
CONFIDENTIAL

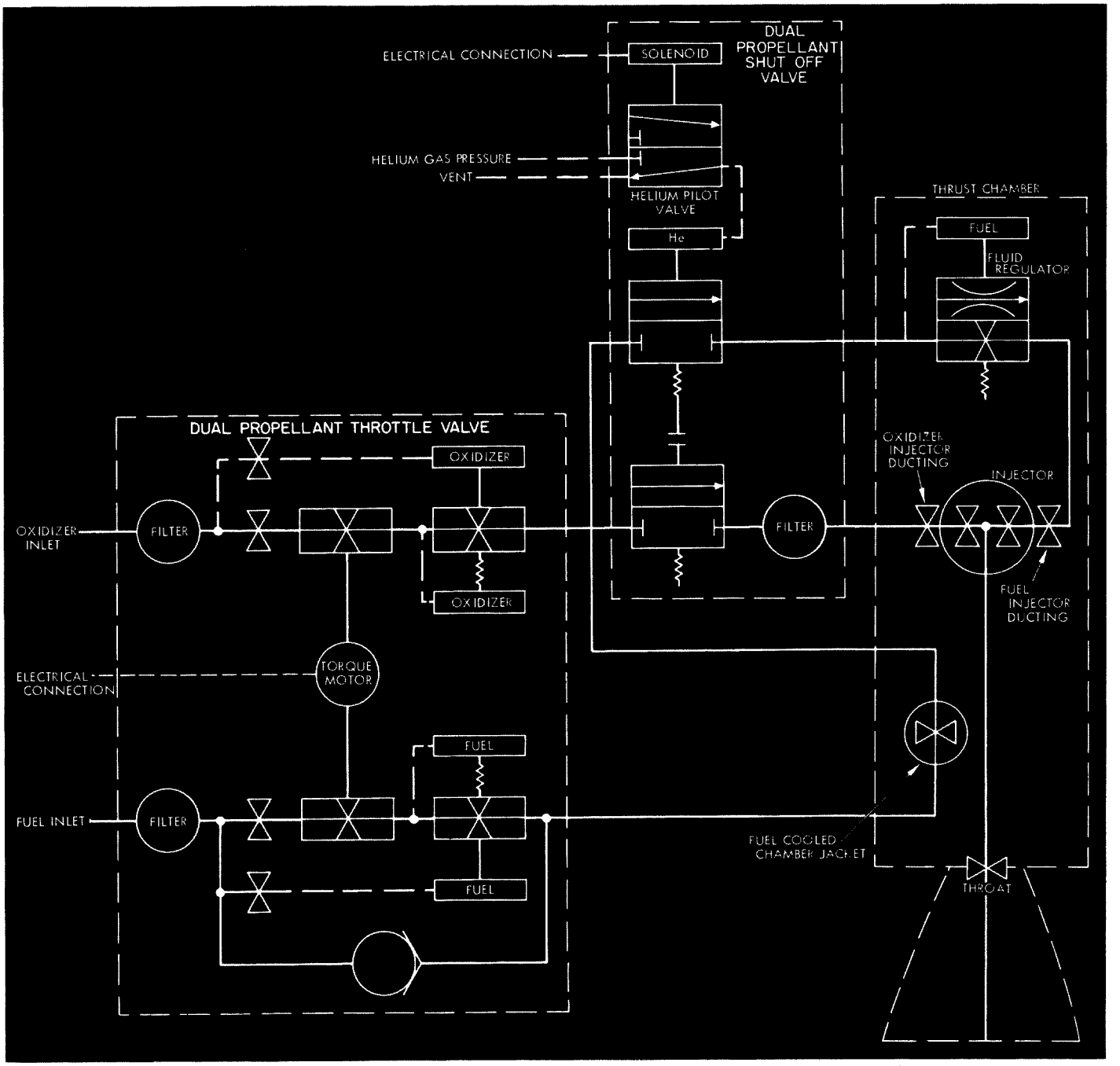

Fig. 49. Vernier engine flow

5. Optical Sensors

a. Canopus sensor. Tests to determine the feasibility of operating the Canopus sensor motor using a modified square wave power source were completed. A breadboard model of a delayed square wave power supply was used for all tests. Performance tests were made at ambient temperatures using the two engineering development model sensors (X-1, -2) and the type approval sensor. The purpose of the tests was to compare the operation of the sensors using 26-v three-phase sine wave power and 26-v three-phase delayed square wave power, as well as to determine the minimum square wave voltage at which the motor would operate. No significant differences in sensor performance were detected in going from 26 v sine wave power to 26- and 16-v square wave power.

UNCLASSIFIED
CONFIDENTIAL

UNCLASSIFIED

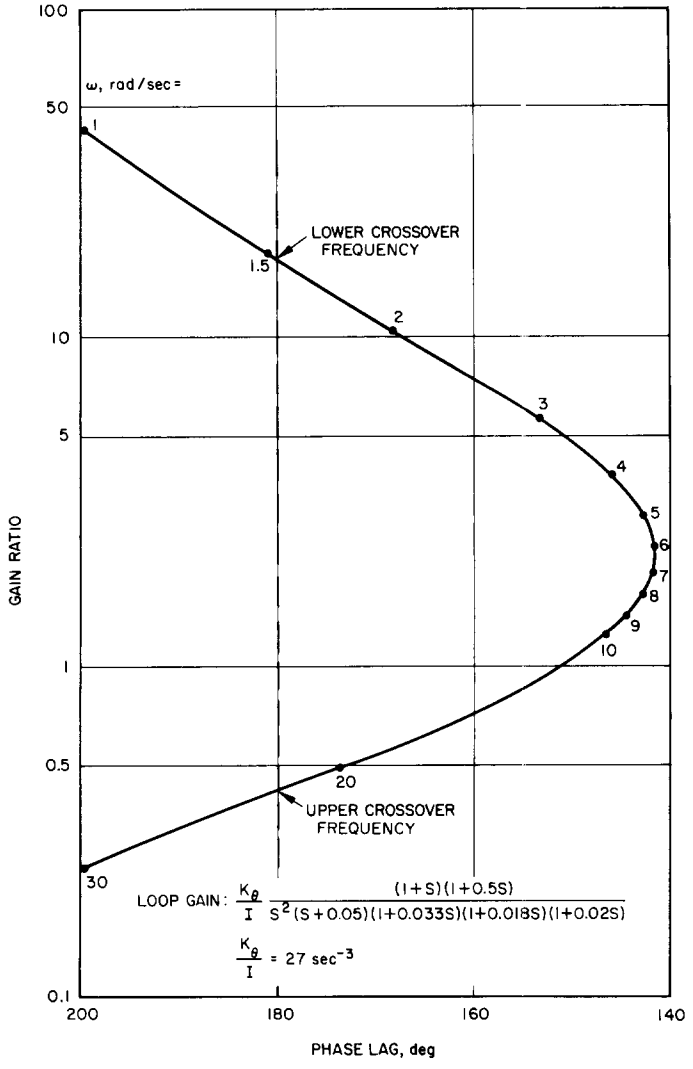

Fig. 50. T-2 inner rate loop open loop gain and phase

The minimum running voltage level for the motor varied from 14 to 16 v. No large differences in motor temperature were noted between sine and square wave operation. Consideration is being given to operating both the Canopus sensor motor and gyro motors on 21 v three-phase square wave power in order to achieve the largest power saving possible. Additional Canopus sensor square wave power tests are planned at the flight control sensor group level.

b. Sun sensors. The decision was made to incorporate the acquisition Sun sensor (described previously in *SPS 37-29*, Vol. I) to the first flight spacecraft. The sequence of events that will occur in a normal Sun acquisition is as follows:

(1) The spacecraft will be launched in the rate stabilization mode.

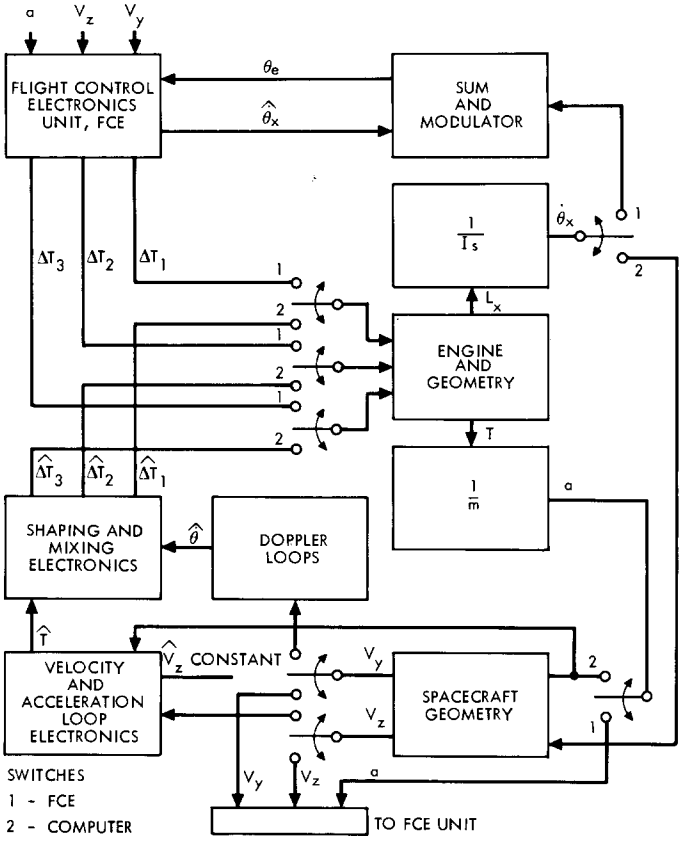

Fig. 51. T-2 flight control electronics mixed simulation

(2) At separation from the *Centaur* vehicle, the separation sensor and legs-down sensors will function to enable the gas jet amplifiers and to initiate a time delay of approximately 51 sec.

(3) Following the time delay, an automatic fixed sequence of maneuvers will take place consisting of a positive rotation about the yaw axis until the Sun line is approximately in the roll-yaw plane (sensor slit illuminated) followed immediately by a rotation about the pitch axis until the primary Sun sensor is illuminated. A yaw maneuver will normally not occur again unless "Sun acquisition" is commanded.

The acquisition sequence was verified by an analog computer study that also considered the effect on system dynamic performance of variations in gas jet thrust, precession torquing rates, and cell slit width. For a maximum expected slit width of ±3 deg, the system overshoot following the initial illumination of a sensor cell did not exceed 2.5 deg over the ranges of gas jet thrust and torquing rates investigated (Fig. 52a and b). Overshoot is defined as the maximum angle attained following initial interception of the slit field-of-view boundary.

UNCLASSIFIED

UNCLASSIFIED
CONFIDENTIAL

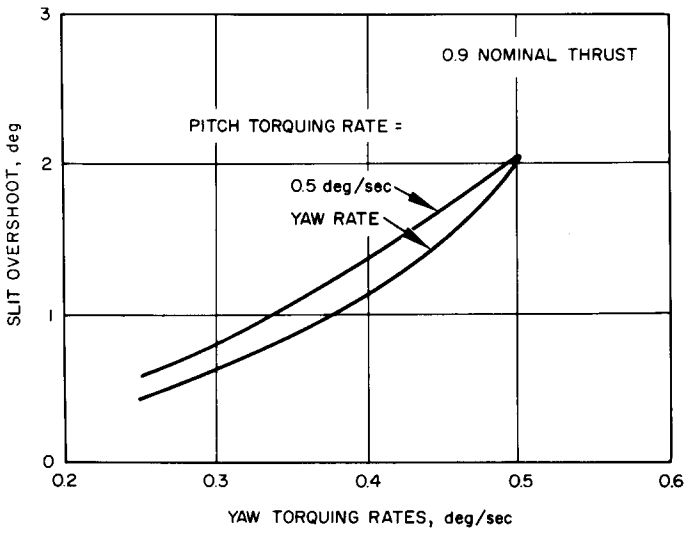

(a) Effect of changes in torquing rates

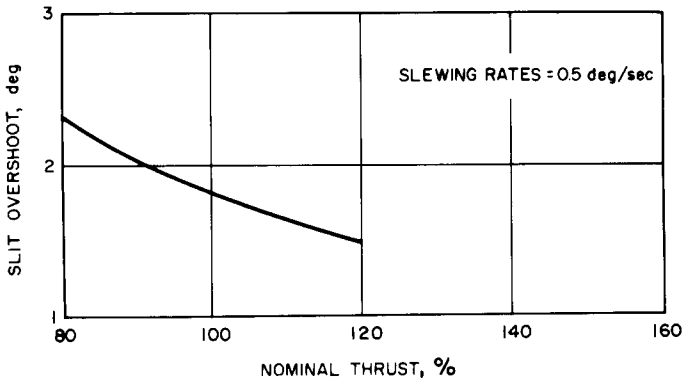

(b) Effect of changes in gas jet thrust

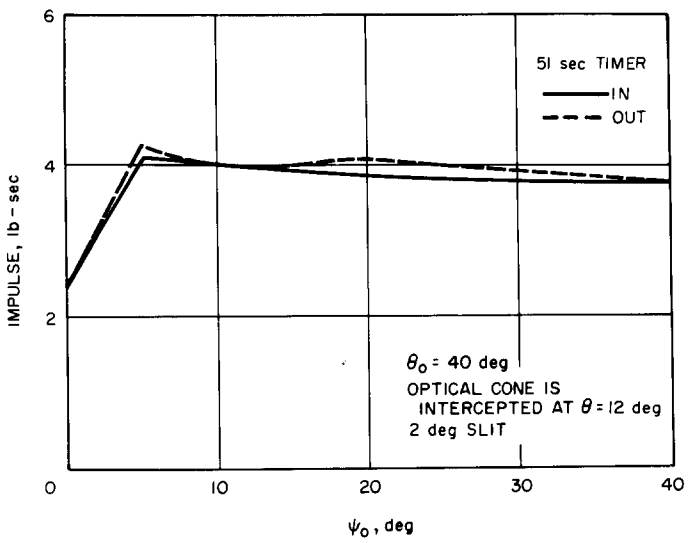

(c) Time delay effect

Fig. 52. Acquisition Sun sensor performance data

System overshoot was chosen as a convenient parameter with which to compare system performance. Since one-shot logic will be used for the acquisition Sun sensor, system overshoot is not a factor in determining a successful acquisition. The Sun acquisition response of a sensor with the nominal ±2-deg slit width was essentially the same as that for the ±3-deg sensor. Computer results also indicated that a time delay between the yaw and pitch maneuver is not required (Fig. 52c).

Operation of both cells will be telemetered digitally and will always be sampled in the same modes as the gyro and primary Sun sensor telemetered error signals. The five secondary Sun sensor cells will continue to be telemetered as before.

Performance tests are presently being conducted on an engineering model of the slit sensor consisting of a one-piece aluminum housing and bracket assembly, four shadow masks, and two photo-conductive cells (Fig. 53).

6. Gas Jet System

a. Gas tank. Gas tank tests that consist of a series of 15-day cycles of continuous exposure to 110% of maximum working pressure are in progress.

Based on a cleanliness evaluation of gas tanks that were in a clean-state storage for approximately 2 yr, it may be necessary to improve gas cleanliness by either installing a gas tank discharge filter or coating the inside

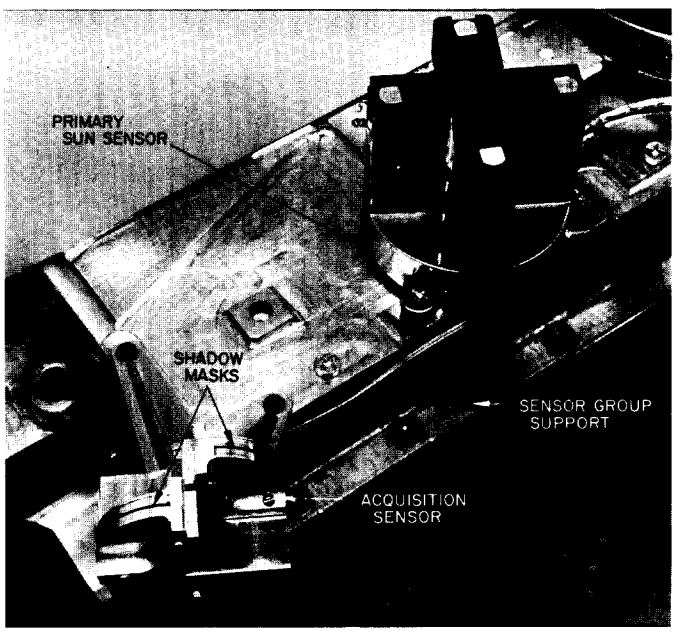

Fig. 53. Engineering model of acquisition Sun sensor

UNCLASSIFIED
CONFIDENTIAL

UNCLASSIFIED
CONFIDENTIAL

of the gas tank to bed-down surface contamination. Ultrasonic cleaning of one tank revealed a considerable quantity of metallic particles which can be removed from the surface.

b. Regulator pressure relief valve. A pressure relief valve successfully completed two additional 24- and 36-day storage cycle tests which subject the valve to twice the normal seating load. Cracking and reseat pressures at both ambient and low temperature in a vacuum environment indicated no degradation in performance.

c. Pressure regulator. An engineering unit of the modified regulator design successfully completed the engineering test program which consisted of functional testing at environmental temperature limits and vibration testing to modified type approval test levels. The vibration test fixture is shown in Fig. 54. A second unit is being life cycle tested and has accumulated approximately 500,000 operational cycles.

The first two flight units (S/N-5 and -6) successfully completed flight approval testing. Assembly test performance of S/N-5 is summarized in Table 17.

d. Jet valves. Flight acceptance tests were completed on the attitude jet valves for the first flight spacecraft and the valves are available for installation. Six additional jet valves are in various stages of assembly, thermal coating, and flight acceptance testing. A summary of assembly test leakage performance data for four valves is presented in Table 18.

Thrust vector tests are presently being conducted on a jet valve mounted on an air bearing supported test table as shown in Fig. 55. Other testing in progress includes a limit cycle performance test on one jet valve.

e. System. A reevaluation of the gas supply transit and mid-course temperature limits resulted in a reduction in operational temperature limits to —30 to 120°F from —70 to 120°F.

Testing of the gas manifold cleanliness was performed on the S-2 spacecraft. Gas samples from the manifold prior to three axis vibration are being compared to post-vibration gas samples. Separate tests of the flexible line portion prior to and after vibration are planned. These tests were previously made to evaluate a design change in the flexible line.

The T-21 gas supply (Fig. 56) was reworked to provide an improved pressure regulator and thermal finish.

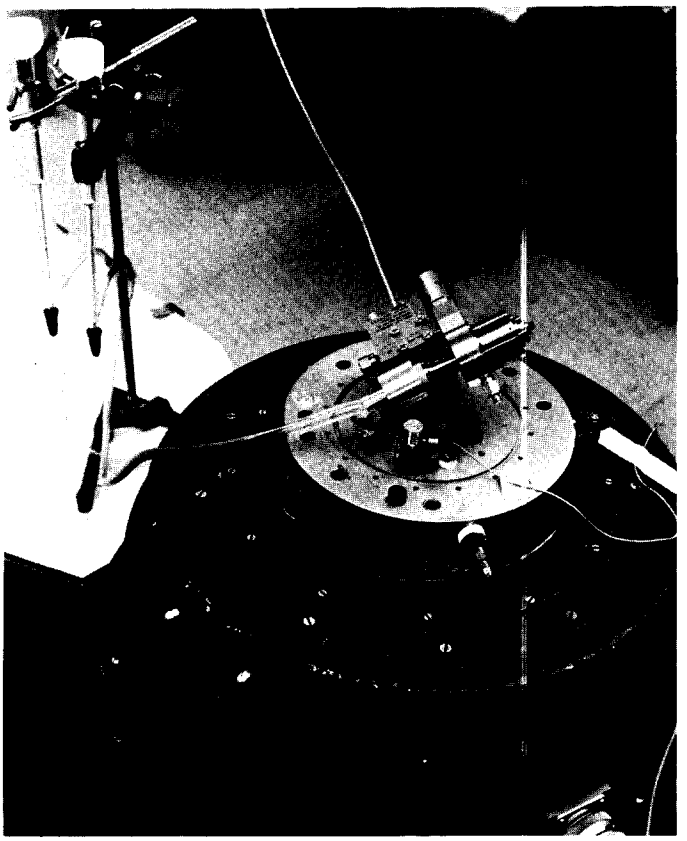

Fig. 54. Pressure regulator vibration tests

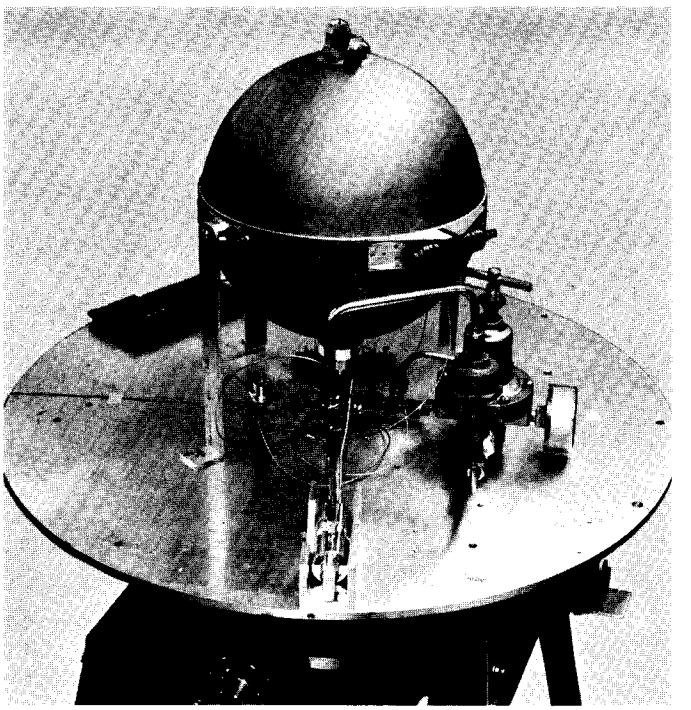

Fig. 55. Gas jet valve air bearing table tests

CONFIDENTIAL
UNCLASSIFIED

UNCLASSIFIED
CONFIDENTIAL

Table 17. Pressure regulator assembly test performance

Supply pressure, psig	Regulated pressure,[a] psig	Flow, scfm	Initial lock, psig	Final lock (5 min),[b] psig
SERIAL NO. 5				
5000	40.6	2.15		
4500	40.4	2.13		
4000	39.7	2.10	42.5	43.0
3500	38.9	2.09		
3000	38.6	2.06		
2500	38.4	2.05		
2000	38.1	2.03		
1500	37.6	2.01		
1000	37.3	1.99		
500	36.4	1.95		
250	36.0	1.91		
SERIAL NO. 6				
5000	40.5	2.15		
4500	40.1	2.13		
4000	39.9	2.12	42.5	45.0
3500	39.6	2.11		
3000	39.1	2.10		
2500	38.6	2.09		
2000	38.3	2.07		
1500	37.9	2.05		
1000	37.4	2.03		
500	36.9	2.00		
250	36.1	1.97		

[a]Specification = 32.0 psig (minimum).
[b]Specification = 50.0 psig (maximum).

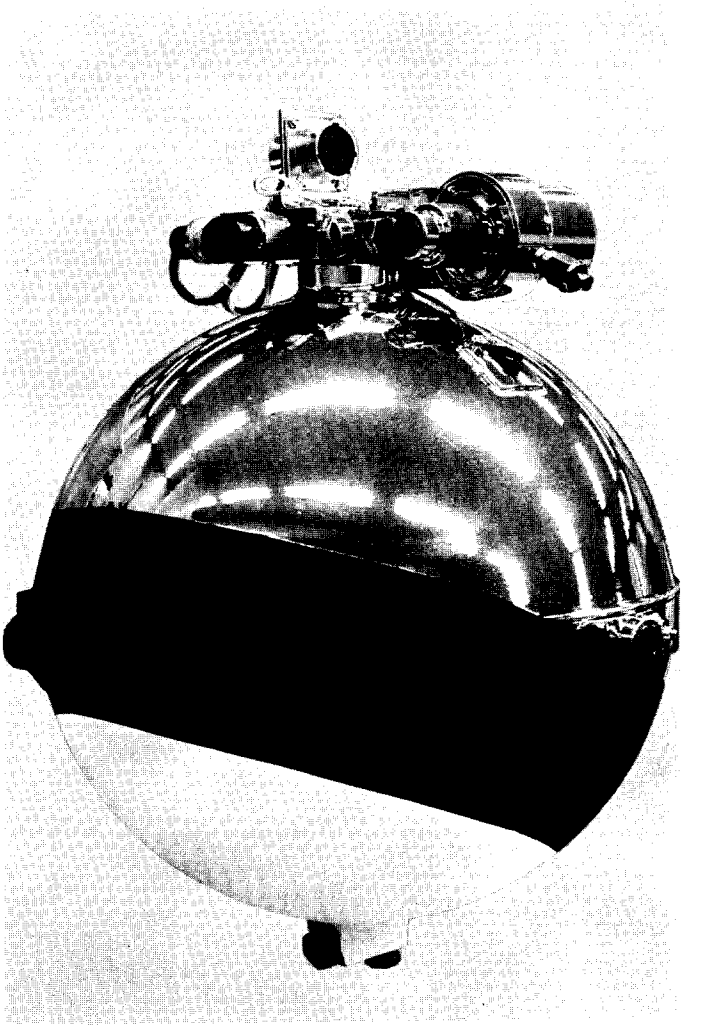

Fig. 56. T-21 gas supply

Table 18. Jet valve performance

Valve number	Side number	Leak rate, cc/hr[a]								
		First 5000 cycles			Second 5000 cycles			Third 5000 cycles		
		Minimum	Maximum	Average	Minimum	Maximum	Average	Minimum	Maximum	Average
1	L1	1.0	1.0	1.0	1.0	1.3	1.02	1.0	3.6	2.4
	L2	1.0	1.0	1.0	1.0	1.0	1.0	1.0	1.0	1.0
2	L1	1.0	3.9	1.2	1.0	1.0	1.0	1.0	1.6	1.13
	L2	1.0	1.0	1.0	1.0	1.0	1.0	1.0	1.0	1.0
3	L1	1.0	1.3	1.01	1.0	2.12	1.58	1.0	4.4	2.27
	L2	1.0	1.0	1.0	1.0	2.2	1.57	1.0	2.75	1.9
4	L1	1.0	1.8	1.07	1.0	1.0	1.0	(Not completed)		
	L2	1.0	3.0	1.8	1.0	3.1	1.9			

[a]Maximum allowable leak rate after 10,000 cycles is 18 cc/hr.

UNCLASSIFIED
CONFIDENTIAL

UNCLASSIFIED
CONFIDENTIAL

7. Roll Actuator

Evaluation tests were initiated on an engineering model of the redesigned roll actuator for use with the Reaction Motors Division vernier engine. Following completion of functional tests, the unit was subjected to vibration equivalent to that expected to be encountered on the spacecraft. Preliminary results of post-vibration functional tests indicated that the unit performance was not significantly affected. During all tests, the actuator was mounted in a test fixture with a simulated vernier engine load (Fig. 57). This load consisted of a ballast representing the vernier engine mass and a spring assembly to simulate the fuel lines. A geared dial and potentiometer were attached to the pivot shaft of the engine ballast to permit accurate measurement of phase lag and amplitude ratio.

The dynamic face seal formerly used on the output shaft was replaced by a standard shaft seal. Leak tests over the expected operating temperature range from 0 to 200°F using this seal resulted in leak rates less than or equivalent to rates measured using the dynamic face seal. Assembly of the actuator is also expected to be facilitated by use of this seal.

8. Electronics Unit

Type approval tests were successfully completed on the electronics unit following a mechanical redesign of

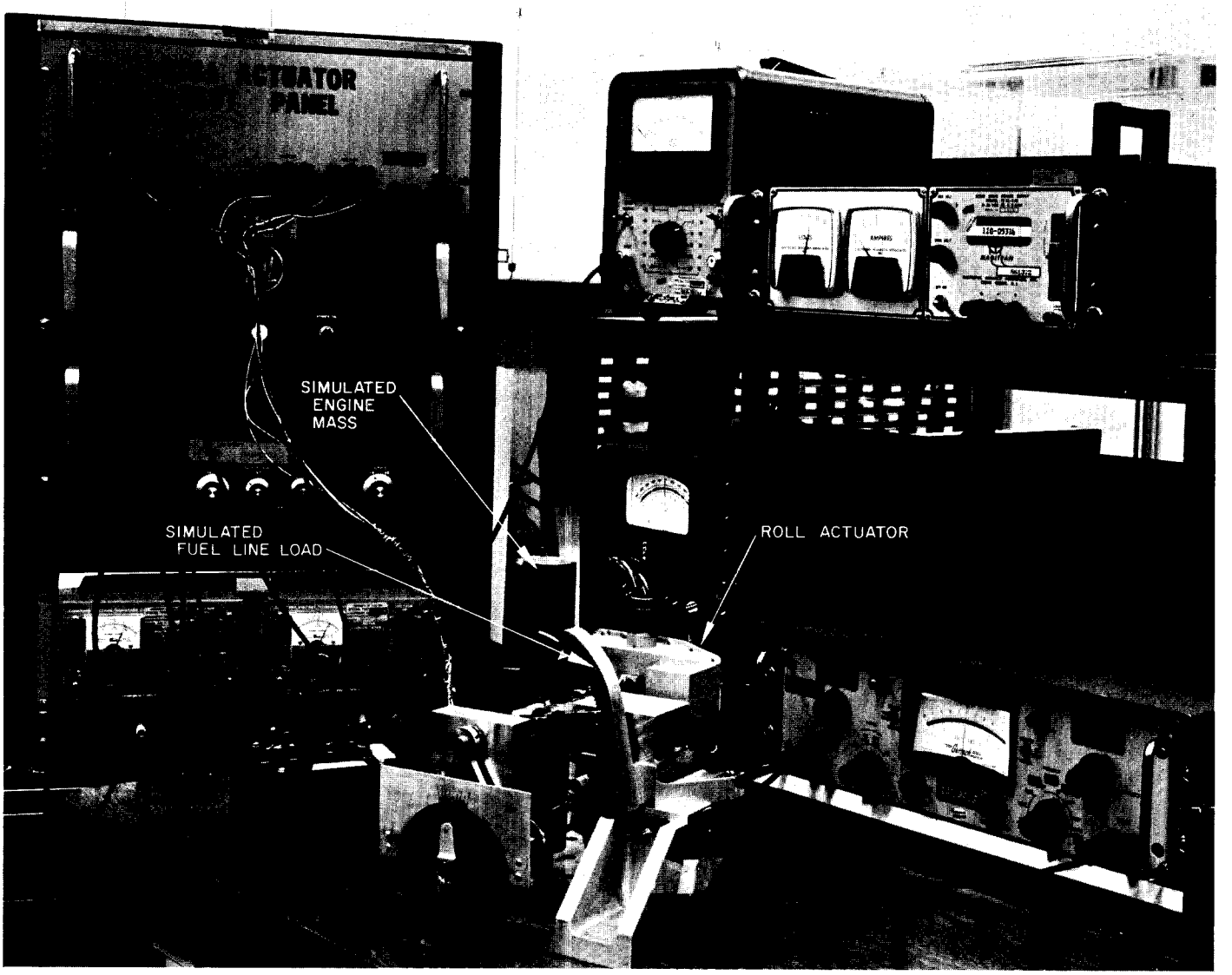

Fig. 57. Roll actuator test fixture

UNCLASSIFIED
CONFIDENTIAL

CONFIDENTIAL
UNCLASSIFIED

the chassis to use honeycomb material instead of polyurethane foam for the core material. No structural failures occurred during vibration tests. Unit performance was satisfactory during additional low level retro mode vibration tests after installation of new non-microphonic transformers. Following completion of type approval tests, the unit was integrated with the T-21 sensor group and delivered to the spacecraft for system testing.

A study to determine the effect of radiative heating from the retro-rocket exhaust plume on electronics unit chassis temperatures indicated that for the worst case radiative heat loading, the maximum increase in chassis temperature remains below allowed design values.

The third flight model of the electronics unit was delivered to the subsystem test area for functional verification, circuit balance, and calibration tests.

CONFIDENTIAL
UNCLASSIFIED

UNCLASSIFIED
CONFIDENTIAL

E. Electronics

1. Introduction

The systems of the spacecraft used for receiving and processing commands and transmitting data to Earth are discussed in this section and include the following: (1) the radio frequency components consisting of two sets of redundant receivers and transmitters, transponder interconnection circuits for operating the receivers and transmitters in the transponder mode, and the planar array (high-gain) and two omnidirectional antennas; (2) command decoding circuitry which receives Earth commands from the receivers and provides output signals to command all spacecraft functions; and (3) signal processing circuitry for processing data for individual scientific experiments and for processing basic spacecraft data through the engineering signal processor, as well as final processing and multiplexing of data which modulates the transmitter. Also included are radar systems associated with flight control functions of the spacecraft.

The television system, spacecraft flight control electronics, and power management are discussed in Sections B, D, and F, respectively.

2. Transmitters

Two identical transmitters are included in each spacecraft to assure reliability through redundancy. High or low power from either transmitter may be directed into any of the three antennas.

a. Receiver phase jitter. Recent changes in the foam encapsulation for the transmitter and receiver oscillator crystals have markedly improved their phase jitter performance. Both transmitter and receiver meet the operational requirements during vibrational phases of the spacecraft mission; under touchdown shock conditions, however, the transmitter phase jitter is still unacceptable and receiver phase jitter is marginal. For these reasons, a new type of crystal mounting technique has been investigated that promises exceptional phase jitter characteristics (see *Space Programs Summary No. 37-28*, Vol. I, dated July 31, 1964). This type of crystal is a ribbon-mounted device, commonly called a Telstar crystal from its early application.

Preliminary tests of a ribbon-mounted crystal used in the PHOENIX program and with a ribbon-mounted crystal blank recently used in both *Surveyor* transmitter and receiver resulted in an order of magnitude phase jitter improvement.

Ribbon-mounted crystal suppliers have been contacted and pilot quantities are being ordered for qualification. This crystal change will be implemented at the earliest possible date. All lunar landing spacecraft configurations are planned to have the ribbon-mounted crystal.

b. RF transfer switch drive circuitry redesign. Recent investigation into T-21 spacecraft equipment failures has revealed that the transfer switch drive circuitry contained within the transmitter has failure modes that could endanger both equipment under test and during a mission. In particular, these failure modes are: (1) failure of the transfer switch to actuate at low battery voltage at high temperatures, causing excessive battery drain and drive circuitry burnout; (2) transfer switch failure causing damage to the drive circuitry and excessive battery drain; (3) coupling of transients generated by inductive switching into command lines causing damage to command decoders; (4) generation of transients if the transfer switch chatters; and (5) generation of a transient when 22-v power is removed in the test area to stop chattering of the transfer switch.

A circuitry redesign was undertaken and the following basic circuit additions were deemed necessary:

(1) A power transistor was added in series with the SCRs to provide definite turn-on and turn-off modes.

(2) A monostable multivibrator was added to drive the power transistor switch.

(3) Diodes were added to provide transient protection on transfer switches.

(4) The transfer switches were moved to the 22-v bus to isolate command lines from transients.

In addition to the above mentioned changes, a study was made to improve the circuit transient immunity.

The redesigned circuitry was breadboard tested (which included temperature testing), results were satisfactory from all design goals. Product design of the changes is approaching completion, and hardware is being built. The planned effectivity of the change is transmitter S/N-16. Fuses and diodes are being added in units below S/N-16 as an interim protective measure.

3. Engineering Mechanisms Auxiliary

The principal functions of the engineering mechanisms auxiliary (EMA) include power switching in various regulated and unregulated voltage circuits, generation and application of constant current pulses to squib firing circuits, and decoding of appropriate switching commands received from the central command decoder.

CONFIDENTIAL
UNCLASSIFIED

UNCLASSIFIED

The EMA OR gate, fed by external command lines, has been changed consistent with the philosophy of desensitizing all command input lines. The function of the OR gate is to provide a path for incoming squib firing commands to enable the constant current generator turn-on switch while preventing mutual feedback. The change was accomplished by addition of a zener diode in the OR gate output (Fig. 58). Specifically, the change consists in removing the zener diode, formerly in series with lead L of the OR gate portion of the AND/OR module, and placing it in series with lead A of the module as shown in Fig. 58.

System tests of the *Surveyor* spacecraft have indicated that silicon-controlled rectifier (SCR) power switching devices tend to be susceptible to anode switching transients and noise at the gate circuits. The EMA utilizes a number of SCR circuits. Although, operationally, a combination of several normally independent conditions must exist simultaneously for RFI to cause EMA misfiring problems (since a current pulse and an SCR ON signal must occur together), a study action plan is in progress to develop approaches for desensitizing those circuits found to be susceptible to RFI, static discharges, transients, etc.

4. Battery Charge Regulator

The voltage potential applied to the bypass silicon controlled rectifier (SCR) drive stage was increased to ensure reliable operation on command. A redundancy factor was realized by applying an additional source of power to this circuit (see Fig. 59).

Emitter voltage for the optimum charge regulator (OCR) bypass driver amplifier transistor was originally 24-v derived from the solar panel bus. Since the collector is tied to the 22-v unregulated bus, the collector to emitter voltage, V_{ec}, of this transistor will vary inversely with changes in the battery and the 22-v unregulated bus voltage. Under conditions of high battery voltage, V_{ec} became so low as to cause marginal operation of the transistor at 0°F.

The change modifies the circuit to provide 29-v dc emitter voltage for the transistor from the 29-v regulated nonessential/solar bus and thus ensures sufficient V_{ec} for reliable operation over the temperature range 0 to 125°F. This change has been incorporated in all battery charge regulator units including the T-21 test model.

5. Auxiliary Battery Control

The auxiliary battery control (ABC) (Fig. 60) automatic transfer from the main battery mode to the auxiliary battery mode has been made a function of the auxiliary battery terminal voltage when the auxiliary battery falls below approximately 22 v. When the auxiliary battery is above approximately 22 v, automatic transfer will occur when the main battery decreases to 20 ±0.1 v (Fig. 61). Prior to the change, the automatic transfer had been set at a fixed unregulated bus level of 17.5 v. The design improvement will prevent: (1) unregulated bus transfer to a discharged or shorted auxiliary battery, and (2) overload/undervoltage trip circuit (OTC) trip due to low boost regulator (BR) input voltage (17.00 ±0.25 v) during automatic transfer because of main battery series diode and line voltage drops. The removal of the auxiliary battery series diodes precludes a high voltage condition on the unregulated bus when in the auxiliary battery mode due to excess solar panel/battery charge regulator

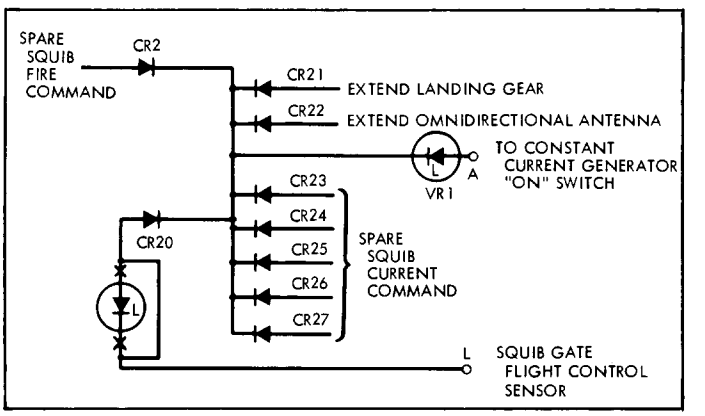

Fig. 58. AND/OR gate module

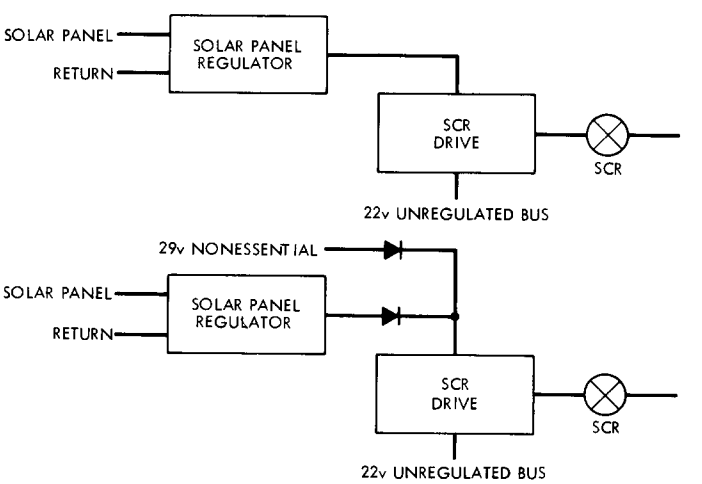

Fig. 59. Battery charge regulator power source changes in SCR drive circuit

CONFIDENTIAL
UNCLASSIFIED

UNCLASSIFIED
CONFIDENTIAL

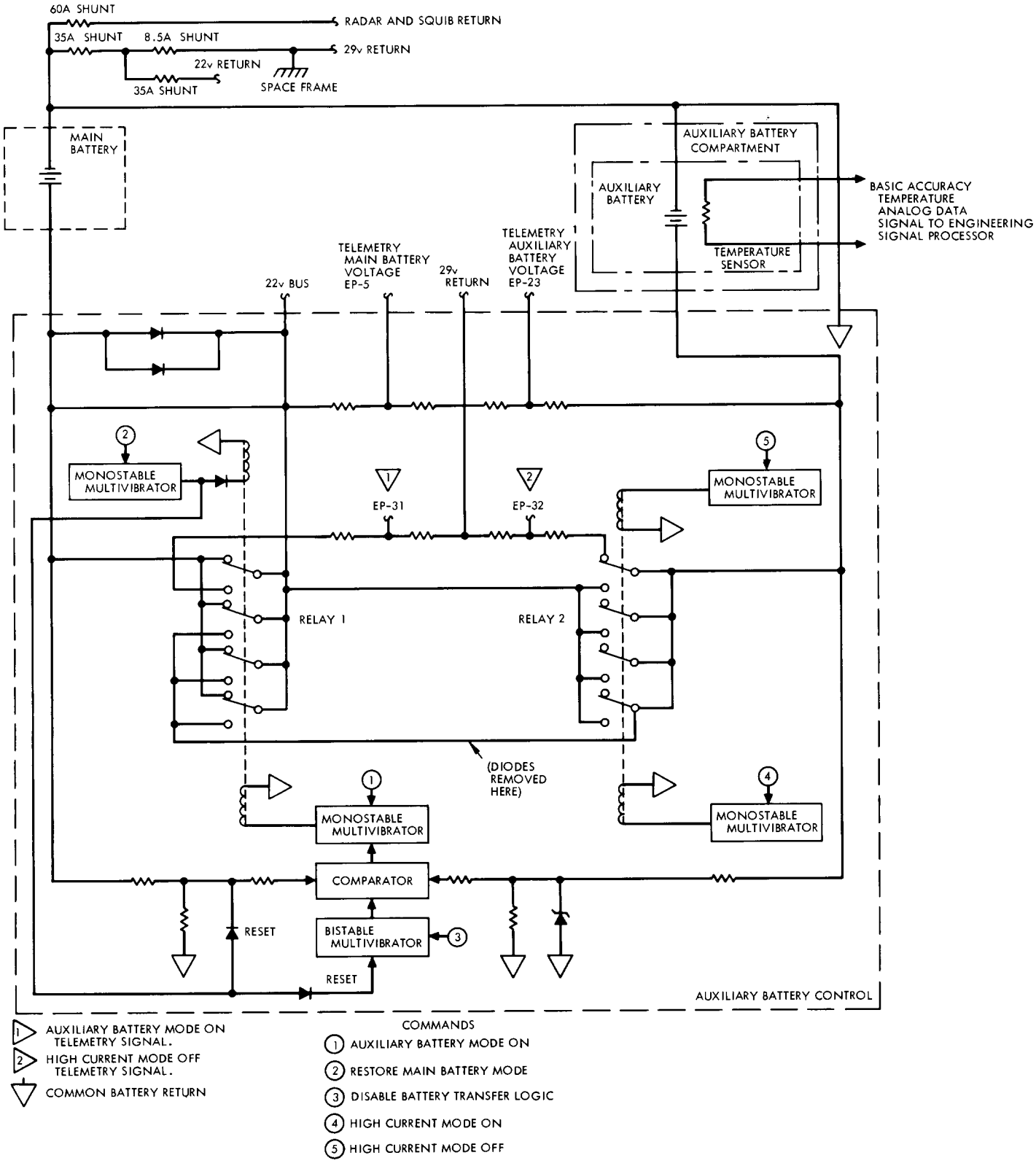

Fig. 60. Auxiliary battery control functional schematic

UNCLASSIFIED
CONFIDENTIAL

UNCLASSIFIED
CONFIDENTIAL

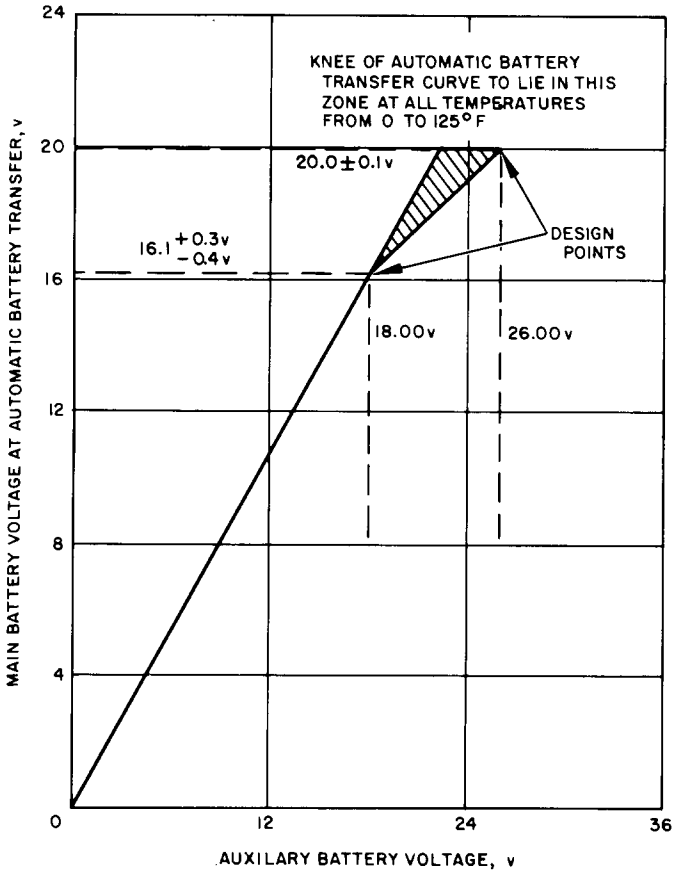

Fig. 61. Automatic battery transfer criteria

(BCR) power. This design improvement ensures constant battery load on the BCR.

Voltage dividers have been added to the ABC unit to provide digital telemetry information of the battery relay positions (see Fig. 60). Prior to this change, the main, auxiliary, and high current modes of operation were determined by analyzing battery and unregulated bus telemetry voltage data.

6. Boost Regulator

The overload/undervoltage trip circuit of the boost regulator will turn off the nonessential bus to protect the BR and the nonessential loads under the fault conditions of nonessential bus overload, low unregulated input voltage, and low nonessential bus voltage caused by an overload. The overcurrent trip circuit level is 7.0 ± 0.9 amp. During T-21 systems test it was revealed that the combination of transmitter (high power) and signal processing loads is sufficient to trip the OTC and drop out all nonessential bus loads. The transmitter draws a surge current of approximately 9 amp for approximately 2 msec and 5.5 amp for the duration of the 20-msec transmitter high-power command pulse. Once the current through the current sensing tunnel diodes in the OTC exceeds the overcurrent trip level, the OTC will trip following a 20-msec delay, unless the current drops below the tunnel diode valley current of approximately 5.5 amp during the 20-msec delay.

This problem has been eliminated by removing the overcurrent trip circuit from the OTC. With a BR unregulated input voltage of 22 volts, the OTC will trip in the low nonessential bus voltage mode at an overcurrent of approximately 11 amp. This inherent trip capability adequately protects the OTC series transistor which is rated for a continuous current of 20 amp. This modification was completely tested and incorporated into all boost regulator units, including the T-21 test model.

UNCLASSIFIED
CONFIDENTIAL

UNCLASSIFIED
CONFIDENTIAL

F. Electrical Power Supply

1. Introduction

Electrical power for the *Surveyor* spacecraft is supplied by a Sun-tracking planar solar panel and a sealed, secondary silver-zinc main battery. On the first four spacecraft, an auxiliary battery will be utilized to provide additional peak load capability and increased energy storage capacity during transit and the lunar day; the main battery provides the electrical energy for operation during the lunar night.

The power management system is composed of a central power control unit and a variety of voltage converters, regulators, and power switches located in other units that provide power management for the various instruments and subsystems. The central power control unit provides power conversion from the solar panel, main bus regulation, overload sensing, main battery charge control, and several switching functions. The optimum-charge regulator circuit provides efficient conversion of solar panel power for use in battery charging. The battery output voltage from the unregulated bus is converted to the main regulated bus voltage by a boost regulator. A main overload trip circuit using tunnel-diode sensing removes all nonessential spacecraft loads when an overload condition is detected. The main battery charge logic system controls the charging current to the spacecraft main battery. Normally, the system operates in the automatic mode and the main battery is charged until its voltage reaches a predetermined level. A command mode is available whereby the battery may be commanded to be charged.

The auxiliary battery control unit provides battery voltage sensing circuitry, automatic control and selection of either the auxiliary or both batteries, and provision for command override of the automatic control mode. A main power switch provides capability to disconnect all spacecraft power.

2. Progress Summary

The redesign of the solar panel wiring harness was incorporated by means of retrofit or rework to previously fabricated panels. S/N-1 and S/N-2 panels received a functional check after incorporation of the change and were delivered to bonded stores. The S/N-3 panel was reworked and after successful completion of the flight acceptance test (FAT) program is awaiting secondary Sun sensor installation. Fabrication of the S/N-4 panel has been resumed. The reliability test panel was fabricated and the panel is undergoing FAT.

A developmental solar panel was subjected to gas impingement tests at the NASA Lewis Research Center. The panel demonstrated no indication of significant damage. JPL successfully completed three balloon flights that included space calibration of six Hughes solar cells. These cells will be used as primary standards for sunlight tests of solar cell modules and solar panels. The Heliotek solar cell module deliveries have been completed. Five lots remain to be inspected at Hughes Aircraft Company. Infrared radiometry is currently being evaluated for possible application in solar array testing. Preliminary results are encouraging.

Five prototype main batteries have successfully passed type approval test vibration and shock. Of the five batteries, four passed a 300-hr type approval thermal–vacuum test. Final evaluation of the auxiliary battery relief valve verified that the valve will provide reliable pressure release.

The auxiliary battery thermal control surface has been redesigned to compensate for an increased power dissipation profile. The reliability test program of eight flight-model auxiliary batteries was completed. Flight acceptance test of flight batteries S/N-9 through 12 was also completed.

A main power switch has been added to the electrical power system. The switch permits command disconnect of electrical power from the spacecraft subsystems.

3. Solar Panel

a. ***Wiring harness redesign.*** Redesign of the solar panel wiring harness to provide a compatible connection to the mast harness was completed and incorporated into solar panel drawings during the latter part of July. Rework or retrofit of existing solar panels was begun immediately thereafter.

b. ***Flight hardware***

S/N-1 solar panel. Flight solar panel S/N-1 was withdrawn from bonded stores for wiring harness retrofit on July 26, 1964. Fig. 62 shows the rear side of the panel after completion of retrofit. Portions of the subgroup test harness are visible. A post-retrofit sunlight functional check was performed at the Hughes El Segundo facility using secondary space-calibrated solar cells. Table 19 shows the performance of the solar panel for air mass zero conditions at 25°C. The retrofitted panel was deemed acceptable and was returned to bonded stores on August 12, 1964. A flight acceptance test program report for the S/N-1 panel will be published during the current report period.

CONFIDENTIAL
UNCLASSIFIED

UNCLASSIFIED
CONFIDENTIAL

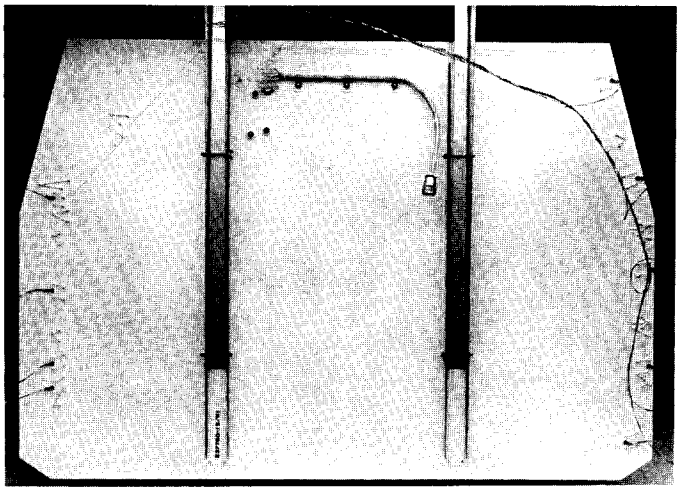

Fig. 62. S/N-1 solar panel after wiring harness retrofit

Table 19. Performance of flight solar panel S/N-1

Item	Power, watts, at air mass zero, 140 mw/cm², 25°C	
	Power requirement	Power output
Total panel	95.8	104.9
Subgroups		
V-1	10.79	11.67
V-2	10.79	11.63
V-3	10.79	11.69
V-4	10.79	11.55
V-5	10.79	11.64
V-6	10.79	11.64
V-7	10.79	11.75
V-8	10.79	11.62
V-9	10.79	11.65

S/N-2 solar panel. After completion of FAT on June 23, 1964, delivery of flight solar panel S/N-2 was postponed for wiring harness rework. Rework was completed, followed by a sunlight functional check at the Hughes El Segundo facility using secondary space-calibrated solar cells. Table 20 shows performance of the panel under air mass zero conditions and at 25°C. The performance was acceptable and delivery to bonded stores took place on August 21, 1964. A flight acceptance test report will be published in October.

S/N-3 solar panel. Following completion of fabrication of flight solar panel S/N-3 on August 3, 1964, the panel was subjected to the flight acceptance test sequence which included pre-environmental sunlight electrical performance testing at Table Mountain, vibration testing, post-vibration sunlight electrical performance testing at Table Mountain, thermal–vacuum testing, and post thermal–vacuum sunlight electrical performance testing at Table Mountain. Electrical performance testing was conducted to the revised FAT specification, which incorporated the optional use of secondary space-calibrated solar cells. A summary of electrical performance testing for the S/N-3 is shown in Table 21. Results of flight acceptance testing were acceptable, with panel performance remaining about 6% over the specification requirement throughout the flight acceptance test sequence. Following completion of flight acceptance testing on August 31, 1964, the panel was placed in interim storage awaiting installation of the secondary Sun sensor. Due to unavailability of the secondary Sun sensor, panel delivery to bonded stores is expected to be postponed about 1 mo.

Table 20. Performance of flight solar panel S/N-2

Item	Power, watts, at air mass zero, 140 mw/cm², 25°C	
	Power requirement	Power output
Total panel	95.8	104.8
Subgroups		
V-1	10.79	11.69
V-2	10.79	11.81
V-3	10.79	11.57
V-4	10.79	11.65
V-5	10.79	11.88
V-6	10.79	11.83
V-7	10.79	11.69
V-8	10.79	11.80
V-9	10.79	11.82

S/N-4 solar panel. Fabrication of flight panel S/N-4, temporarily suspended to permit fabrication of the reliability assurance test solar panel, has been resumed. Module installation is presently under way. A slight delay has been incurred due to relocation of fabrication facilities.

Reliability assurance test solar panel. Fabrication of the reliability solar panel was completed. Pre-environmental sunlight electrical performance testing at Table Mountain has been conducted, as well as flight acceptance vibration testing. A 1-mo delay in flight acceptance thermal–vacuum testing is anticipated due to higher priority occcupancy of environmental test chambers. Table 22 shows the results of the pre-environmental sunlight electrical performance tests. Results were acceptable with performance more than 6% over the minimum requirement.

UNCLASSIFIED
CONFIDENTIAL

UNCLASSIFIED CONFIDENTIAL

Table 21. Performance tests at Table Mountain of S/N-3 solar panel

Item	Specification requirement[a]	Specification requirement[b]	After fabrication[b]	After vibration[a]	After thermal-vacuum[a]
Total panel	79.2	95.8	102.1	83.5	84.6
Subgroups					
V-1	8.8	10.79	11.41	9.50	9.52
V-2	8.8	10.79	11.57	9.37	9.64
V-3	8.8	10.79	11.39	9.45	9.55
V-4	8.8	10.79	11.53	9.58	9.50
V-5	8.8	10.79	11.47	9.39	9.50
V-6	8.8	10.79	11.29	9.41	9.41
V-7	8.8	10.79	11.59	9.46	9.43
V-8	8.8	10.79	11.47	9.45	9.34
V-9	8.8	10.79	11.62	9.40	9.44

[a]Power, watts, at air mass one, 100 mw/cm², 25°C; data reduction per Procedure 1 of Flight Acceptance Test Specification.
[b]Power, watts, at air mass zero, 140 mw/cm², 25°C; data reduction per Procedure 2 of Flight Acceptance Test Specification using secondary space-calibrated standard solar cells.

Table 22. Pre-environmental performance of reliability test solar panel

Item	Power output, watts, at 100 mw/cm², 25°C	
	Specification requirement	After fabrication
Total panel	44.0	46.72
Subgroups[a]		
V-1	8.8	9.43
V-3	8.8	9.41
V-5	8.8	9.36
V-7	8.8	9.28
V-9	8.8	9.30

[a]The reliability panel has five subgroups compared to nine subgroups on a flight panel.

c. ***Solar panel shipping containers.*** A third test container has been purchased and is to be modified to permit elevated-temperature tests of solar panels.

A contract for six shipping containers to be used for storage and shipment of flight panels to Cape Kennedy has been placed with Zero Manufacturing Co.

d. ***Gas impingement tests.*** Development Solar Panel 2, partially filled with solar cell modules, underwent gas impingement testing at Lewis Research Center to determine the effects of gas impingement occurring during nose cone ejection. On the basis of detailed inspection records made prior to panel shipment to Lewis Research Center, no significant damage to the solar panel resulted from the test. Gas impingement tests are scheduled for continuation at the end of October.

e. ***JPL balloon flights.*** Three sets of *Surveyor* solar cells (two per set) were tested by JPL at an altitude of 80,000 ft. At this altitude, the short circuit current of each solar cell was measured and telemetered back to ground. The solar cell output under near-space conditions (air mass zero and 135 mw/cm²) was thereby calibrated. After the test period was concluded, the specimen package was returned to Earth via a parachute. The telemetry information is now undergoing data reduction and it is expected that several flight-calibrated primary standard cells will be available soon.

The solar panel flight acceptance test specification has been revised to incorporate the balloon-calibrated cells as a standard reference. The new FAT procedure will permit the testing of solar panels under less than optimum sky conditions, thus reducing the cost and time of the total FAT program.

f. ***Solar cell modules.*** The Heliotek hardware subcontract has been completed with the delivery of Lot 27 to Hughes. A total of 10,800 solar cell modules have been delivered. To date, approximately 1% of the modules have been scrapped due to damage sustained during handling, test, panel fabrication, and module rework. Hughes has completed flight acceptance testing on all lots through Lot 22.

The third solar cell module type approval test (TAT) program (TA-3) is in the final stages of electrical performance testing. All environmental exposures have been

UNCLASSIFIED CONFIDENTIAL

UNCLASSIFIED
CONFIDENTIAL

completed; it is estimated the TA-3 test will be completed by October 1.

g. *Investigation of infrared test techniques.* Tests have begun to evaluate infrared radiometry as applied to the testing of solar arrays. A high level forward bias is utilized to produce internal heat generation, which raises the temperature of the solar cells a few degrees above ambient. Thermal gradients are then measured using an infrared radiometer. It is expected that damaged areas will be detected because of different heat generation rates. Both fixed spot and scanning systems are being considered. Fig. 63 is an infrared photograph of six *Surveyor* solar cell modules. The photo was taken with a Barnes Engineering Company scanning camera. As noted on the photograph, major defects are easily detectable. An analysis of these premilinary test results is in progress.

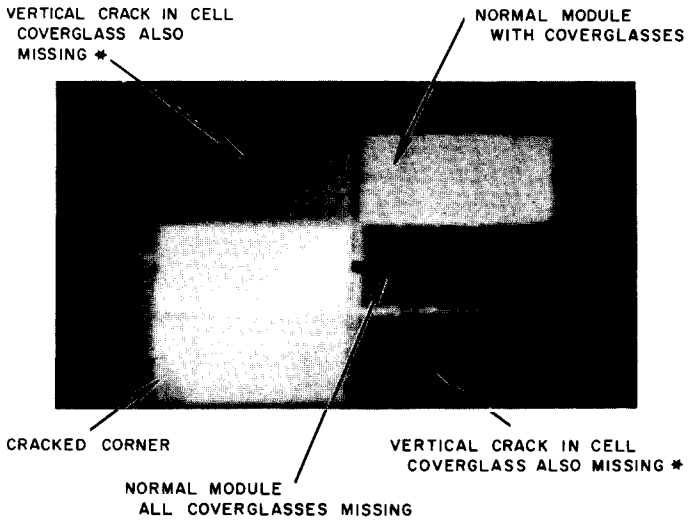
VERTICAL CRACK IN CELL COVERGLASS ALSO MISSING *
NORMAL MODULE WITH COVERGLASSES
CRACKED CORNER
VERTICAL CRACK IN CELL COVERGLASS ALSO MISSING *
NORMAL MODULE ALL COVERGLASSES MISSING
* ENTIRE MODULE IS COOLER (DARKER) THAN NORMAL. ALL CELLS WITH EXCEPTION OF CRACKED CELL HAVE COVERGLASSES INTACT.

Fig. 63. Infrared photograph of *Surveyor* modules

4. Batteries

a. *Main battery.* Prototype battery S/N X-43 has successfully passed type approval vibration and shock testing. This makes a total of five batteries qualified at type approval levels of vibration and shock. X-43 has all molded plates, whereas the other four batteries qualified were a mixture of hand-made and molded plates. For this reason, X-43 was subjected to TAT levels of vibration and shock.

Flight batteries S/N-1, 2, 3, 5, and 6 have successfully passed FAT. Flight batteries S/N-4, 7, 8, and 9 have com-

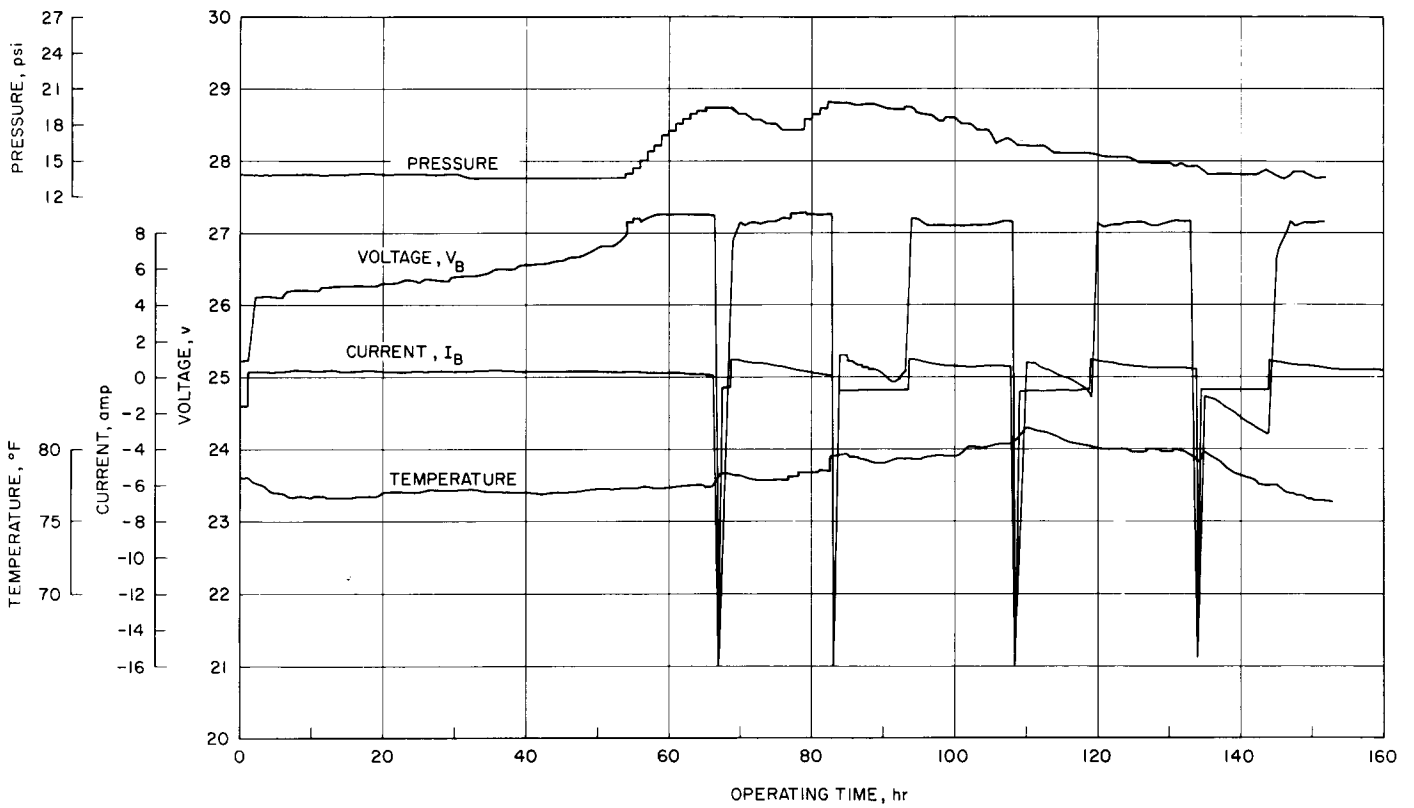

Fig. 64. Battery performance during thermal–vacuum test

UNCLASSIFIED
CONFIDENTIAL

UNCLASSIFIED
CONFIDENTIAL

pleted preliminary acceptance tests and are now ready for FAT vibration tests.

Prototype batteries S/N X-37 through X-40 successfully passed a 300-hr TAT thermal–vacuum test. Fig. 64 illustrates the X-39 battery performance as a function of operating time.

Battery matrix tests are under way; the tests consist of a series of charge and discharge cycles on a number of prototype batteries with different operating conditions on each cycle. Portions of the test have been completed. Analysis of the results indicate more data are necessary to obtain a repetition of points before a statistical battery with definable confidence level can be established.

b. ***Auxiliary battery.*** As previously reported, ten auxiliary battery valve assemblies of identical design underwent cycle life tests at 0, 70°, and 130°F under an ambient pressure of 10^{-4} Torr. Each valve was opened and closed ten times at each temperature in the following sequence: 70°, 130°, 0°, 70°, 130°, and 0°F.

The relief valve submitted to this test was a simple adjustable-coil spring-loaded valve designed to open between 9 and 15 lb/in.^{2} and reclose at a minimum pressure of 5 lb/in.^{2}. Sealing is accomplished by the action of the valve and O-ring seal assembly on the valve seat. Fig. 65 shows the valve construction.

Nine of the ten relief valves successfully passed the sequence of tests, including a leak rate check at the conclusion of cycling. The measured leak rates were in the order of 10^{-6} cc of Helium per second. One valve failed to completely reseat under a decaying pressure, although it fully opened within specified limits. The valve was examined and it was noted that a piece of foreign

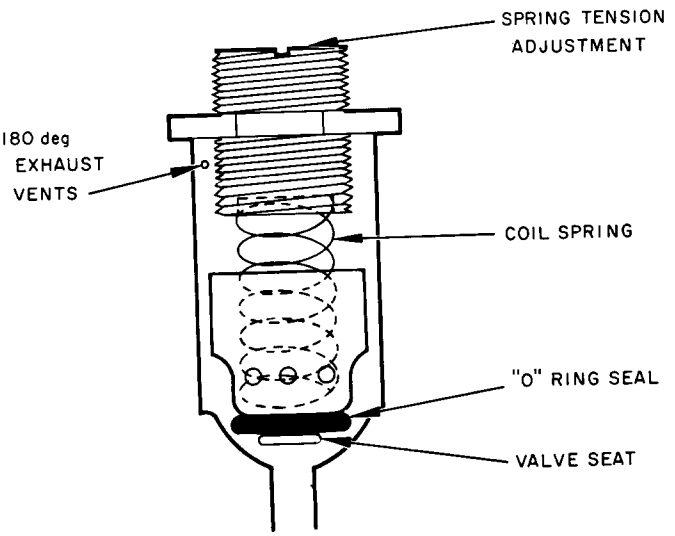

Fig. 65. Pressure relief valve

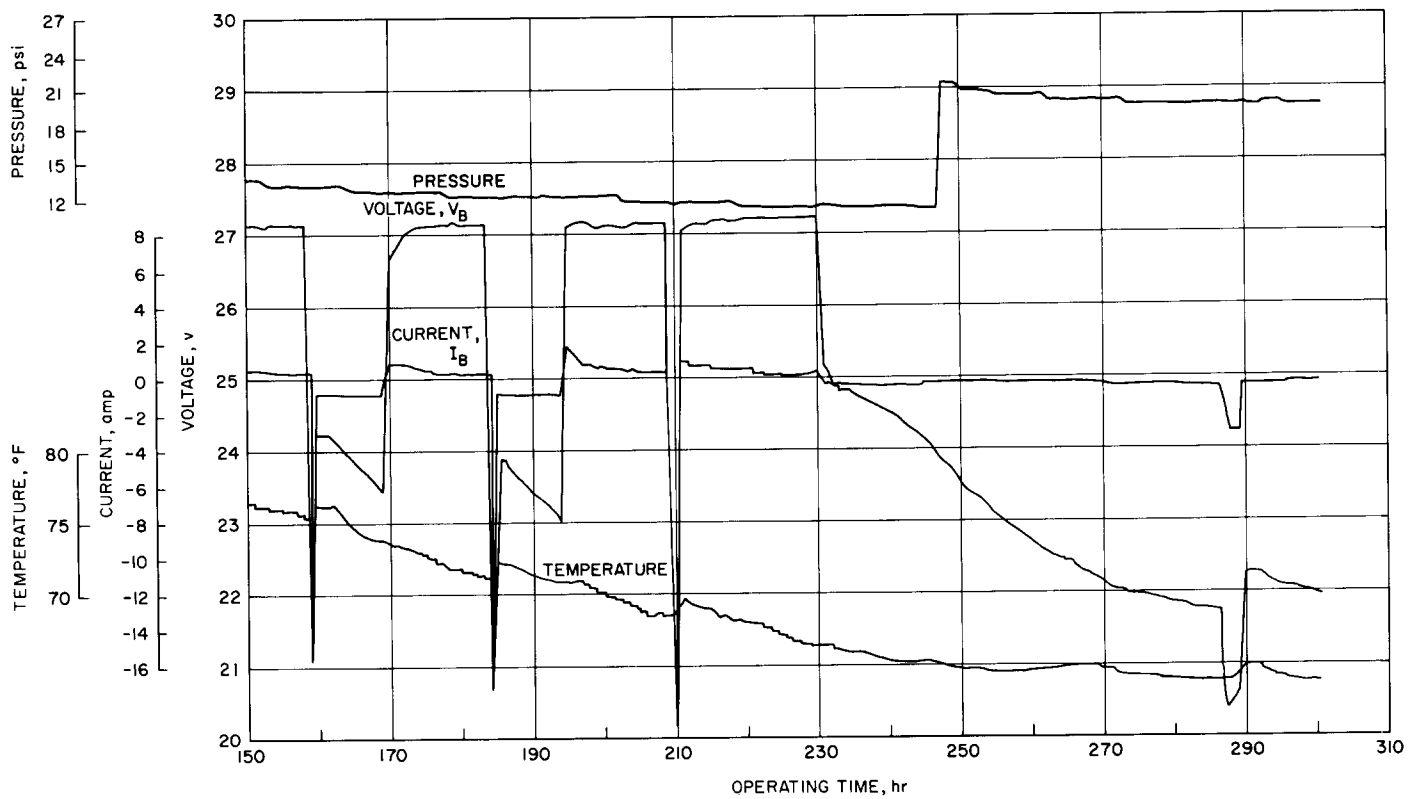

Fig. 64 continued. Battery performance during thermal–vacuum test

CONFIDENTIAL
UNCLASSIFIED

UNCLASSIFIED
CONFIDENTIAL

material had adhered to the O-ring seal. After cleaning, the valve performed satisfactorily. Based on results of the test program, it was concluded the relief valve operates satisfactorily under environmental conditions, thus insuring reliable pressure release for the auxiliary battery.

The auxiliary battery thermal control surface has been redesigned to compensate for an increased power dissipation profile. The new surface treatment includes the use of aluminum foil on the exposed magnesium case and white inorganic paint on the aluminum cover. Thermal analysis indicates that a maximum temperature of 114 ± 15°F will occur in transit during the terminal descent. An evaluation of the accuracy of the thermal analysis will take place after the T-21 thermal–vacuum tests.

The reliability test program of eight flight-model batteries has been completed. The test program was designed to determine the battery capacity as a function of activated stand time and temperature. The results are reported in Section K.

Flight acceptance test of flight batteries S/N-9 through 12 has been completed; the batteries will be delivered to bonded stores for use in system vehicle testing. Batteries S/N-13 through 16 were delivered by Eagle-Picher to Hughes in mid-October.

5. Surveyor Main Power Switch

A main power switch has been added to the electrical power system for the purpose of disconnecting all spacecraft power if required. The power cutoff switch is a single-pole, single-throw, motor-driven switch. When open, the switch removes all spacecraft power including the battery charge regulator output, from bus TB-1 as shown in Fig. 66.

The switch will be located above the main battery in Compartment A of the spacecraft. It weights about 1 lb and occupies 16.9 in.^{3} The voltage drop will be less than 50 mv. At 50 amp through the main contacts, the nominal motor voltage is 28 v. Kinetics Corporation has been chosen to supply the switch, designated Model No. M936-3. The unit will be qualification tested beginning in late December. The first switch is scheduled to be delivered on December 15, 1964.

6. Power System Integration Testing

Simulation tests of the *Surveyor* transit mission were conducted during this report period. The transit power sequence was not completed due to depletion of the system's stored energy (an auxiliary battery was not used

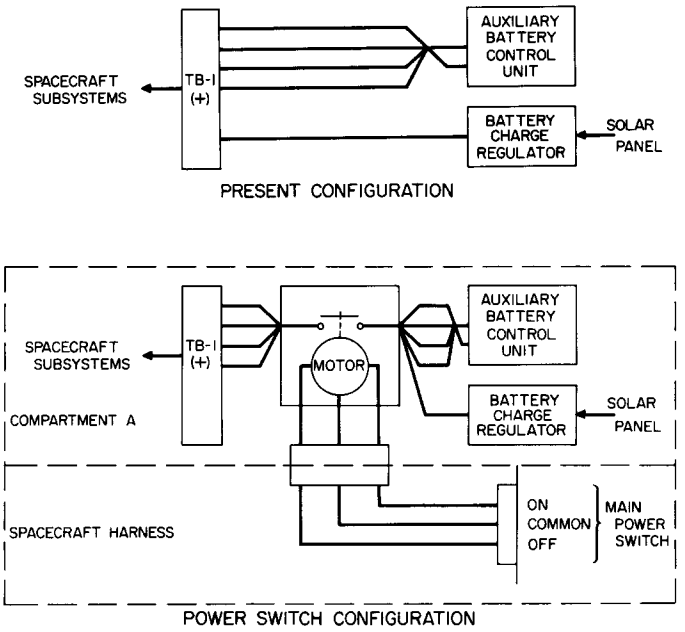

Fig. 66. Main power switch wiring

to supply power). The test was repeated a second time to verify the results. The power depletion was caused by an inefficient solar panel-optimum charge regulator (OCR) interface. Power from the solar panel was only fractionally utilized because of the large voltage swing at the input to the OCR. The unconducted power during transit totaled at least 500 w-hr and was the cause of depletion of stored energy more rapidly than had been anticipated. To correct the problem, several minor changes in the OCR breadboard circuitry were made.

In the last report period, it was reported that the breadboard model OCR did not track the solar panel maximum power point after the panel power output dropped below 60 w. This problem has also been corrected by the same OCR circuitry changes previously noted.

Tests to be conducted will continue with use of a *Surveyor* solar panel. Tests scheduled during the next reporting period include measurement of response times to various command signals and the simulation of failure modes.

7. Boost Regulator Battery Charge Regulator

A circuit redesign to improve the overall system operating efficiency during the transit phase was described in the preceding report. Dissipated power was reduced by approximately 9 w by delivering charging power from the OCR directly to the preregulated bus. This mode of operation is of particular advantage during the transit

CONFIDENTIAL
UNCLASSIFIED

UNCLASSIFIED
CONFIDENTIAL

phase when the power demands are approximately equal to the charging power.

Satisfactory results were achieved in the breadboard tests of the new circuits. Design of the new product packages was started in August and the drafting effort is nearing completion at the end of this report period. The new packages will be mechanically and electrically interchangeable in the spacecraft interface. Delivery of the first units for assembly is expected early in May 1965.

CONFIDENTIAL
UNCLASSIFIED

UNCLASSIFIED
CONFIDENTIAL

G. Thermal Control

1. Introduction

The *Surveyor* thermal control system consists of the individual subsystems or unit thermal control systems integrated to provide acceptable thermal environments for all components during all phases of spacecraft operation. The passive and active methods employed include (1) special preparation of spacecraft external surfaces to achieve optimum thermal absorption and emission characteristics, (2) superinsulated compartments to house critical equipment, and (3) electrical heaters and thermal conduction paths controlled by bimetallically operated thermal switches to maintain compartment temperatures within acceptable limits.

System integration of spacecraft thermal control subsystems and thermal compatibility of proposed mission sequence operations are verified. Thermal switches and spacecraft coatings are developed; subsystem thermal-vacuum performance is evaluated by hardware tests with the MT-1 vehicle and other thermal models. Qualification of the spacecraft prototype thermal design is to be performed on the T-21 vehicle. Mission operation activities are supported by the development of Space Flight Operations Facility (SFOF) thermal management procedures.

2. Progress Summary

The compartment thermal dissipating capabilities during lunar surface operation have been reexamined for both the A-21 and A-21A to incorporate the latest information available on both the compartment design and the surrounding spacecraft environment. The study shows that for the A-21 compartment a positive nominal lunar noon dissipating capability is available and that the total compartment system lunar night heat loss will be approximately 20 w instead of 60 w as previously estimated.

New retro propellant temperature distributions were calculated to include the effects of both the revised values of propellant thermal properties and the changes to the geometry of the propellant envelope. The study considered a 1230-lb loading, a 1250-lb loading, and a 1250-lb initial loading cut back to 1230 lb. In all cases, the minimum temperature point remained at the skirt attach point and did not exceed the 20°F allowable lower limit. The study indicated that the maximum propellant temperature gradient at terminal descent attributable to shading would be less than 5°F between a shaded region and an illuminated region.

Vernier engine pre-test temperature predictions have been completed for the T-21 thermal-vacuum test. Vernier Engine 2 has been fitted with a development type integral solar collector. Testing of the integral collector during the T-21 solar-thermal-vacuum test will provide experimental evaluation of the proposed design.

Review of the helium tank thermal control design indicates that the tank could exceed its upper temperature limit during transit phases in the T-21 thermal-vacuum test and in actual flight. As a result, the thermal paint pattern has been modified.

The design point nominal temperatures for the passive thermal design of the RADVS system have been revised to be compatible with the recently expanded activation temperature range. Based on the revised nominal temperatures, the T-21 RADVS thermal finish patterns are being changed on the T-21 hardware. A development test procedure has been formulated to verify nominal temperatures, internal temperature ranges, and transient thermal characteristics of the T-21 RADVS units during the T-21 solar-thermal-vacuum test.

The analysis of the attitude control system attitude jets has been updated to include the MT-1 thermal-vacuum landing gear test data. The study indicated a necessity for minor modifications in the roll jet mounting bracket conductance.

The thermal study of the micrometeorite ejecta detector sensor head has been completed and submitted to JPL. The study recommended that Hughes inorganic white paint should be applied to the exterior surfaces of the electronics case and that the maximum temperature limit be increased to 213°F.

Definition of the special test hardware required to simulate a flight environment in the T-21 solar-thermal-vacuum test has been completed. The test plan has been established and includes a system functional test of 30 hr duration and a thermal control evaluation test of 75 hr duration. The thermal control evaluation test combines a mission sequence, a RADVS thermal development test, and an engineering data gathering sequence. The "fit and function" thermal evaluation test has been completed. The test verified the adequacy of the auxiliary data monitoring system. The test also showed that the shadow patterns on T-21 resulting from the use of the liquid nitrogen shadow shrouds are quite similar to those on an actual flight vehicle. Experience was obtained in operational procedures to be used in T-21 testing and in coordination among participating groups.

A detailed operating procedure to be used by the SPAC thermal specialist during the transit portions of the *Surveyor* missions has been prepared. A study of

UNCLASSIFIED
CONFIDENTIAL

UNCLASSIFIED
CONFIDENTIAL

the equipment required by the SPAC thermal specialist for purposes of *Surveyor* nonstandard and lunar thermal operation analyses has been completed. The study provides preliminary sketches of the equipment, cost estimates, and a discussion of the equipment use. Incorporation of the equipment into the SPAC system is awaiting JPL concurrence.

The initial quality of the lapped contact surfaces of the first production thermal switches has been found to be inadequate and rework of these parts is in progress. The thin-wall thermal switch cases failed during the axial vibration of S-2A at TAT levels. As a result, the case wall thickness has been increased from 0.004 to 0.0055 in. The new case design will be tested on the S-2A vehicle in mid-October.

A thermal control model (TCM) test program has been proposed to JPL. Hughes has been authorized to proceed immediately on the initial phase. The purpose of the TCM test program is to provide thermal control system information to supplement the data obtained from the MT-1 sector test, the T-21, and T-21A spacecraft tests, and to provide a test medium by which the limitations imposed by the existence of operable spacecraft control items can be circumvented.

The program to study the ultraviolet degradation of the *Surveyor* white inorganic paint was completed. The study indicated no irregular instabilities, and the paint is concluded to be entirely suitable for *Surveyor* use.

The main retro exhaust plume spacecraft radiation heating study has continued. Thermal measurements were made during recent main retro firing tests at AEDC. The preliminary test data is reported. Intensive study of the particle and energy distribution within the plume is underway. Preliminary results indicate the high energy envelope has been overestimated and the severity of spacecraft heating is less than originally anticipated.

3. *Subsystem Thermal Analysis and Design*

a. Compartment system. The compartment system thermal dissipating capabilities during lunar operation have been reexamined for both A-21 and A-21A to incorporate the latest information available on both the compartment design and surrounding spacecraft thermal environment. In the analysis, the planar array antenna was assumed to have a temperature profile corresponding to a horizontal position throughout the lunar day since this yields the most severe thermal environment for the compartments during the lunar noon interval. The solar panel was assumed to be receiving normal incident solar illumination throughout the lunar day. As a further refinement percent solar illumination was introduced as a parameter since each compartment can be partially shaded depending on the orientation of the planar array antenna and solar panel during any given time.

Fig. 67 shows lunar day nominal thermal performance of the A-21 and A-21A compartment systems respectively. A thermal performance tolerance of ±6 w is applicable to the Model A-21A compartment system design; tolerances of the Model A-21 compartment design are being evaluated. The performance difference between the two models is related to the type of wire harness used with each. It was reported in the preceding report that, contrary to previous opinion, the anticipated conductance coupling between the compartment wiring harnesses and the connector plates is small. Consequently, the heat leak into the compartments employing an all-copper wiring harness (as in A-21) is determined by the equilibrium temperature of the wiring harness and is not a function of spaceframe temperature. The wiring harness, wrapped with aluminized teflon (teflon side out, $\alpha = 0.18$, $\epsilon = 0.63$), will not become sufficiently hot to provide a significant heat input to the compartments during the lunar noon interval. The only difference between A-21 and A-21A compartment system thermal performance during lunar day will be near terminator and during lunar night when the heat losses through the all-copper wiring harnesses on A-21 become significant. Tables 23 and 24 contain the current lunar night heat loss summaries for the A-21 and A-21A compartment systems, respectively.

The study has shown a significant improvement in the expected A-21 compartment system lunar surface thermal performance. Previous compartment thermal performance evaluations indicated that no spacecraft operational capability existed at the lunar noon interval unless the compartment radiators were shaded. Similarly, large

Table 23. Lunar night heat losses for A-21 compartment system

Heat path	Heat loss, w	
	Compartment A, 50°F	Compartment B, 10°F
Supports	1.52	0.75
Thermal switches	1.41	0.84
Mylar insulation	2.32	1.38
Thermal tunnel	0.76	0
Subtotal	6.01	2.97
Wire harness	5.0	4.0
Total	≈11.0	≈7.0

CONFIDENTIAL
UNCLASSIFIED

UNCLASSIFIED
CONFIDENTIAL

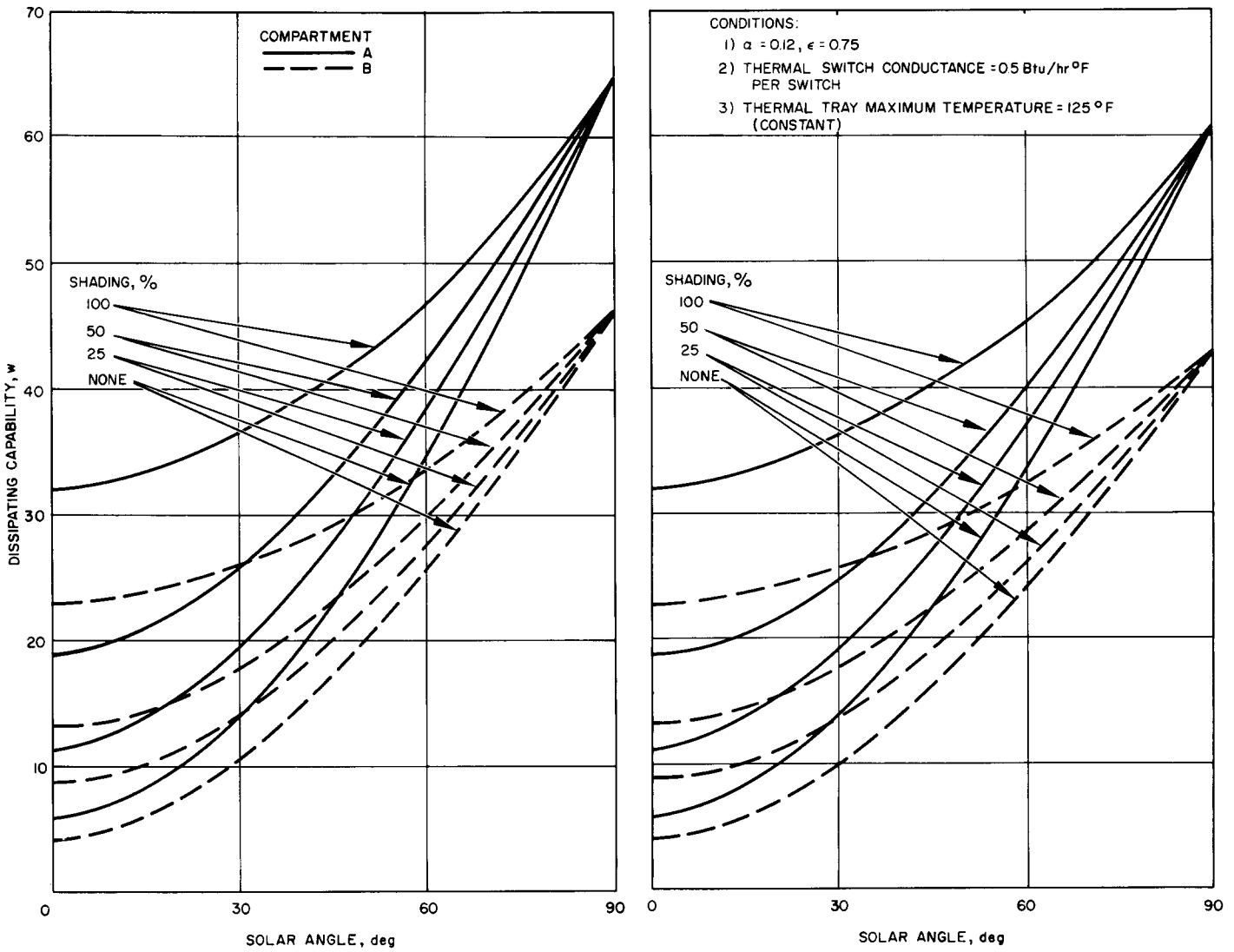

(a) A-21 spacecraft **(b) A-21A spacecraft**

Fig. 67. Compartment system thermal performance

copper wiring harness heat losses during lunar night caused rapid depletion of battery electrical energy.

Based on the present study, positive normal lunar noon dissipating capabilities will be available for the A-21 compartments. The total compartment system lunar night heat loss is approximately 20 w instead of 60 w as previously estimated.

b. Retro-engine. New retro propellant temperature distributions were calculated to include the effects of (1) revised values of propellant thermal properties and (2) changes to the geometry of the propellant envelope. The principal thermal property change was an increased thermal conductivity from 0.20 Btu/hr°F-ft to 0.30 Btu/hr°F-ft which resulted in reduced propellant temperature gradients and higher minimum temperatures at the time of ignition (66 hr after launch). The results of the study are summarized in Table 25. The table presents temperatures for a 1230-lb loading, a 1250-lb loading, and an initial 1250-lb loading cut back to 1230 lb by using a 20-in. diameter mandrel. In no case did the coldest point in the propellant shift to a location different from that established in the earlier analysis. The cold point remained at the skirt attach point for all configurations and did not exceed the 20°F allowable lower limit.

The exterior surface of the super-insulation blanket surrounding the retro motor case provides the boundary

CONFIDENTIAL
UNCLASSIFIED

UNCLASSIFIED CONFIDENTIAL

Table 24. Lunar night heat losses for A-21A compartment system

Heat path	Heat loss, w	
	Compartment A, 50°F	Compartment B, 10°F
Basic compartment less wiring harness		
Supports	1.52	0.75
Thermal switches	1.41	0.84
Mylar super insulation	2.32	1.38
Thermal tunnel	0.76	0
Subtotal	6.01	2.97
Wiring harness		
Basic bus		
Low conductance inserts	0.34	0.68
Three coax cables, low conductance	0.26	0
Tear strip (34 strips)	0.16	0
Subtotal	0.76	0.68
Scientific payload		
TV Cameras 2, 3, and 4	0.16	0.06
Surface sampler	0	0.16
Seismometer	0	0.06
Alpha scattering experiment	Negligible	0.09
Micrometeorite experiment	0.16	0
Subtotal	0.32	0.37
Total	~7.0 ± 0.5	~4.0 ± 0.25

Table 25. Retro-engine propellant temperature at ignition

Propellant loading configuration, lb	Propellant temperature, ~°F		
	Maximum	Minimum	Minimum at aft burning surface
1230	63 ± 4	32 ± 11	33 ± 11
1250	63 ± 4	32 ± 11	33 ± 11
1250 cutback to 1230	63 ± 4	32 ± 11	33 ± 11

temperature for thermal radition losses through the insulation blanket. The effect of blanket asymmetrical exterior surface temperatures on propellant temperature was examined since portions of the retro upper hemisphere are shaded by the solar panel and will be much colder than the solar illuminated portions. The study indicated that the maximum propellant temperature gradient caused by shading would be $\leq 5°F$ between a shaded region and an illuminated region after 66 hr. The study concluded that shaded portions of the insulation blanket will not cause significant temperature gradients in the propellant.

c. Vernier propulsion system. Vernier engine pre-test temperature predictions have been completed for the T-21 thermal-vacuum test. All special effects, due to testing in a solar simulation chamber and to changes in design, were included. Among the important considerations were: (1) changes in radiation properties due to solar mismatch; (2) the use of non-firable RMD engines of an earlier configuration; and (3) a shadow pattern on the T-21 engines different from that expected in actual flight due to the use of the old RMD vernier inner mounting brackets. A Vernier 2 integral solar collector has been fabricated for installation on the engine. Although there is a difference in paint patterns between the flight and test engine, the testing of the integral collector will permit experimental evaluation of this type of collector.

Review of the helium tank thermal control design has shown that the tank could exceed its upper temperature limit during transit phases for both the T-21 thermal-vacuum test (~150°F) and during actual flight (~130°F). Fig. 68 shows the new paint pattern required and the range of temperatures that can be expected in flight for both the helium tank and the helium gas. The SC-1 helium tank, which differs from the T-21 helium tank in weight, material, and orientation, will have the same

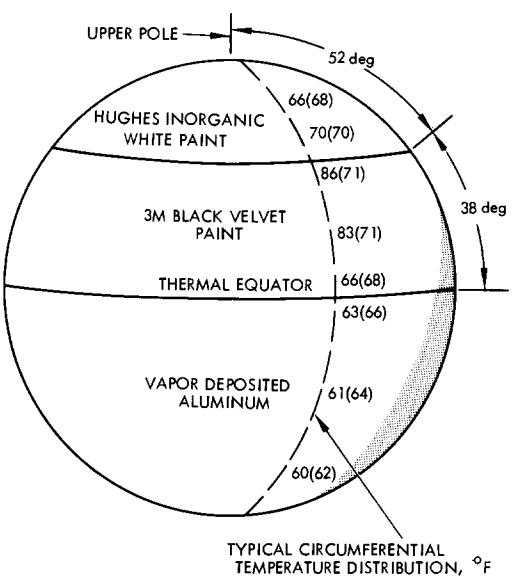

1) ALL TEMPERATURES ± 18°F
2) α OF HUGHES INORGANIC WHITE = 0.18 ± 0.02
3) TRANSIT TEMPERATURES AT 100% JOHNSON SUN
4) ( ) INDICATES GAS TEMPERATURE
5) CHANGE OF α AT HIGH ANGLES OF INCIDENCE FOR THE 3M BLACK VELVET PAINT INCLUDED.

Fig. 68. T-21 helium tank temperatures for flight conditions

CONFIDENTIAL UNCLASSIFIED

CONFIDENTIAL UNCLASSIFIED

basic thermal control design as the T-21 tank with minor paint pattern modifications.

d. RADVS. The design point nominal temperatures for the passive thermal design of the RADVS subsystem have been revised to be more compatible with the recently expanded activation temperature range specified in Table 26. Based on the revised nominal temperatures, the T-21 RADVS thermal finish patterns are being changed on the T-21 hardware. The thermal finishes were defined prior to completion of the reevaluation of subsystem unit performance; consequently, slight differences appear in design point nominal values and the calculated nominals for T-21 hardware as reported in Table 26. The differences will be corrected by making minor adjustments to the thermal finish patterns for subsequent spacecrafts.

A combination of white paint, polished aluminum, and vacuum-deposited aluminum (VDA) is used for the KPSM thermal finish design. To optimize predictability, the thermal finish pattern was established to minimize (1) the absorbed solar reflected energy, (2) the effect of ultraviolet (UV) degradation on solar absorptance, (3) the solar absorptance mismatch between flight and simulated solar environments, and (4) the infrared coupling between the spacecraft and the unit. This optimization was achieved by using both low emittance and solar absorptance on surfaces which "see" the spacecraft and by using polished aluminum and VDA, each of which are relatively insensitive to absorptance mismatch and are UV stable, on the primary solar absorbing surfaces. Predictability accuracy was improved by using the high emittance white paint on surfaces that exhibit large view factors to space. The same design rationale was used for the KPSM velocity sensor klystron tube assembly to achieve the type of optimization in predictability indicated above.

Table 26. T-21 RADVS thermal requirements/performance summary

Unit	Revised activation temperature range (4 min mission), °F	Nominal design point bulk average flight temperature, °F	Nominal bulk average flight temperature predictions for T-21 thermal design, °F
Klystron power supply modulator			
Without velocity sensor klystron assembly	−26 to 116	25	15[a]
Velocity sensor klystron tube assembly	−49 to 100	25	19
Signal data converter			
Motherboard assemblies	30 to 95	60	50[a]
Low voltage power supply	25 to 104	60	50[b]
Preamplifiers			
Altitude/velocity antenna	−40 to 100	35	34
Velocity sensor antenna	−40 to 100	35	26

[a] Nominal temperature spreads are estimated to be between ±10 and ±15°F.
[b] Nominal temperature spread is estimated at ±8°F.

An analytical model of the velocity sensor klystron tube assembly has been programmed to facilitate computer calculations. Preliminary results for the T-21 design indicate that the nominal bulk average temperature of the velocity sensor klystron assembly is 19°F for an assumed 30°F nominal waveguide temperature, 15°F nominal KPSM average temperature with a ±13°F nominal internal temperature spread, an effective conductive waveguide length of 12 in., and a nominal overall conductance of 0.05 Btu/hr°F between the KPSM and the klystron assembly. Additional investigations revealed that average klystron tube assembly temperatures will vary from 16 to 24°F for the assumed boundary temperatures and waveguide effective length when the overall conductance between the KPSM and klystron assembly is varied from 0 to 0.9 Btu/hr°F, the bounds of the actual attachment conductance. Further studies are in progress.

The SDC thermal design has been optimized using techniques that minimize unit susceptibility to uncertainties. For this optimization, polished aluminum and alumized teflon are used on primary solar absorbing surfaces while the aluminized teflon is used on primary radiating surfaces. This thermal finish selectivity minimizes solar absorptance mismatch effects since both polished aluminum and aluminized teflon exhibit approximately identical α values for both the simulated and flight solar environments. The effect of ultraviolet degradation is minimized since both polished aluminum and aluminized teflon are inherently ultraviolet stable. The IR coupling with the spacecraft is also minimized by using the high emittance teflon on surfaces that have maximum view factor to space. To further improve the predictability, a thermal blanket has been incorporated to cover three sides of the SDC to thermally "desensitize" the unit from the SDC surroundings.

Combinations of VDA and white paint are used on the receiver-transmitter assemblies in the same manner to minimize uncertainties. Black paint is used to increase the absorbed solar energy. Further analytical studies on the RADVS subsystem units are in progress to establish

CONFIDENTIAL UNCLASSIFIED

UNCLASSIFIED
CONFIDENTIAL

and define the thermal performance of the present T-21 RADVS thermal design. A development test procedure has been formulated to evaluate major thermal aspects of the T-21 RADVS during T-21 thermal-vacuum testing. The test will verify nominal temperatures, internal temperature spreads, and transient thermal characteristics of the unit.

e. Attitude control system. The thermal design of attitude control system gas jets has been reviewed and the analysis updated to include the MT-1 thermal-vacuum landing gear test data. Table 27 summarizes the predicted flight thermal performance. The pitch and yaw attitude jets will perform within the specified temperature limits; however, the equilibrium temperature of the roll jet can exceed the operating upper temperature limit. Because the temperature of the jets is sensitive to the magnitude of conductance through the low conductance attachment assembly, which connects the jets to the leg assemblies, various methods of reducing the roll attitude jet temperature were investigated. To correct the roll jet problem the thickness of the fiberglass isolator will be reduced to approximately one-third of the existing thickness. Table 27 also includes the temperature data associated with the design modification.

f. Scientific payload

Micrometeorite ejecta detector sensor head thermal study. The thermal study of the micrometeorite ejecta detector sensor head was submitted to JPL on September 4, 1964. The study determined the thermal behavior of the instrument throughout the transit and lunar day phases of the mission. The hardware design, survival and operational temperature limits, and optimum paint pattern are shown in Fig. 69.

The predicted equilibrium temperature of the electronics case during transit is −39 ±23°F. A maximum temperature drop of 85°F can occur during a 1-hr solar eclipse. Since the non-operating survival temperature limits are −297 to 207°F, the thermal behavior of the instruments is entirely compatible with the design requirements during transit.

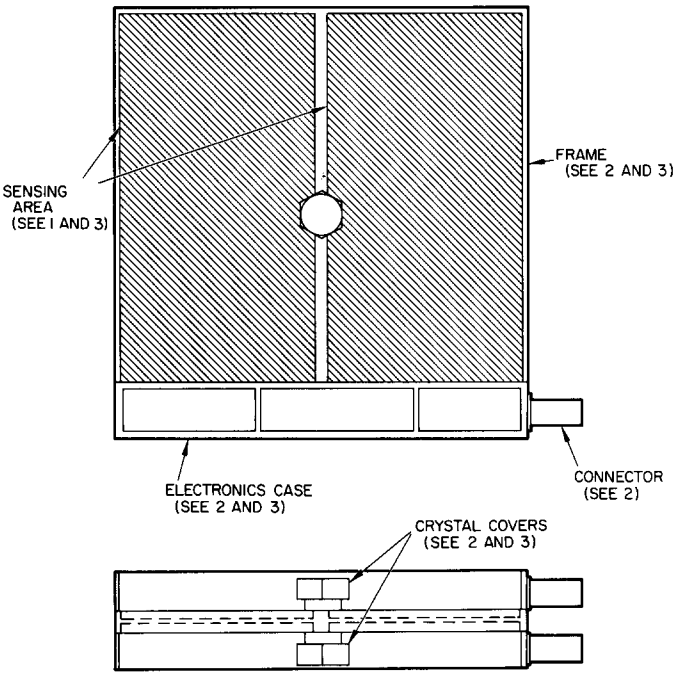
SENSING AREA (SEE 1 AND 3)
FRAME (SEE 2 AND 3)
ELECTRONICS CASE (SEE 2 AND 3)
CONNECTOR (SEE 2)
CRYSTAL COVERS (SEE 2 AND 3)
1. BOTH SIDES OF SENSING AREA NOT TO BE THERMALLY COATED
2. ALL SURFACES OF THESE ITEMS TO BE THERMALLY COATED WITH HUGHES INORGANIC WHITE PAINT
3. TREATED AS ONE NODE IN ANALYTICAL THERMAL MODEL
4. OPERATIONAL TEMPERATURE LIMITS: -67°F TO +180°F
SURVIVAL TEMPERATURE LIMITS: -297°F TO +207°F

Fig. 69. Configuration and paint pattern of micrometeorite ejecta detector

Fig. 70 indicates the thermal performance during maximum heating and minimum heating for lunar surface operation. Maximum heating occurs with 100% solar illumination with the Sun traversing as shown in Fig. 70a. Minimum heating occurs when the instrument is shaded

Table 27. Predicted temperatures for attitude jets

Components	Predicted flight temperatures, ~ °F				
	Operational temperature limits	Prelaunch	Acquisition, solar eclipse up to 1 hr	Equlibrium temperatures, normal transit attitude	Midcourse or terminal descent, solar eclipse up to 30 min
Pitch and yaw jets	−50 to +160	+85 (±5)	+25 (±30)	30 (±30)	0 (±30)
Roll jet (existing design)	−50 to +160	+85 (±5)	+25 (±30)	150 ± 30	120 ± 30
Roll jet (modified design)	−50 to +160	+85 (±5)	+25 (±30)	82 ± 32	52 ± 32

CONFIDENTIAL
UNCLASSIFIED

CONFIDENTIAL
UNCLASSIFIED

by the planar array antenna and solar panel. During lunar operation, the instrument can exceed the upper operational temperature limit (180°F) at solar angles up to 52 deg on either side of lunar noon. Under the most severe conditions, it is possible for the instrument to exceed its survival temperature limit of 207°F during a time period defined by lunar noon ±7 deg solar angle. During this time period, the temperature of the instrument can reach 213°F.

The existing heater capability of 1 w appears to be adequate for all conditions except the completely shaded condition (Fig. 70b). The temperature of the instrument could drop below the —67°F lower operational limit after 85 deg solar angle if the available heater power were limited to 1 w. A 2-w heater would maintain temperatures within the operating range out to the day-to-night terminator under all conditions.

The existing hardware has gold plating on the exterior surface of the electronics case. An analysis was performed to determine the temperatures that would exist if the electronics case were gold plated instead of being painted with white paint. The resulting temperatures were well above the 207°F survival limit through the lunar day.

Based on the results of the thermal study, the following recommendations were made:

(1) Remove the gold plating on the exterior surfaces of the electronics case and apply Hughes inorganic white paint. (Hughes inorganic white paint will not adhere to a gold plated substrate).

(2) Change the requirement that the instrument must operate after 85 deg solar angle to eliminate any increase in heater requirements.

(3) Increase the upper range of the —67 to 180°F operational temperature requirement to at least the predicted maximum temperature of 213°F if unlimited operational capability is desired throughout the lunar noon period.

(4) Examine survival temperature limit to determine if it could be increased from 207 to 213°F to be compatible with the maximum expected temperature.

4. T-21 System Test Support

Definition of the special test hardware required to simulate a flight environment in the T-21 solar-thermal-vacuum tests has been completed and efforts have been concentrated on test operations. Prior to performing the test during the October and November 1964 period, it is appropriate to review the entire thermal test program with emphasis on how the vehicle, the STEA, the chamber, and the auxiliary data monitoring system (ADMS) are used as a system.

a. Test plan. The T-21 solar-thermal-vacuum test is comprised of two distinct phases — a systems functional test and a thermal control evaluation test. The systems functional test is essentially a condensed mission sequence of 30-hr duration. The thermal control evaluation test is of 75-hr duration and combines a mission sequence, a RADVS thermal development test, and engineering data gathering sequences. During the test, the mission thermal performance capability will be verified, the primary heat transfer parameters affecting the RADVS system will be determined, and the thermal

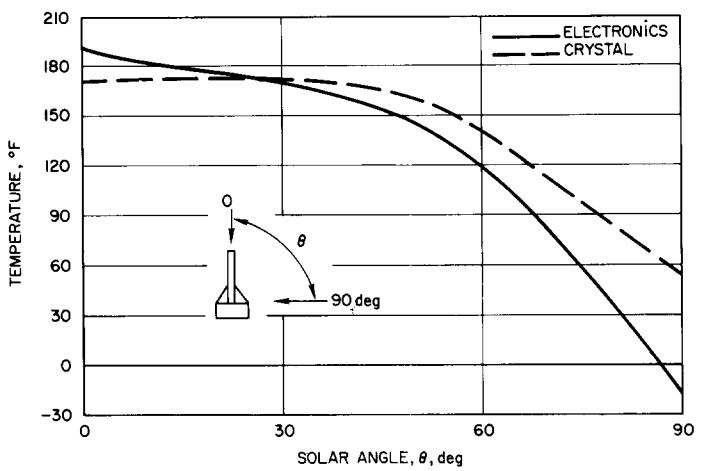

(a) Nonshaded condition

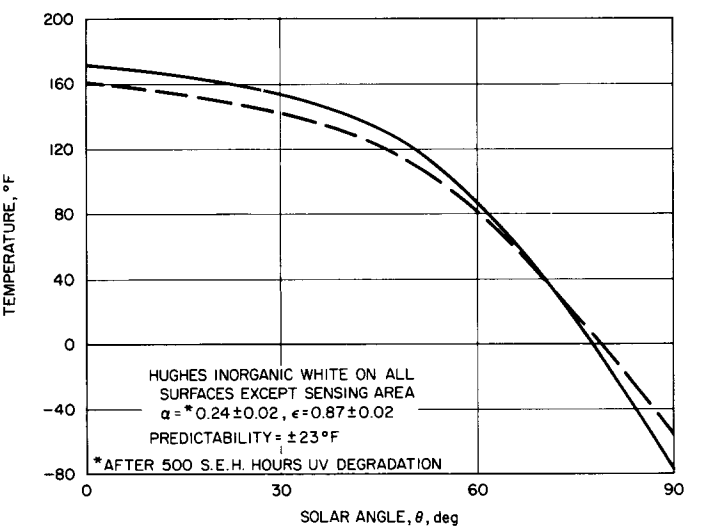
TEMPERATURE, °F
SOLAR ANGLE, θ, deg
HUGHES INORGANIC WHITE ON ALL SURFACES EXCEPT SENSING AREA
α = *0.24±0.02, ε = 0.87±0.02
PREDICTABILITY = ±23°F
*AFTER 500 S.E.H. HOURS UV DEGRADATION

(b) Shaded condition

Fig. 70. Temperature versus solar angle for micrometeorite ejecta detector

CONFIDENTIAL
UNCLASSIFIED

UNCLASSIFIED
CONFIDENTIAL

system capability during transient and nonstandard flight conditions will be examined.

b. Vehicle configuration and environment during thermal control evaluation phase. The special test equipment required for functional testing comprises: (1) the *Canopus* anti-reflection hood, (2) the TV 4 target, (3) the test waveguide plumbing, (4) feedhorn adapters for the RADVS and AMR systems, (5) pneumatic plumbing for the attitude jets, (6) the spacecraft mounting fixture, and (7) the hardline test harnesses. An appropriate thermal installation (see Table 28) is required for these items so that their presence does not degrade the thermal environment. It will be possible to remove the *Canopus* hood, the test waveguide and feedhorn adapters, the TV 4 target, the test pneumatic plumbing, and much of the hardline test access during the thermal control evaluation phase. This will identify any differences in the thermal environment caused by the presence of these test equipments.

A system of liquid nitrogen cooled shadow shrouds, as shown in Fig. 71 and described in *Space Programs Summary No. 37-27*, Vol. I, are required in both test phases so that the shadowing caused by the solar panel is simulated on the T-21 vehicle. The solar panel, removed during the T-21 solar thermal vacuum tests, is inadequate since the collimation angle of the solar simulator is much greater than that of the actual Sun. Decollimated energy intercepted at the height of the solar panel would create a region of varying intensity 15 to 25 in. wide at the plane of the spacecraft instead of the required 1-in. shadow line. The problem is eliminated by placing the shadow shrouds in a plane directly above the component in question. The landing legs and attitude jets are outside of the 8-ft test circle of the simulated solar beam. Blocking heater installations are provided to assure that these units provide the proper conductive and radiative environment to other spacecraft components.

c. Facility. A deficiency in present day solar simulation facilities is spectral mismatch between the energy distribution of the simulator and the actual Sun. This phenomenon causes thermal coatings to exhibit different solar absorptance in the test chamber than in space. An evaluation of the solar simulation was reported in *Space Programs Summary No. 37-29*, Vol. I. The largest change in solar absorptance is exhibited by the inorganic and organic white paints. Thermal performance analysis will take the change in solar absorptance into account. It is necessary to establish that the temperatures of the systems which use these finishes (for example, the nitrogen gas supply tank, the helium gas supply tank, and the flight control sensor group) will not be in excess of the upper temperature limits for the solar intensity level planned for T-21 testing.

The test plane has been defined as 45 in. above the chamber floor I-beams. During the entire systems functional test and the first 64 hr of the thermal control evaluation test, a test intensity of one solar constant will be set at the test plane. Since the intensity varies in the vertical direction, the intensity at the plane of the compartment radiators will be 106% of a solar constant. This permits Compartments A and B to be tested conserva-

Table 28. T-21 Special test equipment and modifications required for thermal-vacuum/functional testing compatibility

Item	Test phase	Thermal installation
Canopus antireflection hood	Systems functional test only	Enclosed in shroud cooled by LN_2 (below —300°F) and painted on exterior with 3M Black Velvet paint.
Television 4 target system	Systems functional test only	Enclosed in shroud cooled by liquid nitrogen (below —300°F) and painted on exterior with 3M Black Velvet paint.
Test waveguide and feedhorn adapters for RADVS and AMR antennas	Systems functional test only	Fiberglass waveguides internally silver plated and inserted into RADVS and AMR test plumbing to provide thermal conduction isolation. Feedhorn adapters polished externally to provide low emittance surface and minimize radiation heat sink.
Spacecraft mounting fixture	Both systems functional test and thermal control environmental test	Low thermal conduction isolation used with conductance less than 0.015 Btu/hr °F.
Test pneumatic plumbing for attitude jets	Systems functional test only	Attitude jets have blocking heaters to maintain proper temperature.
Hardline test harnesses	All present in systems functional test and some present in thermal control evaluation test	Blocking heaters and/or thermal wrap required on some harnesses. Those harnesses not required to perform the thermal control evaluation test are removed in this phase.

CONFIDENTIAL
UNCLASSIFIED

UNCLASSIFIED
CONFIDENTIAL

tively in an environment more severe than that anticipated in space. During the latter part of the thermal evaluation test, the intensity will be reduced to 85% of a solar constant to have an additional test point for evaluation purposes.

One of the more operationally complex parts of the test is the pumpdown, chamber wall chilldown, solar simulator turnon, and spacecraft preconditioning cycle. This sequence must be synchronized so that the vehicle remains within acceptable temperature limits while the vehicle simulated launch environment and chamber solar-thermal-vacuum equilibrium conditions are established. The spacecraft operations which must be performed during this interval are: (1) turnon of the spacecraft electronics; (2) preconditioning of the main retro propellant, AMR electronics, Compartments A and B, and the IRU gyros; (3) obtaining equilibrium temperatures on the surfaces controlled by blocking heaters (e.g., the legs, shock absorbers, attitude jets, and Compartments A and B test harnesses); and (4) enabling the thermostats on the AMR, vernier lines, and vernier tanks. One of the primary responsibilities of the thermal project engineer will be the protection of the vehicle during test. At the completion of this environment preparation phase, the thermal project engineer will review the temperature performance on all spacecraft systems to determine if it is safe to proceed into the actual operational testing phase. If abnormal performance is found, an appropriate course of action ranging from aborting the test for the purpose of making modifications to proceeding with the test at a reduced solar intensity will be recommended. Pre-test planning has included chamber operational procedures for emergency conditions. Time periods in which the ambient environment must be restored, so as to not damage the vehicle, have been defined for a complete building and spacecraft power failure and for a spacecraft power system failure.

d. Auxiliary data monitoring system (ADMS) and temperature data display. The ADMS system will be used to transmit the measurements from the 500 thermocouples on the spacecraft in the test chamber at El Segundo to the IBM data processing facility at Culver City. The reduced temperatures will be transmitted back to the test site in near-real time for monitoring by the thermal control team. The data will be plotted at the test site for real-time viewing to assist in the test direction and evaluation.

Pre-test predictions are being made to facilitate real-time comparisons with measured temperatures and for

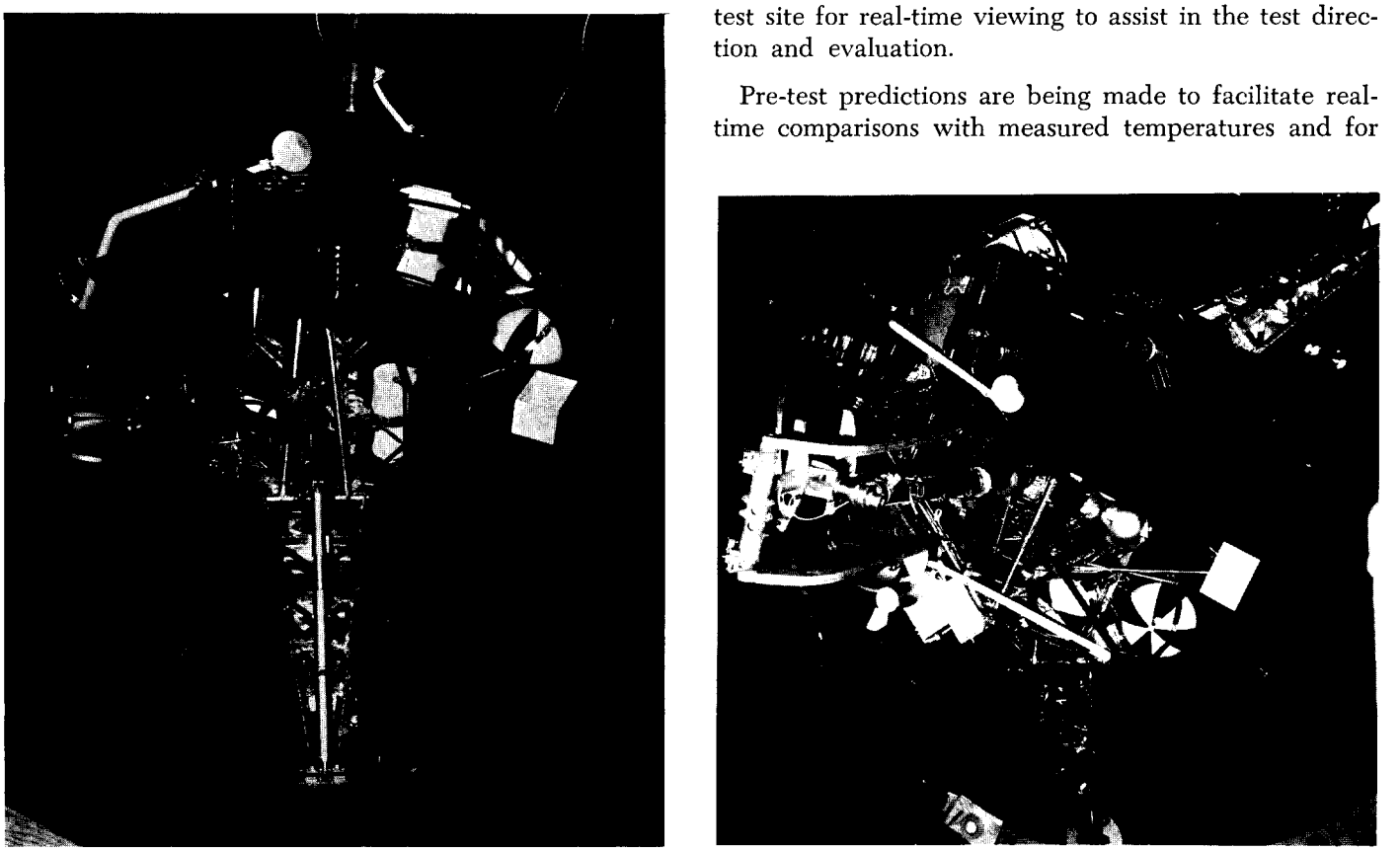

(a) Side

(b) Top

Fig. 71. Liquid nitrogen shadow shrouds on T-21

UNCLASSIFIED
CONFIDENTIAL

UNCLASSIFIED
CONFIDENTIAL

use in post-test data evaluation. The ADMS system has the capability of recalling any previously measured temperatures and of determining the slope of the temperature-time curve in a given period as a criteria for steady state conditions on any system.

A series of high resolution pictures will be taken prior to the test to provide a permanent record of shadow shroud position relative to the spacecraft and for use in establishing shadow lines.

e. Fit and function thermal evaluation test. The environmental phase of the T-21 fit and function test program has been performed using the M-12 mockup vehicle. The overall objective of the test program was to verify fit, function, and procedures for all the equipment used in the upcoming T-21 tests. The thermal objectives are discussed below.

The procedure for sequencing the pumpdown, chilldown, and solar simulator on operation so that temperatures on the vehicle are maintained within relatively narrow limits during this period of rapidly varying chamber environment was performed without difficulty.

The second objective was to demonstrate operational capability of the ADMS and gain familiarity with its use. The near real-time data display performed well. Some minor difficulty was experienced with the recall and slope routines which will be corrected before the start of the T-21 tests.

The third objective was the mapping of the shadow shrouds to determine system effectiveness in duplicating the shadowing of the spacecraft by the solar panel. Performance of the system was excellent. The penumbra (region of varying intensity) was typically 1.0 to 1.5 in. wide on the compartment radiators and Vernier Engine 2, compared to a region of 15 to 25 in. in width if the actual solar panel were used during the T-21 test. These results indicate that shadow patterns on T-21 will be very close to those on an actual flight vehicle.

It was demonstrated during this test that special test equipments like the shadow shrouds, TV4 target, and *Canopus* anti-reflection hood, which are enclosed in liquid nitrogen cooled shrouds, can be maintained at cryogenic temperatures throughout the test phase. This equipment was thoroughly instrumented with thermocouples and no hot spots were detected. Supporting structure, which was not liquid nitrogen cooled, was sufficiently cold so that the environment of the adjacent spacecraft was not degraded. No leaks in the liquid nitrogen system occurred in the solar-thermal-vacuum environment.

5. SPAC Support

A detailed operating procedure to be used by the SPAC thermal specialist during the transit portions of the *Surveyor* mission has been prepared. This procedure describes in chronological order the duties and responsibilities of the thermal specialist during a normal transit mission and specifies the interactions with various other members of the SPAC group. Included in the procedure are the recommended data printout formats for the telemetry, bulk printer, and engineering data reduction program, together with a list of desired thermal sensors that should be used in the automatic alarm program.

The information requested by JPL for use in preparing an analog simulation system for SSAC lunar operation studies has been compiled and transmitted. This information includes gross thermal parameters for Compartment A, Compartment B, and the survey TV camera which describe: (1) the maximum environmental heat addition to the component, (2) the heater operation and electrical dissipation of the component, (3) the dissipating capability to the environment of the component, (4) the thermal storage capability of the component, and (5) the operating characteristics of the compartment thermal switches.

A study of equipment required by the SPAC thermal specialist for purposes of *Surveyor* nonstandard and lunar thermal operations analyses has been completed. This study provides preliminary sketches of the equipment, cost estimates, and a discussion of the equipment use. The terminology chosen to describe this equipment is SPAC Thermal Model System. The Thermal Model System (TMS) includes the following equipment: (1) a one-fifth scale model of *Surveyor*, (2) a gimbal system for the model, (3) a collimated light source, (4) a 35-mm camera, (5) a camera positioning device, (6) a slide projector, and (7) equipment required for making view factor measurements. The TMS is required to obtain solar heating data and infrared radiation parameters necessary for the operation of the Thermal Management Computer Program.

The TMS gimbal system was designed to provide a center of model axis rotation that is located near the center of an imaginary circumscribing sphere and to eliminate the possibility of gimbal structure shadowing during lunar operation analyses. The gimbal system orients the model with respect to the collimated light source or camera (these items simulate the location of the Sun and are used for various parameter measurements). The camera positioning device locates the camera accurately with respect to a spacecraft component.

CONFIDENTIAL
UNCLASSIFIED

CONFIDENTIAL UNCLASSIFIED

The camera and projector are used to measure the projected area of a thermal control surface in a plane normal to the spacecraft sunline (this is a measure of the direct solar energy incident on the surface.) The camera must be located 30 ft or more away from the spacecraft model to minimize parallax errors in the projected area measurements caused by components shadowing each other. The collimated light source will be used to estimate reflected solar energy incident on a component and as a visual aid for detailed component analyses or for rapid thermal decisions with regard to spacecraft operations.

The view factor equipment comprises view factor buttons, beamsplitter mirrors, and a small telescope. This equipment measures data necessary in the calculation of infrared radiation parameters. It will be used primarily during lunar operations when the solar panel and planar array are positioned to new locations. Incorporation of the equipment into the SPAC system is awaiting JPL concurrence.

6. Thermal Switch

The lapped contact surfaces of the first production units have been found to be of insufficient quality to meet the closed switch thermal performance requirement. Extensive rework of these parts is in progress. The engineering requirements on contact surface finish have been tightened; provisions for closer supervision and control are being instituted. In addition, the inner contact teflon coat has been replaced with a more compliant film of RTV-11 silastic rubber charged with molybdenum disulphide. Preliminary testing of this new configuration at TAT levels has been completed.

The thin-wall thermal switch cases failed during the axial vibration of S-2A at TAT levels. As a result, the case wall thickness has been increased from 0.004 to 0.0055 in. This new case configuration will be tested on the S-2A vehicle in mid-October. The increased wall thickness is estimated to cause a 4 to 5% increase in each compartment lunar night heat loss for the A-21A configuration.

The new configuration incorporating both the new contact treatment and the redesigned case will undergo TAT beginning in early November.

7. TCM Program

A thermal control model test program has been proposed to JPL, and Hughes has been authorized to proceed immediately on the initial phase. TCM test program is to provide thermal control system information to supplement the data obtained from the MT-1 sector tests, the T-21, and T-21A spacecraft tests, and to provide a test medium by which the limitations imposed by the existence of operable spacecraft control items can be circumvented.

The four-phase test program has been designed to provide external spacecraft thermal control system performance data, supplemented by more detailed information in subsequent phases as flight-type control items and subsystems become available. Fig. 72 and the following program descriptions indicate the major test phases and milestones of this plan.

a. Phase 1. Phase 1 will consist of one test in the Hughes C-4 chamber and one test at General Electric, Valley Forge to provide steady-state performance data for the thermal control system. During this phase the TCM configuration will be representative of a flight spacecraft, except that the Compartment A and B electronic units will consist of prototype thermal control and heater assemblies and sufficient resistive type heaters to evaluate the external steady-state heat balances. Control items (other than those within the compartments) whose external thermal appearance is significant will be of the appropriate prototype, nonfunctioning prototype, or mockup configuration.

The Hughes test will provide an initial shakedown of the TCM and will utilize special test canisters compartment thermal shells) which are designed to be compatible with all future TCM tests. These canisters will be similar to those currently used on the T-21 vehicle. During this test, as in Phase 2, 3, and 4, liquid nitrogen shadow shrouds will be used, and all passive thermal control systems will be evaluated. Steady-state compartment dissipating capability will be determined. At the conclusion of the tests, flight-type canisters (without special test access) will be substituted for the test canister to verify the test canister concept. During this test, the special test access wiring (thermocouples and heater) will be unplugged and coiled within the compartment. A short "no-Sun" test will be conducted using the thermal control and heater assemblies and a limited number of instrumentation leads (under 10), in addition to the normal wiring harness, to demonstrate the adequacy of the test canister in duplicating the compartment thermal characteristics. Solar eclipse data will also be obtained.

During Phase 1, the TCM will be tested in the General Electric, Valley Forge simulator. The simulator has better collimation (2 to 3 deg as opposed to 6 to 8 deg at Hughes and JPL), although the energy spectrum is different than that of the Sun because the source is pure xenon (Hughes and JPL use mercury-xenon bulbs). The Hughes chamber will, in general, result in vehicle temperatures higher than those expected in space (high

CONFIDENTIAL UNCLASSIFIED

UNCLASSIFIED
CONFIDENTIAL

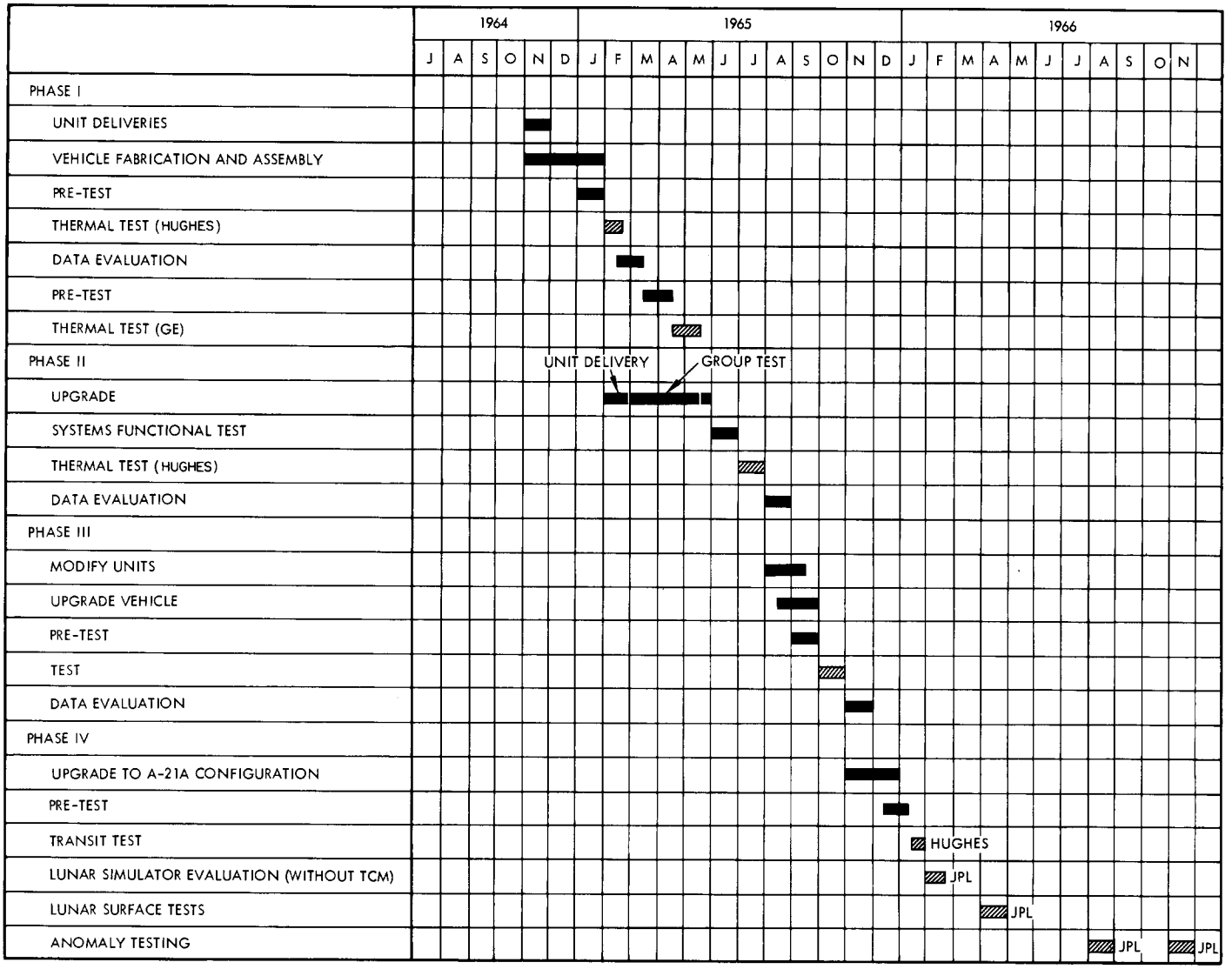

Fig. 72. Program plan for thermal control model

ultraviolet spectrum content), and the General Electric simulator will result in lower temperatures. The initial portion of the General Electric test will utilize the Hughes liquid nitrogen shadow shrouds and will have as a primary objective the exploration of the effect of better collimation.

During the second part of the General Electric tests, the TCM will be fitted with a remotely actuated antenna/solar panel positioner assembly. The subsequent tests will utilize the General Electric gimbal system and are intended to demonstrate that off-normal Sun orientations do not present unexpected thermal problems. These tests will be used to correlate Hughes and General Electric test data and will provide a basis for the conduct of future testing at either Hughes or JPL (25-ft chamber, 15-ft simulator) with a fixed solar orientation.

b. Phase 2. At the conclusion of the General Electric test program, the vehicle will be returned to Hughes, and the flight-type electronic equipment will be installed in the compartments in preparation for the thermal control systems test. This test will examine detailed compartment unit thermal interactions and performance using flight type hardware. The units will be operated in a normal functional manner but without a requirement for specification performance. This requirement is intended to assure that the thermal dissipation is typical of flight hardware. Compartment transient thermal performance will be evaluated, and the data will be catalogued for future correlation with both the Phase 3 and the flight data.

c. Phase 3. At the conclusion of Phase 2, the compartment electronic equipment will be modified to provide

UNCLASSIFIED
CONFIDENTIAL

UNCLASSIFIED
CONFIDENTIAL

variable power dissipation. During the upgrade, individual heaters capable of variable power dissipation will be installed in all compartment-housed units considered to be major dissipators. The heaters will be powered through a special test harness and will be controlled by the TCM test console. The tests will explore the compartment transient capability starting initially with a duplication of a portion of the Phase 2 test plan. The resultant data will be used to demonstrate correlation between dissipation of the units during functional use with their dissipation using heaters. Further testing will examine compartment transient characteristics associated with the transit phase of the mission such as initial acquisition, midcourse maneuver, and terminal descent.

d. Phase 4. Upon completion of the Phase 3 tests, the TCM will be upgraded to the A-21A configuration. An abbreviated transit test will be performed at Hughes, followed by an evaluation of the performance of the improved JPL 25-ft (15-ft simulator) facility, when modified to simulate lunar surface conditions. Lunar surface tests will then be conducted utilizing the TCM in the improved JPL 25-ft facility. Two subsequent special test phases have been scheduled for investigation of anomalies encountered in spacecraft performance and test operations.

8. Thermal Finishes

The program to study ultraviolet degradation of *Surveyor* white inorganic paint was completed during this period, but the zinc oxide phase has been slightly delayed.

Three batches of paint were used for the Hughes test. Batch C-1633-75 was regular Class IV paint, batch C-1633-82 was made from "on hand" raw materials, and batch C-1633-82a was made from newly fired pigment but "on hand" binder.

Data from the tests are shown in Table 29. The samples were exposed to solar intensity in the spectral range of 0.2 to 0.4μ from a BH-6 mercury arc lamp. The exposure times are indicated in Table 29. The sample temperatures were 93°F or less. Considerable scatter exists in the data, all taken by the portable Gier-Dunkle apparatus. Samples grouped together were in the same chamber and are accurate duplicate simulation samples. From this data, it may be concluded that the paint is adequate for realistic lifetime conditions of *Surveyor*.

Some effort has been expended to identify the degradable species in the paint. A series of samples has been taken from Batch C-1633-90 each week and the clear supernatant liquid analyzed for aluminum and other elements. This was predicted on the assumption that the aluminum silicate pigment was being attacked by the highly alkaline potassium silicate, injecting soluble aluminum into the solution. The alkaline stable species would then presumably be unstable in an ultraviolet environment. From the analysis, it is evident that aluminum is not "solubilized." It is possible that attack of the pigment does occur, but that the end products hydrolize to aluminum hydroxide which has been shown to be unstable in vacuum and ultraviolet. The most significant change in the composition of the supernatant liquid was in the potassium content. From an initial value of 8.6% it fell to 5.9% in 4 wk. The exact meaning of the change is not known. If potassium is really removed from solution, then a decrease in alkalinity may be expected, with possible change in adhesion and unknown effects on the ultraviolet stability. Studies are continuing.

Table 29. Change (Δa) in solar absorptance versus time

Batch	Exposure time, hours			
	50	100	200	500
C-1633-75	+0.01[a]	0.01	0.02	0.02
	0.01	0.00	0.03	0.04
C-1633-82	0.01	0.05	+0.01[a]	0.03
	0.03	0.00	0.01	0.03
C-1633-82a	0.02	0.02	0.02	0.05
	0.01	0.01	0.02	0.04

[a]Samples were bleached.

9. Special Studies

a. Exhaust plume heating. The main retro exhaust plume spacecraft radiation heating study accomplishments to date include: (1) experimental determination of exhaust plume heat fluxes, (2) calculation of spacecraft unit temperature rises, and (3) categorization of the results according to problem area, further study area, and non-problem area groups. The degree of plume-induced spacecraft heating depends heavily on (1) the geometry of the aluminum-oxide exhaust particle plume envelope postulated in relation to interpretation of exhaust plume heat flux measurements, and (2) calculation of exhaust plume heat fluxes incident at the spacecraft. The particle plume model is therefore a critical factor in an assessment of the severity of spacecraft heating.

Thermal environment measurements were made during recent main retro-rocket engine tests. The test runs (RP 1429-04, RP 1429-05, and RP 1429-06) were conducted at AEDC on August 26, September 1, and September 9, respectively.

UNCLASSIFIED
CONFIDENTIAL

UNCLASSIFIED CONFIDENTIAL

Two radiometers (Model R-2002-BX-15) with 60-deg conical view angles and two water cooled calorimeters (Model C-1300) were used. All four instruments were manufactured by the HyCal Engineering Company of Santa Fe Springs, California.

Fig. 73 shows the rocket engine nozzle, diffuser, and instrumentation geometry. A calorimeter and radiometer were mounted on both the cradle and diffuser. The cradle radiometer was aimed so as not to view the exterior of the rocket engine nozzle and also maintain its right-hand view extremity within the diffuser. The diffuser radiometer was aimed in such a manner so that its left-hand view extremity did not see the rocket nozzle interior. The view cone centerline of the instruments intersected the exhaust plume centerline.

Fig. 74 shows the results of these tests. The peak values at the beginning and end of each test are from start-up and shutdown transients. The radiometer gave consistently higher values than the calorimeters because it completely viewed the exhaust plume while the calorimeters did not. Valid data was not obtained from the cradle calorimeter during run RP 1429-05.

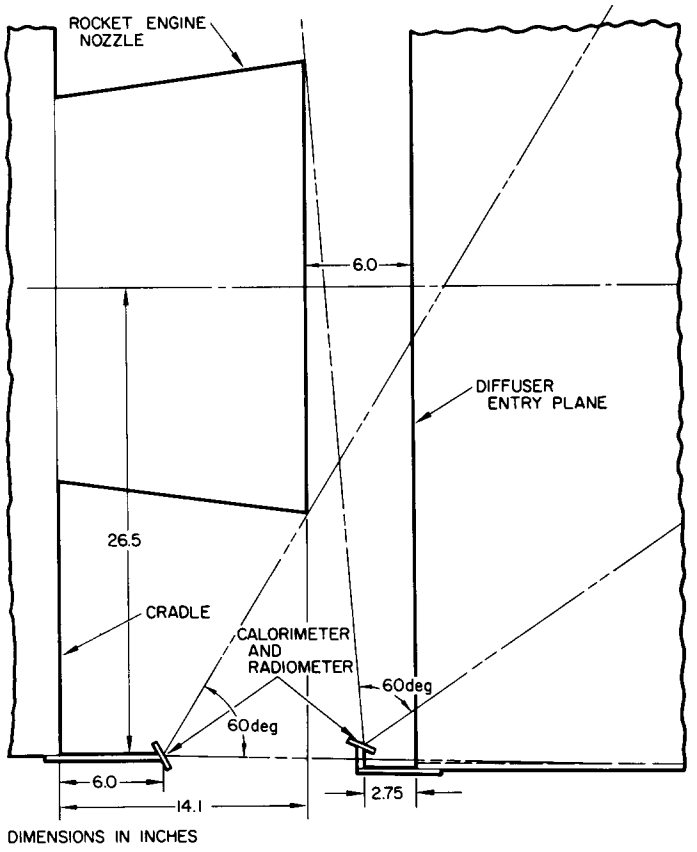

Fig. 73. Radiometer/calorimeter installation for main retro test

A preliminary evaluation of the calorimeter and radiometer data indicates the plume heat flux or radiosity is 5.0 to 6.5 Btu/sec-ft^2. The radiosity range has been established on the basis of measured heat flux data using a model of the aluminum oxide particle plume described by a truncated cone with a 26-deg half angle extending 20 exit diameters from the retro nozzle exit plane. This particle plume model represents a conservative upper limit on the energy content of the particle core and was used with a plume radiosity of 6.5 Btu/sec-ft^2 to calculate heat fluxes incident at the spacecraft in the range 0.5 to 2.0 Btu/sec-ft^2. Temperature rises were calculated for all units on the lower portion of the spacecraft with particular emphasis on those exposed to high incident heat fluxes and having short thermal response characteristics. The results have been categorized according to "problem area," "further study required," and "non-problem area" groups and are presented in Table 30. The criterion for categorization was comparison of maximum expected temperature after 40 sec of retro firing with maximum allowable temperature.

Based on the conservative exhaust plume thermal model used, problem areas where expected temperatures

Table 30. Exhaust plume heat flux study

Problem area group	Further study required group	Non-problem area group
RADVS antennas (2) Skirt, outboard Parabolic dish Skirt, inboard	Klystron power supply modulator, bottom surface	RADVS Antenna septum Waveguide Support structure
Crushable blocks, bottom	Approach TV camera Shutter Lens assembly	Flight control Electronics, bottom radiator
Foot pads, bottom	Omnidirectional antenna, booms	Approach TV camera Vidicon
	Auxiliary battery compartment, bottom face	Helium tank
	TV photometric chart	Vernier propellant lines
	Heater blanket assembly, vernier propellant lines	Roll actuator
	Wiring harnesses Insulation on miscellaneous wires Aluminized teflon covers	Attitude control jets
	Scientific payload	Spaceframe
		Position potentiometer arm, landing leg
		Landing gear leg, bottom skin
		Compartments A and B, bottom skin

UNCLASSIFIED CONFIDENTIAL

UNCLASSIFIED
CONFIDENTIAL

exceed hardware allowables are the RADVS antennas, the three crushable blocks, and the landing leg foot pads. Potential problem areas exist within the further-study group where complex and difficult-to-analyze hardware systems, such as the approach TV camera shutter lens assembly, propellant line heater blankets, and wiring harnesses produce initial results that are subject to doubt and are therefore inconclusive. The remainder of the

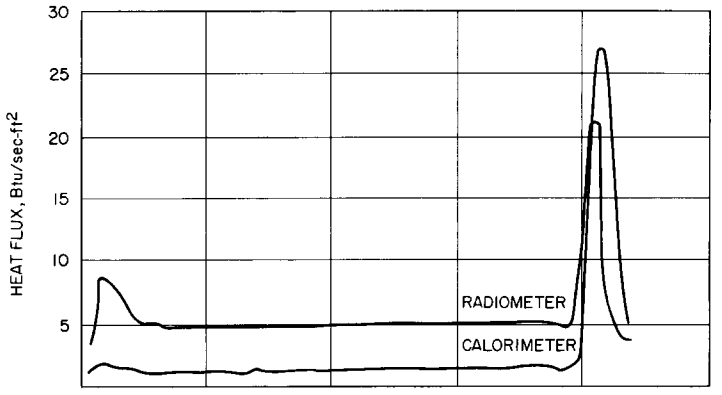

(a) From cradle instruments in run RP1429-04

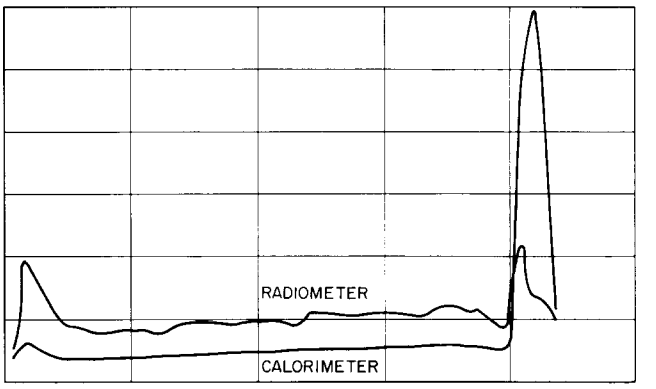

(b) From diffuser instruments in run RP1429-04

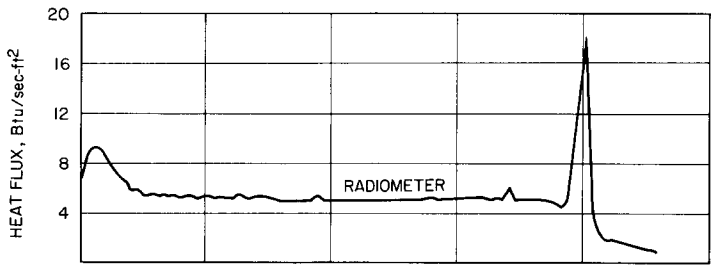

(c) From cradle radiometer in run RP1429-05

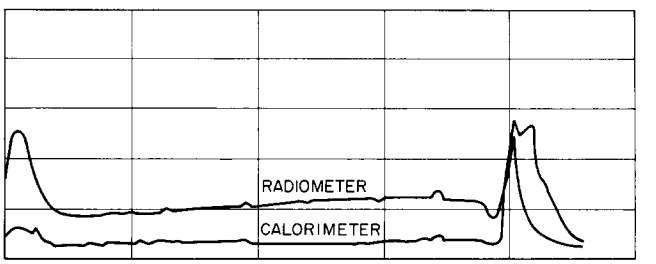

(d) From diffuser instruments in run RP1429-05

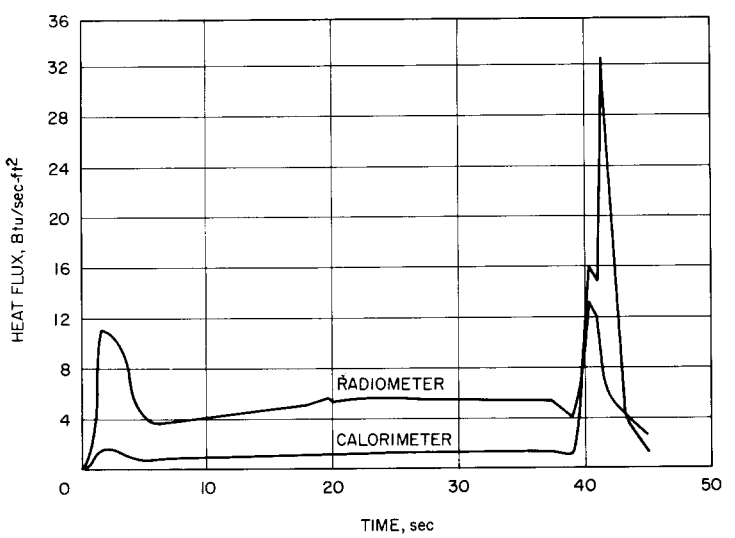

(e) From diffuser instruments in run RP1429-06

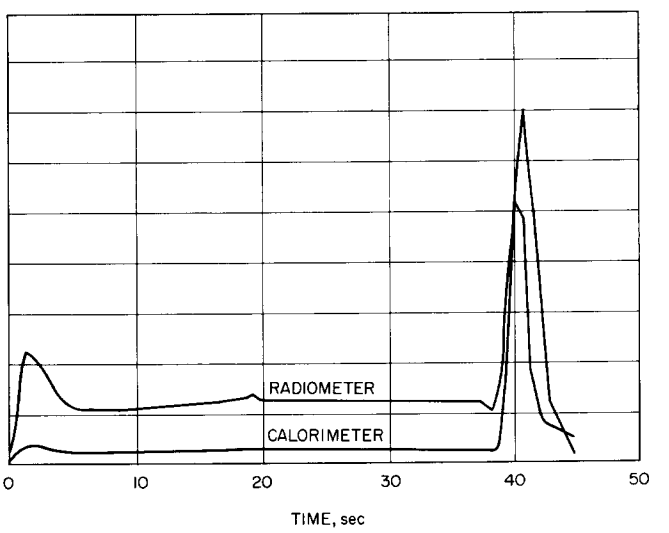

(f) From cradle instruments in run RP1429-06

Fig. 74. Retro-rocket plume heating tests

CONFIDENTIAL
UNCLASSIFIED

UNCLASSIFIED
CONFIDENTIAL

items listed are not expected to have an overheating problem.

The current course of action encompasses two parallel efforts. The first postulates that the heat flux values incident at the spacecraft are realistic and hence some form of spacecraft thermal protection is required. Conceptual protection designs have been devised employing both insulation and heat capacity techniques. The second effort questions the validity of the conservative particle plume envelope; intensive study of the particle and energy distribution within the plume is underway. Preliminary results indicate that the high energy envelope has been overestimated. Based on the initial results, the severity of the problem can be greatly reduced and possibly eliminated.

CONFIDENTIAL
UNCLASSIFIED

UNCLASSIFIED
CONFIDENTIAL

H. Engineering Mechanics

1. Introduction

The activities reported in this section include touchdown dynamics, static and dynamic structural analyses, and structural tests. Touchdown dynamics includes the specification, analysis, and testing of the soft-landing system. A significant portion of this work pertains to procurement of the landing gear shock absorbers. A similar activity is the specification of design and test parameters for spacecraft retro-engine separation. This section also covers stress and dynamic analyses on major spacecraft structures, the specification of loads and other design criteria, and the determination of structural test requirements. The results of the static and dynamic testing of structural models, including full-scale simulated spacecraft, are reported. This task includes procurement of flight engineering instrumentation, such as accelerometers, amplifiers, deflection potentiometers, and strain gage amplifiers.

2. Progress Summary

The forced-response computer program for landing is being used to determine S-2A drop test conditions so that maximum load levels will be achieved during the forthcoming drop tests. Premature failures that have recently developed during proof testing of the beryllium copper tubes used in the shock absorber have been traced to excessive chuck pressures during machining operations. The machining operation has been changed and proof pressure levels have been increased to 12,500 lb/in^2. In addition, ultrasonic crack detection after machining is now being utilized to inspect the tubes.

Work continues on revising the mathematical model used in the forced response programs to include the redesigned antenna/solar panel positioner in the new location. Data reduction has been completed for the elevation motor housing failure which occurred during vibration tests on S-2A, and the loads were verified using independent checks. Plans for the forthcoming modal survey in the landing configuration are essentially complete. Data from four retro-rocket test firings at Arnold Engineering Development Center have been collected and are being analyzed. Preliminary results indicate that the engine outputs are repeatable and that the dynamic forcing functions are transient in nature, rather than continuous or periodic.

Recent structural failures that have occurred in the retro-rocket separation device have been analyzed and corrective measures have been instituted. The retro-rocket support structure has been analyzed, and changes have been instituted to substitute a solid pin for the spring pin in the attachment strut, and a stress concentration area has been changed in the same member by increasing the radii in the critical area. The analysis and redesign of the compartment upper supports are described.

3. Landing Dynamics

To supplement results obtained using the rigid body mathematical model, an investigation is proceeding to establish landing loads using the IBM forced-response program. Results of this investigation will be used to determine S-2A drop test conditions, wherein vertical drops under Earth gravity will yield load levels as close as possible to the highest load levels expected during lunar touchdown. The chief effects of lateral velocity in lunar landing are planned to be simulated by varying the spacecraft incidence angle in the Earth drop test.

4. Shock Absorber

During proof pressure testing to 10,500 lb/in.^{2} of the beryllium copper tubes designated for flight models, a longitudinal split of one unit occurred at 5000 lb/in.^{2} (The burst test unit failed at 18,400 lb/in.^{2} in a similar manner, as reported in *Space Programs Summary No. 37-29*, Vol. I.) In the ensuing investigation, during which all remaining tubes were tested, a second failure of the same type occurred at 2000 lb/in.^{2} and a unit deliberately subjected to burst pressure failed at 18,500 lb/in.^{2} Cause of the premature failures has been determined to be interior longitudinal cracks produced by excessive chuck pressures during a machining operation.

As a result of the investigation, proof pressure levels have been raised from 10,500 to 12,500 lb/in.^{2}, and all tubes are subjected to ultrasonic crack detection after completion of machining. All flight units have been subjected successfully to these test revisions and are now in the process of being welded to the temperature compensating bellows.

All gas cylinders have been welded satisfactorily to the rod ends and all storage brackets have been installed on the cylinders. Grinding of the flame plate on the hydraulic cylinders is near completion. Piston fabrication is near completion and all aluminum housings, with squib firing mounts installed, are complete. Final adjustments are being made to the cam profile preparatory to cutting the metering rod slots.

5. Dynamic Analyses

a. Mathematical model. Analyses for converting the modal data from tests of the S-2 vehicle to data applic-

CONFIDENTIAL
UNCLASSIFIED

UNCLASSIFIED
CONFIDENTIAL

able to the upgraded S-2A vehicle have continued. The modal data of S-2 in the boost configuration have been used to generate a flexibility influence coefficient matrix C whose typical element C_{ij} is the displacement of coordinate i due to a unit load on coordinate j. The restraint of the vehicle for the influence coefficient matrix C is the restraint at the base of the GD/A adapter provided by the floor fixity in the modal vibration test of S-2 in the boost configuration.

The principal change in upgrading S-2 to S-2A is the redesign of the mast and antenna solar panel positioner. The revised structure begins at the three upper corners of the spaceframe to which the tripod mast supports are attached. To isolate the revised structure for detailed analyses, the influence coefficient matrix C is transformed into an influence coefficient matrix $\overline{C}$ which represents the vehicle restrained at the upper three corners of the spaceframe. The restraint at the three corners is statically determinate: one corner is restrained in three directions, one corner is restrained in two directions, and one corner is restrained in one direction. With these statically determinate restraints, the transformation of influence coefficients results from a static loads analysis which reduces to the matrix operation:

$$\overline{C} = P^T C P$$

where

$C = NxN$ influence coefficient matrix for restraint at base of GD/A adapter

$\overline{C} = NxN$ influence coefficient matrix for restraint at three upper corners of spaceframe

$P = NxN$ load matrix. The jth column of P contains the jth unit load and loads at the three upper corners of spaceframe which equilibrate the jth unit load.

P^T = transposed matrix of P

The matrix P is developed from the rigid body modal matrix $R = 6 \times N$ matrix of rigid body modes written as rows. The six columns of R, which correspond to the six restrained coordinates at the upper spaceframe, are used to form the 6×6 matrix r. The inverse of r is obtained as the 6×6 matrix $f = r^{-1}$, and f is expanded with zeros to form the $N \times 6$ matrix F. Finally, the matrix P is given as:

$$P = I - FR$$

where I is the identity matrix to provide the unit loads, and the product FR provides the equilibrating loads at the three corners of the upper spaceframe.

Derivation of the matrix operation $\overline{C} = P^T C P$ is obtained by consideration of the displacement matrix $Y = CP$. Y is an $N \times N$ matrix of displacements referenced to the base of the GD/A adapter. Since the loads in each column of P are self-equilibrating, the reactions at the base of the GD/A adapter are zero and the loads at the upper three corners of the spaceframe may be considered to be the reactions to the unit loads. The matrix Y thus gives displacements for the loads and restraint conditions of the required matrix $\overline{C}$, but the displacements are referenced to the base of the GD/A adapter instead of to the upper three corners of the spaceframe. It can be shown that premultiplication of the matrix Y by the matrix P^T provides the required change of reference. An heuristic argument for this procedure is that the matrix $Y = CP$ has all of the properties of the required influence coefficient matrix $\overline{C}$ except the property of symmetry, and this property is obtained by premultiplication by P^T to give $\overline{C} = P^T Y = P^T C P$.

This procedure has been programmed on the IBM computer and the influence coefficient matrix for the S-2 in the boost configuration has been transformed to an influence coefficient matrix with restraint at the upper three corners of the space-frame. The mast and antenna/solar panel positioner are thus isolated for incorporating the changes made in the redesign of the S-2 to the S-2A vehicle. In addition to relocation and reorientation, the redesign included the structure of the mast support and the mast, and the structure of the planar array and solar panel supports and bracketry. These structural changes have been evaluated to some degree by the vibration tests (see Table 34 for torsional spring between planar array and mast) and will be evaluated further by analyses of structural flexibilities and by static tests to determine flexibilities. These flexibilities will be incorporated in the influence coefficient matrix with restraint at the top of the spaceframe. Transformation of restraint to the base of the GD/A adapter will provide the influence matrix for calculating modes and frequencies of the S-2A in the boost configuration.

A modal vibration test is planned for obtaining the modes and frequencies of S-2A in the landing configuration. In this modal vibration test, the free-free condition of landing will be simulated by supporting the test article with soft springs at each of the three footpads. In addition to surveying the antenna/solar panel positioner (A/SPP) in the landing configurations, it is planned to obtain modes and frequencies in the free-free condition with the A/SPP in the boost configuration. Modes and frequencies measured in this vibration test will be used to generate an inertia influence coefficient matrix in which restraint will be provided by inertia. Reference

CONFIDENTIAL
UNCLASSIFIED

UNCLASSIFIED
CONFIDENTIAL

axes for displacements will coincide with the principal axes of inertia. The inertia influence coefficient matrix may be transformed to an influence coefficient matrix with restraint at the upper three corners of the space-frame in the same manner that is outlined above. This influence coefficient matrix isolates the ASPP and may be used to refine further the S-2A modal data in the boost configuration.

6. Dynamic Tests

a. S-2A spacecraft. The S-2A is the upgraded structural test vehicle that corresponds to the A-21 spacecraft. During this report period, the type-approval vibration tests as summarized in Table 31 were conducted, with the exception of Tests 8 and 9 and a portion of Test 7. In Test 7, while shaking S-2A in the direction normal to Leg 3 during the lateral vibration test, the A/SPP elevation motor housing failed in bending at 9.6 cps. Fig. 75 shows the spacecraft in position on the lateral test fixture prior to Test 7; Fig. 76 shows a closeup view of the failed motor housing. Strain gage data and accelerometer data recorded at the time of failure are listed in Table 32.

The strain gage and accelerometer data of Table 32 shows that at the time of failure the response of the A/SPP was essentially a two-dimensional response corresponding to the direction of table excitation, i.e., the lateral accelerations parallel to the planes of the planar array and the solar panel were negligible. A visual record of this two-dimensional response was obtained by a camera which viewed the mast and the vertical edges of the planar array and solar panel. Film speed of 96 frames

Table 31. Summary of S-2A vibration tests

Test number	Description	Input, g, (0 to peak)	Frequency, cps	Test number	Description	Input, g, (0 to peak)	Frequency, cps
1	Exploratory along Leg 1, lateral	0.25	5 to 100	12G	Mast investigation, lateral (perpendicular to Leg 3)	0.75	5 to 15
2	Exploratory along Leg 2, lateral	0.25	5 to 100	12H	Mast investigation, lateral (perpendicular to Leg 3), sponge inserted between planar array and mast	0.75	5 to 15
3	Exploratory along Leg 3, lateral	0.25	5 to 100	12J	Mast investigation, lateral (perpendicular to Leg 3), sponge inserted between both planar array and solar panel and mast	0.75	5 to 15
4	Low level, longitudinal	0.25	5 to 1500	13A	Mast investigation, lateral (parallel to Leg 3), sponge inserted between both planar array and solar panel and mast	0.25	5 to 15
5	Type approval level, longitudinal	2.5 2.00	5 to 40 40 to 200	13B	Mast investigation, lateral (parallel to Leg 3), sponge inserted between both planar array and solar panel and mast	0.50	5 to 15
6	Low level, perpendicular to most deleterious direction, lateral	0.25	5 to 1500	13C	Mast investigation, lateral (parallel to Leg 3), sponge inserted between both planar array and solar panel and mast	0.75	5 to 15
7 (Not completed[a])	Type approval level, perpendicular to most deleterious direction, lateral	1.25 2.00	5 to 40 40 to 200	13D	Mast investigation, lateral (parallel to Leg 3), sponge inserted between both planar array and solar panel and mast	0.875	5 to 15
8 (not run)		0.25	5 to 1500	13E	Mast investigation, lateral (parallel to Leg 3)	0.25	5 to 15
9 (not run)		1.25 2.00	5 to 40 40 to 200	13F	Mast investigation, lateral (parallel to Leg 3)	0.50	5 to 15
10	Intermediate level for compartment checkout, parallel to Leg 3, lateral	0.75	15 to 200	13G	Mast investigation, lateral (parallel to Leg 3)	0.75	5 to 15
11	Intermediate level for compartment checkout, perpendicular to Leg 3, lateral	0.75	15 to 200	14A	Partial type approval level, lateral, parallel to Leg 3	1.05 2.00	15 to 50 50 to 1500
12A	Mast investigation, lateral (perpendicular to Leg 3)	0.25	5 to 15	14B	Type approval level, lateral, parallel to Leg 3	1.20 2.00	15 to 50 50 to 1500
12B	Aborted run			15A	Partial type approval level, lateral, perpendicular to Leg 3	1.05	15 to 50
12C	Aborted run			15B	Type approval level, lateral, perpendicular to Leg 3	1.20 2.00	15 to 50 50 to 1500
12D	Mast investigation, lateral (perpendicular to Leg 3)	0.50	5 to 15				
12E	Mast investigation, lateral (perpendicular to Leg 3), fast sweep (2 octaves/min) to determine its effect	0.50	5 to 15				
12F	Mast investigation, lateral (perpendicular to Leg 3), reverse sweep to determine its effect	0.25	15 to 5				

[a]Test stopped at 9.6 cps due to housing failure.

UNCLASSIFIED
CONFIDENTIAL

UNCLASSIFIED
CONFIDENTIAL

Table 32. Mast loads and stresses at time of motor housing failure

Accelerometer number	Location	Response, g
10	Input	1.33
11	Retro-rocket perpendicular to Leg 3	1.37
19	Retro-rocket parallel to Leg 3	0.46
26	Solar panel, radial	23.0
28	Solar panel, vertical	8.1
30	Planar array radial	18.5
32	Planar array, vertical	7.66
Strain gage number	**Location**	**Response, thousands of lb/ft²**
101	A/SPP bending	1.49
102	A/SPP bending	27.20[a]
103	A/SPP planar array support tube bending	3.67
104	A/SPP planar array support tube bending	9.80[a]
105	A/SPP solar panel support arm bending	5.85
106	A/SPP solar panel support arm bending	6.03
107	A/SPP planar array support tube torsion	2.23

[a]Strain gage 102 leads 104 by 90 deg at 9.6 cps.

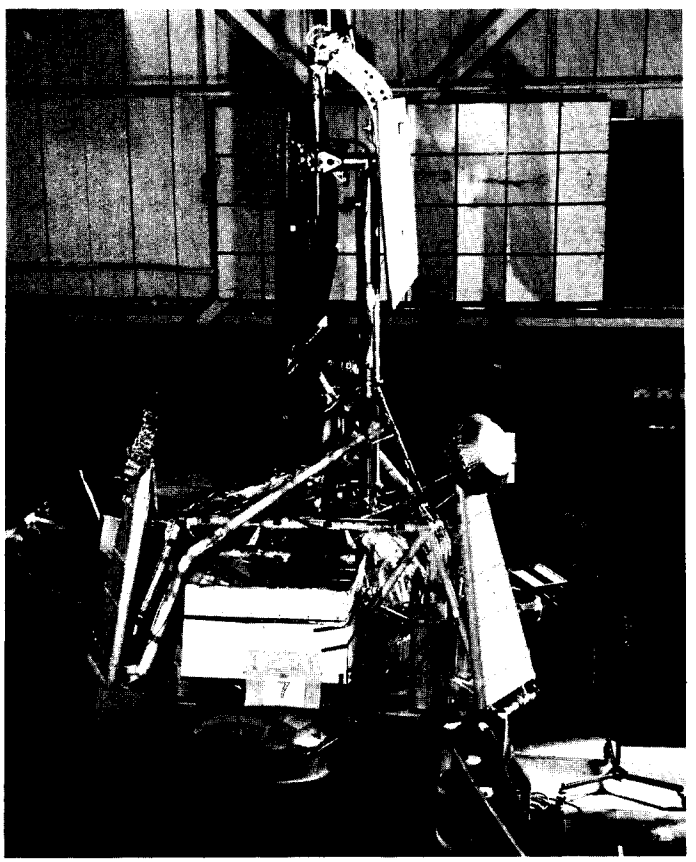

Fig. 75. S-2A lateral vibration test

per sec provided 10 frames per cycle of response at the time of the failure which occurred at the frequency of 9.6 cps. The dynamic conditions of the A/SPP prior to the failure and the events during the failure have been determined from examination of a sequence of 40 frames of the film.

In Fig. 77, significant displacements of the A/SPP are plotted for each of 40 frames of the film.

Fig. 78 shows Frame 9 with the peak displacement in the positive direction and Fig. 79 shows Frame 15 with the peak displacements in the negative direction. In Fig. 77 at Frame 21, the rotation of the planar array does not recover from the peak rotation and this is taken to define the initiation of the failure of the motor housing. Frame 21 is similar to Frame 9 shown in Fig. 78, from this it may be presumed that the failure initiated as a tension failure at the lower surface of the motor housing. The progression of failure events is given in Fig. 77. At Frame 23 a separation of the planar array from the mast was discernible, indicating complete rupture of the motor housing. The impact of the solar panel with the mast in Frame 25 resulted from the complete rupture of the motor housing.

Fig. 77 shows that prior to failure the rotations of the planar array and the solar panel have the same amplitude of $\pm 7\frac{1}{4}$ deg about the static positions of 0 and -5 deg, respectively. The rotation of the solar panel lags the rotation of the planar array by a time less than the time which can be discriminated from the sampling time of the frames; it is estimated that the lag is about one-half of a frame, or one-twentieth of a cycle.

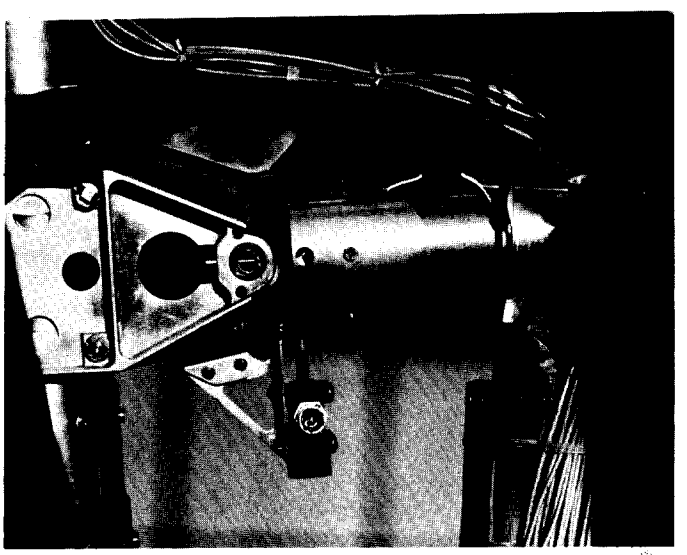

Fig. 76. S-2A elevation motor housing failure

CONFIDENTIAL
UNCLASSIFIED

UNCLASSIFIED
CONFIDENTIAL

The rotations of the planar array and the solar panel are approximately in phase and are of the same amplitude. Examination of frames from the pre-failure period confirms that the motion of the planar array and the solar panel is essentially the motion of a single rigid body. Fig. 78 and 79 show the two extreme positions, in both of which the angle between the planar array and the solar panel is the static angle of 5 deg. With the sim-

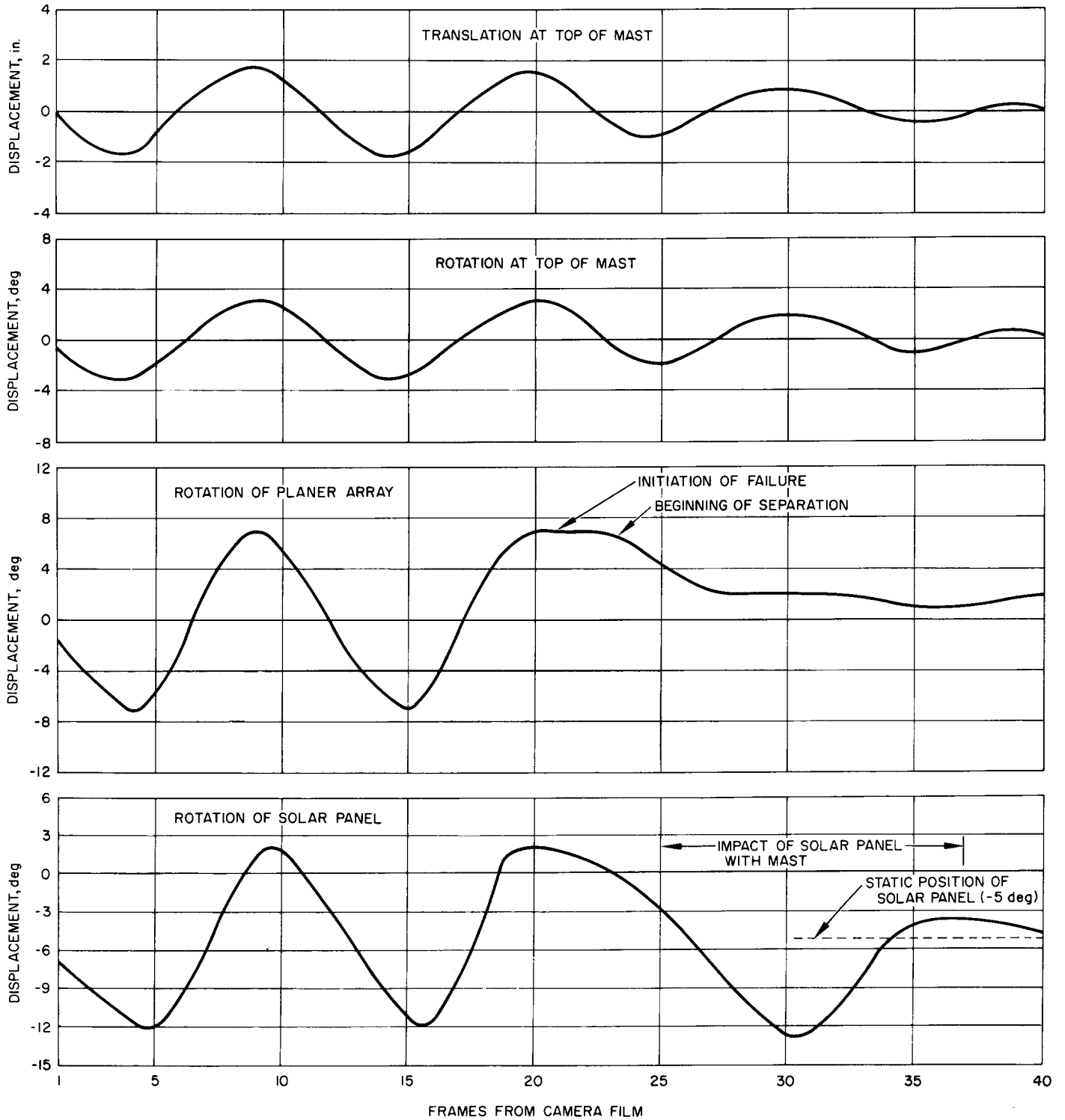

Fig. 77. Displacement of antenna/solar panel positioner

CONFIDENTIAL
UNCLASSIFIED

UNCLASSIFIED
CONFIDENTIAL

plification of a single rigid body for the planar array and solar panel, the motion of the A/SPP can be described by the following terms:

(1) Translation and rotation at the top of the mast.

(2) Translation and rotation of a rigid body consisting of the planar array and the solar panel.

The frames show that the only relative motion which occurs in the system is a rotation of the planar array relative to the mast. Fig. 77 shows that the mast rotation of ±3¼ deg and the planar array rotation of ±7¼ deg give the relative rotation of ±4 deg.

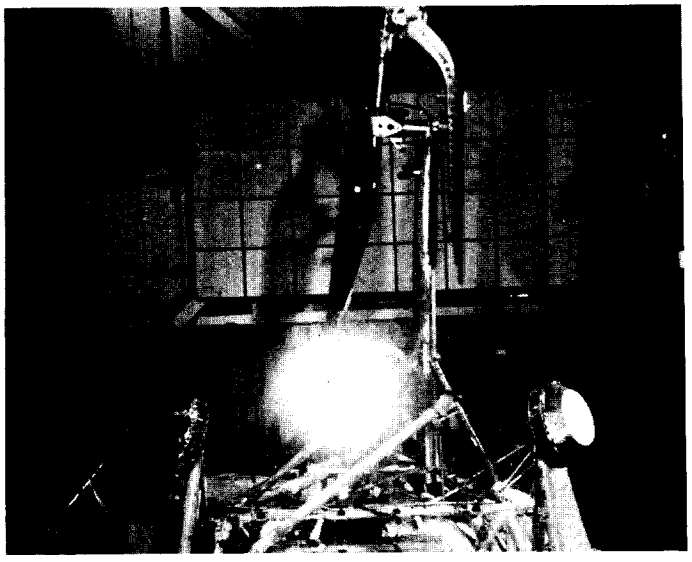

Fig. 78. Enlargement of Frame 9

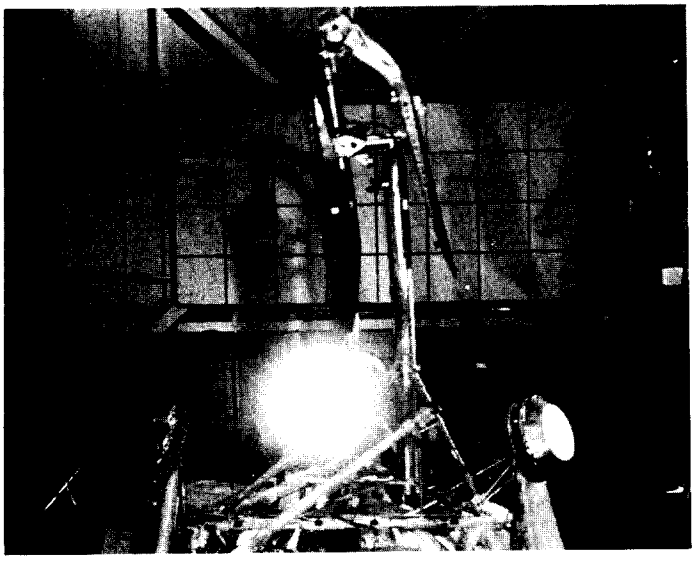

Fig. 79. Enlargement of Frame 15

This relative motion includes backlash of gears and clearances in attachments, but the primary contribution is considered to be the result of elastic deformation. As an initial assumption, the relative motion is ascribed to a torsional spring. The dynamic model of the A/SPP for this condition of two-dimensional response is a flexible mast with a torsional spring attachment to a rigid body comprised of the planar array and the solar panel. The mass properties of the A/SPP corresponding to this model are given in Fig. 80.

For an analysis of the dynamic loads at the time of the motor housing failure, data as summarized in Table 33 were obtained from the motion picture frames and from accelerometers on the planar array and the solar panel. The accelerations of Table 33 with the mass properties of Fig. 80 result in the dynamic loads shown in Table 34, which were acting at the time of the motor housing failure. Table 34 shows that the torsional spring between the planar array and the mast is defined by the moment

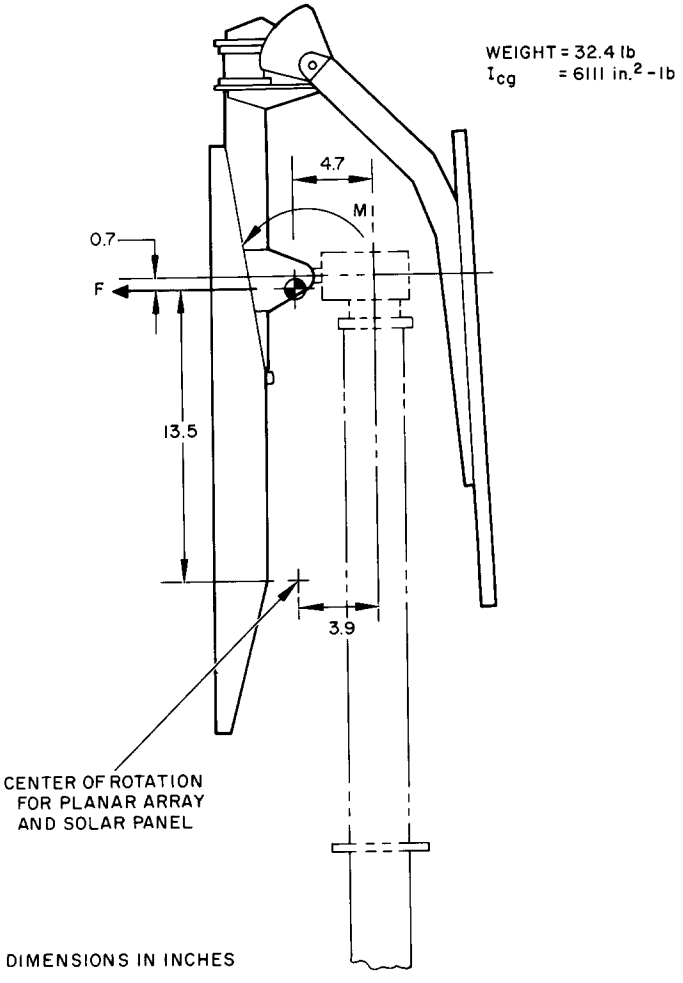

Fig. 80. Loads and mass properties of planar array and solar panel

CONFIDENTIAL
UNCLASSIFIED

UNCLASSIFIED
CONFIDENTIAL

on the motor housing which acts to cause the relative rotation between the planar array and the mast.

The broken housing was repaired with a doubler to allow intermediate-level tests at frequencies from 15 to 200 cps (tests 10 and 11, Table 31). These runs provided data to increase the confidence that remaining components (compartments, auxiliary battery, etc.) would pass TAT level inputs.

The housing was replaced with a new part of the same design, and tests resumed at a reduced input level to explore the cause of failure. The replacement housing had strain gages at the principal bending section to monitor axial (with respect to the motor axis) and shear stresses during the fundamental mast bending and during A/SPP motions from 9 to 11 cps.

Exploratory vibration sweeps were made at 0.25, 0.5, and 0.75 g in both lateral directions over the frequency range of 5 to 15 cps to observe the motor housing stress pattern and to define any increasing stress nonlinearities with input level. The responses of strain gages and accelerometers of the A/SPP were quite linear with the input, except for the strain gages on the motor housing. The responses of the strain gages on the motor housing were nonlinear and were much smaller than expected, and as such gave no clue to the previous failure of the motor housing. Subsequent investigation showed that the ballast unit simulating the transmission and motor weight was installed within the motor housing with a tight fit which does not duplicate the installation of the actual units. The ballast unit provided load path parallel to the motor housing and thus invalidated the strain gage measurements on the housing. The ballast unit has been machined to reduce the diameter to give a typical clearance in the motor housing. It is expected that future tests will provide valid strain gage data for the motor housing.

Tests also were run as high as 0.875 g in one of the lateral directions with a crude sponge rubber absorber inserted between the mast and the antenna and solar panel in an attempt to attenuate the observed large panel motions relative to the mast. For vibration inputs along Leg 3, motion of the antenna and solar panel with respect to the mast were appreciably reduced. Displacement of the edges of the solar panel at a 0.75 g input level with the sponge rubber installed was 65% of that experienced without the absorber.

Tests were conducted in both lateral directions from 15 to 1500 cps at the "B" and "C" levels specified in Revision 1 of JPL Specification 30240D, thus avoiding the A/SPP mast natural frequency range, while conducting further spacecraft evaluations until a strengthened elevation motor housing was available. Apart from two small countersunk screws backing out of their threaded holes in the brace structure of Compartment B, no structural failures or malfunctions occurred during these tests.

Plans for conducting additional tests on the S-2A vehicle include: (1) evaluation of several damping and motion absorber devices to attenuate the mast and A/SPP motions in the 9 to 11-cps range and (2) conducting a demonstration test to the specification "C" levels in both lateral directions with the redesigned A/SPP motor housing in place.

Table 33. Motion of A/SPP at 9.6 cps for excitation perpendicular to Leg 3 (Prior to motor housing failure)

Measurements from camera film prints and accelerometers	Peak-to-peak displacement	Acceleration
Top of mast		
Lateral displacement	3.5 in.	16.5 g
Angular rotation	6½ deg	—
Planar array		
Angular rotation	14½ deg	461 rad/sec²
Lateral displacement at top	6.2 in.	29 g
Lateral displacement at bottom	— 5.3 in.	— 25 g
Accelerometer 30, 7.2 in. from top	See note 1	18.5 g
Solar panel positioner	8.4 in.	39 g
Solar panel		
Angular rotation	14½ deg	461 rad/sec²
Lateral displacement at top	5.7 in.	27 g
Lateral displacement at bottom	— 2.1 in.	— 9.9 g
Accelerometer 26, 3.9 in. from top	See note 1	23 g

Notes:
(1) Accelerometer measurements correlate with accelerations obtained from measured displacements.
(2) All measurements confirm rotation of planar array and solar panel about center of rotation shown in Fig. 80.

Table 34. Internal forces and moments on antenna/solar panel positioner[a]

Force on motor housing	520 lb
Moment on motor housing (7310 — 0.75 × 520)	6,920 in.-lb
Force at top of mast (including inertia force due to weight at top of mast) (520 + 4 × 16.5)	586 lb
Moment at bottom of mast (at location of Strain Gage 102) (6920 + 32 × 586)	25,620 in.-lb
Calculated stress at bottom of mast (25,620/0.92)	27,800 lb/in²
Stress measured at bottom of mast by Strain Gage 102	27,200 lb/in²

Note: The moment on the motor housing causes a relative rotation between the planar array and the mast of ±4 deg. Torsional spring constant $= \frac{6920}{4} = 1730 \frac{\text{in-lb}}{\text{degree}}$

[a]The configuration is shown in Figure 80.

CONFIDENTIAL
UNCLASSIFIED

CONFIDENTIAL UNCLASSIFIED

b. Retro-rocket vibration measurements. Vibration data have been obtained on magnetic tape for four retro-engines fired under simulated altitude conditions at AEDC, Tullahoma, Tennessee. The data are in the form of the oscillatory components of the force output and local accelerations for the engines during burning. Fig. 81 shows the installation of the Endevco force transducer between the retro-engine and test stand.

Visual examination of the data revealed similar burning characteristics for all engines; i.e., the ignition causes the test stand to vibrate axially at its natural frequency for about four cycles of motion before thrust buildup commences. At the peak of thrust buildup, oscillatory forces of about ±250 to ±300 lb at approximately 120 to 230 cps occurred. These forces decayed very rapidly (in less than 1 sec) to the noise level which is composed of a mixture of small random forces and an electrical noise equivalent to about ±25 lb.

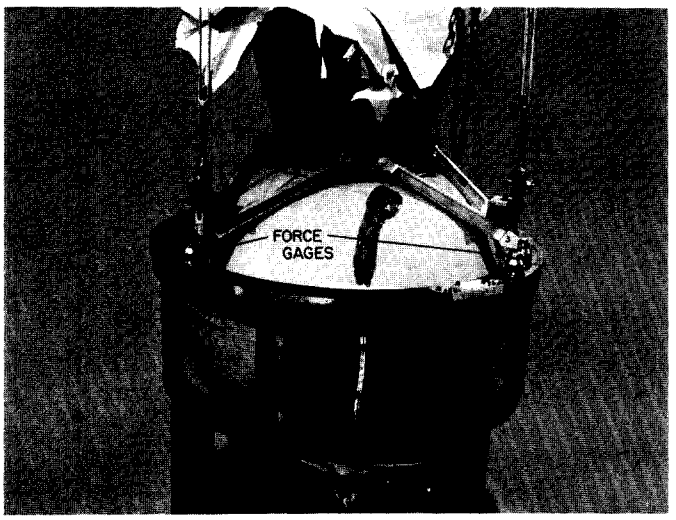

Fig. 81. Force gage installation for retro-engine firing

The sustained firing portions of all traces show several randomly spaced discrete force transients with fast rise times to approximately ±200 lb above the noise level, followed by a damped sinusoidal decay. The frequency content of the decaying sinusoids that can be distinguished are mixtures of 40 cps (test stand frequency) and 120 to 230 cps. The occurrence of the transients has been related to side force responses and are most probably the result of material spalling from the nozzle liner during burning. This is expected to be verified upon examination of AEDC filmed data. Fig. 82 shows the thrust buildup oscillatory forces and sustained firing portion transients.

A quantitative analysis on the taped data is in progress to determine: (1) power spectral densities, (PSD), of quiet (non-transient) portions of the firing for comparison to PSDs of the "prior to firing" condition, (2) probability densities of the quiet portions to establish the spectra of random forces that may exist, and (3) several shock spectrum analyses of the transient phenomena to define the contained frequencies and energy levels. Comparisons of data will be made between engines in an effort to generalize the dynamic characteristics.

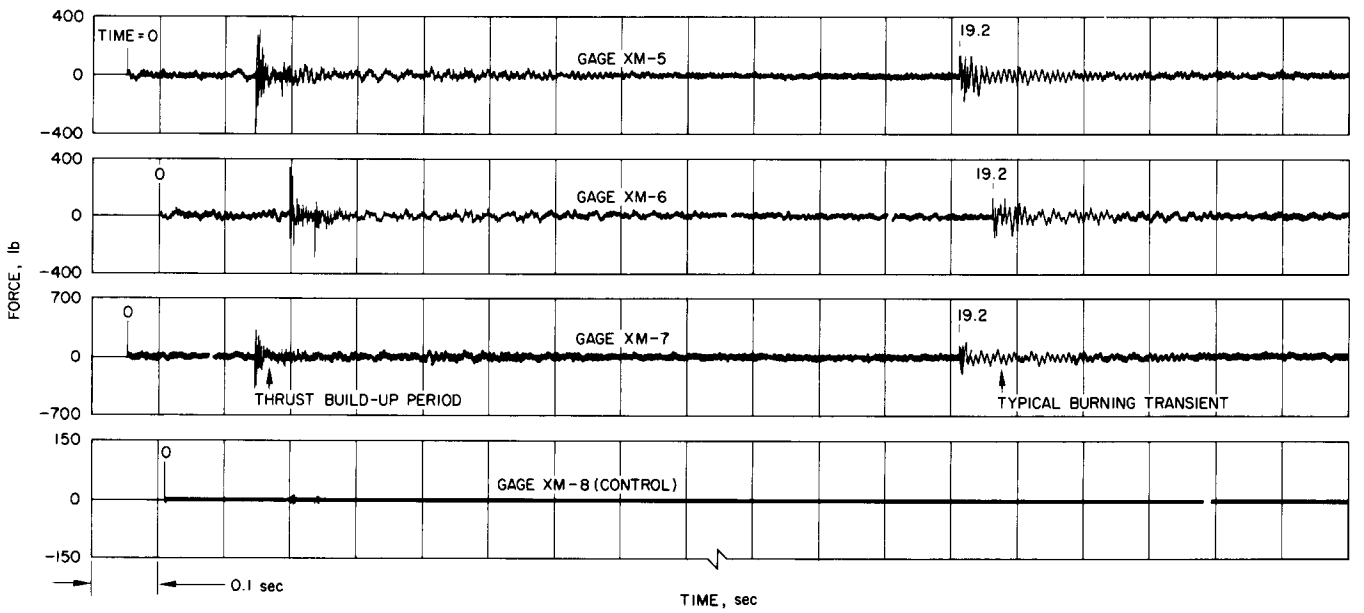

Fig. 82. Force gage response in retro-engine firing

CONFIDENTIAL UNCLASSIFIED

CONFIDENTIAL
UNCLASSIFIED

7. Flight Vehicle Instrumentation

a. Accelerometer-amplifier systems. Complete systems for T-21, SC-1, SC-2, and SP-1 have been delivered; these are units S/N 01 through 33. Delivery of units for SC-3, S/N 33 to 40, is expected in October. The assemblies for T-21 and SC-1 are complete and the assembly for SC-2 is scheduled for mid-October. The accelerometer coax cables located along the bottom of the spaceframe have been rerouted along the main harness to eliminate the possibility of being damaged by corners of the structure. The new routing required cables of different lengths. New cables are now available and rework on some existing cables has been accomplished for T-21 and SC-1; cables for other spacecraft will be procured or reworked after optimum lengths are established.

b. Strain gage amplifiers. Semiconductor Magnetics Incorporated (SMI) notified Hughes that repeated failures at the flight acceptance test level of the strain gage amplifiers have made it unprofitable for SMI to continue supplying the amplifiers at the agreed purchase price. Because of schedule considerations, negotiations are being carried on with SMI for provision of the six additional amplifiers needed for SC-1. Meanwhile, invitation for bids have been sent out to prospective vendors to establish a second source.

c. Leg deflection potentiometers. Units for SC-1, SC-2, and SP-1 have been received from Spectrol. Units for the other spacecraft will be ordered after qualification of the units for electrical operation in a lunar night temperature environment of —300°F and a lunar day environment of +300°F. This is a change in the requirements of the procurement specification which originally required units to operate only between —65° and 275°F. One of the existing units will be tested to determine the effect of the new temperature environments; however, no problems are anticipated.

8. Stress Analysis

a. Retro-rocket separation device. During the design verification tests of the retro-rocket separation device, performed by Hi-Shear Corporation, various failures occurred in the flanged base assembly (see Fig. 83). Failures occurred at the thread relief in the region of the two screws that attach the nut assembly to the spaceframe adapter.

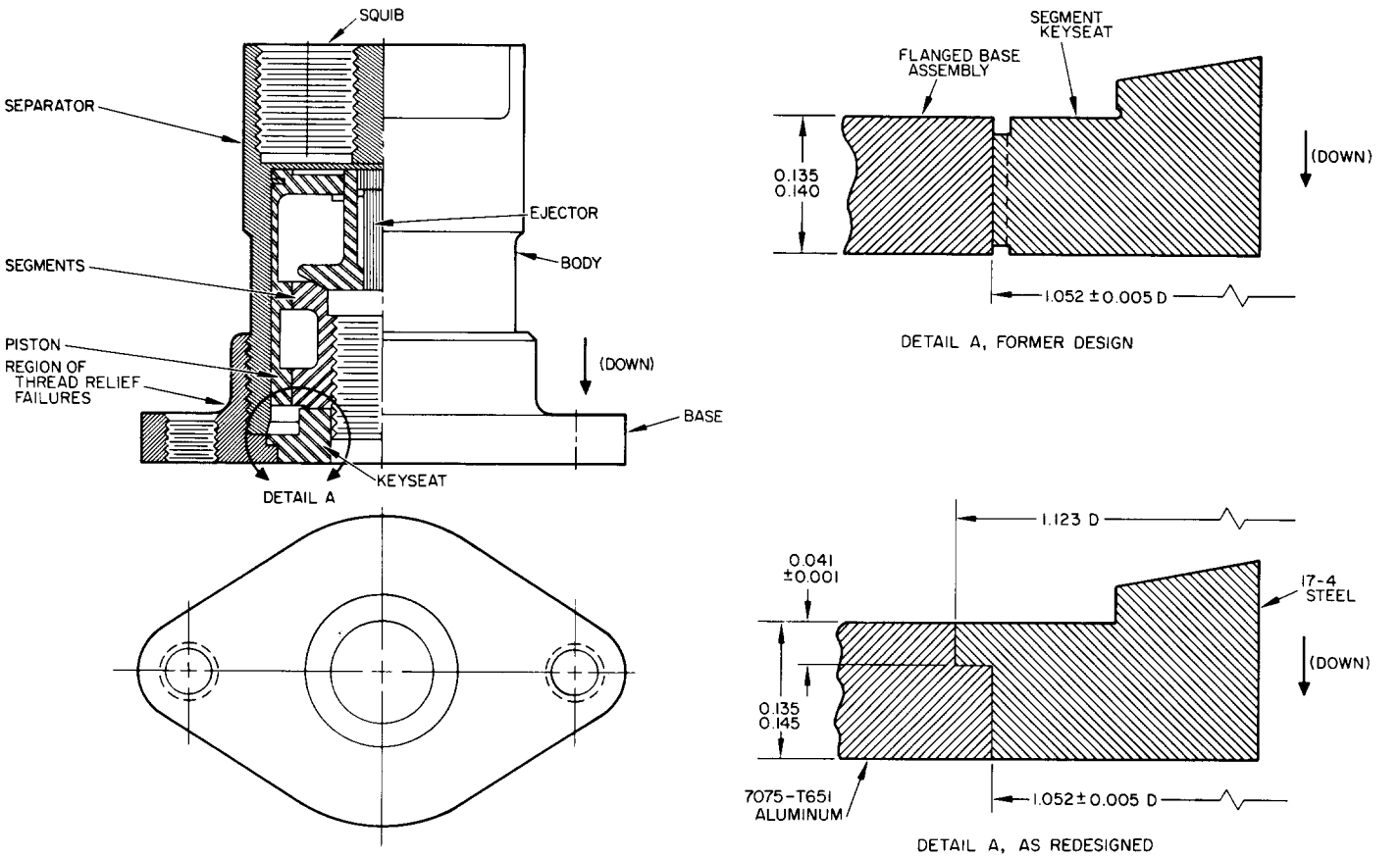

Fig. 83. Redesign of retro-engine separation nut

CONFIDENTIAL
UNCLASSIFIED

UNCLASSIFIED

The manner of operation of the separation device is shown in Fig. 84. (The device on *Surveyor* has two squibs as shown in Fig. 83 but operates the same as the single-squib device in Fig. 84.) The load path for the induced squib pressure in the chamber which operates the device is through the body to the base as shown in Fig. 84. This pressure load is reacted by the two screws which attach the base to the spaceframe adapter. The failures at the thread relief was caused by combined tensile and bending stresses.

To provide an adequate load path to transmit the chamber pressure, a flange was added to the segment keyseat as shown in Fig. 83. This flange and the two screws will carry the chamber pressure before the main bolt is finally ejected. The ratio of flange thicknesses for the keyseat and base was based on the relative shear strength values of the two materials.

Specific chamber pressures as a function of time and piston displacement, measured from the time of squib ignition, are not available, and this information is required before a detailed stress analysis is possible. However, the structural integrity of the device will be proved by tests to be performed by the Hi-Shear Corporation as outlined in the procurement specification. Squibs of various sizes will be fired to determine the maximum charge (two squibs) that the device can withstand without failure. At the other end of the scale, tests will be performed to determine the minimum charge (one squib) required to operate the device. The standard operating charge must be sufficiently smaller than the maximum safe charge (determined by test) to ensure structural reliability.

b. Main retro-engine supports. During vibration tests of the main retro-engine by Thiokol Chemical Corporation, fatigue failures occurred in the attachment strut and spring pin (see Fig. 85). The test history of load levels and number of fatigue cycles were not determined for this particular failure.

Table 35 shows the input levels which have been established for future retro-engine vibration tests. Table 36 gives the retro-engine response in g and pitching moments which are predicted for the inputs of Table 35. Fig. 86 shows the sign convention for the retro-rocket loads in Table 36. The corresponding number of load cycles for each condition are contained in Table 37. The stress analysis of the retro supports for the loading conditions of Tables 36 and 37 is described below.

The hinge-pin attachment provides a load path for transmission of vibratory and thrust loads from the thrust skirt of the retro-rocket engine to the attachment strut (see Fig. 85). Based on static test data from Thiokol Chemical Corp. the assumption has been made that only the center two lugs of the strut hinge are effective in transmitting boost vibration loads.

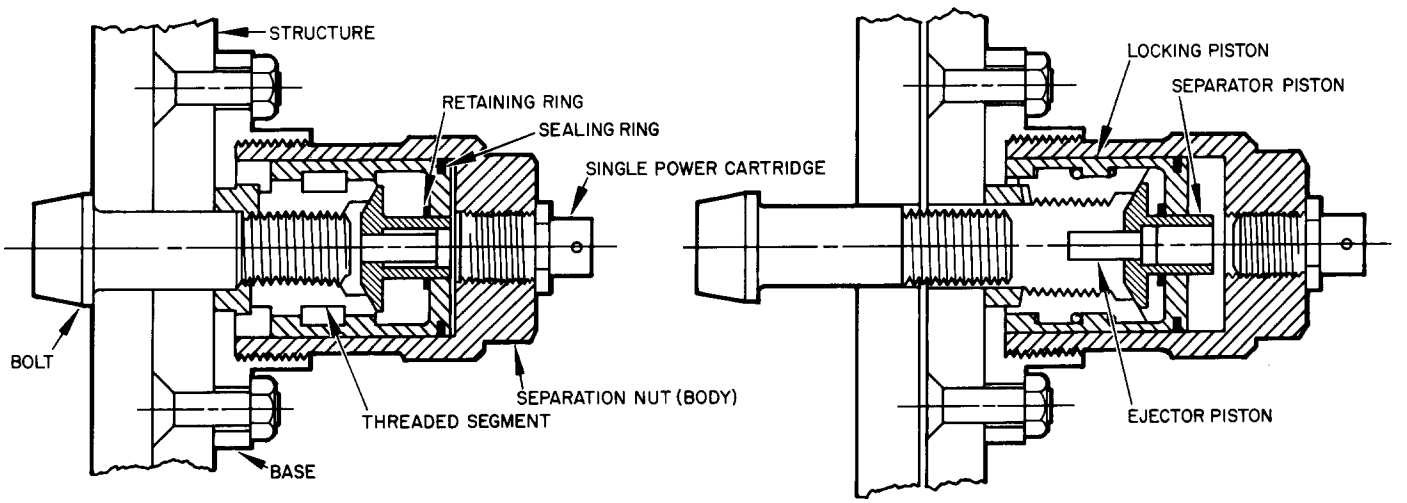

Fig. 84. Retro-engine separation device

UNCLASSIFIED

UNCLASSIFIED
CONFIDENTIAL

Failure of the attachment strut at the point indicated in Fig. 85 was caused by combined biaxial tension and shear stresses which were amplified by a high stress concentration from a small radius of 0.005 in. The strut was reworked to remove the notch at the point of failure by increasing the radius to 0.125 in.

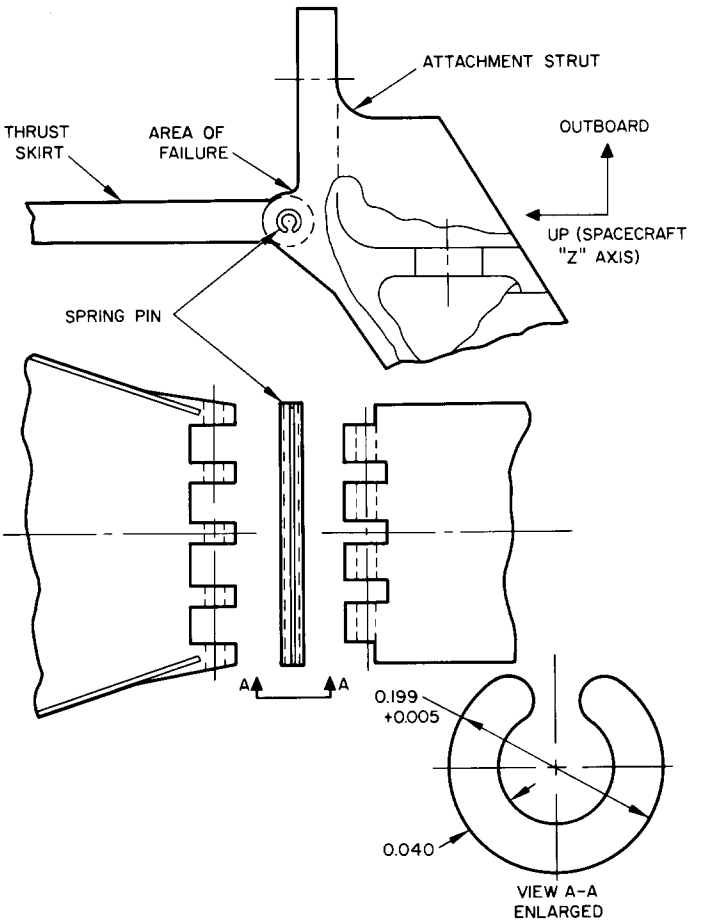

Fig. 85. Retro-engine hinge pin attachment

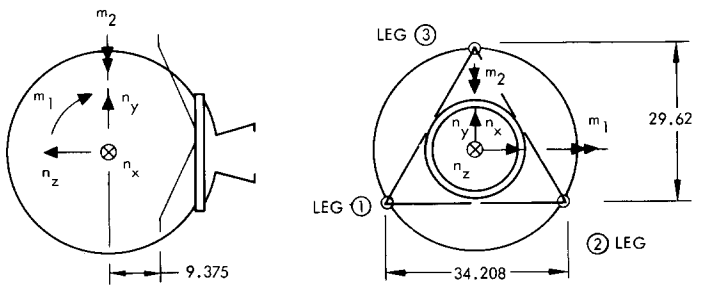

NOTES:
1) LOADS POSITIVE AS SHOWN
2) RIGHT HAND RULE FOR MOMENTS
3) CENTER LINE OF LEG 3 IS IN y-z PLANE
4) X-AXIS IS NORMAL TO y-z PLANE
5) ASSUMED WEIGHT OF ENGINE = 1400 lb

Fig. 86. Sign convention for retro-engine loads

Condition 4 of Table 36 causes the highest loading of the lugs and pin. The maximum principal stress in a lug at the point of failure for Condition 4 is 22,250 lb/in^2. The cumulative damage for all five conditions of Table 36 is less than 1.00. (n/N = 0.2378, using Miner's theory.)

The special spring pin failed during the vibration tests from the following reasons:

(1) The material was too brittle for this particular application.

(2) High installation bending stresses were present in the pin due to an interference fit.

(3) The pin was stressed from transmission of vibratory loads from skirt to strut.

Table 35. Main retro-engine vibration test input

Longitudinal vibration
5 to 40 cps: input 2.5 g as limited by retro-rocket response of 5.0 g
40 to 200 cps: input 2.0 g as limited by retro-rocket response of 4.0 g
Lateral vibration (X and Y)
5 to 40 cps: input 1.25 g as limited by retro-rocket response of 2.5 g
40 to 200 cps: input 2.0 g as limited by retro-rocket response of 4.0 g

Table 36. Retro-rocket load conditions (vibration tests)

Loading Condition	Retro-engine response			Pitching moment	
	$n_{x,g}$	$n_{y,g}$	$n_{z,g}$	m_1, in.-lb	m_2, in.-lb
1	0	0	±5.0	0	0
2	0	±4.0	0	0	0
3	±4.0	0	0	0	0
4[a]	0	±2.5	0	±115,000	0
5[a]	±2.5	0	0	0	±115,000

Note: Load factors are completely alternating (refer to Fig. 86 for sign convention).
[a]positive n acts with positive m and vice versa.

Table 37. Loading schedule, number of load cycles

Load, %	Loading condition (of Table 36)				
	1	2	3	4	5
100	1220	350	350	175	175
90	260	180	180	90	90
80	260	180	180	90	90
70	260	180	180	90	90
60	440	1000	1000	90	90
50	—	—	—	180	180
40	—	—	—	180	180

Note: The load cycles of the five conditions are cumulative.

CONFIDENTIAL
UNCLASSIFIED

UNCLASSIFIED
CONFIDENTIAL

The spring pin was changed from an ESNA roll pin to a solid pin so that it would be adequate for the fatigue load spectrum of Table 37. Also, it appeared that the following items should be considered in arriving at an optimum overall design:

(1) Heat treatment of the material should be revised to reduce brittleness

(2) Holes in the hinges for the pin should be drilled on assembly to prevent preloading of pin and lugs from possible misalignments.

The maximum shear stress for the solid pin for Condition 4 is 58,300 lb/in^2. Using a stress concentration factor of $K_T = 1.0$, the pin will be adequate for a fatigue life of 15,000 cycles. The cumulative fatigue damage of all five conditions of Table 36 is less than 1.0 (Σ n/N = 0.0555 using Miner's theory).

The Hughes stress analysis assumes that the magnitude of the preload acting on the pin as a result of the hole misalignment is small compared to design loads. To substantiate this assumption, the approximate magnitude of the preload corresponding to maximum misalignment of the strut and skirt holes must be determined by test.

c. Structural redesign of Compartments A and B. During the S-2 type approval vibration tests conducted in January 1964, the upper supports of Compartment B failed. In the original design, the Compartment B upper supports were designed primarily to resist axial loads. During the S-2 vibration tests, the monitored axial strain gage readings in the upper supports indicated that the axial stress levels in the upper supports were not high enough to cause any fatigue failure. It was concluded that high secondary bending stresses were induced in the upper supports from the motion of the supporting spaceframe structure combined with internal deflections of the compartments between support points.

At that time it was decided to change the material of the upper supports from magnesium to aluminum. The support configuration for Compartment B was changed to two tripods, rather than a single member and one bipod; the Compartment A support configuration was unchanged. The analysis for the redesign used the data obtained in the S-2 type approval test. However, because of the limited space envelope, it was evident that this redesign resulted in a significant increase in weight and a loss in thermal performance.

During April 1964, the design of the upper support structures for Compartments A and B was again changed to a simpler and lower weight design. This change was justified by a compartment load reduction based on an alternate interpretation of the effects of main retro resonance in depressing vibration inputs as presented in JPL Specification 30240C.

As a result of the load reduction, the material of the Compartment A upper supports was changed from magnesium to aluminum and a more reliable plastic was substituted for the original plastic. The following changes were made to Compartment B (see Fig. 87).

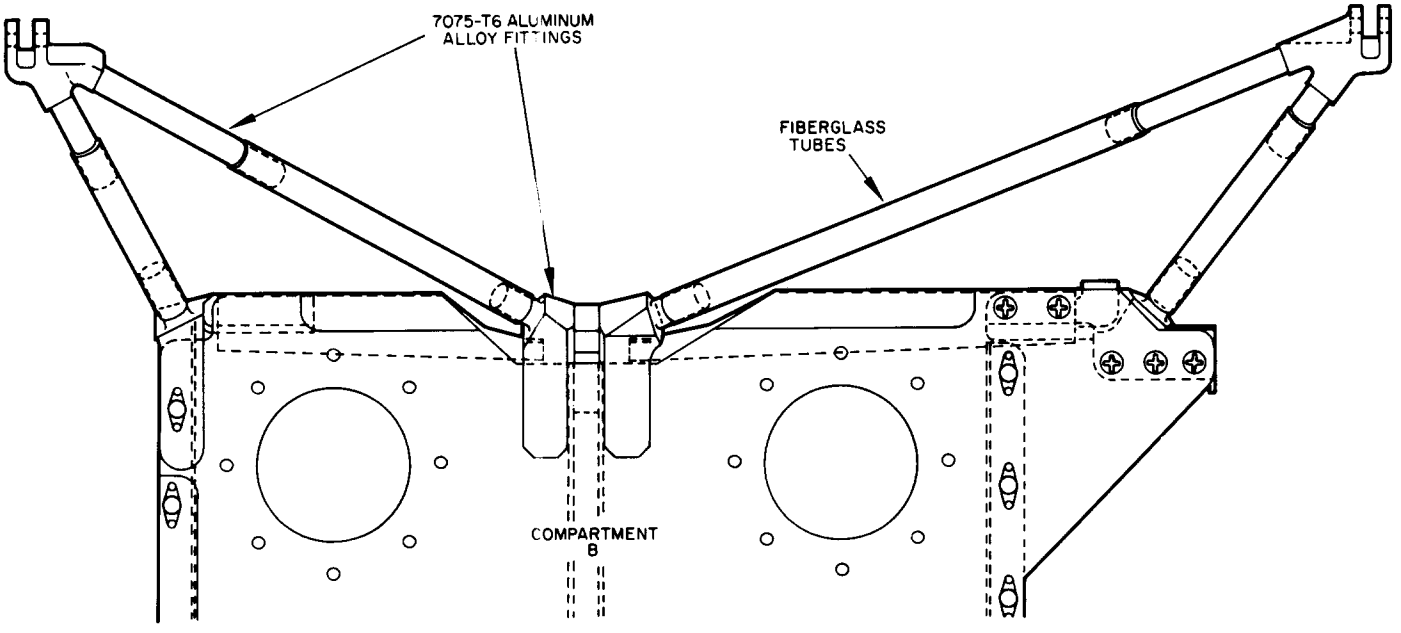

Fig. 87. Latest design of Compartment B upper supports

CONFIDENTIAL
UNCLASSIFIED

CONFIDENTIAL
UNCLASSIFIED

(1) The strength of the upper supports was increased by making two bipod assemblies of aluminum and plastic.

(2) The top plate was extended locally and a new fitting was made to replace the original built-in channel fitting assembly.

(3) New fittings at the point of intersection of the inner bipod members were designed to increase the local moment-carrying capability.

In addition, the knurling in the bonded areas for both compartments was eliminated and thermal standoffs were added to stabilize the outer cannisters and to prevent the cannisters from striking the mirrors on the thermal switches located on the upper surface of both compartments.

In September 1964, Compartments A and B, ballasted to the maximum possible weights, passed the S-2A type approval tests. Two screws in Compartment B vibrated loose during the last test. Safety wiring or locktite will be used to prevent future loosening of screws in the TAT vibration environment.

Tables 38 and 39 show the peak stress levels recorded in the upper supports of Compartments A and B during the recent test. These peak stress levels occurred at approximately 21 cps. Fig. 88 shows the location of the various strain gages. The bending strain gages were not located at the point of maximum stress because discontinuities at these points would have prevented obtaining good data. Maximum stress levels were calculated using the recorded data from the S-2A tests. At the critical Compartment B upper strut section, the maximum bending stress of 30,000 lb/in.^{2} was added to the axial stress of 14,300 lb/in.^{2} resulting in a peak stress of 44,300 lb/in.^{2}. During the test, the stress increased to a peak value for a limited time and then decreased to lower values. Data from the tests is being reduced to determine the complete fatigue spectrum. Preliminary observation of the data and since the fact that the compartments went through the complete vibration test twice (see stress levels in Tables 38 and 39 indicates that no fatigue problem exists. Until the data is completely reduced, no conclusions can be made as to how much fatigue life remains in the S-2A compartment supports.

When the original failure occurred in Compartment B, no bending stresses were recorded. The latest S-2A TAT verifies the original conclusion that excessive bending stresses caused the fatigue failure in the magnesium upper supports.

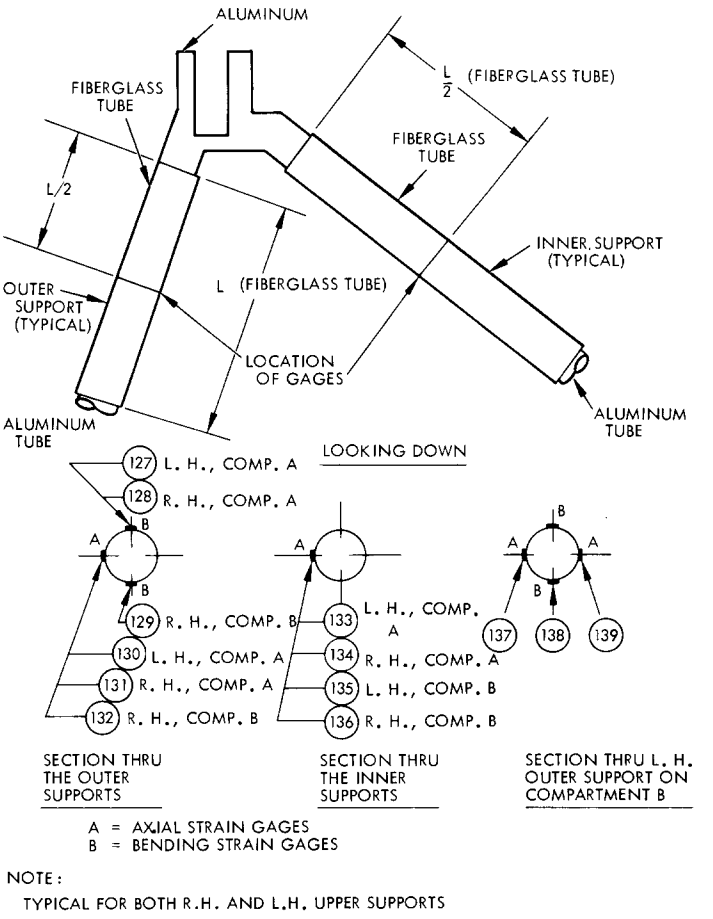

Fig. 88. S-2A Compartment A and B strain gage locations

Table 38. Compartment A stress levels, lb/in^2.

Test	Strain gage numbers				
	127B	128B	130A	133A	134A
14A	2980	2800	3370	—	—
14B	3060	3280	2460	—	—
15A	3710	4040	4060	3860	2140
15B	3930	4590	5160	3820	2360

Table 39. Compartment B stress levels, lb/in^2.

Test	Strain gage numbers					
	129B	132A	135A	136A	137A	138B
14A	4150	5900	630	—	2420	5740
14B	4270	3860	1290	1570	2640	6490
15A	5280	6090	1610	1270	3520	9370
15B	—	6810	2120	1390	3370	9160

CONFIDENTIAL
UNCLASSIFIED

UNCLASSIFIED CONFIDENTIAL

I. Propulsion

1. Introduction

The spacecraft propulsion system comprises a spherical, solid-propellant main retro-rocket engine, and a liquid-propellant vernier propulsion system. The retro-rocket engine, developed by the Elkton Division of Thiokol Chemical Corporation under a subcontract, provides most of the deceleration of the spacecraft during approach to the lunar surface. The vernier propulsion system is used for the midcourse maneuver, attitude control during retro-rocket engine burning, and terminal descent. The vernier system thrust chamber assembly will be furnished to Hughes by Reaction Motors Division (RMD) of Thiokol Chemical Corporation under subcontract to JPL.

2. Progress Summary

a. Main retro-rocket engine. The first four quality assurance test engines were tested in the multicomponent test stand at Arnold Engineering Development Center (AEDC). Ballistic performance of the engines was within specification limits. The vacuum-specific impulse of the propellant is in excess of 291 lb-sec/lb. Preliminary thrust vector excursion data is within specification limits. Final thrust excursion data will be evaluated during the next reporting period.

Vibration testing of inert engine A-21-F with the modified hinge joint was completed. Engines A-21-19 and A-21-22 will be modified and subjected to vibration testing in early November 1964.

b. Vernier propulsion system. Two expulsion unbalance tests were completed using simulated propellants on the S-6 vehicle at the Air Force Missile Development Center (AFMDC). Following completion of the evaluation of the vehicle suspension system, expulsion testing with live propellants will commence. The S-7 vehicle 30-day storage test program was started on October 4, 1964 at AFMDC. The propulsion system was loaded with actual propellants and pressurized through the helium manifolding. As part of the surveillance operation, the engines were test fired for a 6-sec duration on October 6, 1964. This will be performed at 5-day intervals during the storage period.

The 6A1-4Va helium and propellant tank programs, under subcontract to Airtek Dynamics, are progressing satisfactorily. Type approval testing of the propellant tanks, which is complete except for the vibration phase, has been successful. A helium tank expulsion test was conducted, confirming that the current helium tank design has adequate volume to complete the vernier propulsion mission.

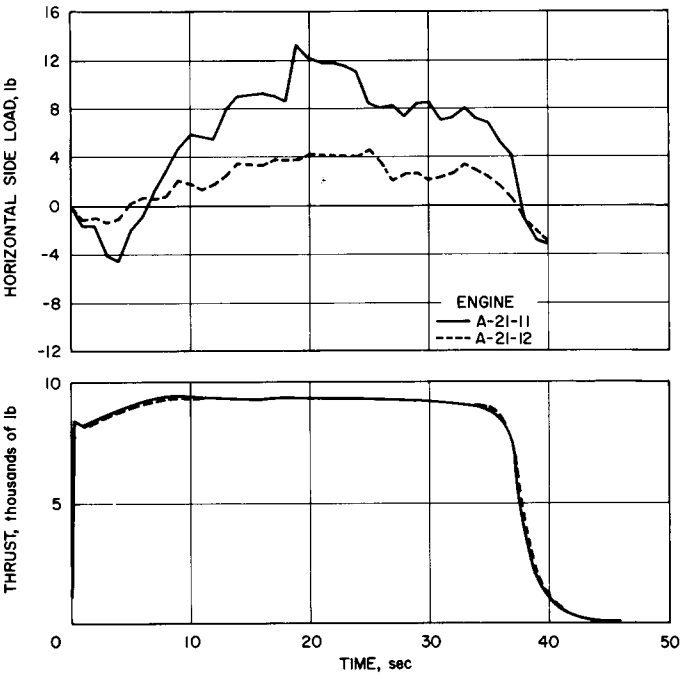

Fig. 89. Thrust and side load in firing engines A-21-11 and A-21-12

The helium pressure regulator dome seals showed deterioration after propellant vapor exposure. A program is underway to effect a seal more resistant to propellant vapors. The squib and squib valve qualification program has been stopped because of the failure of two dump squibs to fire. Modifications to the squib design are in progress.

The RMD Model TD 339 thrust chamber–spacecraft interface document has been submitted to JPL for approval.

3. Main Retro-Rocket Engine

a. Developmental engine tests. The last two developmental engines, A-21-11 and A-21-12, were tested under simulated altitude conditions in the J-5 facility at AEDC on July 6 and July 15 respectively. The engines were preconditioned to 50°F before test. Performance of these engines was within specification limits and is summarized in Table 40. Of particular interest on these tests is the side force or thrust vector excursion experienced during burning. Side force measurements were restricted to the horizontal plane for these two tests and are presented in Fig. 89.

b. Quality assurance test program. The first four retro-rocket engines subjected to quality assurance testing were fired in the six component horizontal test stand at AEDC. Prior to firing, the engines were conditioned to

CONFIDENTIAL UNCLASSIFIED

CONFIDENTIAL UNCLASSIFIED

an equilibrium 50°F temperature. Fig. 90 depicts a typical engine installation in the J-5 facility.

Ballistic performance of the four engines, corrected to vacuum conditions, is presented in Table 41. The variation in total impulse from 358,314 to 359,661 lb-sec is well within the spacecraft design limits of ±1%. These variations can be attributed to the thrust stand measurement accuracy, propellant batch-to-batch variations, and the ±3.0 lb inaccuracy of the propellant weight determination. The propellant specific impulse range of 291.5 to 291.9 lb-sec/lb is indicative of the tolerance control of the engine and propellant formulation.

The complexity of six component measurements and the interdependency of the load cells requires that a comprehensive force interaction calibration be conducted prior to and after completion of the test series. The alignment of each engine with respect to the thrust stand was measured at an equilibrium temperature of 50°F before and after each test as shown in Fig. 91. Pre- and post-test force calibrations and selected interaction calibrations were conducted at sea level and vacuum conditions. The force interaction, calibration, and measured load data is subjected to a computer analysis prior to release of final data by AEDC.

Table 40. Ballistic performance corrected to vacuum conditions

Parameters	Engine number/test date	
	A-21-11 July 6, 1964	A-21-12 July 15, 1964
Action time, sec	39.87	39.96
Total impulse, lb-sec	348,795	348,196
Propellant weight, lb	1197.8	1198.8
Specific impulse, lb-sec/lb	290.4	291.2
Maximum pressure, psia	587	582
Average pressure, psia	527	529
Throat erosion, % area	7.4	7.8
Test altitude, ft	97,000	101,000
Maximum thrust, lb	9,323	9,298
Average thrust, lb	8,525	8,621

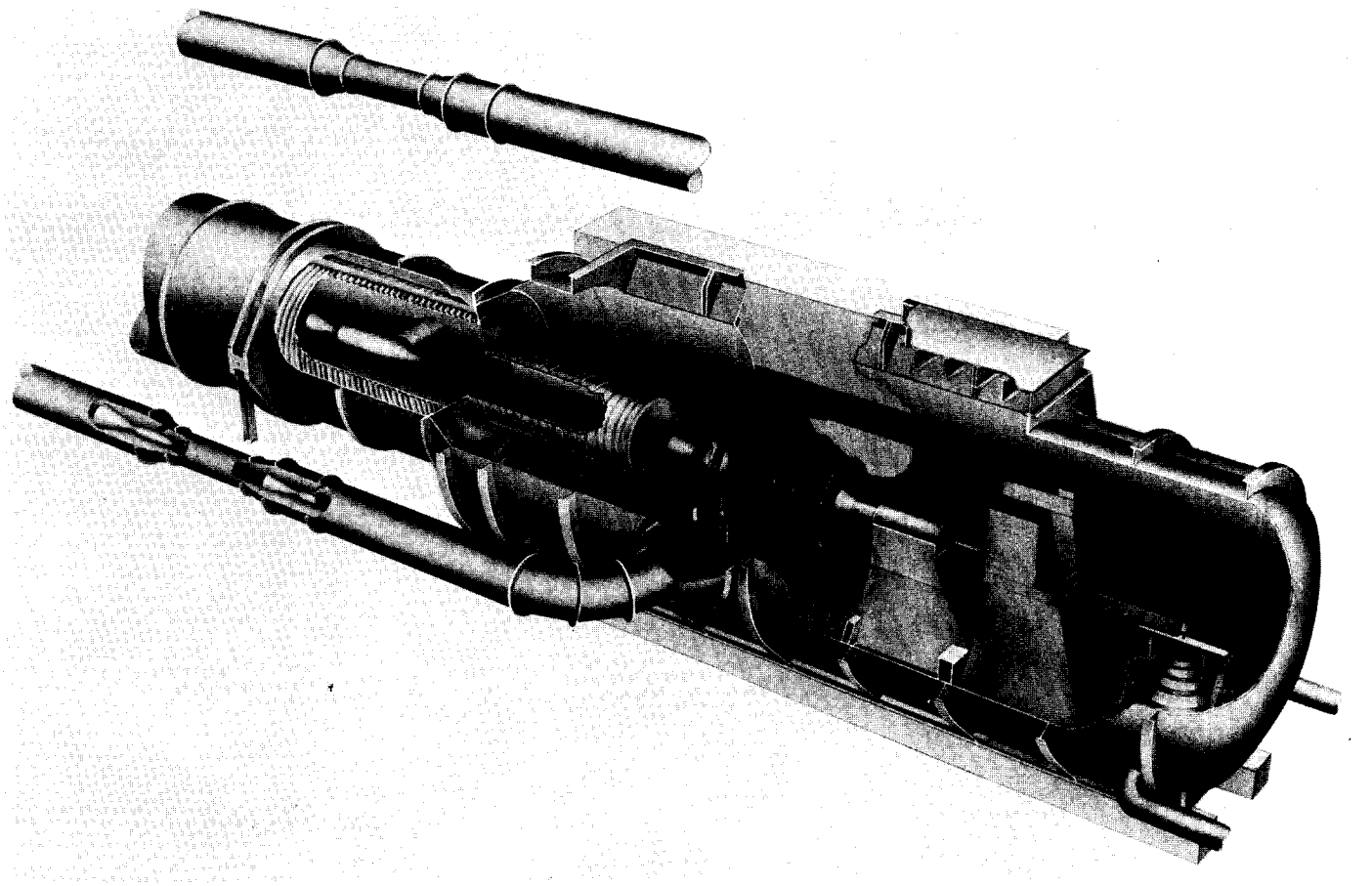

Fig. 90. Retro-rocket engine installation in AEDC J-5 test cell

CONFIDENTIAL UNCLASSIFIED

UNCLASSIFIED

Table 41. Ballistic performance corrected to vacuum conditions

Parameters	Engine number/test date			
	A-21-17 August 18, 1964	A-21-18 August 26, 1964	A-21-23 Sept. 1, 1964	A-21-24 Sept. 9, 1964
Total impulse, lb-sec	358,314	358,880	358,775	359,661
Propellant weight, lb	1228.9	1229.5	1229.0	1231.8
Specific impulse, lb-sec/lb	291.5	291.8	291.9	291.9
Action time, sec	40.45	40.55	40.98	40.35
Maximum thrust, lb	9,546	9,722	9,447	9,647
Average thrust, lb	8,736	8,711	8,579	8,767
Maximum pressure, psia	579	571	572	582
Average pressure, psia	536	534	531	537
Throat erosion, % area	8.1	8.1	8.8	9.1

Preliminary thrust vector excursion data indicates that the measured side forces are within specification limits with the exception of instantaneous forces measured on engine A-21-23. The disturbances would not affect spacecraft stability. Each nozzle experienced spalling and blistering, as shown in Fig. 92. The nozzle from engine A-21-23, shown in Fig. 92c and 92d, represents the most severe condition of spalling observed to date. Blistering, as evident by the material remaining, is a cooling-down effect. Final conclusions regarding thrust vector excursion is dependent on receipt and evaluation of the final test data.

In addition to the ballistic and thrust vector excursion data, engine induced vibration data was obtained on the four engine tests. Exhaust plume radiation measurements were conducted on engines A-21-18, -23, and -24. Two altitude marking radar (AMR) antenna ejection tests were conducted with engines A-21-17 and A-21-18. The vibration and AMR ejection data are presented in other sections of this report.

Fig. 91. Retro-rocket engine alignment check

UNCLASSIFIED

UNCLASSIFIED
CONFIDENTIAL

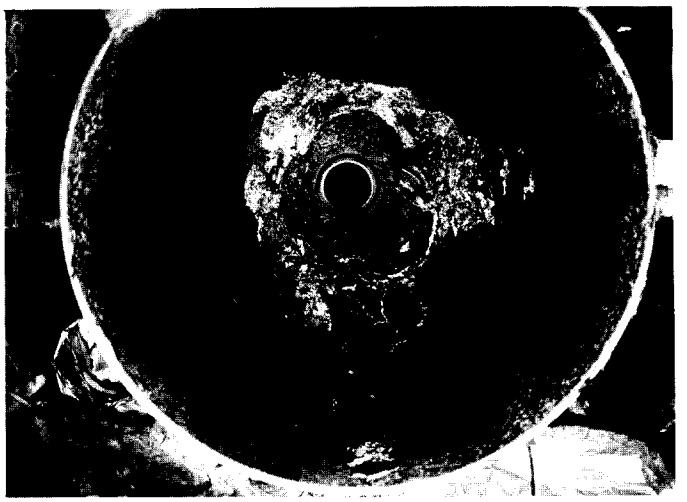

(a) Engine A-21-17 nozzle

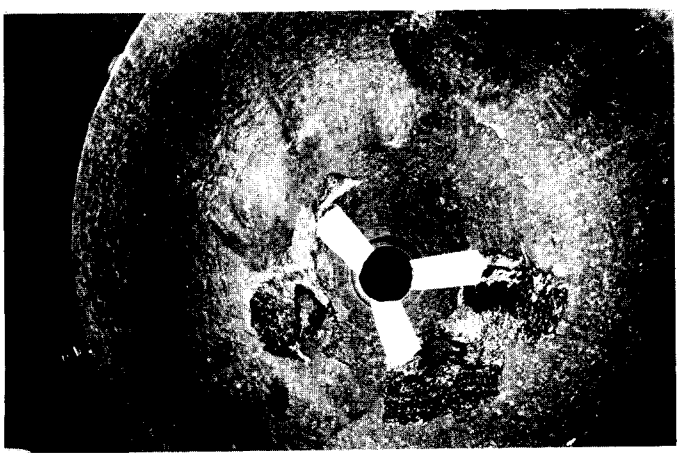

(b) Engine A-21-18 nozzle

(c) Engine A-21-23 nozzle (closeup)

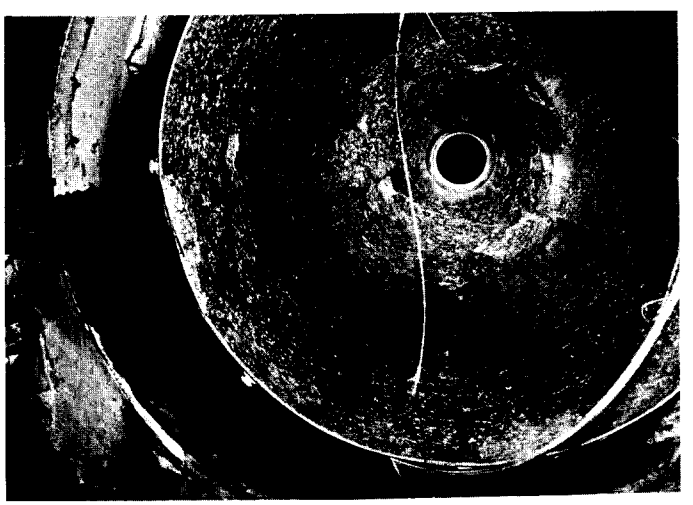

(d) Engine A-21-23 nozzle

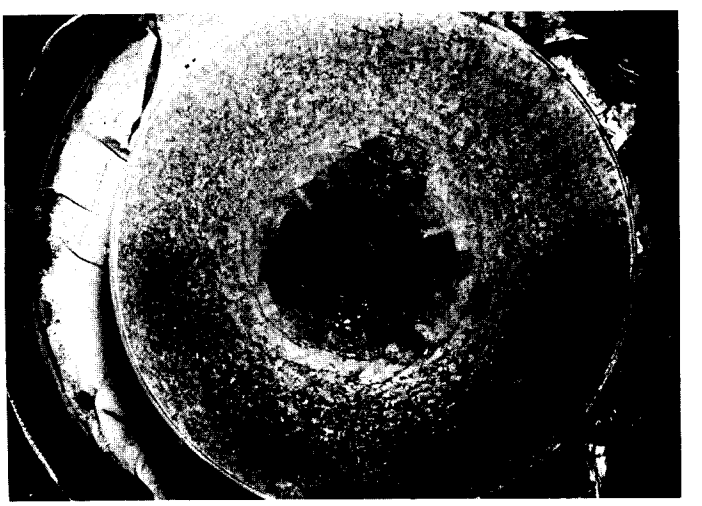

(e) Engine A-21-24 nozzle

Fig. 92. Post-firing effects on engine nozzles

Quality assurance testing of the remaining six retro-rocket engines at the Elkton Division has been delayed pending evaluation of outstanding action items between Hughes and JPL.

c. Safe and arm assembly. Quality assurance testing of the safe and arm assembly by the Elkton Division is being conducted with retro-rocket engine testing. As a demonstration of ignition system reliability, engines A-21-23 and -24 were ignited with only one of the two squibs. The initial initiator free volume was increased significantly in both tests because of the five pressure transducers (Fig. 93) mounted on the safe and arm assembly, which provides additional confirmation of an adequate squib charge.

CONFIDENTIAL
UNCLASSIFIED

UNCLASSIFIED
CONFIDENTIAL

Two incidents occurred during the arming phase of the test of engine A-21-18. The initial safe and arm electrical assembly, S/N 301, would not arm because of burned contacts caused by the external arming circuitry. A replacement electromechanical assembly, S/N 304, was installed at the test site and subsequently would not arm from mechanical binding of the rotor shaft and drive mechanism. Binding of the shaft was eliminated by loosening the four screws joining the upper and lower housings and the test was completed at AEDC. Post-test inspection of the units substantiated the adverse tolerance condition which prevented interchangeability of the electromechanical assemblies.

Engineering and manufacturing records show that four units, S/N 301 through 304, were fabricated by the Bristol Division prior to detection and correction of the adverse tolerance condition. Subsequent units are interchangeable.

A review of the acceptance test program by Hughes has delayed initiation of acceptance testing of the PC-37 squibs at the Hi-Shear Corporation. Acceptance testing and delivery is scheduled for completion by November 15, 1964.

d. Vibration testing. Inert engine A-21-F was subjected to vibration testing in early October 1964. Prior to testing, the engine attachments were modified in the hinge joint area to eliminate the notch effect and to incorporate a solid pin in place of the roll pin. Engine A-21-19 and A-21-22 will be modified and subjected to vibration testing in the next reporting period.

e. Thermal control. A temperature conditioning test was conducted on a thermocoupled engine containing live propellant to determine the time interval required to condition the engine from 70°F to the 85 ± 5°F prelaunch temperature at the Air Force Eastern Test Range (AFETR). The conditioning test results indicate that a time in excess of 48 hr will be required at AFETR.

Installation of thermal control components on inert engine A-21-E was completed for use in the T-21 test program.

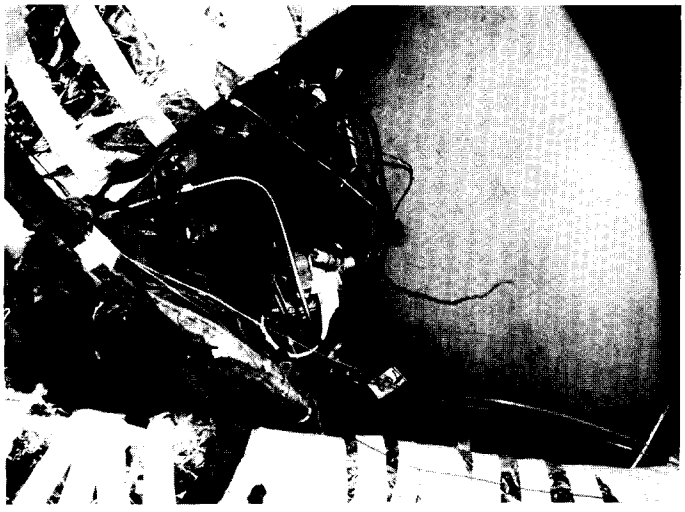

Fig. 93. Transducer installation on safe and arm assembly

4. Vernier Propulsion System

a. System development. The S-6 system modifications for propellant unbalance expulsion testing were completed. These modifications include: (1) installation of engine simulation flow blocks; (2) propellant discharge lines, flow meters; and (3) installation of insulation on the helium tank and lines (Fig. 94). Also, instrumentation was installed and the data link was checked out.

A three point suspension system incorporating load cells was installed for determining the shift in cg during propellant expulsion (Fig. 94). Tension rods were initially employed in the suspension system as shown in Fig. 94, but were replaced with cables to eliminate side loading effects. The evaluation of the suspension system will be completed early in the next report period.

Two expulsion unbalance tests were completed using simulated propellants. Tests using actual propellants will be conducted at ambient and various thermal environments to determine the shift in cg during operation.

The 30-day storage test program to be conducted on the S-7 vehicle began the last week of this report period. Modifications from the previous S-7 configuration included:

(1) Installation of Hughes fabricated propellant tanks.

(2) Installation of an unused helium bottle from T-21.

(3) Instrumenting of propellant manifolds.

(4) Valving to bypass the helium squib release valve.

(5) Addition of valves upstream of the thrust chamber assemblies to permit disconnection and removal of the thrust chamber assemblies for inspection between firings.

(6) Extensions for remote location of the helium fill connection and for helium unloading from the propellant tanks downstream of the system check valves. (These are required for personnel safety.)

During the 30-day storage test program, the engines will be fired periodically to verify the functional acceptability of the system. Also, it is planned to conduct the

CONFIDENTIAL
UNCLASSIFIED

UNCLASSIFIED

acceptance test firing of the new RMD engines with fuel regulators on S-7 prior to installation on the T-2S vehicle.

The gas entrapment device laboratory tests, discussed in the last report, were conducted. Future use of the device will be made during the S-6 and S-7 vehicle tests to determine the amount of entrained gas after loading propellants.

The propellant migration test setup, discussed in the previous report, will be ready for the start of testing early in the next report period. The first phase of the propellant migration program, the free standing bladder tests, was completed and the report released at the end of this period. A composite curve of the results of these tests is shown in Fig. 95. The maximum amount of hysteresis at ambient temperature and at 30% expulsion is approximately 1×10^{-3} psi from Fig. 95. At 0°F this hysteresis increased to approximately 18×10^{-3} lb/in.^{2}.

b. Component development

Relief valve. Detailed drawings of the helium relief valve received from the vendor have been approved by Hughes. Detail parts fabrication for the type approval test (TAT) relief valve assemblies is in progress. TAT testing is expected to commence in late November.

Quick disconnect. It has been determined that the fuel coupler failure, previously reported, resulted from frictional abrasion of the O-ring seal during coupling and

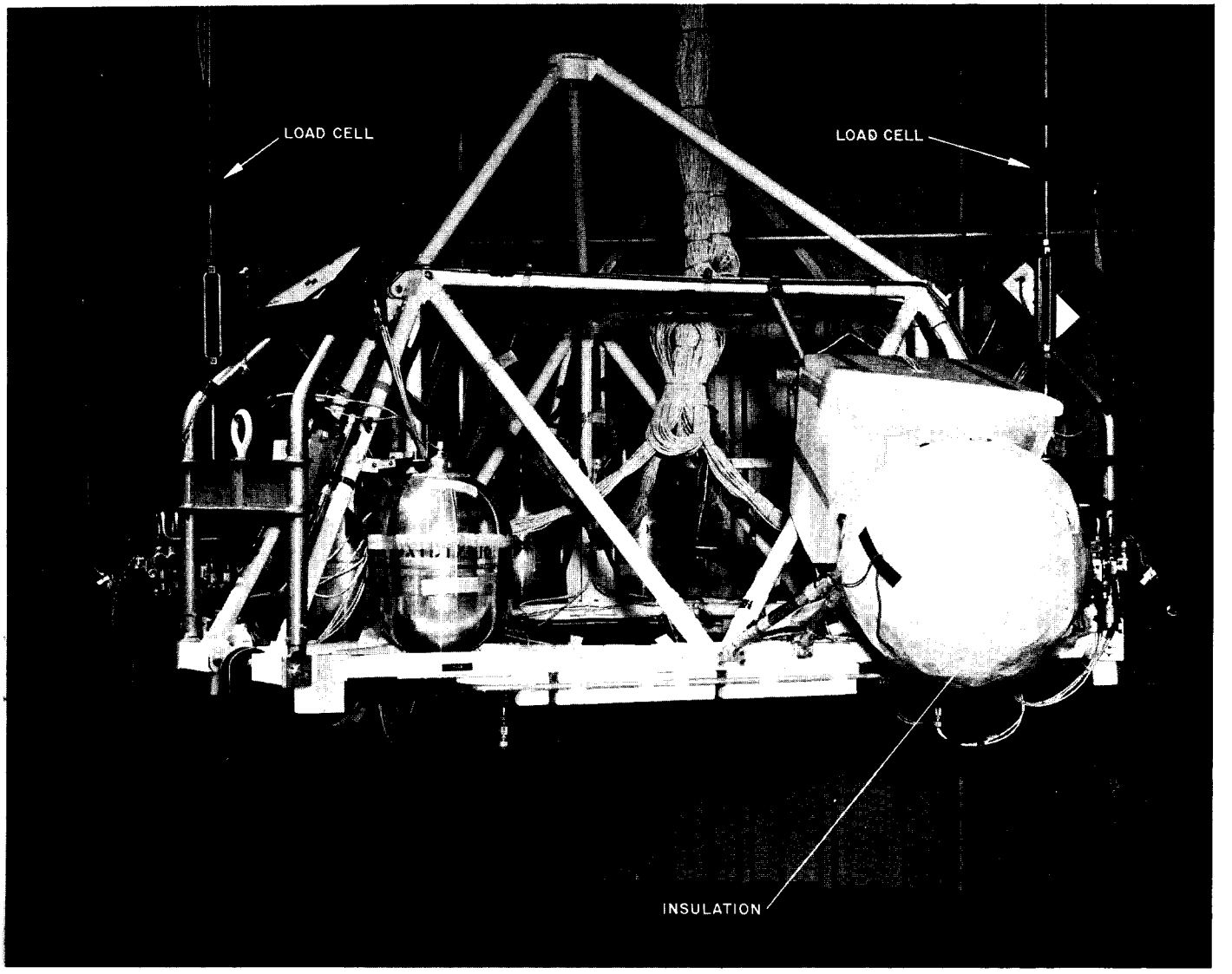

Fig. 94. S-6 vehicle expulsion test setup

UNCLASSIFIED

UNCLASSIFIED
CONFIDENTIAL

uncoupling. Furthermore, swelling of the O-ring from vapor exposure was evident. Alternate seals have been investigated. Testing, which is in progress, indicates that favorable results can be expected by utilization of an Omni-Seal in this application. Two coupler units have been subject to coupling tests to date. One unit has been cycled 1000 times with no evidence of leakage and a second unit has completed 200 cycles without leakage. Six additional units will be subjected to the coupling tests. At the completion of cycling tests, these units will undergo propellant exposure tests.

Check valve. Functional testing of the check valve assembly following propellant exposure was completed. Visual examination of the unit after disassembly showed no deterioration of the detail parts from vapor exposure.

Pressure regulator. Disassembly of the regulator assembly following propellant vapor exposure showed that one of the butyl O-ring dome seals had severely deteriorated. A review of the development history of the regulator assembly revealed that RMD had changed the dome seal material from Viton A to butyl rubber to overcome a problem encountered with sealing at low temperatures (0°F), but had not subjected the regulator assembly to propellant vapors.

The regulator subcontractor was contacted regarding the failure after propellant exposure and the previously encountered low temperature sealing problem. The vendor was of the opinion that the Viton dome seal would be effective if the dome were pressurized prior to reducing the temperature of the regulator to 0°F. To test this procedure, two regulators were returned to the vendor for incorporation of the Viton A O-ring dome seals. The regulators have been returned to Hughes for low temperature testing. Prior to conditioning the regulators to 0°F, the dome of one was pressurized to 300 psig and the second was pressurized to 700 psig. Notwithstanding the pressurization prior to conditioning, both regulators leaked excessively through the dome. A program is in progress to develop a seal groove configuration using Viton material in the low temperature environment. Alternate seal configurations such as K-seals and Omni-seals are also being investigated.

Squibs and squib valve. Qualification testing of the squibs and squib valve commenced early in the report period, but has now been suspended. Although the reliability margins test and Bruceton test phases of the program were completed, two dump squib failures were encountered during the squib valve qualification tests. Analysis has indicated that both failures were the result of a shock wave generated by the release squib firing

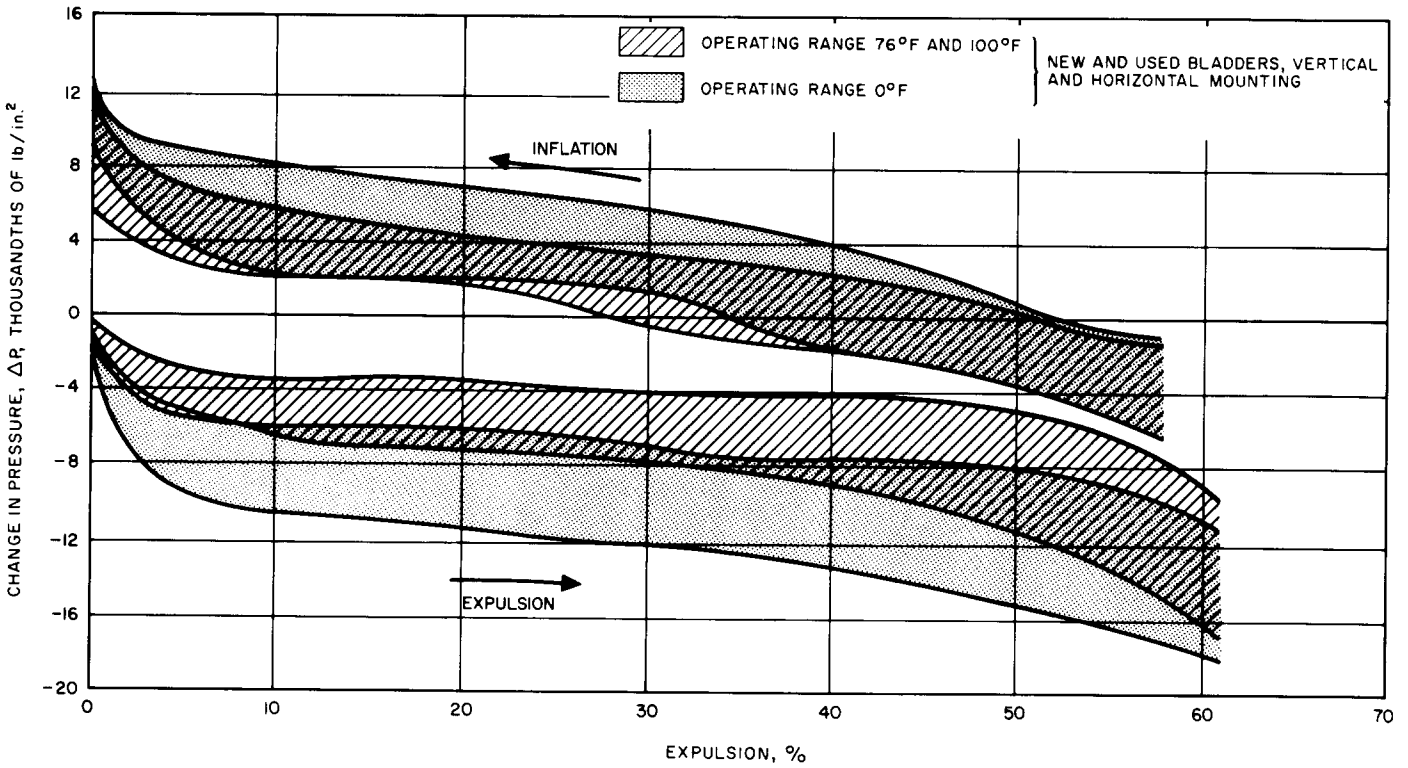

Fig. 95. Composite data of bladder expulsion characteristics

CONFIDENTIAL
UNCLASSIFIED

UNCLASSIFIED
CONFIDENTIAL

causing movement of the cup which houses the primer charge and bridge wires, thereby shearing the bridge wires. To correct the problem, the squib design will be modified to incorporate a cup retention mechanism. No valve design changes are contemplated because of the squib failures.

Helium expulsion testing. To verify the adequacy of the helium storage tank volume, the test configuration shown in Fig. 96 was established using six propellant tanks and associated manifolding which is equivalent in volume to the flight design. The lines and tankage were insulated to effect an adiabatic expansion of the stored gas. Three expulsion tests were made with the propellant tanks filled to capacity with liquid, i.e., zero tank ullage. In two of the three tests, a 50 $in.^3$ accumulator was added to the tank manifolding to account for helium consumption required for operation of the vernier engine propellant shutoff valves and for the allowable leakage throughout the manifolding. Results of the tests confirm that the helium tank, as designed, contains a sufficient volume of gas to complete the vernier propulsion mission.

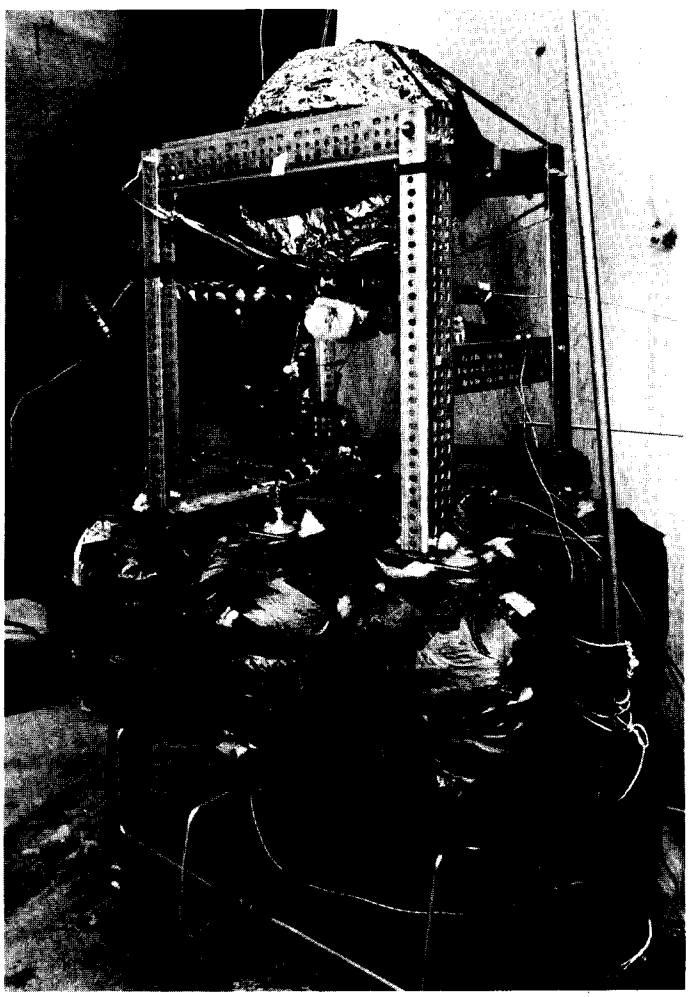

Fig. 96. Helium expulsion efficiency test setup

The 6Al-4Va titanium alloy helium tank program, under subcontract to Airtek Dynamics, is progressing satisfactorily. Airtek Dynamics has completed the engineering drawings; machine tooling is 95% complete; and the first lot of forgings have been received. No problems are anticipated in meeting the first tank deliveries in November 1964.

A series of tests are in progress at the Placerita Canyon test facility to determine the compatibility of the vernier propulsion system propellants and solvents with the various materials used in the system hardware. The results of one of the compatibility tests indicate that the aluminum-stainless steel couples and the aluminum samples exposed to wet nitrogen tetroxide-Freon TF solvent solutions were corroded and the anodizing of the aluminum attacked. The samples exposed to the dry solution were relatively unaffected by the exposure for 115 hr at ambient temperature. This confirms that if moisture in the oxidizer system is avoided, corrosion will not be a problem and that Freon TF is a satisfactory flushing solvent. Anodizing or other aluminum surface treatements offer no advantages and their use on internal surfaces is discouraged.

A set of Parker Viton A O-rings was exposed to MON-10 oxidizer with and without Freon TF flush, with very little difference in effects being noted. Approximately the same permanent set resulted in both cases, indicating that Freon TF is a suitable flushing solvent.

An evaluation of the effect of immersion in propellant upon various standard surface treatments for aluminum has been initiated. Samples of 5052-0 aluminum tubing have been prepared with chromate coatings, sulfuric acid anodize, electroless nickel coatings, and bare, passivated aluminum surfaces. These samples are presently being exposed to MON-10, monomethyl hydrazine, and monomethyl hydrazine monohydrate for periods of up to 6 wk. The results of these exposure tests will be available in the next report period.

c. Propellant tank development. The subcontract with Airtek Dynamics for the 6Al-4Va titanium propellant tanks has been issued. The development, type approval tests and fabrication of flight tankage are progressing on schedule.

The bulk yield and burst tests were conducted on three tank shells. Results of these tests established 1050 psig to be the minimum bulk yield pressure; burst pressures derived from the tests were 1400, 1380, and 1390 psig for S/N 01, 02, and 06, respectively. By specification requirement, the minimum design burst was set at 1038 psig.

CONFIDENTIAL
UNCLASSIFIED

UNCLASSIFIED
CONFIDENTIAL

Type approval tests, which are complete except for the vibration tests, have been successful. During vibration tests, the test fixture failed at an input of 18 g and 147 cps. A redesign of the vibration fixture is underway. The vibration tests will be completed during the next report period. Type approval tests completed consisted of three proof cycles at 945 psig (90% of bulk yield), one proof cycle at −300°F and 1323 psig (1.4 × ambient proof pressure), a 150-hr hold at the maximum operating pressure of 830 psig, and 300 pressurization cycles of 0 to 830 psig.

A minor problem remains in the fabrication of flight tankage. The girth weld porosity is in excess of specification requirements. A weld porosity improvement program is in effect and will be complete in October. The first group of flight production tanks, which had girth weld porosity in excess of the allowable, passed the bulk yield, burst, and a major portion of the type approval tests successfully. Future units will not be accepted from the vendor until a satisfactory improvement in the weld porosity has been achieved.

During the pre-test checkout of the S-7 vehicle preparatory to storage tests, several expulsion bladder failures were experienced because of the sharp weld protrusions on the interior surface of the aluminum tanks fabricated by Hughes. A weld shaving process was developed which machined the weld bead flush with the tank inside diameter. To verify the structural integrity of the aluminum tanks after weld shaving, type approval tests similar to the type approval tests for the titanium tanks are in process and will be complete early in the next report period.

d. Thrust chamber assembly. An interface document detailing the *Surveyor* requirements of the RMD Model TD 339 thrust chamber assembly (TCA) has been prepared with joint RMD, JPL, and Hughes participation and has been submitted to JPL.

RMD completed a demonstration program on hardware refurbished to the TD 339 configuration. Six thrust chambers were run through two complete series of complex down-throttling missions at both 0° and 100°F with no evidence of overheating or excessive heat rejection, demonstrating that the use of monomethyl hydrazine monohydrate in conjunction with TCA passivation has eliminated the down-throttle problem exhibited by the former TD 280 configuration.

The new features incorporated in TD 339 are:

(1) Use of 72% MMH and 28% water as the fuel.

(2) Elimination of the jacket vent and reprime valve.

(3) Stiffened torque motor on the throttle valve.

(4) Modified seat in the on-off valve.

The four thrust chambers assembled by Hughes and scheduled for use on the T-2S vehicle in Test 17 were acceptance tested at the Hughes Propulsion System Field Laboratory at Placerita Canyon. New thrust chamber assemblies with fuel regulators have been received from RMD for Test 18. These new thrust chambers will be test fired on the S-7 vehicle prior to installation on T-2S.

UNCLASSIFIED
CONFIDENTIAL

UNCLASSIFIED

J. Spacecraft Vehicle and Mechanisms for Basic Bus

1. Spacecraft Vehicle

Vehicle activities reported in this section include status of the design and fabrication of spaceframe and substructures and the assembly of complete vehicles for flight and test spacecraft. Fabrication, assembly, and tests of the thermally controlled equipment compartments, wiring harness, landing gear, and ground handling equipment are also reported here. Overall spacecraft configuration studies, weight reports, etc., are reported in Section A.

a. Vehicle status

T-21 — system type approval test vehicle. This vehicle completed the Phase III upgrade and was returned to systems test for a preliminary checkout prior to installation in the space chamber for the thermal-vacuum phase of environmental testing (see Fig. 97).

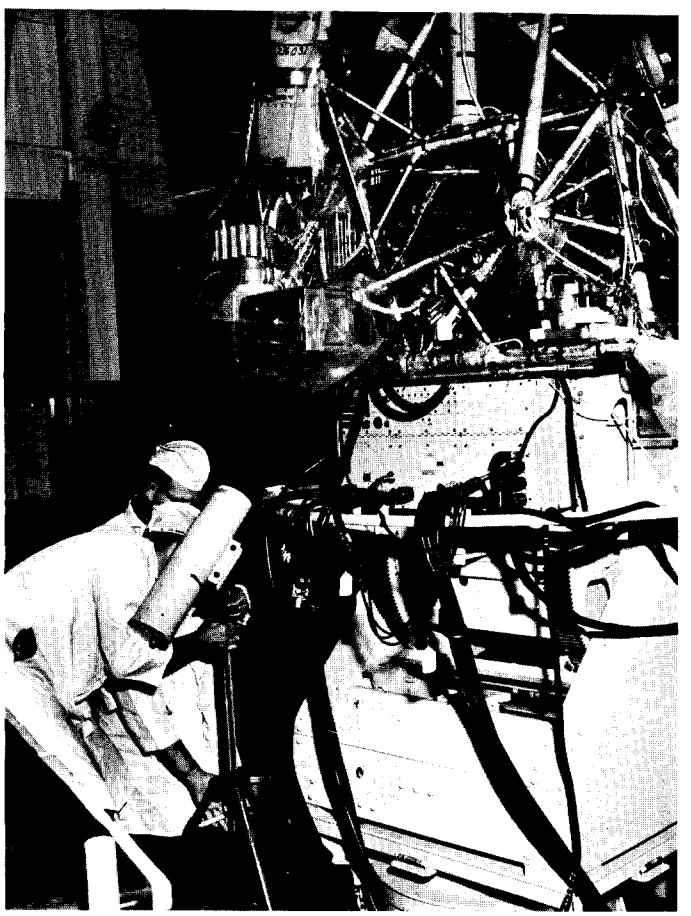

Fig. 97. T-21 in RF screen room after Upgrade III

T-21A — system type approval test model. This vehicle is being reprogrammed for delivery to systems testing in mid-July 1965. Engineering, fabrication, and assembly is proceeding on this new schedule.

T-1 separation type approval test model. Detail parts are being fabricated to upgrade this vehicle for retrorocket separation tests scheduled for the next reporting period (see Fig. 98).

T-2SS — backup vehicle for T-2 drop tests. Final assembly is near completion. Delivery of this test vehicle to Air Force Missile Development Center (AFMDC) is scheduled for October (see Fig. 99).

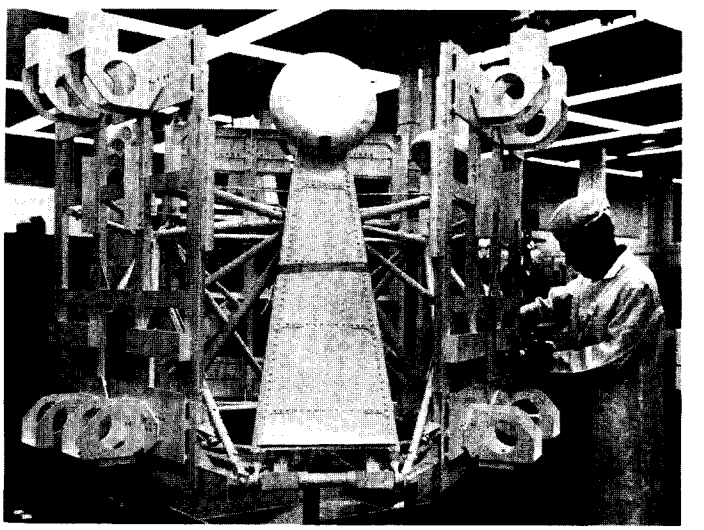

Fig. 98. T-1 vehicle during upgrade for retro-engine separation tests

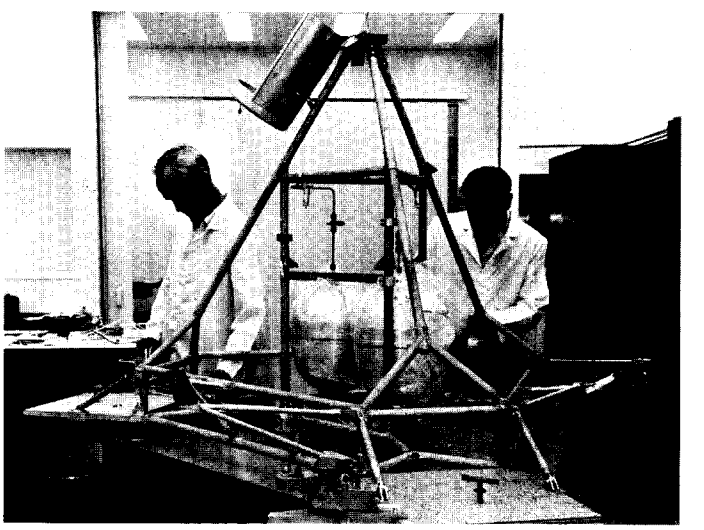

Fig. 99. Assembly of T-2SS vehicle

UNCLASSIFIED

UNCLASSIFIED
CONFIDENTIAL

S-2A — structural test vehicle. The S-2A vehicle is continuing vibration testing. The redesigned thermal compartments have withstood the vibration environment. This vehicle is being used to type approval test the flight configuration compartments which had failed during earlier tests.

S-6, S-7 — vernier propulsion system qualification vehicles. These vehicles are undergoing tests at AFMDC. Preparations are being made for an upgrade of S-7 for the A-21 flight configuration vernier propulsion system which includes new thrust chamber assemblies and a new helium tank. The S-7 substructure is also being upgraded to withstand the full type approval test (TAT) level vibration loads. Vibration tests are scheduled for January 1965.

S-8 — tether test vehicle. This vehicle was prepared for a series of tests of the radar altimeter and doppler velocity sensor noise interaction with the vernier engine system (Fig. 100). After tests scheduled for the next reporting period, the test spacecraft will be returned for upgrade to its ultimate usage as a buzz test vehicle at AFMDC. Tests were made of the suspension system on the Aerobee Tower at AFMDC with a dummy weight. The system performs within specification. For further details see Section K.

SC-1 — first flight spacecraft. This vehicle was delivered to systems test during this reporting period (Fig. 101). It will be returned to the final assembly area in November for a short upgrade in which the new structure for the modified helium tank will be installed and Compartment A and the wiring harness retrofitted for the newly added power cutoff switch (see Section K).

SC-2 — second flight spacecraft. Fabrication continues on this vehicle for completion during the next reporting period (Fig. 102).

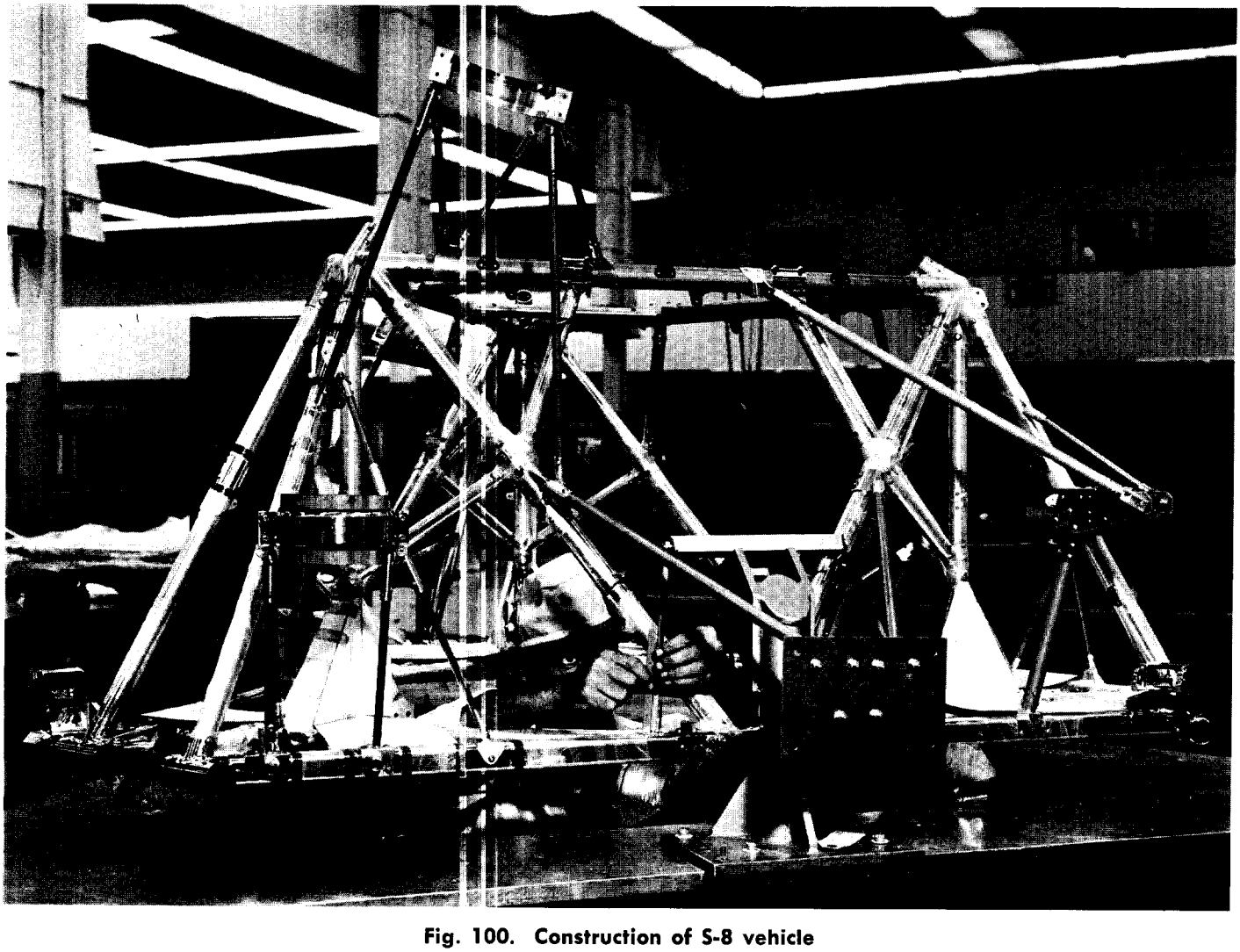

Fig. 100. Construction of S-8 vehicle

CONFIDENTIAL
UNCLASSIFIED

UNCLASSIFIED

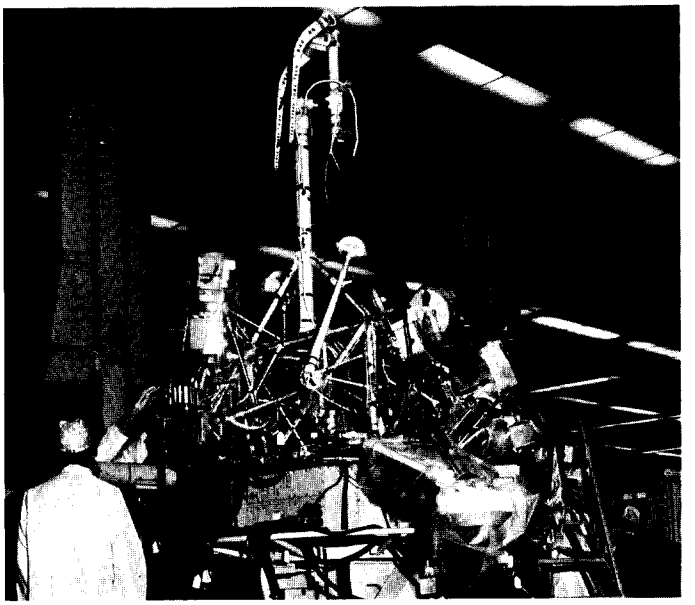

Fig. 101. SC-1 spacecraft in systems test

b. Testing status. To improve the reliability of the flexible line on the attitude jet plumbing system, a change in manufacturing method resulted in a slightly stiffer line. A type approval deployment test was run to ensure that this stiffer flexible line had not impaired the deployment capability of the landing gear. These tests were concluded successfully during the month of September (Fig. 103).

All TAT testing of the altitude marking radar separation latches has been completed.

2. Mechanisms for Basic Bus

a. Omnidirectional antenna mechanisms. The two omnidirectional antenna mechanisms (designated A and B) use tapered, fiberglass cloth tubes bonded to aluminum hinge bracket assemblies. They deploy and lock the two omnidirectional antennas into operating position prior to separation from the *Centaur*.

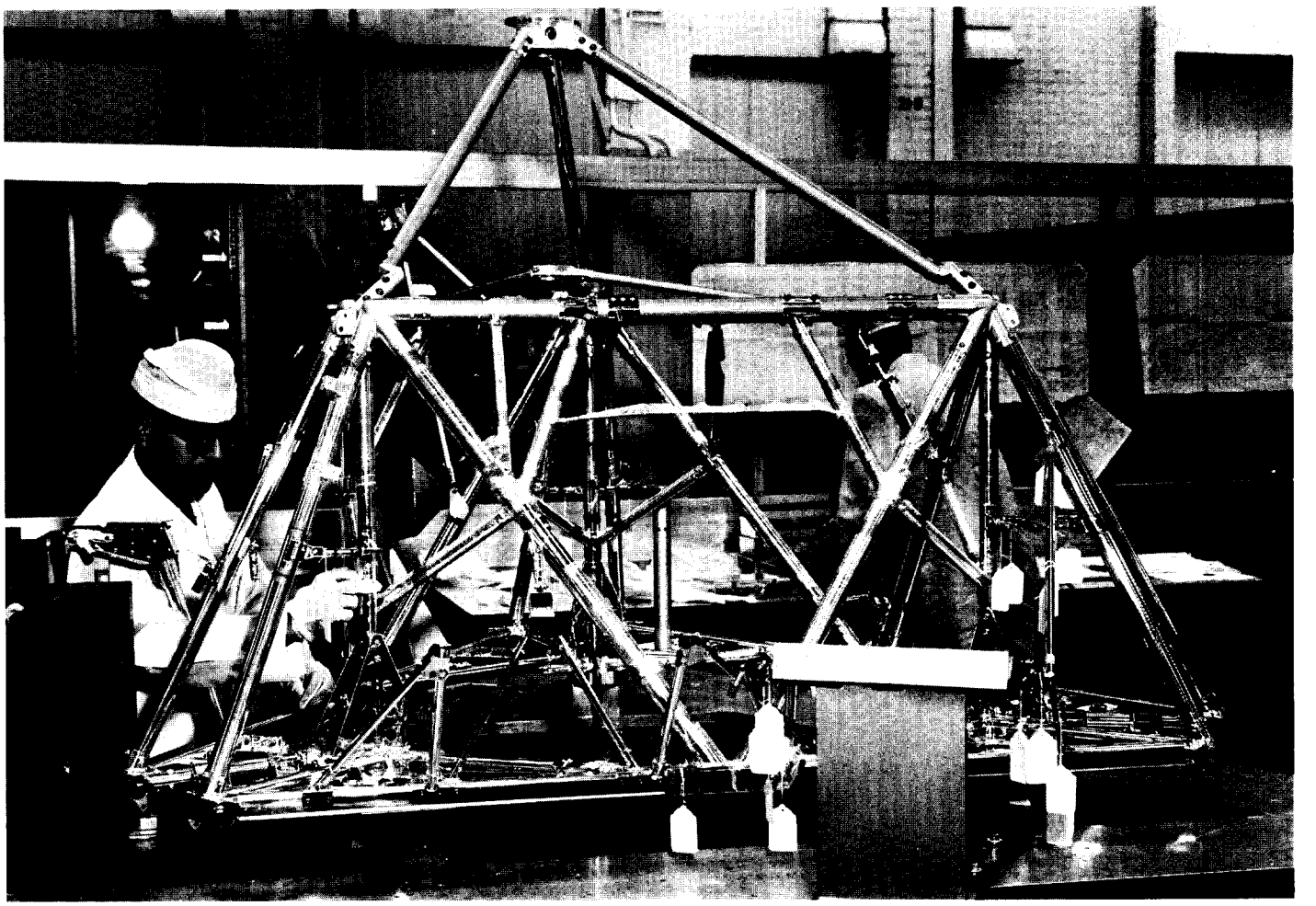

Fig. 102. SC-2 spacecraft assembly

UNCLASSIFIED
CONFIDENTIAL

UNCLASSIFIED
CONFIDENTIAL

Upgraded mechanisms for the two antennas have performed satisfactorily in vibration tests of the S-2A vehicle.

The A and B mechanisms for SC-1 were delivered during this report period. The A and B mechanisms for T-21 are being upgraded and will be reinstalled in October.

Hardware redesigned to strengthen the A mechanism is being fabricated. The hardware change will be retrofitted on T-21 and SC-1.

b. Antenna/solar panel positioner. The positioner provides mounting, positioning, position indicators, and launch and landing locks for the planar array antenna and solar panel. The antenna support structure has three controllable axes; the solar panel is mounted to the antenna support structure by a single controllable axis. The roll, elevation, and solar axis drives each utilize a three-stage planetary gear reduction. The polar axis drive uses a single-stage planetary and a double enveloping worm gear drive. Each drive uses a solenoid stepper motor for power and a wire-wound potentiometer for position indication.

The developmental unit X-1, redesigned for higher loads, was installed on the S-2A spacecraft for type approval vibration tests. Structural Failure in the elevation axis motor housing (Fig. 104) occurred at approximately 100% of full type approval load. The elevation axis housing, pin puller brackets, solar panel cover fittings, and solar panel tube support fittings have been redesigned and are in fabrication. The solar panel tube support fittings have been completed and retrofitted into the X-1 unit. Type approval testing will be resumed when a new elevation housing is installed in the unit. After completion of the type approval level vibration and shock tests on the S-2A vehicle, the units will be subjected to type approval level thermal-vacuum tests. Individual class IV units incorporating the above changes will be delivered every 4 wk starting in mid-November 1964.

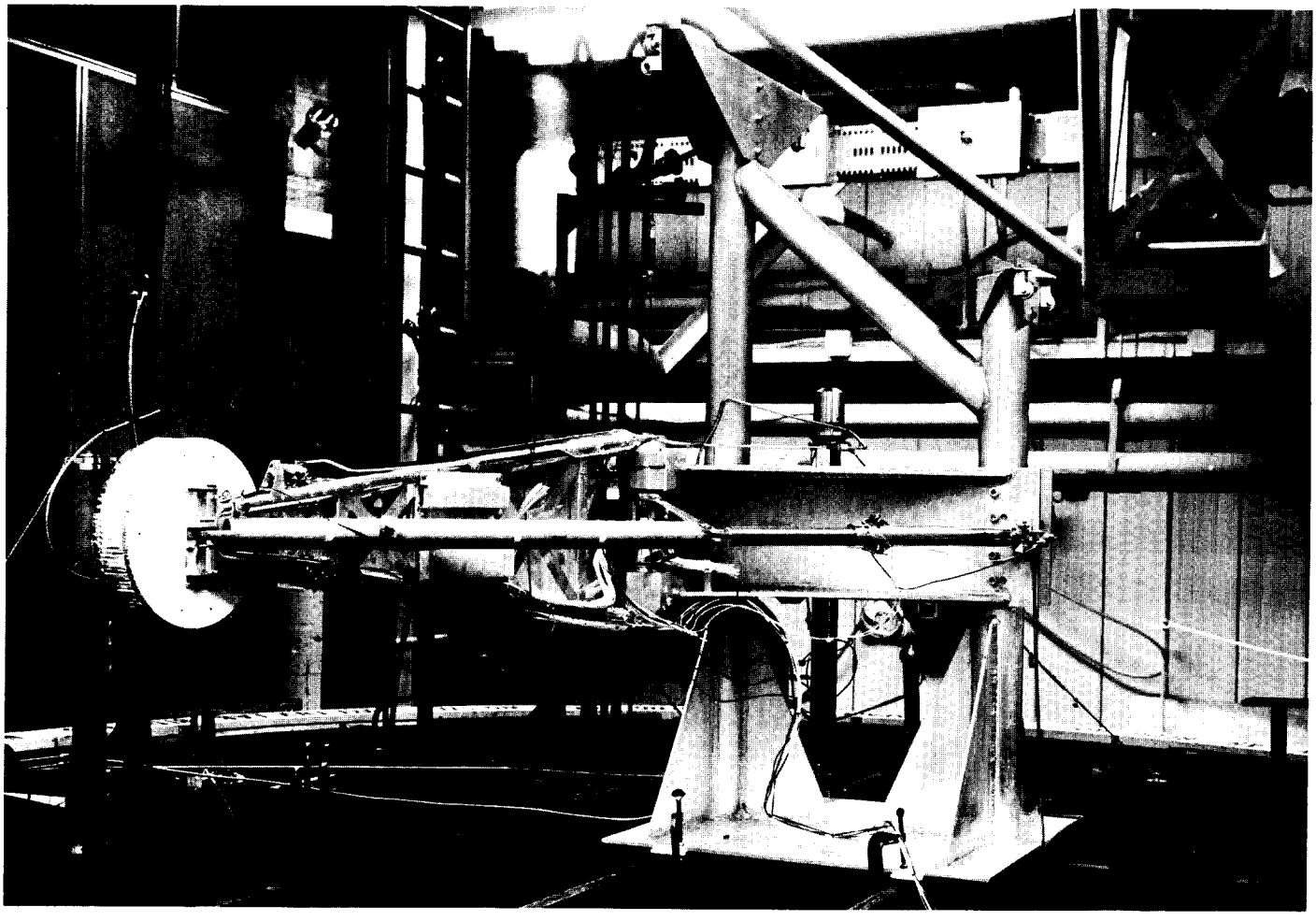

Fig. 103. Testing of attitude jet flexible line

CONFIDENTIAL
UNCLASSIFIED

UNCLASSIFIED

During the type approval vibration tests, large motions of the positioner were observed. "Breadboard" hardware to stiffen the mast and dampen the motion of the antenna and solar panel is in fabrication. This hardware will be tested on the X-1 unit installed on the S-2A vehicle.

The solar panel launch-lock pin-pullers were fired at −216°F with no damage to the taper pins. The spring loaded taper pin will be tested at −216°F when parts are available.

c. Motors and mechanisms drive units. Ledex stepping motors are used to drive the antenna/solar panel positioner. The drives in two positioners (T-21 and SC-1) were tested for load capabilities. The tests were performed under laboratory conditions with the supply voltage lowered to compensate for the effect of high temperature and minimum spacecraft battery voltage. The polar axis drive functional requirement has been revised to include two parameters: (1) 50% stepping efficiency at 100% lunar load, and (2) 100% stepping efficiency after unloading the polar axis by repositioning the solar panel through an angle not to exceed ±60 deg (maximum load after repositioning is 40 in-lb.). Fig 105 represents the performance of three units in this axis based on unbalanced load and stepping efficiency. In terms of maximum lunar load conditions, the following capabilities were measured.

Positioner 1		
Solar panel axis		200%
Roll axis		155%
Elevation axis		185%
Polar axis	144%[a]	162%[b]
Positioner 2		
Solar panel axis		163%
Roll axis		166%
Elevation axis		160%
Polar axis	136%[a]	140%[b]

[a]Related to 59.5 in.-lb
[b]Related to 40 in.-lb

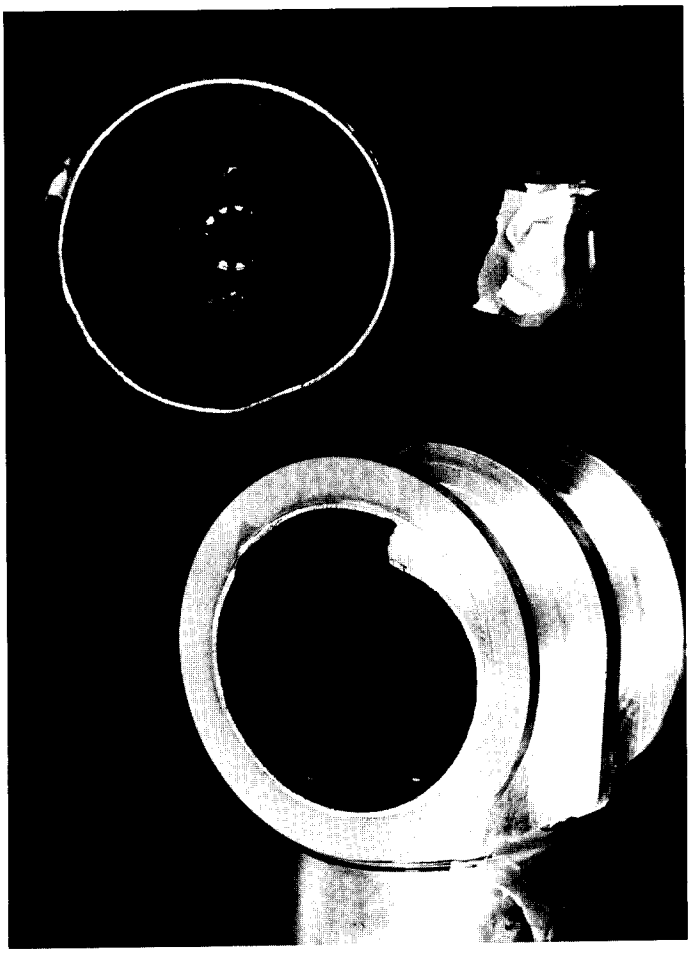

Fig. 104. Elevation axis motor housing failure

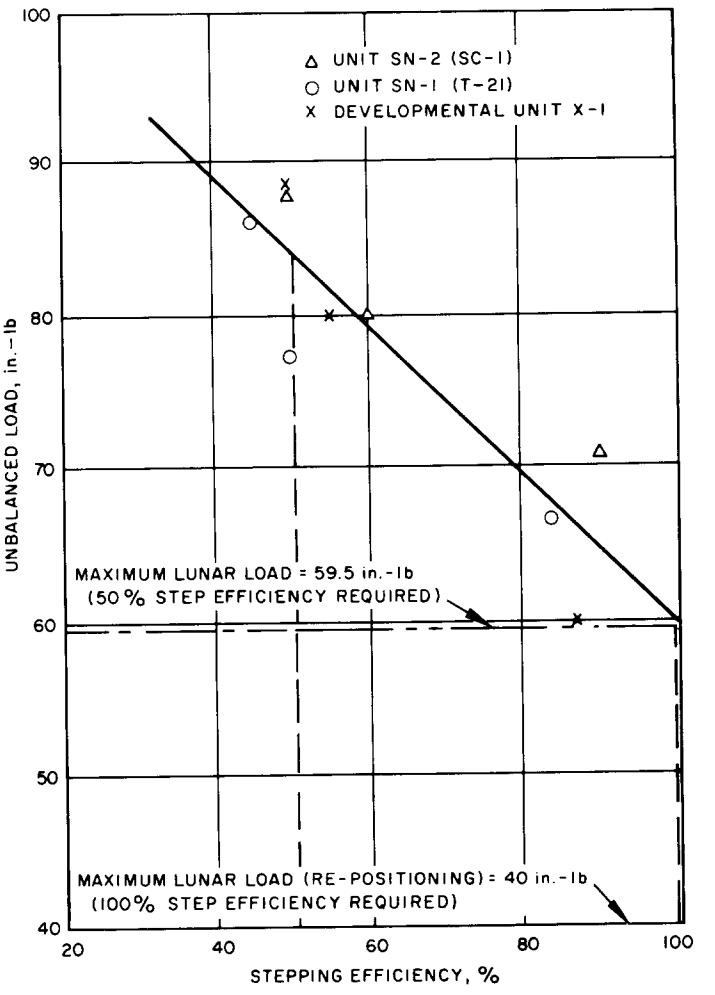

Fig. 105. Polar axis drive performance

UNCLASSIFIED

UNCLASSIFIED
CONFIDENTIAL

The results are comparable with those obtained from the developmental positioner (X-1).

The TV mirror assembly is driven in both axes (roll and elevation) by Abrams (Curtiss-Wright) stepping motors. Testing of the external motor detent, described in previous reports, was continued. This detent had previously been tested for life under laboratory conditions. Two types of lubricant found to be acceptable under laboratory conditions were Microseal and molybdenum disulphide. The life tests were continued in the thermal-vacuum environment. Motors containing a detent using each type of lubrication were exposed to vacuum under temperature cycling simulating lunar operation, (temperature range 175° to —50°F, vacuum 3 X 10^{-8} Torr). The motors were stepped through their life cycles with response and minimum drive voltage monitored as a check for degradation. Results of the test indicated a rapid degradation in the high stress areas of the detent using Microseal. The motor detent lubricated with powdered molybdenum disulphide completed the life test without degradation. The superior results obtained using molybdenum disulphide were due to a reservoir of powdered molybdenum disulphide retained in the spring cavity of the detent. This reservoir replenishes the powder in the highly stressed areas between the detent ball and its track during operation. The detent lubricated with Microseal will be relubricated with powdered molybdenum disulphide and resubmitted to thermal-vacuum life test to confirm this choice of lubrication.

d. Separation sensing and arming device. These devices (three per spacecraft) provide redundant interruption for the post-separation squib firing circuits and the vernier engine solenoid circuit until after the spacecraft separates from the *Centaur*.

Five sets of flight hardware (three devices per set) have been flight acceptance tested and are available for spacecraft assembly. The next set of hardware is being assembled prior to undergoing flight acceptance test.

e. Pyrotechnic devices

Squibs. The squib TAT program is approximately 99% complete. Three hundred and seventy squibs have been expended. This total was comprised of the following squib configurations and quantities: configuration 236472-1, 213 squibs; configuration 236472-2, 115 squibs; configuration 236472-4, 42 squibs. The remaining tests include the post-firing test, hermetic seal check of the glass headers, and resistance between all pins and between pins and case.

During the firing tests of the remaining 236472-4 squibs, it was determined that excessive shock caused two squibs to fail to fire when one bridge circuit was energized; however, both squibs fired when the second bridge wire was energized. The shock environment was measured by accelerometers mounted on the surface of the firing fixture approximating the squib location. The maximum g detected during this test was 800 g axial and 5000 g lateral. It can be assumed that the squib which is screwed into the fixture would experience shocks in excess of the test results. It is believed that this shock imposed by an unrealistic firing procedure contributed to the malfunction of the two detonators. The firing procedure has been modified to correct this condition.

Ninety-eight 236472-2 squibs have been delivered to JPL. These units are to be utilized by JPL to develop a seismometer cable cutting device for the *Surveyor*. The transfer of these units was initiated after JPL informed Hughes that the pressurized gas power supply and the 236472-2 squib would be deleted from the *Surveyor* requirement.

An abbreviated quality verification test program is being conducted on the squibs for the T-2 vehicle to give assurance that the units will perform reliably. All the squibs will undergo the following tests: bridge resistance, insulation resistance, sealing check, and two x-rays. The test samples from all the squib lots will then be selected by analyzing results of the above tests. The samples will be subjected to the following environments: sinusoidal vibration at +75°F, temperature shock at 140 and —20°F, and a sawtooth mechanical shock of 100 g for 4- to 6-msec duration. Electrical tests are to be conducted after each environmental exposure and prior to firing to determine the effects of environmental degradation. All firings will simulate T-2 firing current and conditions. Remaining samples will be graded as to quality and allocated accordingly to various phases of systems tests and usage.

Pyrotechnic switch. Sixty switch assemblies are being subjected to a TAT program. Fifty-six units have been subjected to vibration tests at temperatures of 0 and 135°F. During the vibration, all switches were monitored for momentary (greater than 1 μsec) openings or closures. All units passed vibration and switch monitoring requirements with no discrepancies or malfunctions. Post-environmental electrical checks indicate no change in electrical characteristics. Tests are continuing.

Four switch assemblies were exposed to RFI tests and none fired. Post-environmental tests are being conducted on the units to determine the effects of the RFI environment.

CONFIDENTIAL
UNCLASSIFIED

UNCLASSIFIED

K. Reliability, Quality Assurance, and System Test

1. Reliability

a. System and subsystem **a priori** *reliability estimates.* The *a priori* reliability estimate for the A-21 spacecraft has increased slightly from 0.834 to 0.836 for the flight and landing phase. These estimates include only the Hughes portion of the vernier propulsion system.

b. Reliability estimates based on test data. Reliability estimates based on the latest available test data for the system and individual subsystems (flight and landing phase) are presented in Table 42.

c. Electropyrotechnics. Atlas has completed the manufacture of a replacement lot of pyrotechnic switches. X-ray examination and reliability testing has been completed. Type approval testing is being performed at Hughes. Type approval testing of Ordnance Associates squibs P/N 236472-1 and 236472-2 has been completed. Histograms of the data show that the operating time and output pressures are normally distributed and within tolerance. A typical histogram is presented in Fig. 106. The firing time at −250°F is 2 msec longer than at +250°F. The output pressure does not vary significantly over this temperature range. A summary of pyrotechnic tests is given in Table 43.

Analysis of two helium dump valve squib failures at Holex is under way. These failures occurred during the type approval test program.

Table 42. Reliability estimates for flight and landing based on test data[a]

Subsystem	Current report	Preceding report	Comments
Command decoding	0.965	0.974	Additional failures during subsystem testing of central command decoder
Signal processing	0.924	0.925	Additional failures during subsystem testing of engineering signal processor.
Structures	0.734	0.723	Increase due to reevaluation of relevant failures on wiring harness.
Thermal controls	0.998	0.998	No change.
Telecommunications	0.985	0.983	Increase due to reevaluation of relevant failures on transmitter.
Flight controls	0.794	0.797	Previously unclassified failures for altitude marking radar and roll actuator judged relevant.
Propulsion	0.959	0.959	No change.
Electrical power	0.828	0.915	Previously unclassified failures for battery charge regulator judged relevant.
Mechanisms	0.964	0.962	Increase attributed to change in the *a priori* estimate of retro-rocket release mechanism.
Probability of system success $= \prod_{i=1} P_i$	0.391	0.429	

[a]Where relevant test data are not available on a unit, the *a priori* estimate of the unit is used in making test data estimate.

d. Subcontractor status

(1) *Vector (subcarrier oscillator).* Four failures experienced to date on units returned to Hughes after rework by Vector to remove potential failure modes result in an estimated reliability of 0.691 at a lower 80% confidence limit as compared to the 0.730 previously reported. These units will undergo an extensive failure analysis as part of a formal failure review board to be held at Vector early in October 1964 to assure responsive diagnosis and corrective action.

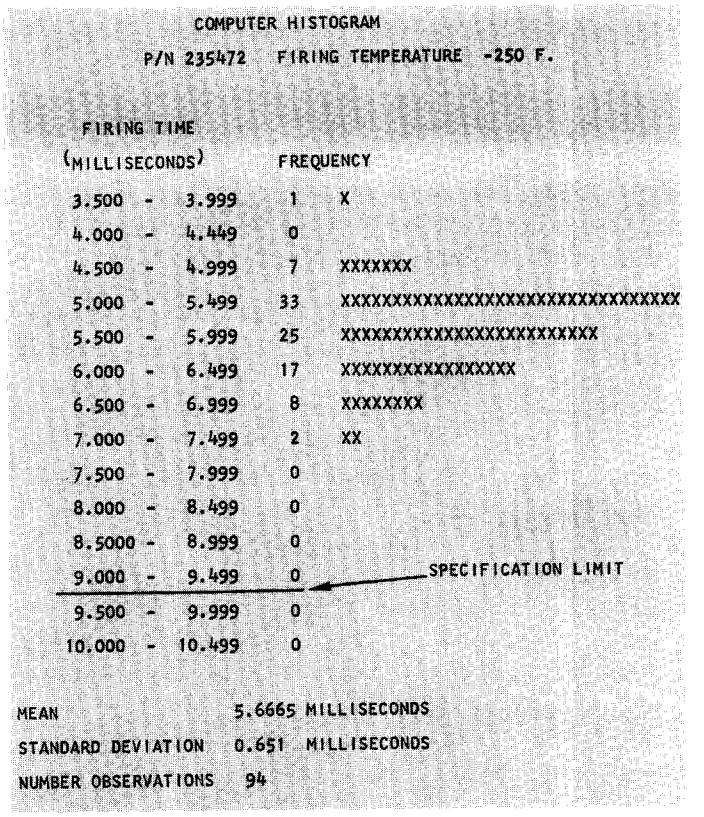
COMPUTER HISTOGRAM
P/N 235472 FIRING TEMPERATURE -250 F.
FIRING TIME (MILLISECONDS)
FREQUENCY
3.500 - 3.999 1 X
4.000 - 4.449 0
4.500 - 4.999 7 XXXXXXX
5.000 - 5.499 33 XXXXXXXXXXXXXXXXXXXXXXXXXXXXXXXX
5.500 - 5.999 25 XXXXXXXXXXXXXXXXXXXXXXX
6.000 - 6.499 17 XXXXXXXXXXXXXXXX
6.500 - 6.999 8 XXXXXXXX
7.000 - 7.499 2 XX
7.500 - 7.999 0
8.000 - 8.499 0
8.5000 - 8.999 0
9.000 - 9.499 0
SPECIFICATION LIMIT
9.500 - 9.999 0
10.000 - 10.499 0
MEAN 5.6665 MILLISECONDS
STANDARD DEVIATION 0.651 MILLISECONDS
NUMBER OBSERVATIONS 94

Fig. 106. Typical computer histogram

CONFIDENTIAL UNCLASSIFIED

UNCLASSIFIED CONFIDENTIAL

Table 43. Pyrotechnics test summary

Type	Lot size	Quantity fired			Results
		Previous report	To date	Future	
Pinpuller/shock absorber squibs	1000	471	501	30	Testing completed successfully.
Attitude jet gas dump squibs	245	135	135	110	No change.
Helium valve squibs	379	0	204	113	Two dump valve squib failures being analyzed.
Separation device squibs	845	0	0	755	New contract.
Pyrotechnic switch squibs	651	0	220	180	
Retro-rocket igniter squibs	300	0	0	125	New lot being fabricated.
Pin pullers	363	51	51	0	Testing completed successfully.
Nitrogen valve	58	12	12	~25	Two valves leaked after squib firing, but this valve is now used for nitrogen dump only; therefore, leakage is of no importance.
Separation devices	307	0	0	244	No change.
Helium valve		0	4		Resolution of two dump valve squib failures in process.

All units have been modified to incorporate sleeving on the leads at the point of stress to eliminate a shorting hazard due to burrs around chassis holes. Vector is updating their reliability program plan, scheduled for completion in late October.

(2) *Ryan (radar altimeter and doppler velocity sensor) (RADVS).* Through a joint effort with Hughes, Ryan is attempting to eliminate fabrication problems with the magnetic components of which 20% still remain on the critical parts list. It is expected that all components will be qualified in the near future. The reliability estimates based on the most recent test data indicate an improvement to 0.985 from the 0.975 previously reported.

Ryan has updated their reliability program plan to reflect future reliability requirements for the RADVS and is being reviewed by Hughes.

During the course of qualification testing Varian Associates' altimeter klystron exceeded all electrical requirements. In an attempt to meet the vibration requirements, Varian changed the grid materials and changed the top cavity construction to brazing from bolting. To date no new problems have occurred with the new improved version in the vibration test environment.

(3) *Thiokol/Elkton (retro-rocket engine).* Four engines (A-21-11, A-21-12, A-21-17, A-21-18) completed qualification tests at Arnold Engineering Development Center. Reduced data from A-21-11 and A-21-12 indicate successful performance. Data from A-21-17 and A-21-18 are in the process of reduction. Two problem areas that developed during the firing of A-21-18 have been corrected: (1) safe-and-arm malfunction was traced to faulty facility circuitry, and (2) interference between upper and lower assemblies was traced to drawing tolerance error.

Previously reported analysis and corrective action on the A-21-22 hinge pin and strut failures are continuing (see Section H). Using inert engine A-21-F, reevaluation is in process on the redesigned struts and the solid pins. Because the engine is not operating during this series of tests, development failures are not included in the retro-engine reliability estimate.

The present reliability achievement based on five development and two qualification test engines is 0.920 at a lower 80% confidence limit. The goal is 0.970 at 80% confidence. The mathematical model is being modified to reflect the potential effects of pre-firing environments and thrust tail-off characteristics. Inability of the present reliability model to reflect these two terminal conditions could result in a biased estimate. Upon completion of the modifications, the new model will be submitted to TCC/Elkton.

A status review of TCC/Elkton failure reports indicates 34 failures attributable to design errors, 4 due to manufacturing process errors, and 9 due to faulty test equipment or procedures, or human errors. All deficiencies have been satisfactorily corrected except the hinge-pin and strut problem.

CONFIDENTIAL UNCLASSIFIED

UNCLASSIFIED

A reliability audit of TCC/Elkton was conducted on July 21. At that time agreement was reached on the revised mathematical model.

(4) *Hughes/JPL/Reaction Motors Division (vernier propulsion system).* Previously reported deficiences in the fuel tank expulsion bladder resulted in tensile and elastic properties tests on the material by Hughes. These tests indicated a deficiency in the tensile properties.

Analysis of previously reported quick-disconnect failures has resulted in a redesign by the vendor. The redesign incorporates two index pins which replace the previous one-pin design resulting in improved contact between the nipple and coupling during pressurization. Additionally, the poppet seating characteristics have been improved. The new units are currently being evaluated. No failures reported to date.

The *a priori* reliability of the gas pressurization subsystem remains at 0.959. The total vernier propulsion system reliability goal is 0.946.

(5) *Systron-Donner Co. (linear force balance accelerometer).* The fluid damped units have logged 298 hr of testing without a relevant failure. The reliability estimate increased to 0.802.

A failure analysis was conducted at Donner on two units which failed at Hughes. The first unit was air damped (S/N 6856A) and failed after vibration at TAT levels. The teardown analysis revealed damaged pivots and bearings caused by the vibration. The air damped unit is known to be marginal for TAT environments and it was for this reason the flight units are now fluid damped. The second unit was fluid damped (S/N 9249F) and failed at the start of special testing for repeatability. This was the first time the unit was operated after the acceptance test. Failure analysis revealed an oil leak at the reservoir cover due to overheating and melting of the solder. This failure is similar to that of S/N 9250F and 9251F. Units S/N 9249F and 9250F had operating times of 5 and 2 hr, respectively, and were acceptance tested with four other units in November 1963. S/N 9251F had 1 hr operating time and was acceptance tested with another unit in December 1963. The investigation is continuing to determine an adequate test program to determine if the other units were overheated.

(6) *Endevco (accelerometer).* Total accumulated test time is 283 hr and 9 min. The corresponding reliability estimate is 0.994. Three failues have occurred to date. With no additional failures, an additional 192 hr operating time will be required to reach the "accept" region of the sequential test plan.

Endevco has submitted a reliability report and two failure analysis reports for the last two failures. These are presently being reviewed.

e. Materials and process studies

Thermal-vacuum testing

(1) Dokyl insulating varnish No. BT3602-1 when cured for a minimum of 2 hr at 455°F was qualified for space environmental applications up to 260°F.

(2) Samples of VITRON rubber glass cloth RF absorber material were tested at a thermal-vacuum condition of 260°F and 10^{-6} Torr for 5 days with no visible signs of outgassing.

(3) Du Ponts fluorocarbon "Slip Spray" was qualified for space environments where the maximum temperature exposure does not exceed 260°F.

(4) A TV camera resolution chart (fiberglass substrate) completely processed was subjected to the thermal-vacuum environment at 260°F for 2 wk without visible deterioration.

(5) A variety of "Electrolized Steel" samples were thermal-vacuum tested to determine the merit of this process as an anti-friction technique for the surface finish of moving parts used in this environment. The results of the test indicated that the process is not an acceptable technique for the intended *Surveyor* application.

(6) The honeycomb core material manufactured by the General Grid Company identified by number 1/8-0.0007P-5052-H19 was found to be suitable for use as *Surveyor* solar panel core material. The results of testing included investigation of the bonding process and mechanical and structural strength.

(7) Califoam X-SS polyurethane foam was selected from five samples tested as the most suitable material for applications such as vibration damping in electronics equipment for space environment. This material is considered qualified for space applications below 160°F.

Thermal control coatings. A white organic paint material specification and a process control document for thermal control applications have been prepared. The following basic characteristics are specified:

(1) Initial absorptance (α)	0.22 maximum
(2) Initial emittance (ϵ)	0.91 minimum

UNCLASSIFIED

UNCLASSIFIED CONFIDENTIAL

(3) Alpha after 350 solar equivalent hours of ultraviolet 0.31 maximum

(4) Minimum outgassing at 260°F and 5 x 10^{-6} Torr.

(5) No deterioration in α or ϵ due to rebaking when necessary to repair damaged surfaces.

(6) Allows cleaning of surfaces contaminated with fingerprints, oil or grease without increasing α by more than 0.03.

f. Failure analysis and review. The failure review board has completed action on three failures previously reported and has initiated action on four new failures on which action has been completed.

(1) *Previously reported failures*

(a) *Flight control sensor group:* The ac electrical conversion unit, which supplies 400-cycle power for the group, had experienced several failures for no apparent reason. An investigation of the circuit and the test setup was initiated, as the unit experienced failures in system test and not in the unit test area. The circuit design and the transistors used in the circuit were found to be adequate, and no indication of component problems existed. The cause of the failures was determined to be in the test equipment; defective pins were discovered in the STEA test connections on the 29-v line into the flight control sensor group. These pins were repaired, and no further failures of this type have been encountered.

(b) *Flight control electronics:* During the vibration portion of the type approval tests (TAT) on the flight control electronics, several components broke loose from the circuit boards, causing a failure in the unit and damage to other components. The failure was attributed to the mounting techniques of the transformers and the marginal structural design of the chassis boards. The transformer mounting techniques were improved. Also, the chassis board construction was modified by replacing the foam core with a honeycomb core and improving the bonding techniques. An electronics unit that was fabricated using the modified chassis boards and transformer mounts has successfully passed the TAT vibration tests.

(c) *Engineering mechanisms auxiliary:* The constant-current generator electrical conversion unit failed due to excessive duty cycle when the unit was not being exercised. The failure review board investigation discovered two possible causes. First, noise was known to exist on some of the STEA-spacecraft lines, which could trigger sensitive circuits in the engineering mechanisms auxiliary (EMA). The sensitive inputs were found and desensitized. Second, a grounding problem in the flight control STEA was causing the EMA constant current generators to go on and stay on. The grounding problem has also been solved.

(2) *New failure investigations*

(a) *Engineering mechanisms auxiliary:* During flight acceptance tests (FAT) of the EMA, one of the command outputs would not operate for approximately 7 min; afterward, the unit functioned normally. After the failure, the unit was subjected to extensive special testing to find any deficiencies, but none could be found. Further investigation indicated that the test equipment may have been at fault; the line carrying this command output through the test equipment has a single-pole toggle switch in series. Dirt or contamination of any sort in the switch mechanism or on the contacts could cause a non-repeatable failure such as this. The switch is to be replaced by a double-pole switch with contacts wired in parallel to prevent a recurrence of this failure.

(b) *Boost regulator, transmitter, and receiver:* During vibration testing of a dynamic model vehicle, the boost regulator failed, inducing failures in the transmitter and receiver by subjecting them to excessive voltages at their inputs. The boost regulator failure was the result of shake table "run away", applying approximately four times the maximum g-load specified. All three of the units were analyzed to determine if reliability degradation had occurred. The boost regulator sustained no significant degradation, as only a few components were subjected to the excessive voltages. In the receiver, all modules and components were subjected to stress due to overvoltage generated by the receiver power supply. The reliability has been degraded by an order of magnitude, and thus the unit will not be accepted as flight approved hardware. The affect of this failure on the transmitter is still being investigated.

CONFIDENTIAL UNCLASSIFIED

UNCLASSIFIED
CONFIDENTIAL

(c) *Inadvertent squib firing:* During system RFI testing, some squibs which were not commanded were found fired and no method existed to determine the exact time or cause of firing. Special testing has been suggested by the failure review board to determine the cause of failure. Changes to the squib assemblies on the spacecraft during test have been initiated to provide adequate indication of squib firing.

(d) *Static discharge testing:* During the performance of the T-21 static discharge testing, numerous engineering signal processor and auxiliary engineering signal processor commutator switches failed and many squibs fired out of sequence. Failure review board investigations are in progress to determine the cause of failure and the necessary corrective action. System studies are being made to determine the nature of the static discharge threat.

g. Reliability assurance test program

(1) *Status and results of tests.*

(a) *Canopus Sensor:* Testing of two Canopus sensors, S/N 3 and S/N 9, has continued through this reporting period. Both of these units incorporate an upgrade instituted as a result of a failure discovered during the early stages of reliability testing. These units have each been subjected to two vibration tests at 155% of flight level, and one vibration test at flight level. Each of these vibration tests was followed by a 66-hr simulated flight sequence while being subjected to a thermal-vacuum environment equivalent to actual transit conditions. Twenty-one additional simulated flight sequences have been performed under thermal-vacuum conditions. The units have both survived this testing with no apparent degradation of operation and no failures. Each unit has been subjected to 1500 hr of operation. Three more simulated flight sequences will be performed to provide a demonstration of Canopus sensor reliability of 0.970 with 80% confidence.

(b) *Auxiliary Batteries:* Auxiliary batteries have completed reliability assurance testing. Six batteries were subjected to a simulated mission test comprised of shock, vibration, and thermal-vacuum environment. These tests were performed to obtain confidence in the battery reliability from test data and determine the effects of activated storage on total power capacity. Tests were performed on batteries stored from 11 to 20 days to simulate possible preflight sequence operations. Six batteries completed the testing. A seventh battery (S/N 1) indicated low voltage prior to test and an eighth battery was destroyed by an error in the activation procedure. Activation procedures have been changed to preclude repetition of this error. Of the six batteries tested, S/N 2 had marginal power capability. S/N 1 and S/N 2 were disassembled and analyzed to determine the failure modes. One cell of each was found to have low voltage after discharge. Suspected failure modes were structural failure of cell plates and connecting grids or internal short circuit paths through the plate separators. Fig. 107a shows the battery case opened to provide access to individual cells. Fig. 107c shows an individual cell and Fig. 107d shows the same cell with its polystyrene case removed. Fig. 107b shows the cell plates with separators removed. No indication of internal short or interplate shorts was evident and the plates and plate connector grids were all intact. The cause of the low voltage was not determined for either of the two batteries examined.

Analysis of the data by the statistical method of analysis of variance did not support the hypothesis that storage time up to 20 days affects a change in discharge capacity. A complete report of the test results will be made during the next reporting period.

(c) *Other Selected Items to Be Tested:* The remaining selected control items to be tested include:

(1) Main batteries (26)

(2) Separation sensing and arming device (8)

(3) Solar panel (1)

(4) Attitude jets (6)

Items 1 and 2 will be tested during the next reporting period. The remaining items will be tested during March of 1965.

2. Quality Assurance

a. Quality of products. Improvements in the control of quality continued during this reporting period. Some of

UNCLASSIFIED
CONFIDENTIAL

UNCLASSIFIED
CONFIDENTIAL

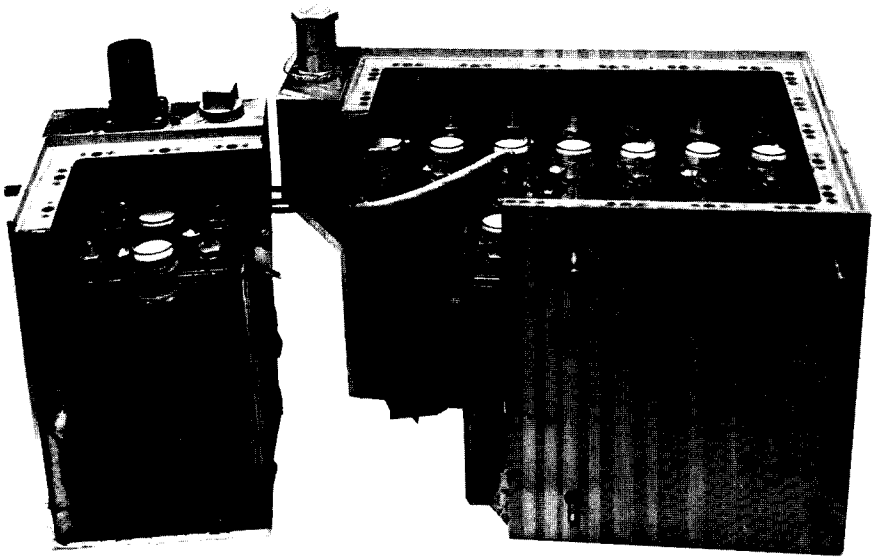

(a) Sectioned for access to cells

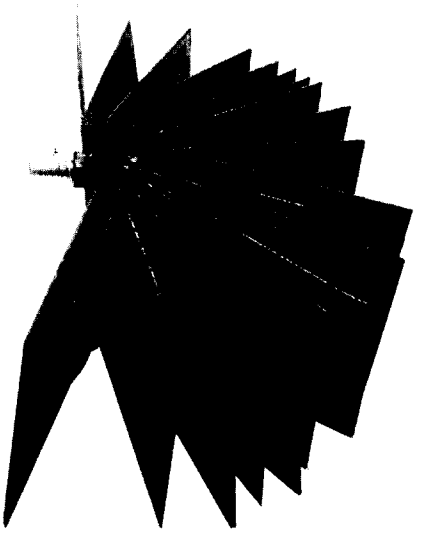

(b) Battery cell plates without separators

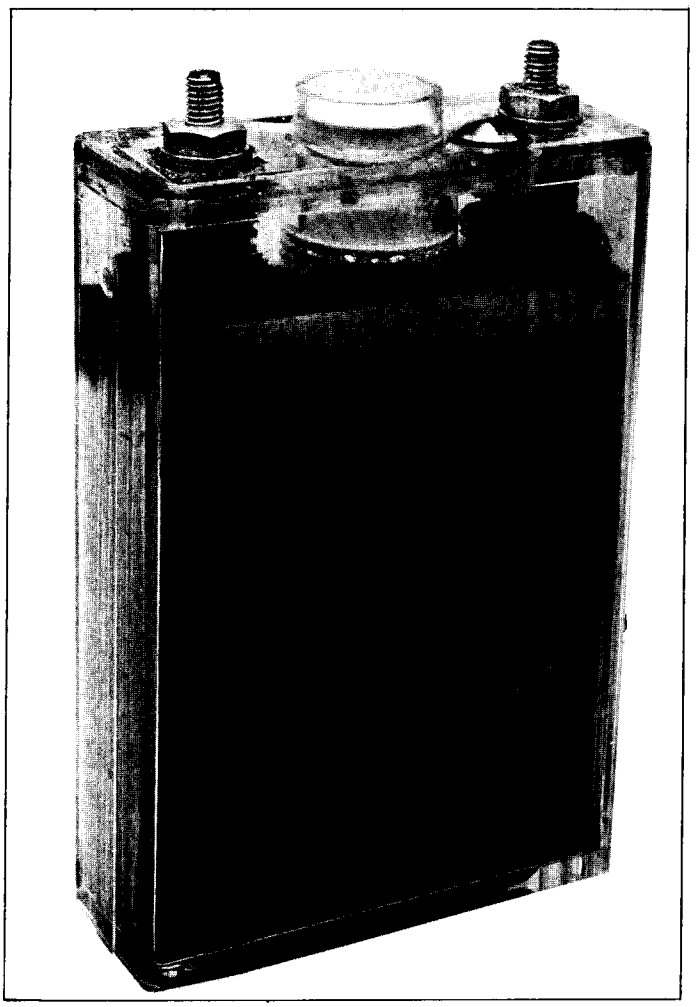

(c) Battery cell

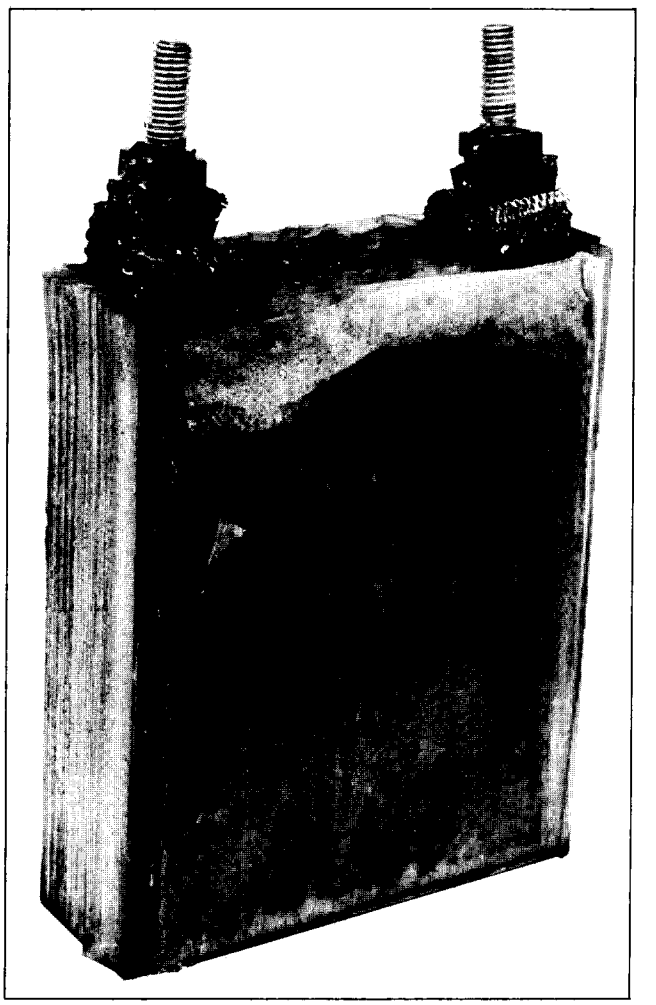

(d) Battery cell without case

Fig. 107. Auxiliary battery

CONFIDENTIAL
UNCLASSIFIED

UNCLASSIFIED
CONFIDENTIAL

the more significant events are discussed below. In some instances, technical problem areas mentioned here are discussed in more detail in other sections of this report.

(1) *Procedures for repair, rework, and modification.* Detailed instructions describing acceptable procedures for the repair, rework, and modification of electronic assemblies have been expanded to include welded modules, soldered modules, feedthrough terminals, and plating repairs.

(2) *Traveling-wave tubes.* All traveling-wave tubes in bonded stores, as well as those installed in spacecraft transmitters, have been x-rayed and found to be acceptable.

(3) *Atlas connectors.* A specification control document has been prepared covering plastic caps for connector protection. Procurement negotiations are in progress and the selection of a source is imminent. Connectors in control item test positions are being repaired or replaced on a non-interference schedule.

(4) *Altitude marking radar.* A task team has been organized to assure prompt resolution of problems relating to this control item. A quality assurance representative has been assigned to the team to assist engineering and production personnel in meeting both the quality requirements and the delivery schedule.

(5) *Vidicon tubes.* A quality assurance representative has been assigned to verify the testing of the vidicon tubes. A flow plan has been prepared describing the movement of the vidicon tubes from receiving, receiving inspection, various specialized test areas at Hughes, transportation to JPL, JPL test, return to Hughes, and reinspection and test. This flow plan has been developed to:

(a) Improve coordination between test areas.

(b) Assure that no additional or repetitive tests are performed that may degrade the vidicon tubes.

(c) Preclude unnecessary handling and the attendant possible damage.

(d) Provide information in the event of tube quality deterioration.

(6) *Spacecraft cleanliness requirements.* Close coordination is being maintained with participating organizations to assure that these personnel are fully aware of the cleanliness requirements for all *Surveyor* hardware. Manpower training in improved maintenance and cleaning techniques and the growing recognition of their effect on the hardware, are receiving close attention by all levels in fabrication, assembly, and test areas. The control of temperatures and humidity as well as the dust count in manufacturing and test areas are under active surveillance.

b. Review board actions. Material review board (MRB) actions totaled 368 and preliminary review board actions (PRBs) totaled 504 for this report period. PRBs comprise about 60% of all review board actions, indicating a continuing downward trend in MRBs versus PRBs as the result of the use of standard dispositions at lower inspection levels.

c. Quality audit/surveillance of* Surveyor *subcontractors. Quality audit/surveillance of subcontractors, under the centralized supplier quality assurance system, has been fully implemented during this reporting period. A summary of significant subcontractor activities are noted below.

(1) *Ryan.* The continuing audit/surveillance by the resident quality assurance representative has resulted in a tightening of controls in deficient areas and increased cooperation between Ryan and its major second-tier subcontractors.

The (QA-1) radar altimeter and doppler velocity sensor (RADVS) was overhauled and modified in accordance with the T-21 Upgrade III program and returned to Hughes. The RADVS system (AM-1) was completed and shipped to Hughes. The type approval tests on RADVS system S/N-1 are still in progress and should be completed during the next reporting period.

(2) *Bell and Howell.* Type approval testing of lens Y-5 is in progress following its upgrade to the latest changes and only two tests remain in the optical laboratory before the start of environmental testing at Inland Test Laboratories. Lenses S/N-7 and S/N-11 were retrofitted and have passed the flight acceptance test. Lens S/N-5 was assembled and optically adjusted but failed the flight acceptance temperature torque test of the zoom and focus systems. Investigation revealed a breakdown of the microseal dry lubrication permitting metal-to-metal contact resulting in galling. Lens S/N-8 failed to meet torque requirements after 1000 break-in cycles. Failure was apparently due to the same causes noted for S/N-5. The disassembled parts have been remicrosealed and are being recycled. All hardware modifications have been completed on S/N-5, 8, 10, 12, and 13. A

CONFIDENTIAL
UNCLASSIFIED

UNCLASSIFIED
CONFIDENTIAL

redesigned evaluation shutter, S/N Y-2, has been equipped with larger latch coils. Each coil bore was increased from 0.090 to 0.140 in. The core of the bobbin has been fabricated of stainless steel and is designed to prevent contact between the moving armature and the carbon steel of the housing and flanges of the bobbin. The length and diameter of the armature were increased; a stronger compression return spring is being used to move the heavier armature back to its return position. Measurements made on the magnetic force at the beginning of the stroke show a 100% increase from the earlier design. This improved shutter was cycled 78,000 times before failure. The armature drive pin was replaced and the unit was cycled an additional 111,000 times before failure occurred again. The cause of this failure was the shearing of the pin which attaches the actuating arm to the shutter blade. This pin was replaced for additional cycling tests.

(3) *National Water Lift.* Final assembly of the first six shock absorber units is scheduled to begin on October 2, 1964, with flight acceptance testing to commence shortly thereafter. The anticipated shipping date for the first six units for S/C-1 and S/C-2 is mid-October.

(4) *General Electrodynamics Corporation (GEC).* The procurement of the first 15 vidicon tubes is essentially completed. GEC has been performing rework or replacement of tubes rejected during final acceptance testing. Negotiations are presently underway between Hughes and GEC for the procurement of 15 additional vidicon tubes. The proposed tube is an improved ruggedized version of the present design.

(5) *Thiokol/Elkton.* Four main retro-rocket engine firings (Engines A-21-17, A-21-18, A-21-23, and A-21-24) were conducted at AEDC. Engines A-21-17 and -18 were fired with AMR antennas and all engines were fired with safe-and-arm devices mounted.

Two failures were experienced with the safe-and-arm device on A-21-18 – one mechanical and the other electrical. Hughes and Thiokol are currently conducting failure analysis and proposing corrective action.

Excessive nozzle side force loading was experienced on A-21-23, plus excessive spalling of the interior of the nozzle. A new nozzle design is under consideration by Thiokol Chemical Corporation, Hughes Aircraft Company, and JPL.

(6) *Vector.* This supplier has recently submitted an inspection plan to Hughes for approval. During this reporting period, Vector commenced the rework program outlined in their rework and test procedure.

(7) *Kearfott.* Kearfott has submitted their flow plan and inspection procedures to Hughes which define how controls were maintained toward the end of the second-buy period. These controls have been reviewed and an agreement has been reached on the specification to be followed for the rework of gyros.

(8) *Dilectrix.* Production and delivery of propellant tank bladders are in progress. Damage to 17 completed bladders occurred when test fixtures used in the final check area were moved and improperly set-up in another location. The damaged bladders were down-graded to class III status for engineering evaluation purposes.

(9) *Electric Storage Battery Company (ESB).* A recent quality audit disclosed that the ESB battery activation procedure was not up to date. Corrective action has been initiated by ESB in this area. Leakage of a Cannon connector employed in the Bourns pressure transducer has been resolved. Five reliability test batteries (R-4 through R-8) have been completed and delivered to ESB for test. Upon completion of vibration at type approval test levels, these batteries will be returned to ESB for lunar load simulator testing.

(10) *Holex.* Reliability tests of the helium dump valve and squib were conducted during this period and no failures occurred. The valve assembly qualification tests were also conducted and two failures were reported. Failure analysis indicated that the shock absorbed by the Phase II squib from the Phase I firing caused movement of the dielectric spacer from its seated position in the body of the cartridge. This movement separated bridge wires AB and CD from the connector pins causing an open circuit. Hughes is presently evaluating design changes to the squib and valve to prevent reoccurrence of this failure.

(11) *Airtek Dynamics.* The supplier was surveyed and approved to produce titanium propulsion tanks and helium tanks. *Surveyor* quality assurance surveillance was specified for all principal operations and test. All material deliveries have been audited. Several test specimens were welded and evaluated before a satisfactory weld schedule could be accomplished. However, the production of a weld

CONFIDENTIAL
UNCLASSIFIED

UNCLASSIFIED

with porosity below the acceptable level has been difficult to attain. It appears that despite repeated review of the pre-weld cleaning process such porosity stems from a cleaning deficiency prior to welding. Type approval testing of three propellant tanks is nearing completion with only the repeated failure of the vibration test fixture causing difficulty. The use of sub-tier contractors for the majority of the processing and testing of these units imposes a specific requirement for the inspection and certification of special processes by both Airtek and Hughes. Seven flight model propulsion tanks have been delivered to Hughes.

d. Quality assurance field operations

(1) *Air Force Missile Development Center (AFMDC) Operations.* Additional quality direction has been provided for *Surveyor* test operations in the form of specific quality assurance procedures, which are in the process of formal release to cognizant organizations.

(2) *Dynamic models.* The dynamic model transponder for SD-1 was given a pre-interim combined systems test (ICST) functional test at GD/A. However, due to the availability delay of the *Centaur* vehicle, the interim combined systems test schedule has slipped, and it is anticipated that ICST will start in late October, 1964. Quality assurance surveillance is being provided.

The dynamic model transponder for SD-2 was accepted by JPL and shipped to Goldstone Deep Space Instrumentation Facility (DSIF) where JPL, with Hughes support, will conduct spacecraft transponder/DSIF compatibility tests. Upon completion of the JPL Goldstone tests, the SD-2 transponder will be returned to Hughes for a functional test.

e. Type approval test reviews. During this period, type approval test reviews involved only one major review of the *Surveyor* main battery, which was accepted by the type approval test review committee.

f. Quality representation status. Quality assurance representation on the T-21 spacecraft task force committee has been continued during this period to assure quality support and coordination for T-21 functional and environmental testing.

3. System Test

a. Preparations for T-21 thermal-vacuum test. Upon completion of the static discharge tests, T-21 entered the Upgrade III modification program, designed primarily to ready the vehicle for solar-thermal-vacuum testing. Upgrade III was completed in early October, and selected group and system tests were started to verify the upgrade changes and to prepare the vehicle for solar-thermal-vacuum testing. It is presently planned to enter the solar-thermal-vacuum test phase at the end of October.

(1) *Solar-thermal-vacuum pre-test implementation status.* The solar-thermal-vacuum pre-test implementation as described in previous reports has been completed with the exception of the pre-test vehicle instrumentation. The remaining vehicle instrumentation will be included as part of the scheduled solar-thermal-vacuum preparatory sequence.

(2) *Solar-thermal-vacuum fit and function test.* A test program was carried out to evaluate all STEA solar-thermal-vacuum test equipment before T-21 solar-thermal-vacuum (STV) testing. This test program included an environmental test under STV conditions using a full-scale engineering mockup of the spacecraft with the STV test equipment. In addition the automatic data monitoring system (ADMS) was operated during the STV portion of the test program to check out the ADMS and its use in providing data for the control of the chamber environment. Several test procedures for T-21 STV testing were verified and improved through the fit and function test program.

The program was divided into two phases based on the hardware delivery schedule. Phase I included the STV test with all the equipment requiring an environmental test. Phase II consisted of a test of the fit of all special test equipment not requiring solar-thermal-vacuum exposure.

(3) *Fit and function Phase I test results.* In general the entire fit and function Phase I test was successful and extremely beneficial in proving test equipment and test procedures to be used in T-21 STV testing. During this testing a maximum vacuum of 3×10^{-5} Torr at a one-Sun solar intensity was achieved. The major accomplishments of this test were as follows:

(a) The shadow cold shrouds were successfully checked for shadowing characteristics and leaks. The cold shrouds performance (see Section G) during environmental testing exceeded pre-test anticipations.

(b) The TV 4 target operated within the STV environment but the light uniformity on the

CONFIDENTIAL
UNCLASSIFIED

UNCLASSIFIED
CONFIDENTIAL

target was below specification limits. The action taken to improve the uniformity was completed and the target retested successfully.

(c) The automatic data monitoring system successfully scanned and recorded over 100 temperatures in near-real-time during STV testing. Minor difficulties with the system have been eliminated by program changes to assure optimum operation during T-21 STV testing.

(d) Bake-out, pump-down, and cool-down procedures for T-21 testing were successfully followed. The procedures for turning on solar lamps to full intensity during cool-down is being studied for improvements to allow better temperature control of the vehicle. Low temperature bake-out of the chamber (130°F) was proved satisfactory.

(e) The emergency shutdown procedures were satisfactorily executed, but the system has to be modified to meet the chamber warmup objectives. The necessary design modifications of the chamber plumbing and valving will be incorporated and tested before T-21 STV testing begins.

(f) The installation procedures for test equipment were shown to be satisfactory; however, several slight modifications were made for improvement.

b. T-21 vibration and shock test

(1) *Vibration pre-test implementation:* A draft of revision A to the T-21 vibration test specification has been completed. Some changes in instrumentation locations are anticipated and will be reflected in Volume I of the Vibration Test Plan. Some changes to upgrade the functional test aspects will be reflected in the functional test requirements. Preparation of the test plan continues; establishment of the final table of requirements, which is also required for the specification, comprises an important milestone of progress.

The vertical test fixture still requires shop work to eliminate an interference problem with the altitude marking radar (AMR) antenna, and to bring weldments into print conformity. The problem of excessive deflection of the vibration table armature, caused by the combined weight of the vehicle and fixture, has been successfully solved by incorporation of the pneumatic suspension boost system. Successful operation was demonstrated during S-2A testing.

Table 44. Vibration test implementation

Item	Percentage completion
Documentation	
Test specification	100
Instrumentation plan	100
Test plan	90
Procedures	10
Hardware and equipment[a]	
Test fixtures	95
Vehicle instrumentation	85
Special facility preparation	65
Vehicle special equipment	40

[a]Includes design, drafting, procurement, fabrication, assembly, and checkout.

Installation of strain gages is virtually completed. Accelerometer installation, and final checkout of strain gages and accelerometers will be accomplished after STV tests are completed.

Tests were made during the S-2A vibration program to determine the magnetic field intensity due to the shaker operation in the area of T-21 components which might be sensitive to strong magnetic fields. Data are being reduced; however, additional surveys are planned prior to T-21 vibration tests.

Table 44 provides a summary of progress for T-21 vibration test implementation.

(2) *Shock pre-test implementation:* A draft of the revisions to the preliminary issue of the shock test specification is being reviewed. Preparation of the test plan continues. As with the vibration test plan and specification, upgrade of test requirements has been an important step in progress of these documents.

The drop test platform has been completed. Design work continues on the release mechanism, and on test access cables required for the retro-separation test.

Table 45 summarizes progress of preparations for T-21 shock tests.

c. T-21 radio frequency interference (RFI) test. The full RFI test phase, including the static discharge test, was concluded during this period.

RFI testing. The reason for the premature firing of the retro-rocket eject squibs and retro-rocket ignitor squibs

CONFIDENTIAL
UNCLASSIFIED

UNCLASSIFIED

Table 45. Shock test implementation

Item	Percentage completion
Documentation	
Test specification	100
Instrumentation plan	100
Test plan	90
Procedures	10
Hardware and equipment[a]	
Test fixtures	50
Vehicle instrumentation	85
Special facility preparation	60
Vehicle special equipment	20

[a]Includes design, drafting, fabrication, assembly and checkout.

during the RFI functional subphase of testing has not yet been fully determined. However, a failure review board (FRB) concluded, on the basis of available squib test information and other data, that the RFI environment was not the cause of firing.

Static discharge test. The static discharge subphase of testing was accomplished during this period and determined that spacecraft susceptibility to electrostatic discharges exists. The susceptibility was evidenced by premature squib firing and failures of commutator transistor switches.

On August 9 the T-21 vehicle was removed from the screen room and placed in flight configuration with inert retro-rocket, altitude marking radar, solar panel, discharge tabs, and live squibs installed. It was then placed in the spacecraft adapter ring in the static discharge test (Fig. 108a and b).

(1) *Positive discharge.* The first series of discharges were from a high voltage source to a grounded spaceframe/adapter ring, Fig. 108c. These discharges caused no malfunction until the TB-2 floating ground was contacted. At this time all preseparation squibs detonated and numerous commutator switches in the engineering signal processor and auxiliary engineering signal processor failed. It was determined that the full 30-kv discharge voltage was developed across three current shunts in series from the discharge point to spaceframe ground. This precipitated the removal from the test procedures of all further discharges to this particular point. Testing continued without incident until the first discharge to spacecraft Ground 1. A sustained arc of 1 to 2 sec duration occurred, accompanied by the firing of the helium dump squib. The malfunction could not be duplicated so testing was continued.

(2) *Negative discharge.* The second series of discharges was accomplished by charging the spacecraft to 30 kv and discharging it to ground, Fig. 108d. The

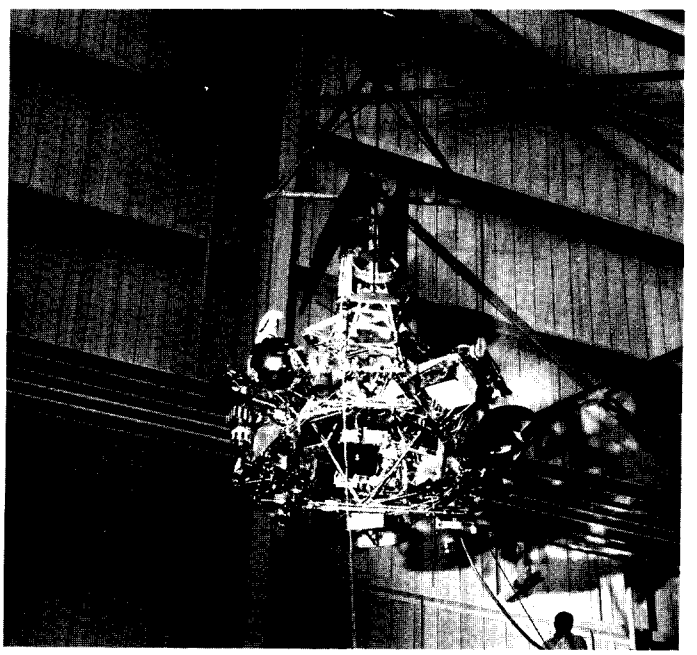

(a) T-21 prior to installation of retro-rocket

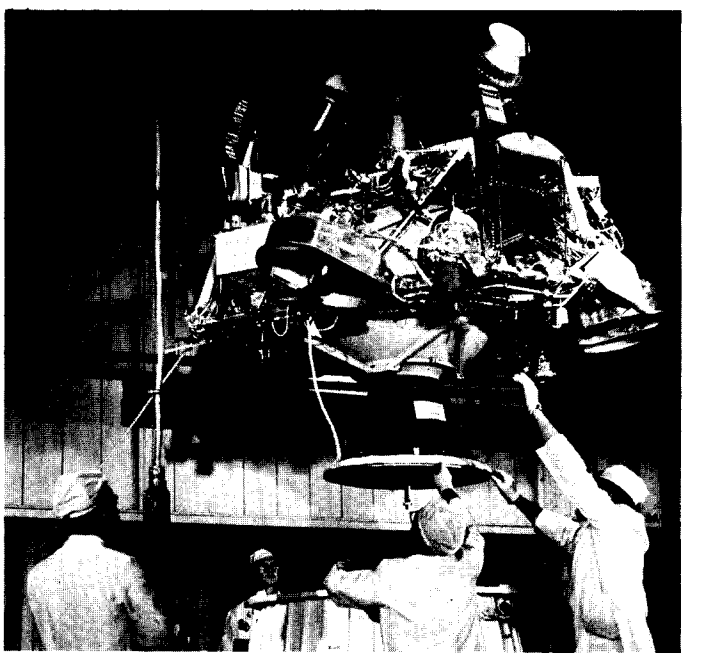

(b) T-21 installation on adapter ring

Fig. 108. T-21 static discharge tests

UNCLASSIFIED

UNCLASSIFIED CONFIDENTIAL

first discharge in this series was conducted from Leg 1. Upon discharge of the spacecraft, the helium dump squib detonated and telemetry indicated a failed commutator transistor switch. Further discharges from Legs 1, 2, and 3 brought forth the following information:

(a) Pulses up to 40-v amplitude and 0.1-sec duration are generated on commutator input lines at the time of discharge.

(b) The flight control system generates a squib gate signal upon discharge.

(c) Squibs not interlocked out by the separation sensing and arming switch will detonate upon discharge.

(d) Commutator transistor switches are caused to fail as a result of discharge.

(e) Momentary disturbances of telemetry data occur at the time of each discharge.

The discharges conducted at the mast and mating ring did not cause any apparent malfunction.

(3) *Lightning simulation.* Simulated lightning discharges were conducted between the spacecraft landing gear in as close proximity of the vehicle as possible (Fig. 108e). With an off-ground vehicle, telemetry was disturbed for arcs between Landing Gears 1 and 3, and 2 and 3, but returned to normal upon cessation of arcing. There was no noticeable disturbance of telemetry information when the spacecraft was grounded.

(4) *Simulated spacecraft separation.* Simulated spacecraft separations were accomplished (Fig. 108f), by lifting the spacecraft from an off-ground charged mating ring. A slow rate of separation caused sustained arcing resulting in loss of phase lock and failures of commutator switches. Rapid rates of separation resulted in short arcing periods and momentary disturbances of telemetry data.

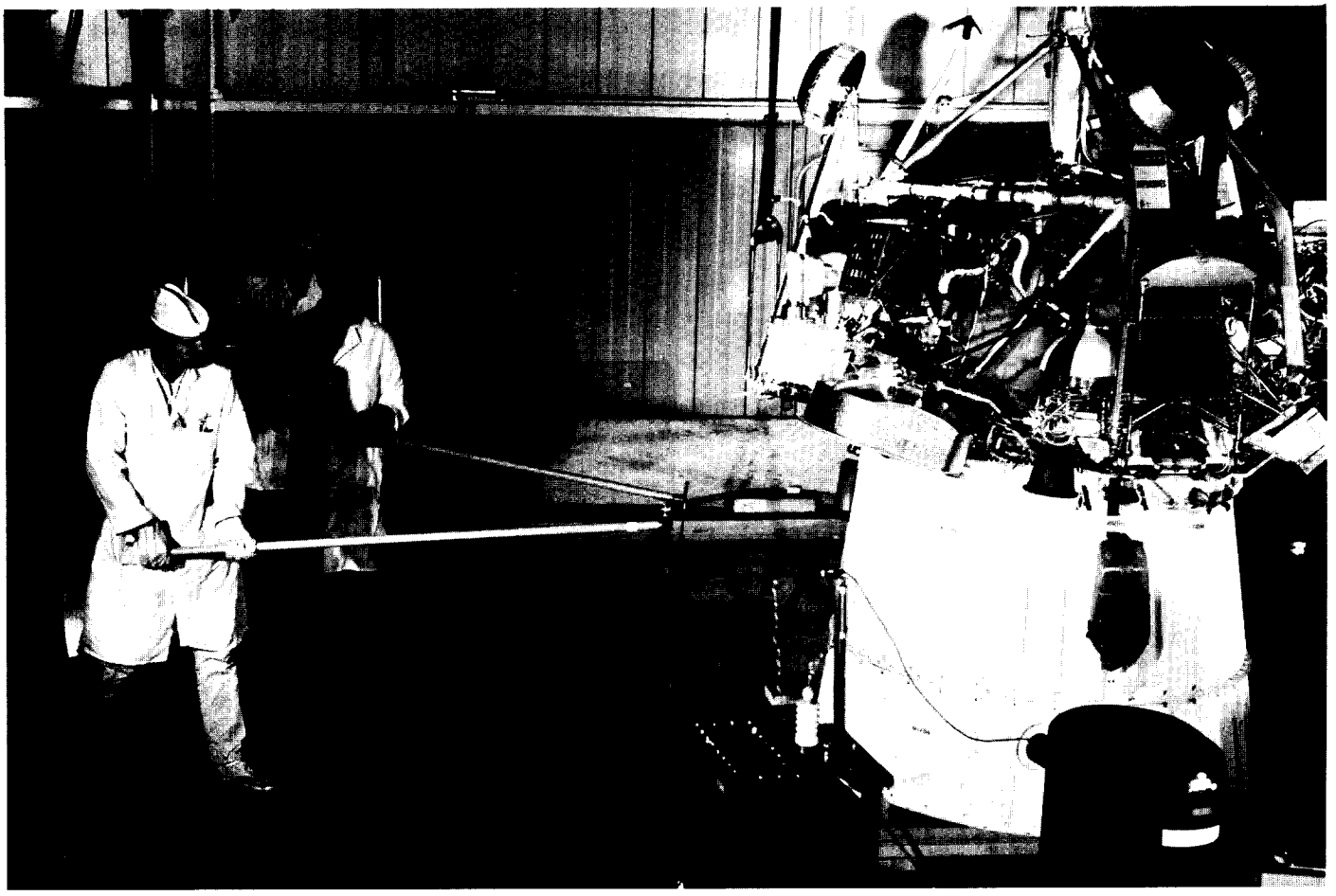

(c) Positive discharge to Leg 3

Fig. 108 (continued). T-21 static discharge tests

UNCLASSIFIED CONFIDENTIAL

UNCLASSIFIED
CONFIDENTIAL

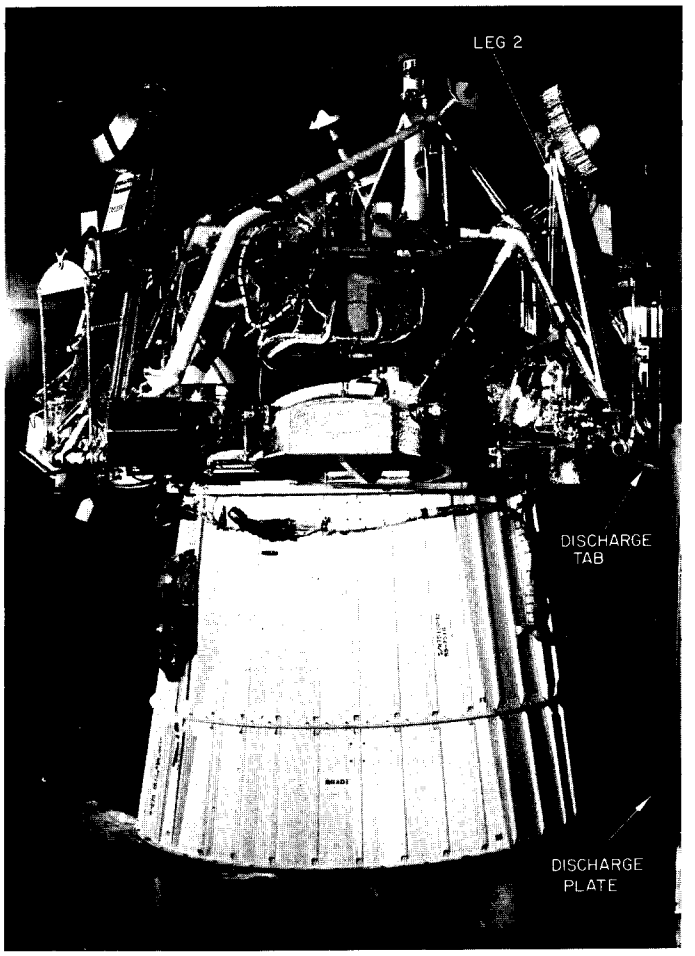

(d) Negative discharge for Leg 2

(e) Lightning simulation between Legs 1 and 3

(5) *Test continuation.* Following completion of the originally planned testing, additional testing was accomplished to attempt to determine more accurately the causes of various malfunctions.

Part of the additional testing conducted was simulated lunar landings of a charged spacecraft. Fig. 108g shows the arcing evident from one of the

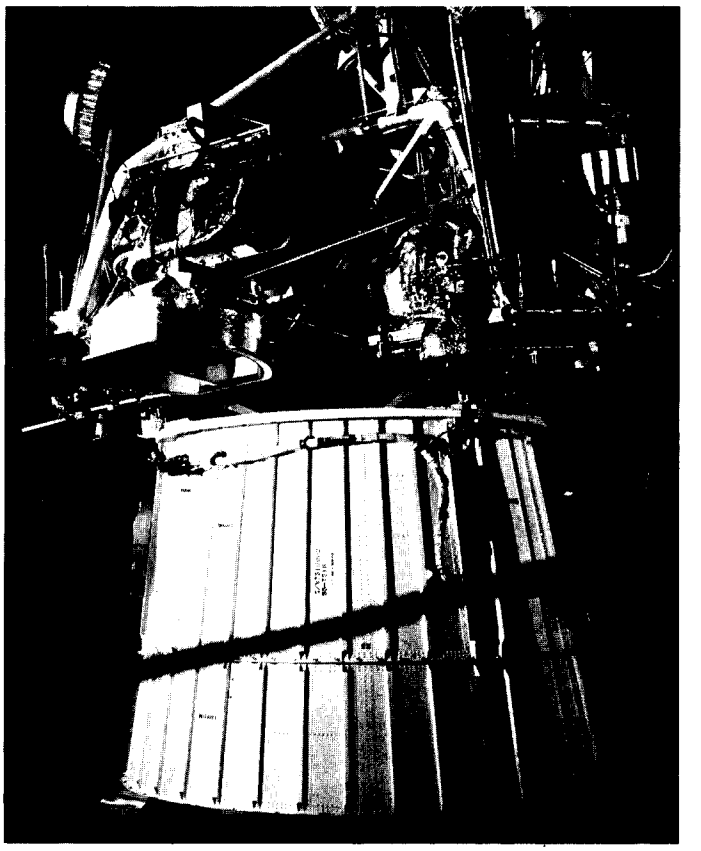

(f) Simulated spacecraft separation

(g) Discharge arcs at footpad during simulated lunar landing

Fig. 108 (continued). T-21 static discharge tests

CONFIDENTIAL
UNCLASSIFIED

UNCLASSIFIED
CONFIDENTIAL

footpads to the ground plane. As in the previous discharge tests, a voltage level of 30-kv was used. The vehicle was rigged so that a specific footpad (leg) would touch first. This testing resulted in disturbed telemetry signals and the failure of a number of commutator switches.

Based on these results Hughes is conducting an extensive investigation into the effects caused by static discharges on spacecraft harness and units. Other investigations are being pursued to determine requirements for making harness and units compatible with static discharge effects.

d. T-21/QA-1 test data analysis. Analysis of test data obtained is continuing with data input from the White Sands Missile Range approximately 90% complete.

Analysis of available data has indicated that a problem area exists in the generation of the RADVS minimum altitude mark (14 ft mark). During approximately 45% of the helicopter passes investigated, where there was no known malfunction in the RADVS or instrumentation system, the minimum altitude mark occurred above the tolerance limit of 14 $\pm$4 ft. Investigation of the problem has been initiated both at Hughes and Ryan.

Analysis of reflectivity data obtained during the tests has produced the following information:

(1) The RADVS reflectivity voltages as transmitted by telemetry are quite noisy. The amplitude of the noise is dependent upon the type of terrain, being somewhat higher for rough terrain than for smooth surfaces.

(2) The reflectivity of the lava beds located at AFMDC was slightly higher than that of flat desert and brush, while the reflectivity of the very fine white sand or gypsum was somewhat lower than the flat desert.

(3) During periods of RADVS preamplifier gain switching, analysis of reflectivity data is practically impossible. At gain switch, the reflectivity voltage analog changes level, and the time constants of the circuits involved cause a delay in the change. If several gain switches occur in rapid succession, the voltage analog represents the average between the two levels, and is useless for data reduction.

e. T-2S vehicle test program. A closed loop simulation of the T-2S Drop Test 17 was completed during this period. Analog simulation was connected electrically to the vehicle, radar test equipment, and the control van. In addition, the range telemetry receiving station was brought on site to receive telemetry from the T-2S vehicle, decommutate, and display the usual signals displayed during an actual drop. The output of the computer was fed into an X-Y plotter which provided a record of the drop profile in range and the V_z velocity component. Radar noise previously recorded during the T-2H helicopter flights was introduced into the system during the tests. The excursion of vernier engine throttling due to this noise was approximately 5 to 7 lb peak-to-peak.

Failure mode simulations were made, such as the loss of an engine, but generally were not too informative due to computer saturation.

As a result of the closed loop simulation tests, the control system mechanization equations were verified. In addition, it was found that the hardware operation matched the theoretical mechanization very closely, and a high confidence was established that the closed loop performance of the hardware can be predicted.

A new propulsion manifold was fabricated, pressure tested, and installed on T-2S in preparation for Drop Test 17. This test is scheduled for October 20, 1964.

f. S-6 propulsion system test program. The S-6 vehicle arrived at AFMDC on June 21, 1964 for a series of tests to examine:

(1) The unbalance in the vehicle resulting from expulsion of propellant from the vehicle storage tanks during periods of unequal thrust chamber demand.

(2) Verification of system performance with temperature conditioning of various sections of the vernier propulsion system.

Encompassed within these test objectives were a number of subobjectives to examine system dynamics, expulsion efficiency, etc.

To accomplish these objectives, it was required to know the vertical force exerted by the vehicle at each of three suspension points within approximately 0.2 lb. From this information an evaluation of vehicle compliance with unbalanced moment specifications could be completed. This resulted in the requirement for a load cell system having 0.1% full-scale accuracy from front-end recording to final data. This requirement was beyond the known state of the art, and a program was initiated to evaluate every possible combination of techniques to achieve the goal. This ranged from statistical smoothing techniques in the data reduction to evaluation of suspension techniques.

A technique has been developed to permit calibrating the load cells, under full vehicle load, immediately prior

CONFIDENTIAL
UNCLASSIFIED

UNCLASSIFIED
CONFIDENTIAL

to each test. Comparison tests of two suspension systems have been completed, using solvents for the expulsion tests, and the data is being analyzed by the statistical program developed for this series of tests. Testing has started, as reported in Section I.

g. S-7 propulsion system test program. The S-7 vehicle was received at AFMDC without thrust chamber assemblies on September 14, 1964. The propulsion system had been upgraded at Hughes El Segundo for the 30-day storage test program. This upgrading included the installation of Hughes fabricated tanks, an unused helium tank from T-21, instrumented manifolds, and the necessary valving required to permit pressurization without squib firing. Additional modifications were made at AFMDC to allow engine removal without deservicing the propulsion system.

The 30-day storage test has started; periodic firings are planned during this storage period. In addition, the new thrust chamber assemblies received for T-2S will be system fired on S-7.

h. S-8/RADVS vibration test. In an attempt to demonstrate suitable operation of the RADVS system on a flight-type spaceframe in an expected vernier engine vibration environment, a vibration test utilizing the S-8 test vehicle and an operational RADVS system is being planned. This test consists of suspending the S-8/RADVS system in an inverted position in a special test fixture and vibrating it as a system by a drive rod connection at each vernier engine location (see Fig. 109).

The input vibration spectrum will be tailored for the RMD engines, based on firing data and the T-21/QA-1 RADVS vibration test. Since the test will be conducted using random vibration inputs (white Gaussian acceleration) from 50 to 2000 cps, the low frequency effect of the A/SSP is not anticipated and hence this unit will not be installed on the vehicle. The retro-rocket will not be simulated because operation of the RADVS will take place after retro-engine ignition and ejection. Vernier engine dummies will be used, but actual plumbing and fuel and oxidizer will be installed. Liquid ballast will be utilized in the tanks to simulate the lunar descent phase.

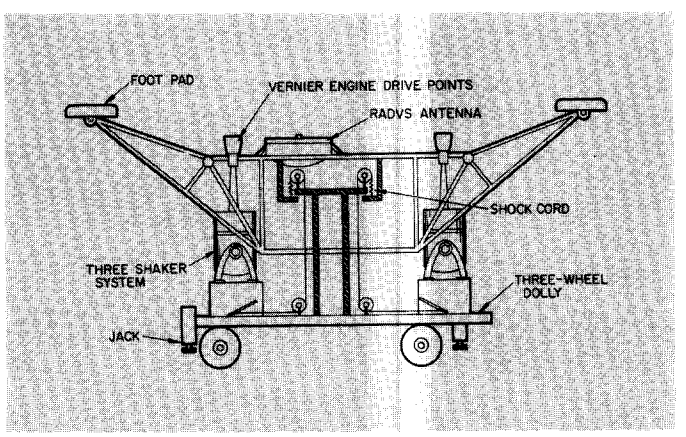

Fig. 109. S-8 RADVS vibration evaluation test

In order to affirm and resolve possible radar interference due to the landing legs and crushable blocks, it is also the intent of this test to verify satisfactory radar operation with landing legs and crushable blocks installed.

The vibration test facility will be composed of three Ling A280 shakers, an RP3/5 power amplifier, and a 26-filter equalizer/analyzer console. Force transducers will be used between the drive rod connection and the vehicle. The shakers will be installed in series and an armature current sensing device will be utilized.

Initial runs of the vibration tests are planned to determine the effects of correlated and uncorrelated inputs. These runs will require testing at one engine location at a time and then combining to shake at all three engine locations simultaneously. Effects of the following methods of testing will also be examined: (1) equalizing at Engine 1 only; (2) summing and averaging force transducers at all three engines; and (3) equalizing on the armature sensing current.

Once the method of testing has been determined, the RADVS will be evaluated in the typical environment without the landing legs extended or the crushable blocks installed. After the RADVS has been deemed operational, the landing legs will be extended and crushable blocks will be installed to determine possible radar interference. If interference is encountered, corrective measures will be taken. These measures will include the installation of aluminum foil around the footpads and crushable blocks. If the latter proves ineffectual, then microwave-absorbent material will be placed around the footpads and crushable blocks and the test rerun.

In addition to evaluating the AM-1 RADVS, S/N-1 and possibly the AM-2 RADVS systems will be evaluated, if time and equipment schedules permit.

i. S-8 flight control vernier propulsion system test. Accelerometer bracket design for the 26 accelerometers to be used to monitor vehicle vibration during the S-8 test has been initiated. A prototype of the accelerometer amplifier package containing three amplifiers is ready for type approval test and calibration with Endevco Model 2213 accelerometers.

The S-8 flight control electronics is being upgraded to the SC-1 configuration from the XT-21 configuration.

CONFIDENTIAL
UNCLASSIFIED

UNCLASSIFIED
CONFIDENTIAL

Fabrication of the signal processing and integral control unit to be installed on the vehicle in compartment B has started. Provisions for an emergency automatic engine shutdown feature in case of engine failure are being considered.

The S-8 vehicle configuration for this test has been defined in the S-8 Test Planning Specification which will be released soon.

S-8 suspension system. The S-8 suspension system was shipped to AFMDC and both the ¾-in. elastic cord system and the ½-in. system were assembled and tested using T-8H (the 2100-lb dummy vehicle) and T-8L (the 700-lb dummy vehicle) respectively. These systems were assembled and suspended from the 30-ft attachment boom on the Aerobee Tower using the winch system which was developed at the El Segundo facility. Fig. 110 shows the suspension system test arrangement supporting the dummy vehicle T-8H. Winch system operation was satisfactory; however, wind velocities exceeding about 5 knots cause the two steel cables supporting each leg to twist together and wind unevenly on the winch drums. Winch operation and control from the blockhouse (approximately 400 ft from the tower) were satisfactory and the ability to establish initial attitude conditions was demonstrated.

Instrumentation for the suspension system tests included both oscillograph, for vehicle motion and elastic cord loading, and photo theodolite coverage for both vehicle motion and induced boom motion. Preliminary results from the oscillograph data indicate that frequency and damping characteristics of both the ¾-in. and ½-in. systems compare favorably with theoretical values. The photo theodolite coverage was provided by Land-Air. The film is being reduced, but results are not yet available. A preliminary review of the film indicates valid data was obtained.

The upper snubber loops were modified so that the vertical free travel of the vehicle after release can be adjusted to any value from zero up. This was tested using the light vehicle, T-8L, and a free travel of 3 ft. After the vehicle was released from an initial condition of 150-lb force, relieved in the elastic cords, the vehicle dropped 3 ft and was snubbed by the short sections of elastic cord in the snubber loops. The snubbing action was satisfactory.

j. Flight acceptance test planning. Test planning effort during this period was directed primarily to the preparation of A-21 test specifications covering (1) system group tests, (2) initial system checkout, and (3) mission sequence tests. In addition, Volume I of the detailed test plan for the mission sequence test has been completed in rough draft form. The status of these documents and the information they contain are described below.

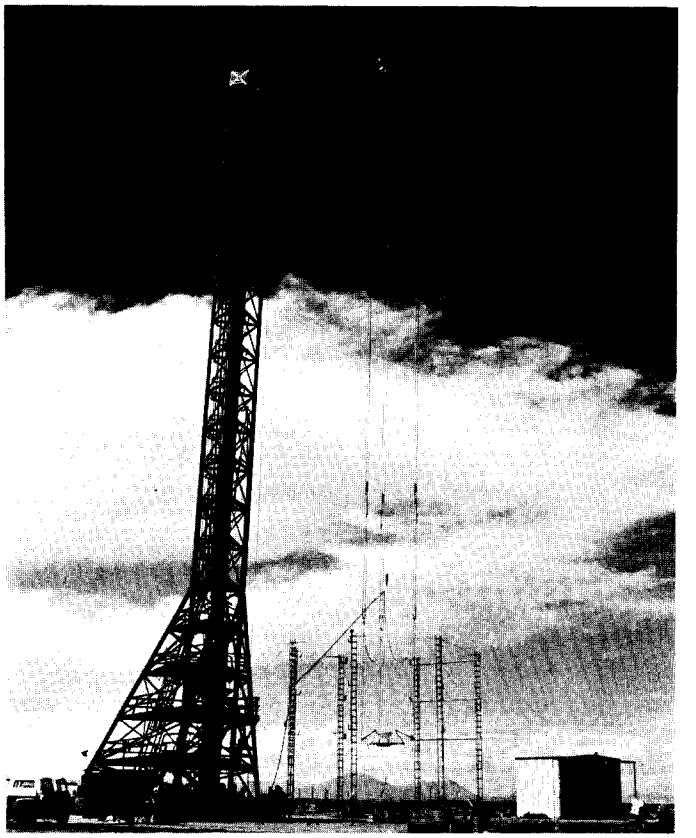

Fig. 110. S-8 suspension system test arrangement on Aerobee Tower

(1) *System group test.* The A-21 System Group Specification (224704) is complete. This specification covers requirements for power and radar subsystems in a group configuration powered from the STEA, television, flight control, radio frequency, mechanisms and vehicle, mechanisms auxiliary and command decoder/signal processing subsystems in a group configuration but powered by the spacecraft power subsystem.

(2) *Initial system checkout.* The A-21 Initial System Checkout Specification (224850) has been prepared. This specification contains requirements for system integration testing and system calibration.

(3) *Mission sequence tests.* The A-21 Mission Sequence Test Phase Specification (224822) for the A-21 flight acceptance test program has been issued. This specification covers the following requirements: readiness, prelaunch and launch, injection, midcourse correction, terminal descent, and post-touchdown.

CONFIDENTIAL
UNCLASSIFIED

UNCLASSIFIED

k. System test equipment. During this period, STEA 2 was completed and readied for test. STEA 1 is presently being modified to accommodate the solar-thermal-vacuum tests, and STEA 3 is in process of final integration and checkout. STEA 3 will be ready for vehicle SC-3 testing in November. Details of the problems encountered in this equipment and other test equipment are discussed in the following paragraphs.

(1) *RADVS.* Special test equipment to be used in conjunction with the RADVS test racks was designed and fabricated for the S-8/RADVS vibration tests to be conducted at Hughes Culver City. This special test equipment included control and junction boxes, intercabling, waveguide installations, and instrumentation equipment.

(2) *Intercom.* The STEA intercom system has been extended to include four additional remote stations outside of the screen room in the Hughes Space Environment Simulation Laboratory. These external stations will assure proper coordination and control during solar-thermal-vacuum tests. Power switching and grounding checks were performed on STEA-1 and STEA-2 in September. These checks disclosed several ground loops that invalidated the single-point grounding system on both STEAs. In addition, several wiring discrepancies were disclosed and corrected.

(3) *Test procedure status.* The following test procedures have been prepared and the T-21 power group procedure has been released.

Power group	T-21
Power group	SC-1
Mechanical auxiliary group	T-21
Mechanical auxiliary group	SC-1
Power mechanical auxiliary group	SC-1
TV solar panel test	T-21

The battery charging procedure for T-21 will be incorporated as an appendix to STV test procedure. The procedure for the STEA power functional checkout, to be performed immediately following power switching and grounding tests, is now being prepared.

(4) *Squib circuit test set (including squib simulators and stray energy monitors).* A new production quantity of 100 stray energy monitors, 250 squib simulators and 33 adapters have been fabricated, tested, and delivered. The squib simulators will be used for T-21 solar-thermal-vacuum testing; stray energy monitors and adapters are for use in SC-1 system functional test.

Thermal-vacuum tests were performed on squib simulators during this period for verifying mechanical survivability and to determine activation time under conditions of hard vacuum and extremely low temperature.

Three devices were activated at each of seven different temperatures ranging from —200° to 100°F. This range covers the squib temperatures expected during solar-thermal-vacuum test of the T-21.

Test results indicate essentially no change in activation time over the temperature range expected for various squib locations on the spacecraft. No mechanical failures were evident subsequent to the test.

Vibration testing of stray energy monitors is planned in the near future to verify mechanical survivability of the device when subjected to vibration levels expected during spacecraft vibration testing.

(5) *Test pattern illuminator.* The test pattern illuminator, commonly called the "light box," was designed to be a source of approximately 6000°K light for testing the following characteristics of the survey television system: sensitivity, dynamic range, photometry, calorimetry, signal output, and vidicon spectral response.

The first of six units of the test pattern illuminator has been fabricated. Checkout tests on the first unit are approximately 50% complete. A set of photometric and spectral measurements has been taken with the lamps and mirrors left in their "as-fabricated" positions. Temperature measurements were also made.

A typical pattern of photometric measurements taken on the face of the light box is shown in Fig. 111. A Spectra Pritchard photometer was used. These values were taken with the lamps operated at 120 v ac. Three sandblasted pyrex diffusion plates were used, but no absorption filters. The greatest drop in intensity is about 9% in a horizontal line, or about 18% over the whole face. The variation of intensity over the whole face is about 12 and —8% from the average intensity. These intensity values will be approximately the maximum obtainable from the light box. Fig. 111b shows the pattern of photometric measurements taken when the center pyrex diffusion plate was replaced with an opal glass plate: Here the greatest intensity drop remains 9% in one line, but is

UNCLASSIFIED

UNCLASSIFIED
CONFIDENTIAL

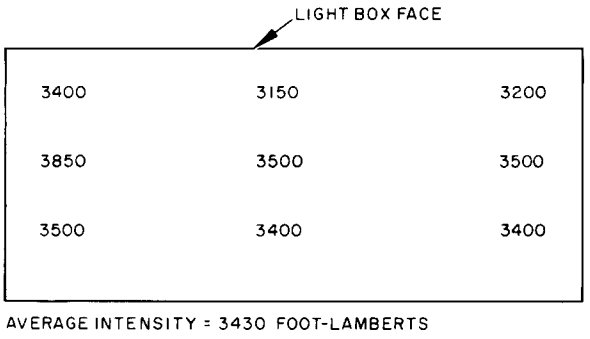

(a) Three pyrex diffusers

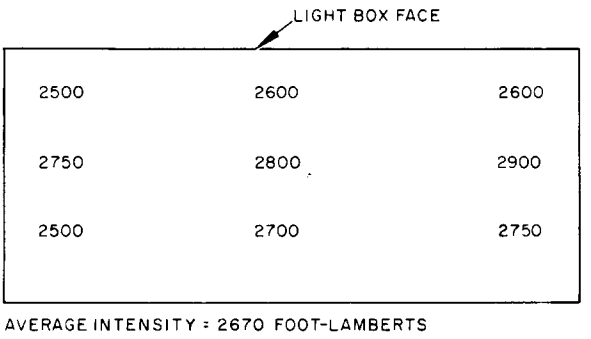

(b) One opal and two pyrex diffusers

Fig. 111. Intensity distribution of test pattern illuminator, foot-lamberts

14% over the whole face. It is again noted that the intensity variation over the whole face is about 8½ and —6½% from the average. Photometric measurements were also obtained with various absorption screens inserted and at lower supply voltages; the test results will be reported in the next issue.

A set of spectral measurements was taken for a similar range of conditions using a Perkin Elmer Model 112 V spectrophotometer. The detector was a blackened thermocouple that has been calibrated by an NBS-checked lamp. Relative spectral responses for both pyrex and opal center diffusion plates are shown in Fig. 112. These measurements are from the center of the light-box face. The lamps were operated at 120 v ac. Color temperature calculations have not been completed, but it is estimated that with a pyrex center-diffuser the temperature will be about 5400°K, and with an opal center-diffuser it will drop to about 5300°K. A difference between the two can be detected visually. A similar red-shift is detected at the sides of the face.

Temperature measurements show that the temperature distribution throughout the light box is satisfactory and the only critical part (the blue filter) reaches a maximum temperature of 145°F, which is uniform from center to corners. Some improvement in the photometric intensity distributions can be expected in subsequent tests when the locations of the lamps and reflectors within the light box are optimized. The measurements already obtained are within the design goals, however.

(6) *Payload system test.* One set of scientific instrument rack mounted STEA equipment has been built for the Payload System Laboratory and is undergoing checkout. Fabrication of a second set,

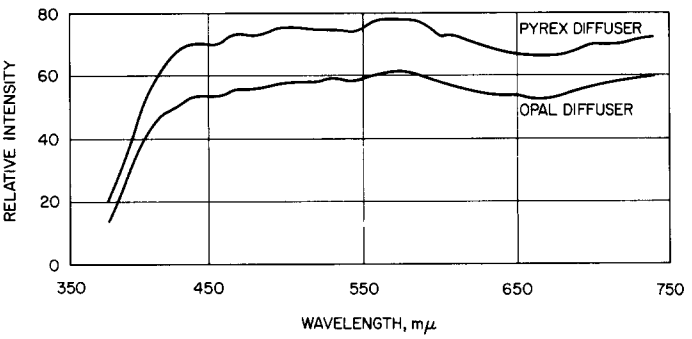

Fig. 112. Spectral responses of test pattern illuminator

to be used in system test operations, will begin in December. Design is nearly complete on the auxiliary (non-rack mounted) test equipment. These auxiliary items include special pulse generators, test devices, and instrument simulators.

(7) *Thermal-vacuum test chart.* A test chart for use inside the thermal-vacuum chamber during approach television thermal-vacuum system tests is being produced. A satisfactory chart with the required gray scale and resolution sections was developed using photographic paper cemented to aluminum. Sample charts were subjected to 260°F temperature at 10^{-6} Torr pressure, and also at liquid nitrogen temperature at 10^{-6} Torr pressure. During these tests no outgassing was observed and the emulsion appeared unaffected.

(8) *Tape recorder calibrator.* Design of this new STEA item and construction of a prototype were completed within this period. This unit will aid in setting up and calibrating the STEA magnetic tape recorders more rapidly and more accurately than in the past. Considerable time will be saved in

CONFIDENTIAL
UNCLASSIFIED

UNCLASSIFIED
CONFIDENTIAL

pretest setup and greater confidence in the tape recorder performance capabilities should be achieved.

The calibrator will provide dc inputs in the range of 0 to 25 v either positive or negative to an accuracy of $\pm 0.01\%$ and ac inputs in the range of 0 to 10 v rms $\pm 1\%$ at frequencies from 5 to 600 kc. In addition, a voice input is available to any selected channel for operator use during calibration. The calibrator will be mounted on casters for portability.

(9) *Flight control closed loop STEA.* Early in this period, engineering for incorporation of the closed loop STEA rack into the STEA complex was completed. Final engineering was released shortly before the end of the period. In addition, new equipment and cables were designed and fabricated for closed loop testing of the T-2 vehicle at AFMDC.

CONFIDENTIAL
UNCLASSIFIED

UNCLASSIFIED
CONFIDENTIAL

L. Launch Operations

1. Combined Systems Test

a. Planning. During this reporting period a meeting with LeRC, JPL, GD/A, and Hughes was conducted at which many of the details of the CST planning were formalized. Test objectives were discussed and agreed upon as follows:

(1) Demonstrate compatibility of the space vehicle electrical system and ground support equipment during a simulated flight from launch through simulated *Centaur* retromaneuver, including operation of the payload.

(2) Obtain data for qualitative evaluation of electromagnetic and radio frequency interference characteristics and compatibilities for the spacecraft in flight configuration.

(3) Demonstrate mechanical compatibility of the *Centaur*, spacecraft and *Centaur*/interstage adapter.

(4) Evaluate the adequacy of the spacecraft launch preparation, handling, and countdown procedures.

(5) Perform confidence tests as required.

The following success criteria shall be demonstrated to meet these test objectives:

(1) Satisfactory demonstration of compatibility of spacecraft electrical systems and ground support equipment during a simulated flight from launch through simulated *Centaur* retromaneuver, including operation of the payload.

(2) Demonstration of satisfactory operation of the telemetry, range safety, and pyrotechnic systems and recording of appropriate data.

(3) Evaluation of thrust vector control loop performance (guidance/autopilot test) of the *Atlas* stage and the *Centaur* stage for nulling, phase, and range during main engine gimbaling tests using ground hydraulic power.

(4) Demonstration of correct performance of the *Atlas* and *Centaur* engines with respect to frequency response and obtaining data on performance.

(5) Demonstration that the *Centaur* guidance and autopilot systems will initiate and functionally perform all programmed commands including commands crossing the *Centaur/Surveyor* interface and obtaining data on performance.

(6) Verification of adequacy and compatibility of AFETR mating and handling procedures.

(7) Verification of adequacy of the temperature control for the electronic equipment and spacecraft in a launch configuration and obtaining data on performance.

(8) Demonstration of satisfactory operation of the *Atlas* pneumatic system and pneumatically actuated or controlled valves in the propulsion system and obtaining data on performance.

(9) Demonstration of satisfactory operation of the *Centaur* pneumatic system including tank "burping."

A handling sequence for the encapsulated *Surveyor* spacecraft has been agreed upon as follows:

(1) Plugs-in test shall be performed with a flight nose fairing.

(2) Plugs-out test shall be performed with a "test" nose fairing.

The test nose fairing will be a flight-type nose fairing with access doors. The purpose of the test nose fairing is to simulate the flight nose fairing while providing access to the spacecraft during the CST plugs-out test. This access will be utilized to check stray energy monitors and replace squibs in the event a test rerun is necessary.

Test nose fairing design requirements, as follows, have been submitted:

(1) General. The basic structure, configuration, and characteristics shall be identical to the flight nose fairing. Deviations due to the access requirement may be made as required.

(2) Access Openings. Test fairing access openings shall be 34 in. wide and extend from *Centaur* station 75.00 to station 125.00 The four openings required shall be centered on the following locations:

(a) Quadrant IV, 10 deg from the +y axis in the x-y plane.

(b) Quadrant III, 50 deg from the −y axis in the x-y plane.

(c) Quadrant III, 40 deg from the −x axis in the x-y plane.

(d) Quadrant II, 30 deg from the +x axis in the x-y plane.

(3) RF Characteristics. The attenuation of RF signals below 5,000 mc shall be within 1 db of the attenuation of the respective areas on the flight nose fairing over 99% of the total surface area.

CONFIDENTIAL
UNCLASSIFIED

UNCLASSIFIED CONFIDENTIAL

(4) Air Conditioning. Air conditioning ducting identical to that provided by the flight nose fairing is required, except that the ducting may be interrupted when any or all access doors are open.

(5) Cleanliness. The test nose fairing with attaching entry hardware and two of the access doors open shall provide and assure cleanliness control equivalent to that provided by the spacecraft environmental control unit.

(6) Television Targets and Lighting. TV targets and lighting shall be installed as required for a flight nose fairing.

(7) Toxic Gas Detector Lines. Toxic gas detector lines shall be installed as required for a flight nose fairing.

A CST documentation tree was agreed on as follows:

(1) *Centaur* Unified Test Plan (UTP) for Combined System Test to be the top document, prepared by GD/A and approved by LeRC with coordination of JPL.

(2) The *Surveyor* Combined Systems Test Directive prepared by Hughes Aircraft Company, requirements to be included in a UTP section and details to be included in Joint Operational Plan (JOP).

(3) CST/JOP to be prepared by GD/A to detail the LeRC approved CST UTP and necessary joint operational requirements; to be approved by LeRC with coordination of JPL.

(4) Daily CST operational reports prepared by GD/A to identify problems with testing and schedule.

(5) Launch-on-time study results pertinent to CST scheduling and operations prepared by GD/A.

(6) Launch Operations schedule prepared by Hughes to show JPL/Hughes time spans required for complete sequence from arrival at CST to launch at ETR.

b. Cleanliness. A review of CST facility cleanliness has been jointly conducted by LeRC/JPL/GD-A/Hughes. During this review it has become evident that present facility provisions do not adequately protect spacecraft cleanliness. Recommendations have been provided by the CST Facility Cleanliness Review Committee. These recommendations are being reviewed by LeRC for cost and schedule impact.

The following recommendations represent minimal modifications deemed necessary to permit adequate control of the environment within the high-bay area containing an exposed *Surveyor* spacecraft.

(1) *Personnel access area.* At least one personnel access area, providing for access control to the high-bay area, is to be provided south of and exterior to high-bay area.

A second personnel access control area is desirable. This second area would be located adjacent to the GSE air lock.

Provisions and features of the access control areas are listed as follows:

(a) The access area will contain a personnel air shower similar to Madl Series 4000 manufactured by Glen Mart Co., Los Angeles.

(b) The access area will contain a "Shoe Scrubber" similar to model CV-1500/CV-9-M-S manufactured by Central Vac Corp. of Los Angeles.

(c) The access area will contain a clothing locker adequate for 30 personnel.

(d) The access area door leading into the high-bay area will be equipped with an electrical door latch (location of control to be determined later).

(e) A clear glass window (approximately 18 by 18 in.) will be located in the wall between the high-bay area and the area adjacent to the personnel access.

(f) A voice communication system will be located at the window (item e above). The system is to permit two-way conversation between the two areas. Some form of signal should be provided.

(g) All personnel doors leading to the high-bay area not equipped for personnel control as described above shall be restricted to use for emergency only.

(2) *GSE air lock.* To provide for control of equipment and hardware entering the high-bay area, an external addition to the building is required. This GSE air lock is to be located outside the present roll-up door.

Provisions and features of the air lock are as follows:

(a) Dimensions inside are to be 20 by 20 by 26 ft high.

(b) A centralized vacuum cleaning system is to be provided with outlets and flexible hoses provided in the air lock such that any point within the air lock can be reached.

UNCLASSIFIED CONFIDENTIAL

UNCLASSIFIED CONFIDENTIAL

(c) The floor of the air lock is to be sealed concrete. JPL will suggest sealant materials at a later date.

(d) Inside surfaces of walls and ceiling are to be finished with non-particle producing materials. Walls and ceiling are to be air-tight.

(e) The entrance door is to be 14 by 26 ft high positioned for straight-through passage to the existing high-bay door. The door should incorporate a seal design which will not allow dust to enter the air lock. Door finish is to be of a non-flaking material.

(f) Lighting is to be at least 50 ft-c generally all over the inside of the air lock.

(g) A concrete pad 20 by 20 ft is to be located outside the GSE air lock adjacent to the entrance door.

(h) A compressed (100 lb/in.^{2}) air outlet and a water outlet (utility) will be located outside the air lock at the concrete pad.

(3) *Vacuum system.* A central vacuum system is to be installed with service outlets (hose attachment points) in the GSE air lock, STEA area, Hughes stock room, and high-bay area. Service outlets shall be positioned such that, with the use of flexible vacuum hoses, any point within each of the areas may be reached, including walls.

c. Activation. An activation sequence consisting of two phase has been prepared for the CST (Fig. 113). This sequence will be utilized to prepare for T-21 operations. The first phase will be utilized to prepare for STEA/CDC installations scheduled for Phase II. Also, all Hughes Aircraft Company equipment interfacing with GD/A equipment will be installed during Phase I.

The Phase II activation activities must be accomplished prior to arrival of T-21 on site. Activities during this period are constrained by the available schedule time. During this period the major portion of the STEA/CDC will arrive on site for installation, calibration, checkout, and integration.

An activation directive is currently in preparation delineating in detail all information necessary for the activation operation.

2. Surveyor Operations Console Launch Control Rack

The three *Surveyor* operations consoles have been received and one (S/N 1) has been placed in the dynamic model configuration. The changes required to modify the console to dynamic model configuration included:

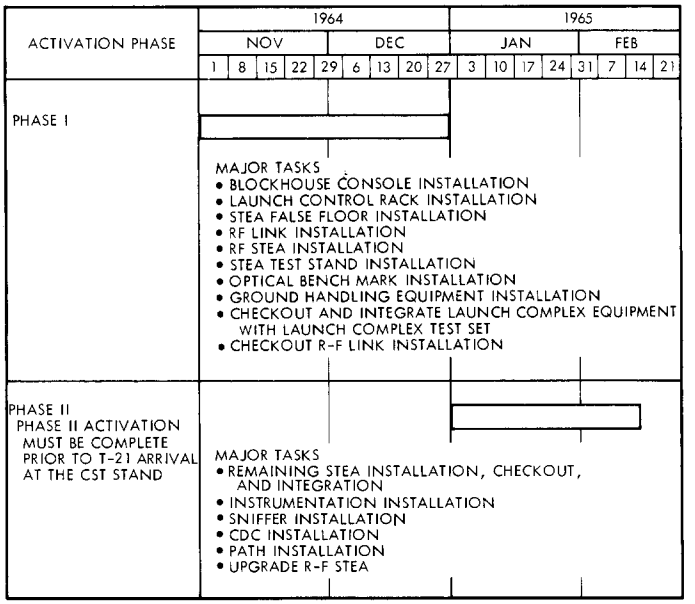
ACTIVATION PHASE
1964
1965
NOV
DEC
JAN
FEB
1 8 15 22 29 6 13 20 27 3 10 17 24 31 7 14 21
PHASE I
MAJOR TASKS
• BLOCKHOUSE CONSOLE INSTALLATION
• LAUNCH CONTROL RACK INSTALLATION
• STEA FALSE FLOOR INSTALLATION
• RF LINK INSTALLATION
• RF STEA INSTALLATION
• STEA TEST STAND INSTALLATION
• OPTICAL BENCH MARK INSTALLATION
• GROUND HANDLING EQUIPMENT INSTALLATION
• CHECKOUT AND INTEGRATE LAUNCH COMPLEX EQUIPMENT WITH LAUNCH COMPLEX TEST SET
• CHECKOUT R-F LINK INSTALLATION
PHASE II
PHASE II ACTIVATION MUST BE COMPLETE PRIOR TO T-21 ARRIVAL AT THE CST STAND
MAJOR TASKS
• REMAINING STEA INSTALLATION, CHECKOUT, AND INTEGRATION
• INSTRUMENTATION INSTALLATION
• SNIFFER INSTALLATION
• CDC INSTALLATION
• PATH INSTALLATION
• UPGRADE R-F STEA

Fig. 113. CST activation schedule

(1) Deletion of the safety panel.

(2) Installation of the control and monitor panel.

(3) Installation of a digital voltmeter.

(4) Installation of the ready-to-launch panel.

(5) Wiring modifications.

Drawings reflecting the console configurations are being released. Design of the console has been directed to simplify the problems associated with incorporating design changes. All interface cabling connectors have many leads to the terminal boards. If a signal must be picked up or moved, it requires a relatively simple terminal board change. In the dynamic model configuration, the control and monitor panel provides hardline commands to the spacecraft. These commands include "transponder on/off" and "transponder high/low power."

The DVM provides a readout of battery pressure, and the ready-to-launch panel provides a signal to the GD/A launch control ladder circuitry permitting completion of the launch vehicle commit sequence.

The safety panel is not required for dynamic models. Its functions, applicable to operational *Surveyors* A-21 and A-21A), are as follows:

(1) Command and monitor main retro safe/arm mechanism.

CONFIDENTIAL UNCLASSIFIED

UNCLASSIFIED
CONFIDENTIAL

(2) Monitor main retro igniter squibs.

(3) Monitor liquid propellant leakage.

(4) Control TV target illumination.

(5) Provide emergency release of high pressure gases.

The power panel will remain in operational *Surveyor* configuration. This panel monitors and controls the prelaunch power supplies in the battery and solar panel simulator modes. The solar panel simulator portion of the console will be inoperable for dynamic models as this supply is not utilized.

The S/N 1 launch control rack has completed fabrication in dynamic model configuration. In this configuration the solar panel simulator has been deleted and some wiring modifications have been made. Again, terminal boards have been utilized to readily accommodate design changes. This rack is currently undergoing configuration and workmanship inspection.

Interface testing between the *Surveyor* operations console and the launch control rack has been accomplished. A test breakout box has been provided that enables insertion of line and load impedances that test the effect of launch complex cabling impedances on the required signal characteristics. This testing has revealed a few design changes in the console and rack that have been incorporated.

The console, rack, and necessary technical data are currently in preparation for buy-off and shipment to AFETR. This equipment will be installed in Launch Complex 36 to support the launches of dynamic models SD-1 and SD-2. Prior to the launch of SC-1, the console and rack will be returned to operational *Surveyor* configuration by on-site modification.

3. Surveyor Operations Scheduling

During this reporting period the Launch Operations J-FACT (Joint Flight Acceptance Composite Test), CST, and AFETR operations sequences have been in process of coordination. The Hughes Aircraft Company version of the operations schedule (Fig. 114) has been distributed to JPL/LeRC/GD/A. This schedule depicts a 100-day operations sequence and will be utilized to establish a baseline schedule for SC-1, A/C-7.

The schedule details of the CST operation have been agreed upon. The CST operation will comprise a 20-day spacecraft sequence and a 45-day *Atlas/Centaur* sequence. The *Atlas/Centaur* sequence includes the period of time required for T-21 verification and proofing runs.

4. Dynamic Model Transponder Compatibility Test

The dynamic model transponder was tested for compatibility with the Deep Space Instrumentation Facility at the Goldstone tracking station (Pioneer site). Participating personnel included the Hughes Aircraft Company SD-1 test team and JPL personnel. DSIF operations were handled by the regularly assigned Bendix personnel. The Hughes Aircraft Company command and data handling console is not utilized on the Dynamic Model Program.

The SD-2 transponder was located in a screen room about 6 mi from the Pioneer Station with transponder output radiated from a dish on a tower outside the screen room. Hills blocking the line of sight between this dish and the Pioneer Station antenna necessitated utilizing a passive repeater on the collimating tower to provide the RF link. A block diagram of the test setup in the screen room is shown in Fig. 115 and the test area is illustrated in Fig. 116.

Testing was begun on September 30. Because the DSIF maser was not available at the start of the test period, the procedure was performed in a different sequence than originally planned. The RF link was calibrated utilizing a DSIF test transponder. The down-link test portion of the procedure was omitted and the testing proceeded with the up-link tests. The following day, because of doubts concerning the validity of the link calibration, this phase was repeated utilizing an S-band signal generator as well as the DSIF test transponder. It was found that the previous down-link calibration was in error because of a mistaken assumed power output of the DSIF test transponder. Following the link recalibration, the up-link tests were completed. A block diagram of the entire link with the path losses is included in Fig. 117.

On the third day of testing, direct communications with the spacecraft omnidirectional antenna was satisfactorily completed. Work proceeded with the down-link tests utilizing the paramp in place of the maser. Later, the telemetry portion of the down-link tests was repeated with the maser. Threshold and acquisition tests were repeated using the maser, and some unscheduled tests to investigate problem areas were performed completing the compatibility test.

A preliminary analysis of the data and observation of the testing indicates several problem areas as discussed

UNCLASSIFIED
CONFIDENTIAL

UNCLASSIFIED
CONFIDENTIAL

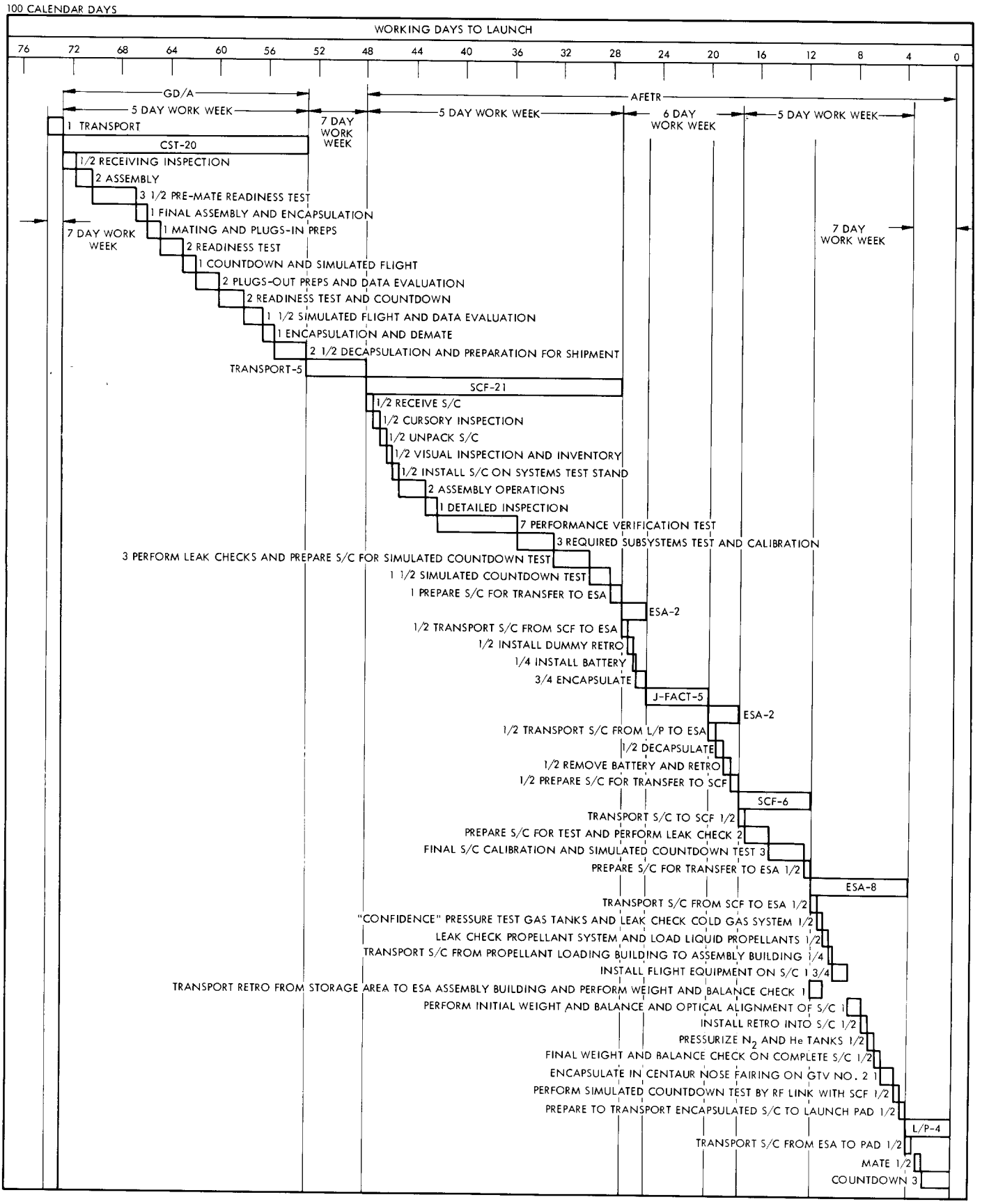
100 CALENDAR DAYS
WORKING DAYS TO LAUNCH
76 72 68 64 60 56 52 48 44 40 36 32 28 24 20 16 12 8 4 0
GD/A
5 DAY WORK WEEK
7 DAY WORK WEEK
AFETR
5 DAY WORK WEEK
6 DAY WORK WEEK
5 DAY WORK WEEK
1 TRANSPORT
CST-20
1/2 RECEIVING INSPECTION
2 ASSEMBLY
3 1/2 PRE-MATE READINESS TEST
1 FINAL ASSEMBLY AND ENCAPSULATION
1 MATING AND PLUGS-IN PREPS
2 READINESS TEST
1 COUNTDOWN AND SIMULATED FLIGHT
2 PLUGS-OUT PREPS AND DATA EVALUATION
2 READINESS TEST AND COUNTDOWN
1 1/2 SIMULATED FLIGHT AND DATA EVALUATION
1 ENCAPSULATION AND DEMATE
2 1/2 DECAPSULATION AND PREPARATION FOR SHIPMENT
TRANSPORT-5
SCF-21
1/2 RECEIVE S/C
1/2 CURSORY INSPECTION
1/2 UNPACK S/C
1/2 VISUAL INSPECTION AND INVENTORY
1/2 INSTALL S/C ON SYSTEMS TEST STAND
2 ASSEMBLY OPERATIONS
1 DETAILED INSPECTION
7 PERFORMANCE VERIFICATION TEST
3 REQUIRED SUBSYSTEMS TEST AND CALIBRATION
3 PERFORM LEAK CHECKS AND PREPARE S/C FOR SIMULATED COUNTDOWN TEST
1 1/2 SIMULATED COUNTDOWN TEST
1 PREPARE S/C FOR TRANSFER TO ESA
ESA-2
1/2 TRANSPORT S/C FROM SCF TO ESA
1/2 INSTALL DUMMY RETRO
1/4 INSTALL BATTERY
3/4 ENCAPSULATE
J-FACT-5
ESA-2
1/2 TRANSPORT S/C FROM L/P TO ESA
1/2 DECAPSULATE
1/2 REMOVE BATTERY AND RETRO
1/2 PREPARE S/C FOR TRANSFER TO SCF
SCF-6
TRANSPORT S/C TO SCF 1/2
PREPARE S/C FOR TEST AND PERFORM LEAK CHECK 2
FINAL S/C CALIBRATION AND SIMULATED COUNTDOWN TEST 3
PREPARE S/C FOR TRANSFER TO ESA 1/2
ESA-8
TRANSPORT S/C FROM SCF TO ESA 1/2
"CONFIDENCE" PRESSURE TEST GAS TANKS AND LEAK CHECK COLD GAS SYSTEM 1/2
LEAK CHECK PROPELLANT SYSTEM AND LOAD LIQUID PROPELLANTS 1/2
TRANSPORT S/C FROM PROPELLANT LOADING BUILDING TO ASSEMBLY BUILDING 1/4
INSTALL FLIGHT EQUIPMENT ON S/C 1 3/4
TRANSPORT RETRO FROM STORAGE AREA TO ESA ASSEMBLY BUILDING AND PERFORM WEIGHT AND BALANCE CHECK 1
PERFORM INITIAL WEIGHT AND BALANCE AND OPTICAL ALIGNMENT OF S/C 1
INSTALL RETRO INTO S/C 1/2
PRESSURIZE N_2 AND He TANKS 1/2
FINAL WEIGHT AND BALANCE CHECK ON COMPLETE S/C 1/2
ENCAPSULATE IN CENTAUR NOSE FAIRING ON GTV NO. 2 1
PERFORM SIMULATED COUNTDOWN TEST BY RF LINK WITH SCF 1/2
PREPARE TO TRANSPORT ENCAPSULATED S/C TO LAUNCH PAD 1/2
L/P-4
TRANSPORT S/C FROM ESA TO PAD 1/2
MATE 1/2
COUNTDOWN 3
7 DAY WORK WEEK
7 DAY WORK WEEK

Fig. 114. Launch operations, J-FACT and CST for SC-1

CONFIDENTIAL
UNCLASSIFIED

UNCLASSIFIED
CONFIDENTIAL

below. None of these were entirely unexpected and, in general, the tests went smoothly and should be termed successful.

(1) In one-way lock (spacecraft to DSIF), undesired modulation is present on the spacecraft signal. This modulation results in carrier suppression of up to 9 db which reduces the acquisition margin. This modulation is evidently the result of interaction between the receiver voltage-controlled crystal oscillator and the transmitter narrow-band voltage-controlled crystal oscillator as it disappears when two-way lock (transmitter narrow-band voltage-controlled crystal oscillator disabled) is achieved or the receiver is disconnected (receiver voltage-controlled crystal oscillator removed) from the transmitter. Elimination of this problem by

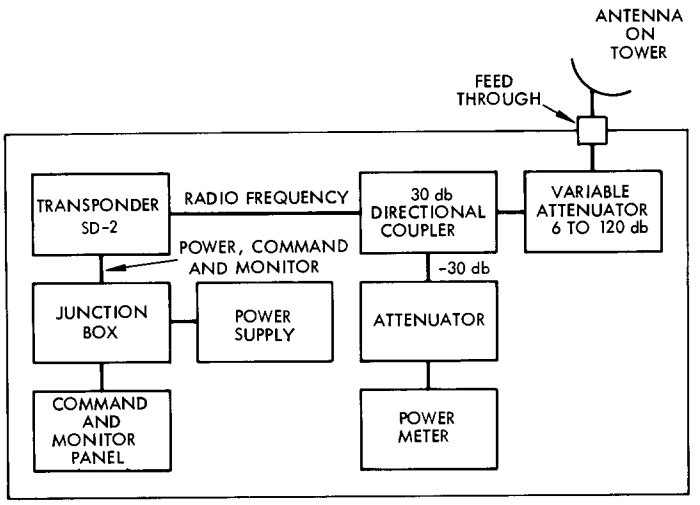

Fig. 115. Screen room setup for transponder test

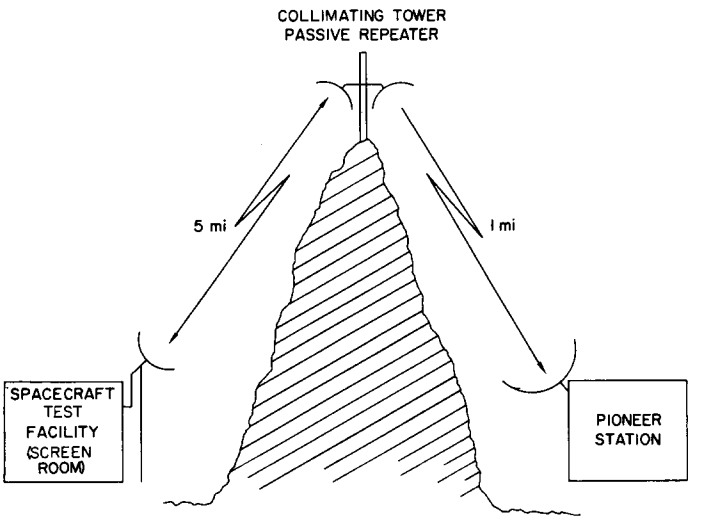

Fig. 116. Transponder test area

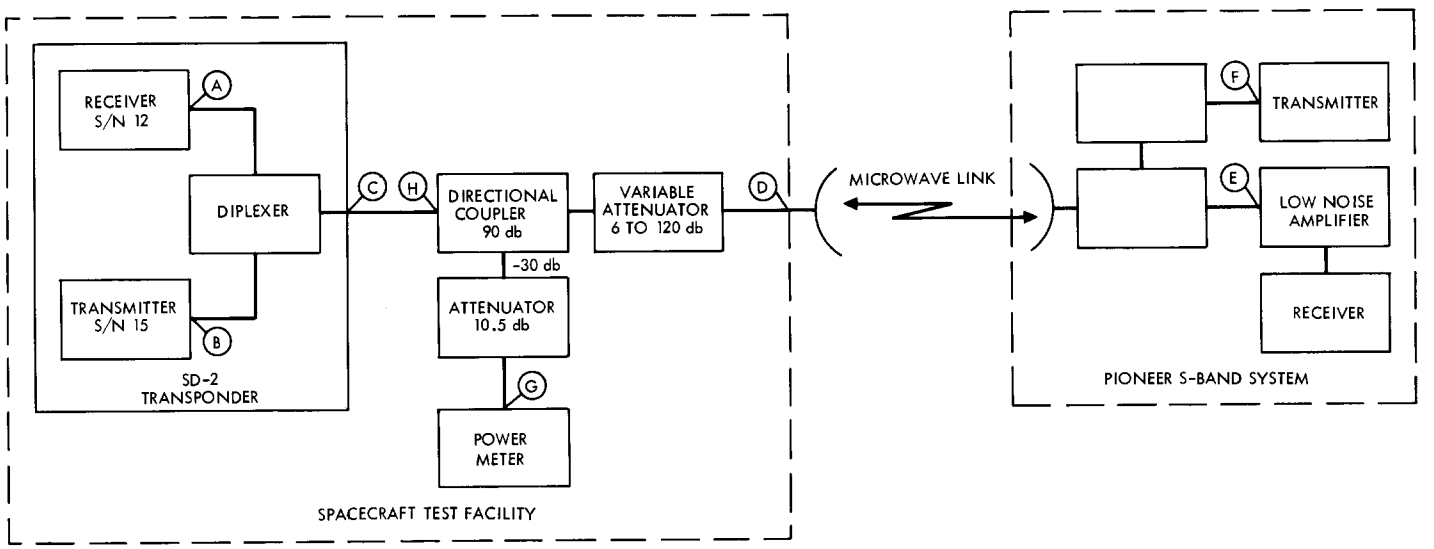

PATH LOSSES

A TO C	1.5 db AT 2113 mc	D TO E	115 db AT 2295 mc
B TO C	1.3 db AT 2295 mc	D TO F	120 db AT 2113 mc
C TO H	0.6 db	*C TO E	128.6 db AT 2295 mc
C TO G	41.1 db	*C TO F	132.0 db AT 2113 mc
C TO D	13.6 db AT 2295 mc 12.0 db AT 2113 mc	*VARIABLE ATTENUATOR	10 db ON DIAL 13 db ACTUAL AT 2295 mc 11.5 db ACTUAL AT 2113 mc

Fig. 117. RF link path losses

CONFIDENTIAL
UNCLASSIFIED

providing more isolation between the receiver and the transmitter is being studied. The modulation frequency drifted between 40 and 100 cps at S-band with the first order sidebands being about 5 db above the carrier with 70 cps and 4 db below the carrier with 95 cps. An effort to determine how much more isolation is needed to eliminate the problem revealed that about 10 db additional was sufficient. However, since the cable between the receiver and transmitter is a frequency determining component of the transmitter narrow-band voltage-controlled crystal oscillator, the attenuation placed in this cable to determine how much additional isolation is necessary could have changed the oscillator frequency resulting in undesired modulation. Therefore, the validity of the inserted 10-db figure is doubtful.

(2) With very high input levels at the spacecraft receiver (about −50 dbm) the receiver locked up when the DSIF transmitter was not at center frequency. It has not been determined whether this is due to receiver overload or transmitter spurs. It is doubtful that signals of this magnitude will be seen by the spacecraft in flight and at reasonable signal levels (below −80 dbm), this anomaly did not appear.

(3) The telemetered static phase error voltage utilizes only about 1.5 v of the allotted 5-v range and the subcarrier oscillator uses only about 5.5 cps of the full 16 cps allotted peak-to-peak deviation. In addition, center frequency does not result in 2.5 v or 560 cps, but in 1.92 v or 558.5 cps. This is a direct result of the telemetry drive voltage from the receiver not having the theoretical 5-v range. As a result of not using the full assigned deviation, it is probable that telemetry threshold will be below that expected.

(4) The output connector of the traveling-wave tube became very hot after long periods (greater than 30 min) of high power operation whereas there were no other apparent hot spots. The TWT itself was only warm to the touch. Several halts were called to allow this connector to cool during the course of the tests. Cool down time was relatively short (less than 5 min).

(5) The power output of the transponder appeared to decrease by about 1.5 db after some period of operation. This decrease was evidently not attributable to the TWT, as high power was a constant 20 db greater than low power in both cold and hot conditions. This phenomena could possibly have been a result of the power meter heating up as it was constantly measuring the output power (see Fig. 115). No second (cold) power meter was available to check this.

All other tests were performed without difficulty. These included transmission through the spacecraft omnidirectional antenna, simulation of spacecraft tumble, spacecraft receiver threshold, acquisition, spectrum, phase jitter, and telemetry tests.

5. Microwave Installation and Test

The installation and testing activity on the Air Force Eastern Test Range microwave link is discussed below.

a. Installation.

(1) *Spacecraft Checkout Facility.* Installation at the AO and AM building is complete (see Fig. 118 and 119). The following changes were made in this area:

(a) The 55 ft of styroflex originally to be used on gantry 36B will be spliced to the last section of cable (within the high-bay area) to complete the link between the antenna and the RF test rack.

(b) The 110 ft of styroflex, fabricated as the last section within the high-bay area, was longer than required. This section was installed between the AO and AM Buildings to be used during dynamic model tests, and replaces the

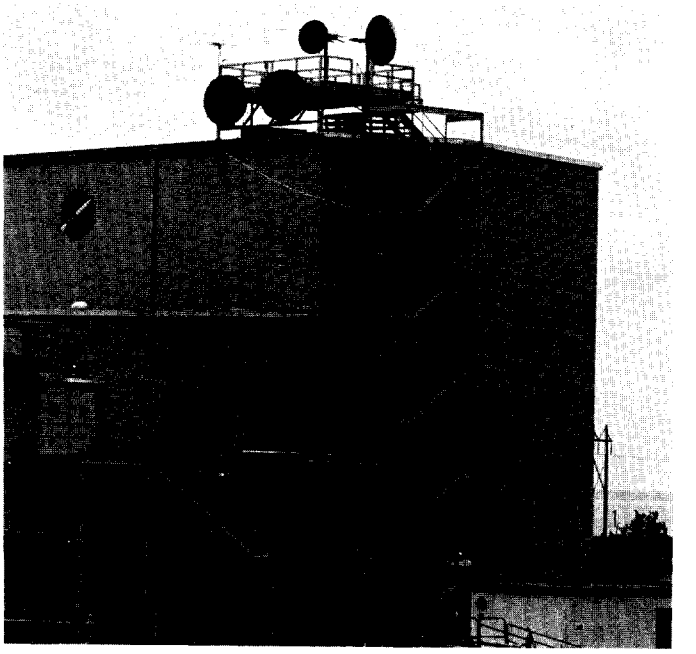

Fig. 118. Antenna platform on building AO at AFETR

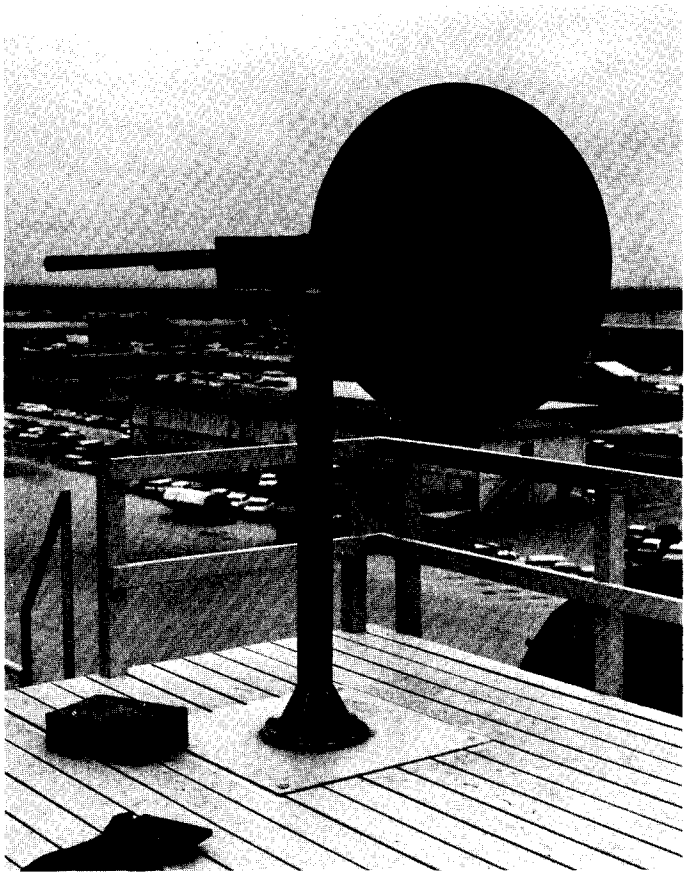

Fig. 119. Hughes trainable antenna on building AO at AFETR

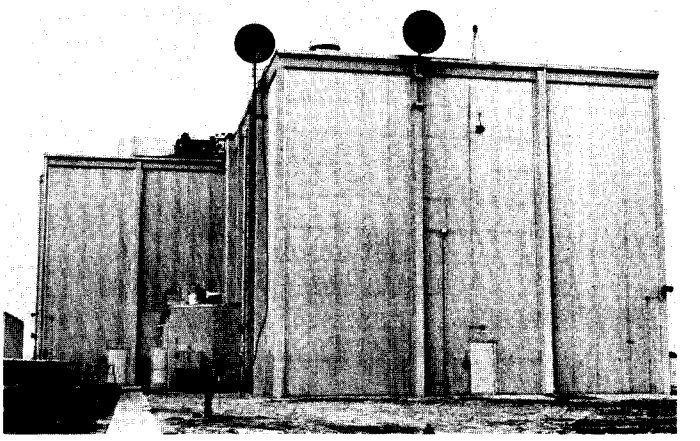

Fig. 120. Final assembly building with Hughes antenna installed

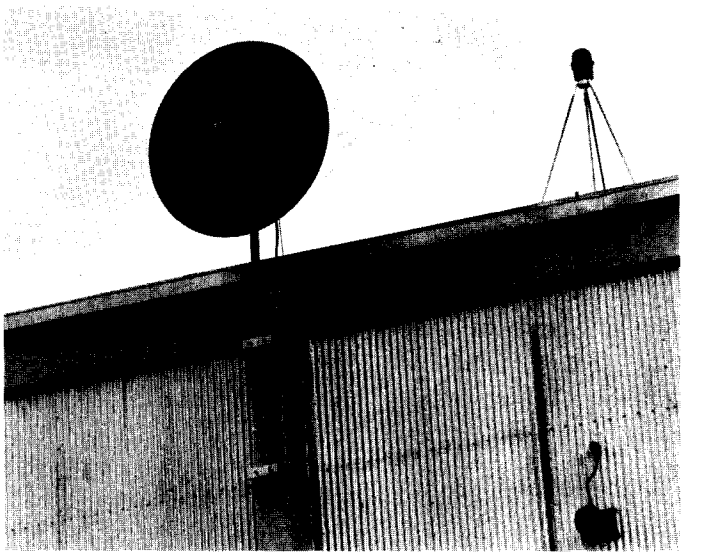

Fig. 121. Antenna installation on ESA final assembly building

55-ft high-bay section of cable during these tests. Both the 110-ft section and the 55-ft section are spliced at the same point to the cable running to the antenna.

(2) *Gantry 36A.* Installation at this gantry is complete. The following change was made in this area: GD/A supplied Hughes with approximately 60 ft of Heliax cable to replace the Hughes 55-ft length of styroflex which could not be installed through the limited accesses within the gantry.

(3) *Gantry 36B.* Installation at this gantry was cancelled by GD/A. Present planning is to schedule all launches from 36A. One 6-ft antenna, antenna mount, and feed will be stored.

(4) *Explosive Safe Area.* The installation of the link at the ESA is complete except for the terminations of the cables (see Fig. 120 and 121). The following changes were made at the ESA:

(a) The cable from the antenna to Laboratory 3 was run down the outside of the building and into the laboratory through a conduit rather than running the cable through the roof and down the inside of the building.

(b) The 55 ft of styroflex originally to be used on 36A will be used as a jumper at the ESA in Laboratory 2 or 3 or the Propellant Laboratory.

b. Testing.

Spacecraft Checkout Facility. Communication between level 12 of gantry 36A and the AO antenna platform was established with the Missile Technical Operations Communication System (MITOC). Channel 19 on the AO/MITOC is connected to Selector Switch 12 on the 36A/

UNCLASSIFIED

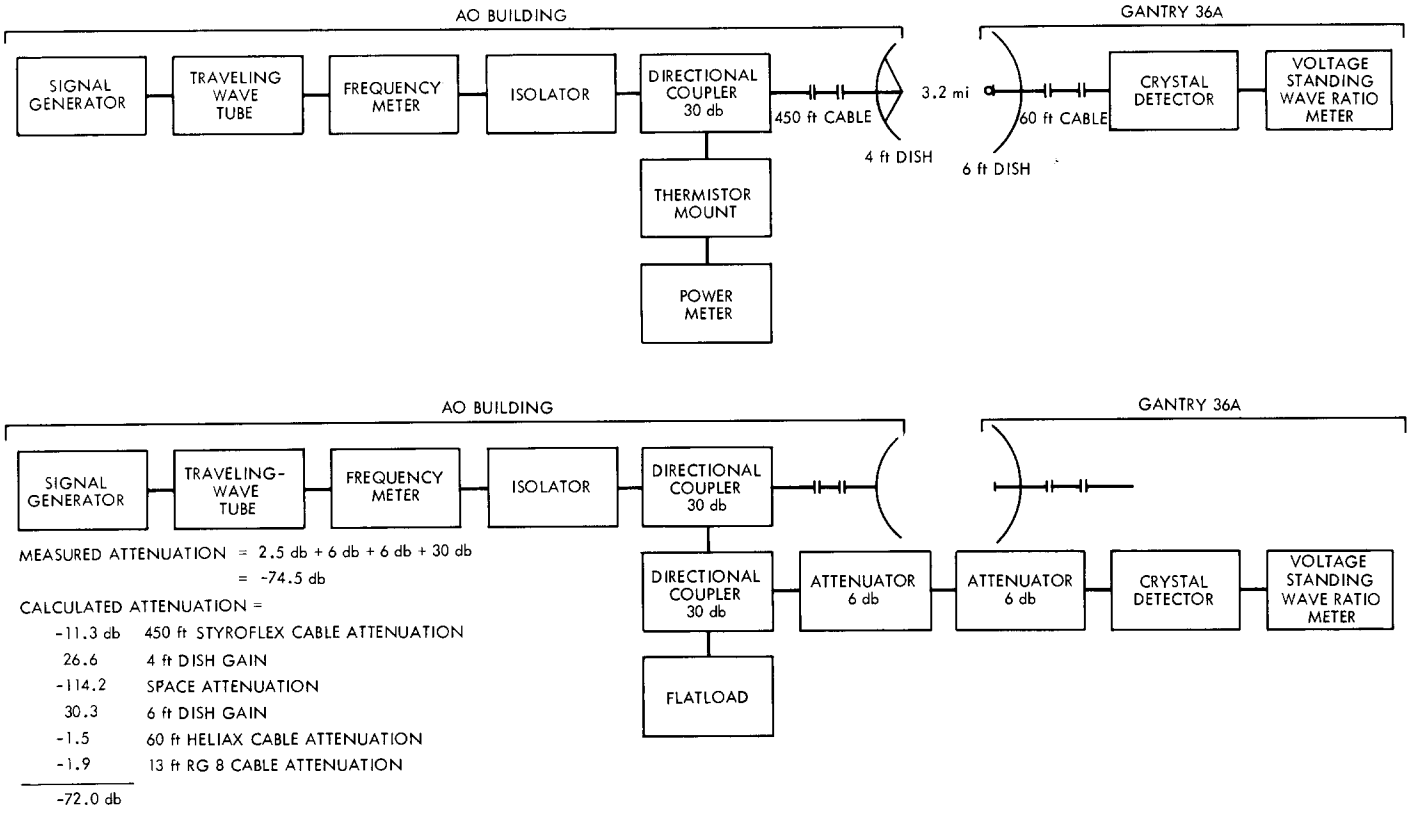

Fig. 122. Microwave link attenuation test, Eastern Test Range

Missile Operations Paging System. JPL will provide assistance to Hughes Aircraft Company in obtaining the necessary communication links at JPL facilities. GD/A will provide this assistance at 36A.

Alignment of the AO to 36A link was accomplished with the MITOC system, rather than walkie-talkies which were also available. The beam width of the 4-ft dish was approximately 6 deg. The gain remained constant within this beam width and dropped off rapidly outside this limit. The optical sight on the 4-ft dish was able to obtain the center point of this beam width when sighted at gantry 36A, 3.2 mi away.

The attenuation through the link between the cable termination in the AM building and the cable termination at gantry 36A was measured using RF substitution. The circulator on the 4-ft dish was bypassed. The antenna radiated a vertically polarized field to the gantry at 2295 mc. The measured attenuation was 74.5 db, and the calculated attenuation was 70.1 db (see Fig. 122). A complete calibration should be conducted on the total link when the RF test rack is available.

UNCLASSIFIED

UNCLASSIFIED
CONFIDENTIAL

M. Support of Study on Critical Data Recorder

During the 2-mo period ending in mid-September, Hughes provided technical support to the Aeronutronics Division of Philco Corporation (ADP) in their study of a critical data recorder (CDR) for installation on the Surveyor spacecraft. The purpose of the CDR is to sense and transmit back to Earth various data regarding the structural integrity and angular orientation of the spacecraft after landing. The CDR is intended to perform this function even with the occurrence of a landing hard enough to render the spacecraft totally inoperative because of structural failures. The CDR package must therefore be designed (within limitations of weight and volume) to withstand a considerably higher level of shock and impact loading than the spacecraft is expected to encounter.

The Hughes effort consisted of coordination with JPL and ADP on all aspects of the study that related to the spacecraft, including CDR mounting, data channel assignments, shock and vibration loads transmitted to the CDR, CDR thermal environment and interaction with the spacecraft RF radiation exposure, and a breakwire system on the spacecraft to sense structural failures. The effects of the CDR on spacecraft system test and operations were studied, and comments were offered on the ADP study report. The Hughes participation is described in the report SSD 4442R, September 1964, *Support of Critical Data Recorder Study for Surveyor Spacecraft*, Hughes Aircraft Company. The Hughes effort is summarized below.

1. Physical Design and Installation Considerations

As a result of coordination among ADP, JPL, and Hughes, the following basic requirements were established to govern the installation of the CDR on the spacecraft:

(1) The CDR package shall be installed as close as possible to the strongest and most rigid portions of the spaceframe in a manner that will minimize the length and weight of the supporting substructure. This is intended to maximize the probability of CDR survival in the event of a hard landing.

(2) The mounting location of the CDR on the spaceframe shall be selected such that removal or relocation of normal spacecraft elements is not required to permit CDR installation. It is desired that installation and removal of the CDR be possible without need for temporary detachment of any normal spacecraft elements.

(3) The placement of the CDR upon the spaceframe shall, insofar as possible, result in an acceptable spacecraft center-of-gravity location for all of the likely CDR/spacecraft equipment offloading combinations.[a]

(4) The CDR package shall be located such that at least part of its surface receives full solar illumination when the spacecraft is in its nominal transit attitude.

(5) The CDR mounting location and method shall be chosen to minimize the conductive and radiative heat transfer in either direction between the CDR and the spacecraft.

To achieve the best tradeoff among these requirements, several locations were considered for installation of the CDR. It was generally recognized that for lateral center-of-gravity purposes the CDR should be installed somewhere on or near the payload sector (Sector 2), and all locations examined were within this sector. Consideration was given to mounting of the CDR at either end of the payload sector near the apex of the triangle formed by the three upper main spaceframe members. This location was potentially attractive from a structural viewpoint because of its close proximity to several major structural members which meet in a cluster. Mounting of the CDR above the upper spaceframe cluster at either end of the payload sector is unacceptable because of blockage of the radiation pattern from either Compartment A or Compartment B as well as being undesirable from both a solar illumination and radio frequency radiation standpoint. Consideration was given to mounting of the CDR in a position just below the upper spaceframe cluster on either end of the payload sector. This position, in an area between the outer surface of the main retro-engine and the inner surfaces of the tubular members in the cluster, limited the CDR envelope to either an unacceptably small volume or one that was oddly shaped. Other than improvement resulting from the reduction in blockage of the compartment radiation pattern, this location suffers from all of the disadvantages of the previous position and, if anything, the RF radiation problem is worse.

The final CDR mounting position selected for this study, although located at a greater distance from a

[a]Items of spacecraft equipment potentially available for removal to help compensate for the weight increase caused by the addition of the CDR as a payload item.

CONFIDENTIAL
UNCLASSIFIED

UNCLASSIFIED
CONFIDENTIAL

main spaceframe cluster, is superior in all other respects to the corner locations. The position selected is located in the center of Sector 2 directly on the Y-axis at a point just above and somewhat inboard from the nitrogen tank. This position permits the CDR to receive almost full solar illumination during transit; it does not interfere with moving elements such as the landing gear and omnidirectional antenna booms; is reasonably free from blockage of RF radiation by the planar array antenna or solar panel; and is nearly optimum from the standpoint of spacecraft lateral center-of-gravity control in combination with the various spacecraft equipment downloading options. The position chosen permits the CDR to be mounted on four supporting struts of minimum length, minimum weight, and maximum strength and rigidity. The four struts are arranged such that their center lines pass through the CDR center of gravity for maximum strength and rigidity in the presence of high landing loads. The close proximity of the CDR to the spaceframe afforded by this arrangement results in essentially no additional blockage of the view from survey TV Camera 3.

The details of CDR mounting and mechanical interfaces with the spacecraft were negotiated with ADP in August. The configuration later proposed by ADP has certain dimensional differences from the negotiated configuration, but it appears capable of integration with the spacecraft with minor design changes. The installation proposed by ADP is shown in Fig. 123 and Fig. 124, and the effects of shadowing of the CDR by the planar antenna and solar panel are shown in Fig. 125.

The shadow patterns of Fig. 125, based on the nominal transit phase orientation of the spacecraft, also provide a crude indication of RF radiation blockage by the solar panel and planar array antenna during the time when the CDR is transmitting. By noting this shadow pattern, recognizing that the planar array/solar panel combination is free to rotate about the spacecraft roll axis after landing, it can be seen when comparing this pattern with the spacecraft general arrangement drawings that there are no other positions on the spaceframe free from interference by the omnidirectional antenna boom and landing legs which afford less interference with the RF radiation pattern from the CDR to earth.

While the CDR installation described in the final ADP report has dimensional differences from the installation negotiated in August and shown here, it appears capable of integration with the spacecraft with minor design changes.

Table 46 shows weight and balance data for the A-21 spacecraft, the effects of adding the CDR, and data for adding the CDR in conjunction with various offloadings of payload items to compensate the weight increase.

2. *Breakwire System*

A preliminary design was performed on a breakdown system for use in conjunction with the CDR. The more important requirements of the breakwire system are as follows:

(1) Provide a positive indication of structural failure of the instrumented spacecraft part and at the

Table 46. Weight and balance data for *Surveyor* Model A-21 with critical data recorder

Configuration description	Basic bus	Engineering payload	Lateral center of gravity			Injected weight[a]	Dry landed weight	Usable propellant		
			X	Y	R			Vernier	Retro	Bouyancy
Model A-21 on September 2, 1964	698.82	62.18	0.03	—0.11	0.11	2157.71	596.40	161.40	1234.50	0.81
Add CDR[b]	698.82	75.57	0.02	—0.43	0.43	2196.20	609.79	163.50	1257.50	0.81
Add CDR less TV4	698.44	75.57	—0.27	—0.14	0.30	2169.42	600.41	162.10	1241.50	0.81
Add CDR less TV3	698.82	55.92	—0.40	0.20	0.45	2140.05	590.14	160.50	1224.00	0.81
Add CDR less auxiliary battery system	698.82	47.44	—0.10	0.90	0.91	2116.27	581.66	159.20	1210.00	0.81
Add CDR less certain items of engineering instrumentation[c]	698.82	63.03	0.46	—0.43	0.63	2160.26	597.25	161.60	1236.00	0.81

[a] No contingency.
[b] Weight of CDR installation includes 11.44-lb critical data recorder unit, 1.35-lb harness (including sensors), and 0.6-lb substructure.
[c] Includes the auxiliary engineering signal processor, four accelerometers and amplifiers, seven strain gages, ten temperature sensors, and two current shunts.

UNCLASSIFIED
CONFIDENTIAL

UNCLASSIFIED
CONFIDENTIAL

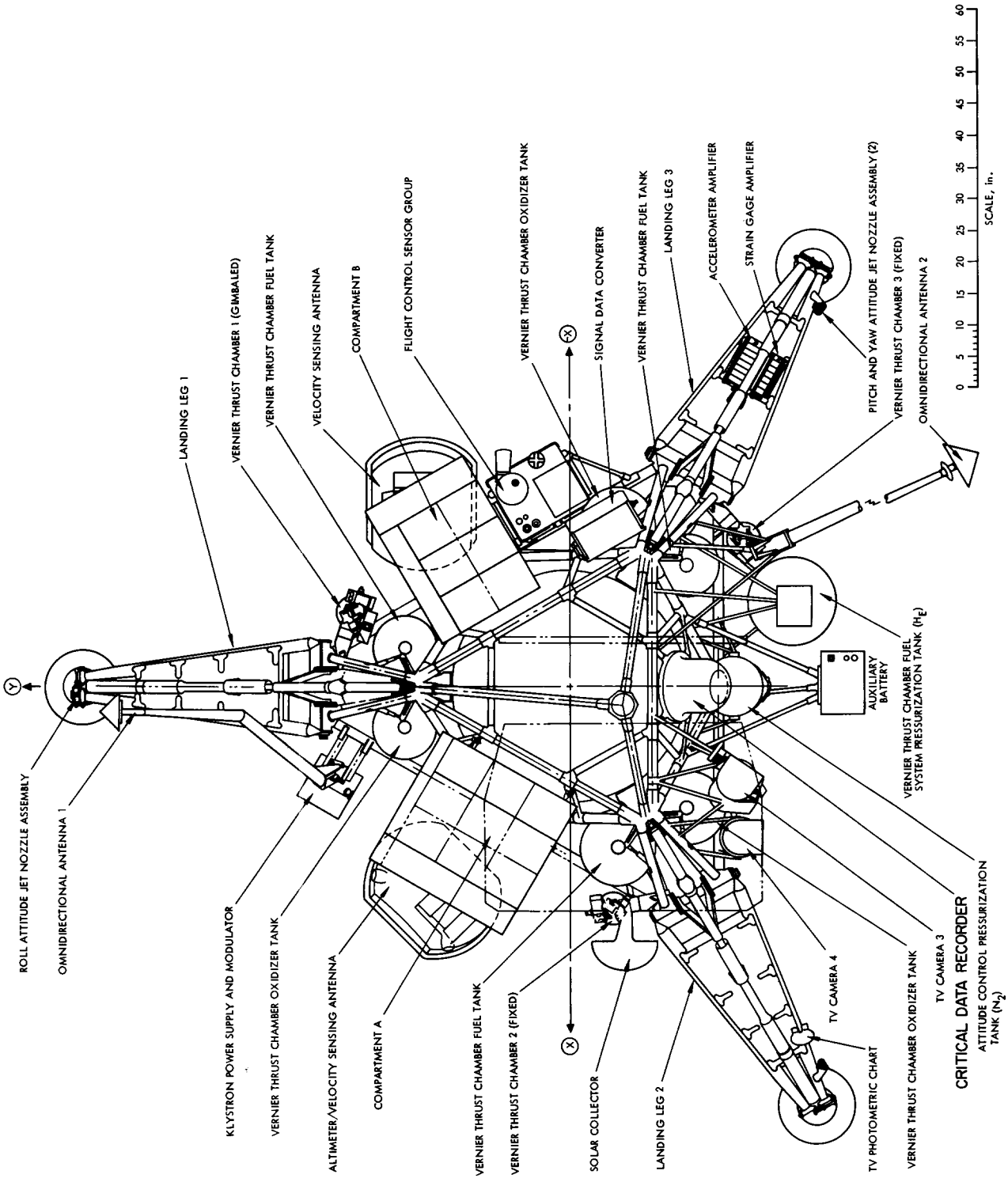
ROLL ATTITUDE JET NOZZLE ASSEMBLY
OMNIDIRECTIONAL ANTENNA 1
KLYSTRON POWER SUPPLY AND MODULATOR
VERNIER THRUST CHAMBER OXIDIZER TANK
ALTIMETER/VELOCITY SENSING ANTENNA
COMPARTMENT A
VERNIER THRUST CHAMBER FUEL TANK
VERNIER THRUST CHAMBER 2 (FIXED)
SOLAR COLLECTOR
LANDING LEG 2
TV PHOTOMETRIC CHART
VERNIER THRUST CHAMBER OXIDIZER TANK
TV CAMERA 3
TV CAMERA 4
CRITICAL DATA RECORDER
ATTITUDE CONTROL PRESSURIZATION TANK (N_2)
VERNIER THRUST CHAMBER FUEL SYSTEM PRESSURIZATION TANK (H_2)
AUXILIARY BATTERY
LANDING LEG 1
VERNIER THRUST CHAMBER 1 (GIMBALED)
VERNIER THRUST CHAMBER FUEL TANK
VELOCITY SENSING ANTENNA
COMPARTMENT B
FLIGHT CONTROL SENSOR GROUP
VERNIER THRUST CHAMBER OXIDIZER TANK
SIGNAL DATA CONVERTER
VERNIER THRUST CHAMBER FUEL TANK
LANDING LEG 3
ACCELEROMETER AMPLIFIER
STRAIN GAGE AMPLIFIER
PITCH AND YAW ATTITUDE JET NOZZLE ASSEMBLY (2)
VERNIER THRUST CHAMBER 3 (FIXED)
OMNIDIRECTIONAL ANTENNA 2
0 5 10 15 20 25 30 35 40 45 50 55 60
SCALE, in.
MIDCOURSE CONFIGURATION
ANTENNA AND SOLAR PANEL POSITIONER HAS BEEN OMITTED FROM THIS VIEW FOR CLARITY

Fig. 123. Spacecraft general arrangement with proposed CDR design

CONFIDENTIAL
UNCLASSIFIED

UNCLASSIFIED
CONFIDENTIAL

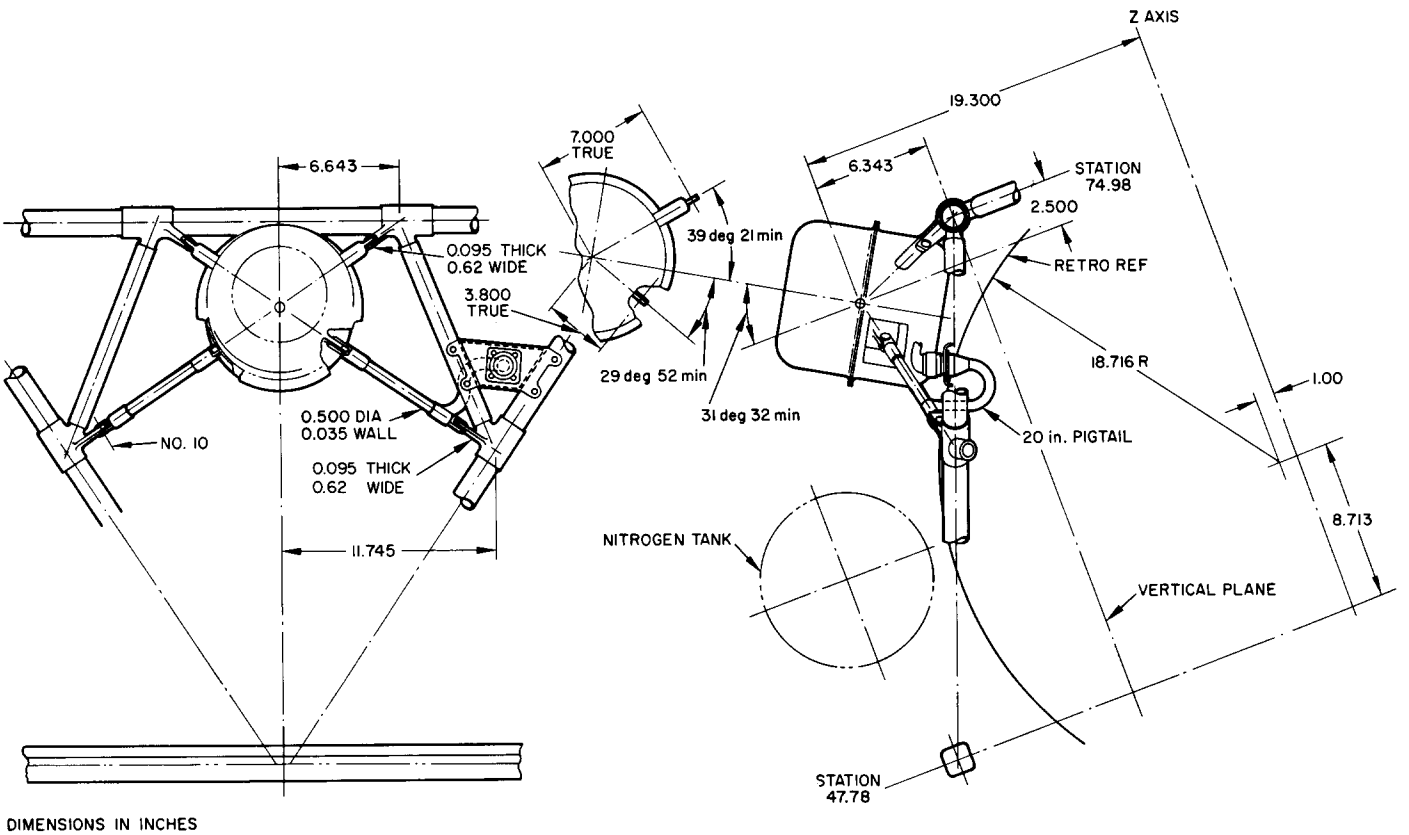

Fig. 124. CDR installation

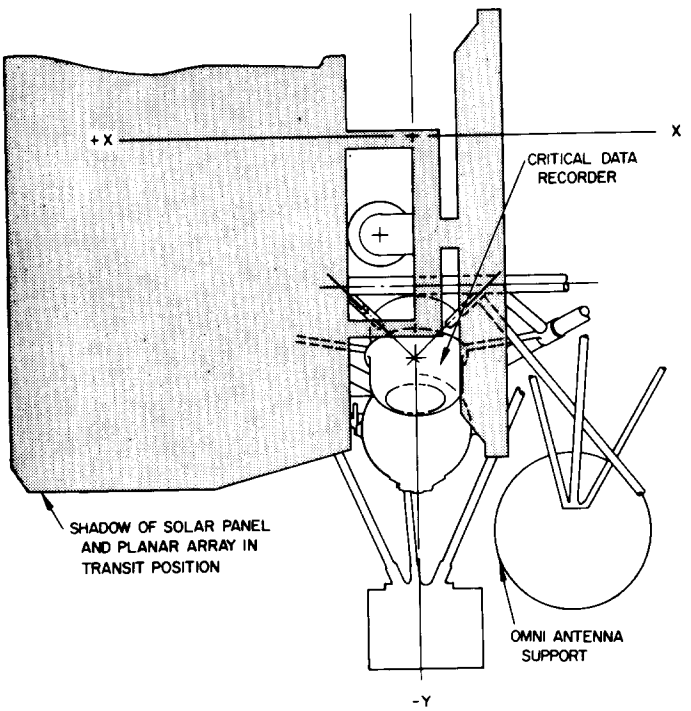

Fig. 125. Shadow pattern on proposed CDR and payload sector for nominal transit

same time be capable of withstanding all vibrational, thermal, and shock environments encountered in a normal *Surveyor* launch and landing.

(2) Permit normal unobstructed operation of all spacecraft moving parts.

(3) Cause minimal effect on spacecraft thermal performance.

(4) Permit the normal installation and removal of the various control items on the spacecraft without degrading the integrity of the breakwire system.

(5) Produce very small effects on the weight and balance of the spacecraft.

The list of breakwire sensors agreed upon by ADP, JPL, and Hughes appears in Table 47. Hughes investigated the placement of the sensors on each item based on a preliminary assessment of the most probable failure mode. The recommended sensor placement appears in Table 47.

a. Sensor design. For all sensors except the crushable block and shock absorber gas cylinder, the devices have been conceived as lengths of conductive material secured to the structure in question so as to guarantee a

UNCLASSIFIED
CONFIDENTIAL

UNCLASSIFIED
CONFIDENTIAL

Table 47. Breakwire sensor list

Sensor number	Item instrumented	Remarks
1	Compartment A support	These six sensors are similar. Each is to run the full length of the particular compartment supporting member to which it is applied.
2	Compartment A support	
3	Compartment A support	
4	Compartment B support	
5	Compartment B support	
6	Compartment B support	
7	Omnidirectional Antenna A	The sensor is to run the full length of the tubular antenna boom along the upper surface.
8	Omnidirectional Antenna B	
9	Planar array antenna	The sensor is to run along the planar array channel structure at the attachment brackets.
10	CDR attachment flange	The sensor is to run along the upper surface of one CDR mounting foot.
11	CDR breakwire connector	A short loop of conventional wire connects two connector pins together.
12	Solar panel bracket	The sensor is to run along the upper surface of each of the solar panel supporting arms.
13	Solar panel bracket	
14	Shock Absorber Gas Cylinder 1	One circumferential wrap of wire around each of the shock absorber gas cylinders is provided to detect cylinder explosion.
15	Shock Absorber Gas Cylinder 2	
16	Shock Absorber Gas Cylinder 3	
17	Crushable Block 1	A breakwire sensor is used on each block to detect when it crushes more than 5 in.
18	Crushable Block 2	
19	Crushable Block 3	
20	Main mast	One breakwire sensor with four different runs connected in series is used to sense the four sides of the mast.

complete break (open circuit) in the event of structure failure. Two configurations of conductor material have been considered: round wire and flat foil, suitably insulated electrically. Flat copper or aluminum foil appears preferable because it presents greater bonding area, separation under lower loads, and tends to lose insulation over a lesser length when broken.

To meet the requirements of the spacecraft harnessing, it is essential that at some point there be a transition from the breakwire element to stranded copper hookup wire through a terminal arrangement. This transition area must exhibit high reliability mechanically and electrically. Assuming foil construction, this termination can consist of a metallic clip, crimped and soldered to the junction of stranded wire sensor pigtail and foil (see Fig. 126).

Since the shock absorber gas cylinder will explode under excessive loads, a circumferential breakwire band about the structure should give an indication of failure. Fig. 127 through 130 illustrate typical breakwire installations on various spacecraft items to be instrumented for structural failure.

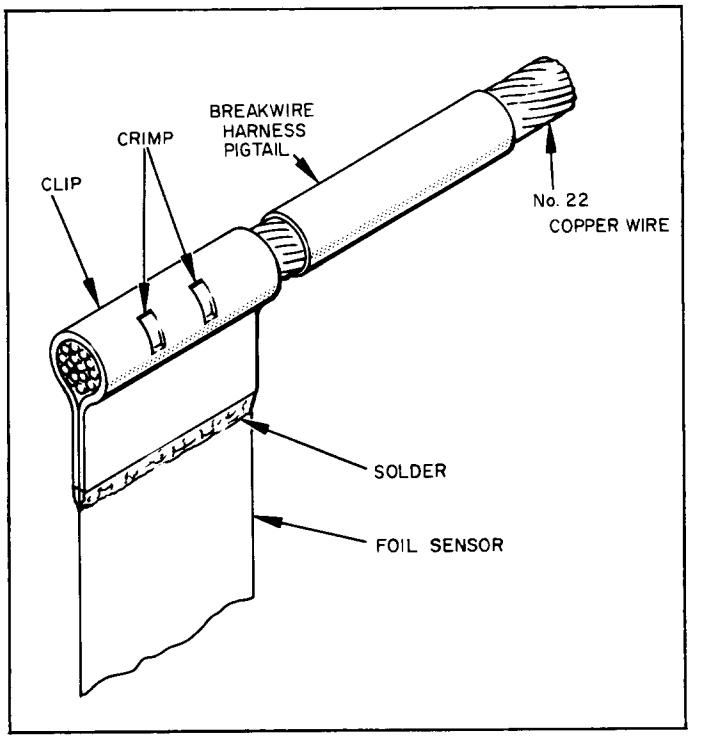

Fig. 126. Foil-to-harness connection

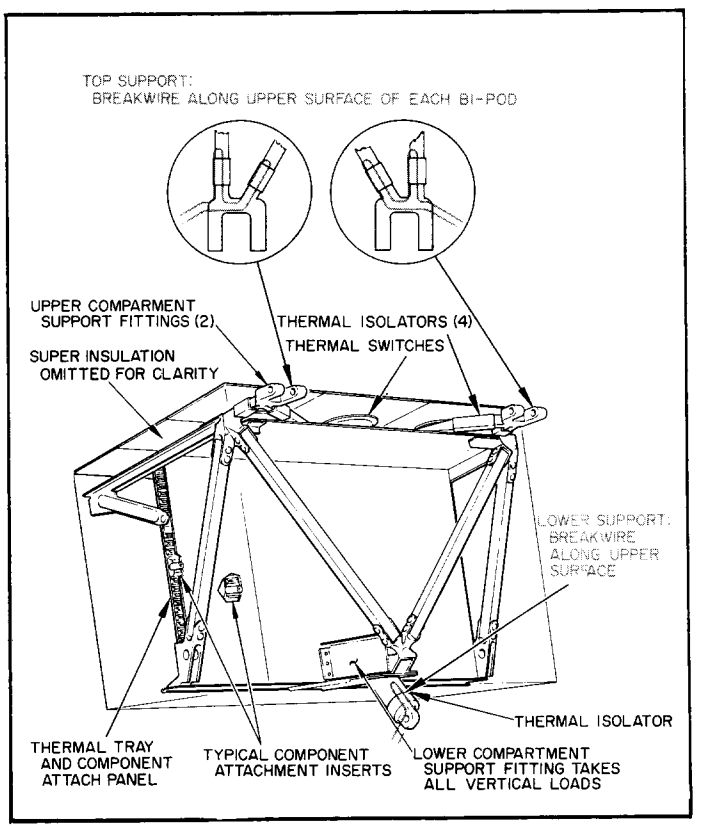
TOP SUPPORT: BREAKWIRE ALONG UPPER SURFACE OF EACH BI-POD
UPPER COMPARMENT SUPPORT FITTINGS (2)
THERMAL ISOLATORS (4)
THERMAL SWITCHES
SUPER INSULATION OMITTED FOR CLARITY
LOWER SUPPORT: BREAKWIRE ALONG UPPER SURFACE
THERMAL ISOLATOR
THERMAL TRAY AND COMPONENT ATTACH PANEL
TYPICAL COMPONENT ATTACHMENT INSERTS
LOWER COMPARTMENT SUPPORT FITTING TAKES ALL VERTICAL LOADS

Fig. 127. Typical breakwire sensor installation on compartment supports

CONFIDENTIAL
UNCLASSIFIED

UNCLASSIFIED
CONFIDENTIAL

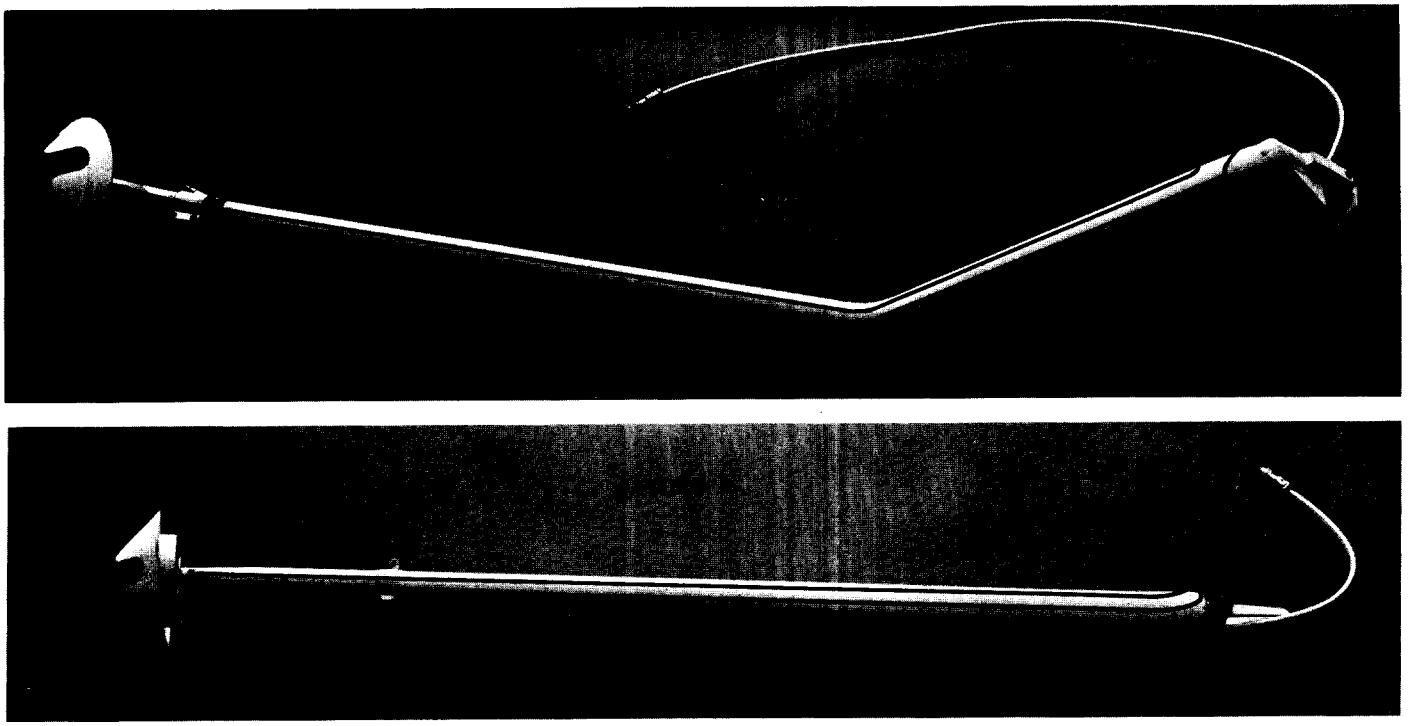

Fig. 128. Breakwire sensor installation on omnidirectional antenna booms

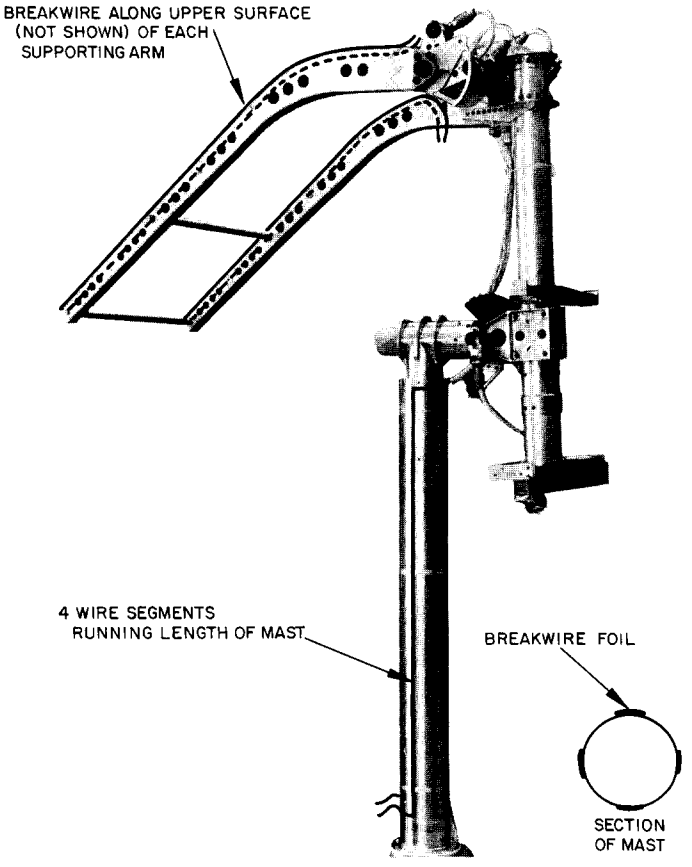

Fig. 129. Installation of breakwire sensors on solar panel brackets and main mast

The crushable block sensors are unique in that they act as penetration indicators rather than as sensors of structure failure due to abnormal loads. Fig. 131 indicates one possible arrangement in which a rod is employed to sense when the compression of the crushable honeycomb structure exceeds 5 in., thereby transmitting some of the crushing force into a breakwire segment causing it to rupture. A reliable snap action switch with overtravel provisions could be substituted to provide a similar sensing arrangement with some increase in weight.

b. Harness design. The harness, together with the CDR, must survive impact shock in excess of normal *Surveyor* requirements. Since the harness is, in effect, an integral element of the spaceframe, dependent upon the basic structure for support and protection, independent survival appears to be an incompatible requirement. In practice, however, a high level of confidence in harness survival after hard impact may be achieved provided terminations are adequately treated. The interface connector PTS07E-22-55P proposed by ADP, is more rugged at weight expense than normal *Surveyor* connectors and appears to be a good compromise for this application. Examination of Fig. 132, which illustrates the general placement of the proposed breakwire sensors on the spacecraft, will infer the general routing requirements and relative complexity of the breakwire harness.

UNCLASSIFIED
CONFIDENTIAL

UNCLASSIFIED
CONFIDENTIAL

3. System Test Implications

It appears that the CDR should receive testing corresponding to that of any other payload item on the spacecraft. A prototype CDR should be required to pass unit type approval tests, followed by system type approval testing as installed on a prototype spacecraft. System type approval testing should be completed prior to flight acceptance testing of the flight-type CDRs. A CDR test console will be required to support system testing. The study included detailed programming of the CDR into the overall spacecraft test schedule.

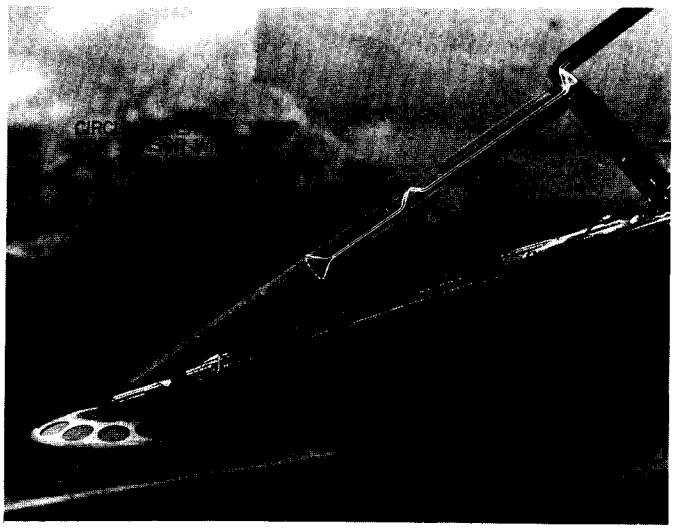

Fig. 130. Breakwire sensor installation on shock absorber

4. Operational Considerations

From a preliminary examination of launch operations, the following recommendations were made.

(1) The flight model CDR should not be employed in the spacecraft/*Centaur* combined system tests, since the CDR transmitter does not operate during the launch period.

(2) Because of time constraints and hazardous operations in the Explosive Safe Area (ESA), the CDR should be installed earlier in the Spacecraft Checkout Facility (about 22 days before launch).

(3) The CDR should receive a final prelaunch checkout in the ESA just prior to encapsulation of the spacecraft.

A detailed sequence of events for CDR installation and prelaunch checkout was formulated.

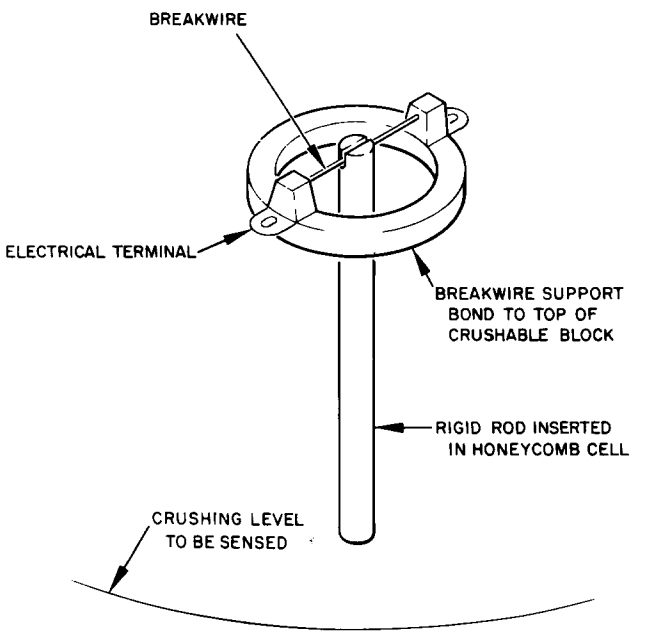
BREAKWIRE
ELECTRICAL TERMINAL
BREAKWIRE SUPPORT BOND TO TOP OF CRUSHABLE BLOCK
RIGID ROD INSERTED IN HONEYCOMB CELL
CRUSHING LEVEL TO BE SENSED

DETAIL OF BREAKWIRE SENSOR DEVICE

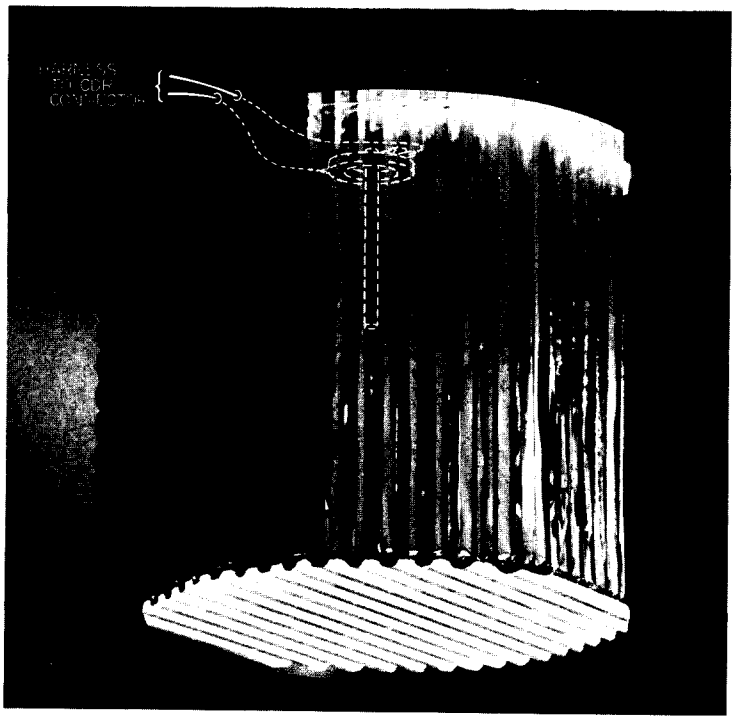

CRUSHABLE BLOCK

Fig. 131. Installation of breakwire sensor on crushable block

UNCLASSIFIED
CONFIDENTIAL

UNCLASSIFIED
CONFIDENTIAL

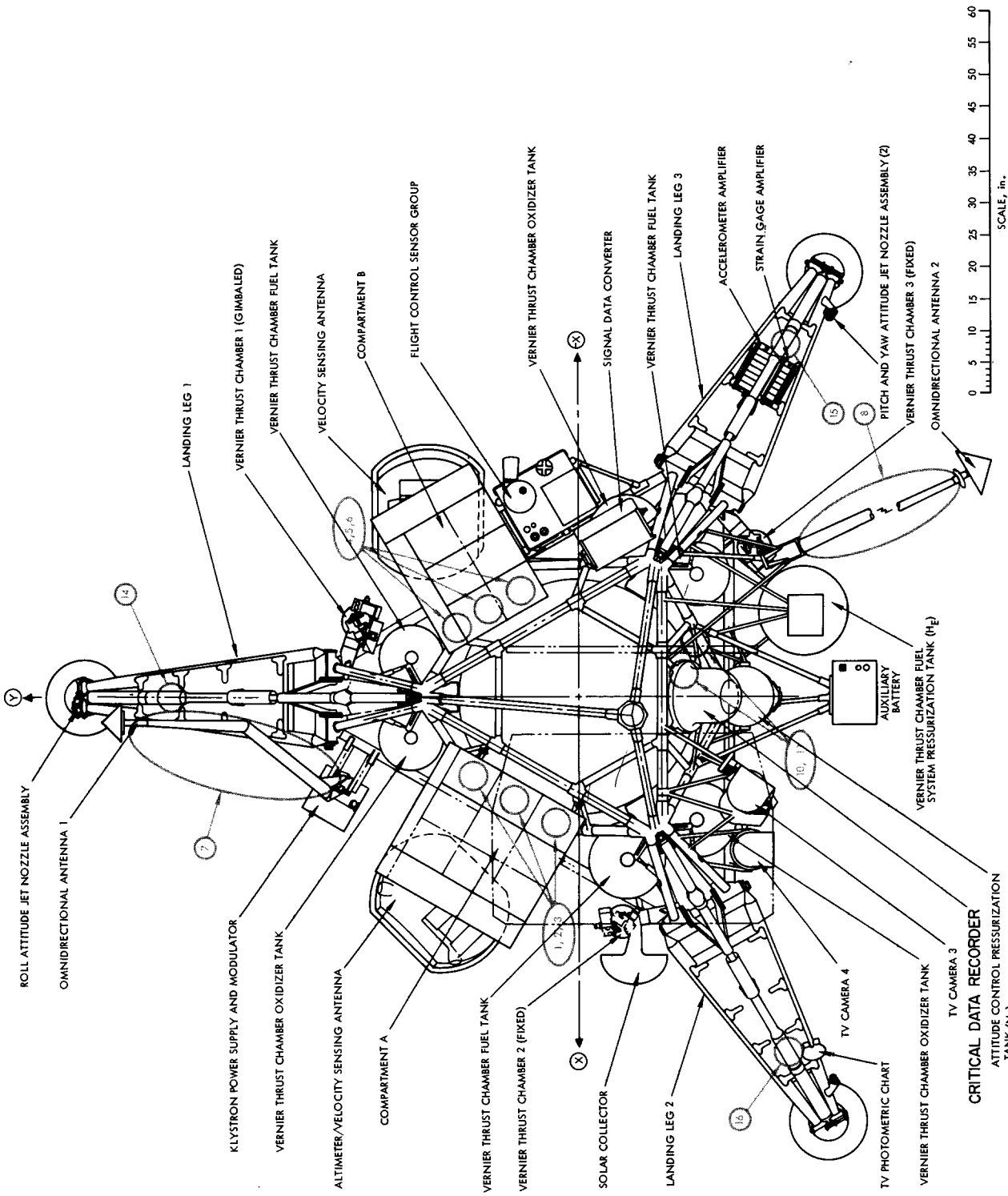
ROLL ATTITUDE JET NOZZLE ASSEMBLY
OMNIDIRECTIONAL ANTENNA 1
KLYSTRON POWER SUPPLY AND MODULATOR
VERNIER THRUST CHAMBER OXIDIZER TANK
ALTIMETER/VELOCITY SENSING ANTENNA
COMPARTMENT A
VERNIER THRUST CHAMBER FUEL TANK
VERNIER THRUST CHAMBER 2 (FIXED)
SOLAR COLLECTOR
LANDING LEG 2
TV PHOTOMETRIC CHART
VERNIER THRUST CHAMBER OXIDIZER TANK
TV CAMERA 3
TV CAMERA 4
CRITICAL DATA RECORDER
ATTITUDE CONTROL PRESSURIZATION TANK (N_2)
VERNIER THRUST CHAMBER FUEL SYSTEM PRESSURIZATION TANK (H_2)
AUXILIARY BATTERY
LANDING LEG 1
VERNIER THRUST CHAMBER 1 (GIMBALED)
VERNIER THRUST CHAMBER FUEL TANK
VELOCITY SENSING ANTENNA
COMPARTMENT B
FLIGHT CONTROL SENSOR GROUP
VERNIER THRUST CHAMBER OXIDIZER TANK
SIGNAL DATA CONVERTER
VERNIER THRUST CHAMBER FUEL TANK
LANDING LEG 3
ACCELEROMETER AMPLIFIER
STRAIN GAGE AMPLIFIER
PITCH AND YAW ATTITUDE JET NOZZLE ASSEMBLY (2)
VERNIER THRUST CHAMBER 3 (FIXED)
OMNIDIRECTIONAL ANTENNA 2
SCALE, in.
0 5 10 15 20 25 30 35 40 45 50 55 60
MIDCOURSE CONFIGURATION
ANTENNA AND SOLAR PANEL POSITIONER HAS BEEN OMITTED FROM THIS VIEW FOR CLARITY

Fig. 132. Placement of breakwire sensors on spacecraft

UNCLASSIFIED
CONFIDENTIAL

UNCLASSIFIED
CONFIDENTIAL

References

1. "*Surveyor* Spacecraft System," *SPS 37-28*, Vol. I, pp. 31–173, Jet Propulsion Laboratory, Pasadena, California, July 31, 1964.
2. Thornton, T. H., Jr., *A Statistical Analysis of a Multiple-Purpose Guidance System for Space Mission,* Technical Memorandum No. 312-408, Jet Propulsion Laboratory, Pasadena, California, March 24, 1964.
3. "*Surveyor* Spacecraft System," *SPS 37-29*, Vol. I, pp. 66–207, Jet Propulsion Laboratory, Pasadena, California, September 30, 1964.
4. Preliminary Surveyor Midcourse and Terminal Guidance Equations, SSD 3296 R, Hughes Aircraft Company, Space Systems Division, May 1963.
5. Blanchard, L. E., Meier, O., *Mission Analysis Study for Soil Mechanics Surface Sampler Experiment,* SSD 4482 M, Hughes Aircraft Company, Space Systems Division, September 14, 1964.

UNCLASSIFIED
CONFIDENTIAL